Imperial College London

TARGETING MAML FOR THE INHIBITION OF NOTCH SIGNALLING, USING ANTP FUSION PROTEINS

SILVIA COLUCCI

THESIS SUBMITTED FOR THE DEGREE OF DOCTOR OF PHILOSOPHY OF IMPERIAL COLLEGE LONDON

DEPARTMENT OF LIFE SCIENCES
IMPERIAL COLLEGE LONDON
FEBRUARY 2013

For Nonno Ciccio, Arnaldo Bravo and Tata

Declaration of Originality

I, Silvia Colucci, hereby declare that the work presented in this thesis was carried out by myself unless otherwise stated.

Silvia Colucci

Abstract

The highly conserved Notch signalling pathway plays a major role in both metazoan development and adult tissue renewal. Deregulation of this pathway is linked to several diseases, including cancer. Various strategies for Notch signalling inhibition are now being investigated as promising new approaches for cancer therapy. Notch receptor activation results in the release of the Notch cytoplasmic domain (N^{IC}) which translocates to the nucleus to bind the transcription factor CSL. Subsequent recruitment of MAML-1 is necessary to form the active complex that initiates transcription of Notch target genes. In this study, the strategy used to inhibit Notch signalling consists of blocking the CSL-N^{IC}-MAML tripartite complex formation by targeting MAML-1 interactions with N^{IC} and CSL. The first tool is a fusion protein composed of the membrane translocating protein Antennapedia (Antp) and a dominant negative version of MAML-1 (DN-MAML1). A Notch activity reporter-gene assay revealed that addition of Antp-DN-MAML1 leads to a dose dependent decrease in luminescence, corresponding to an inhibition of Notch signalling. At the transcriptional level, treatment of MDA-MB-231 and bone marrow dendritic cells with Antp-DN-MAML1 resulted in a significant decrease in the mRNA levels of Notch target gene Hes1. In a cell proliferation assay, addition of Antp-DN-MAML1 had a strong growth-inhibitory effect when added to MDA-MB-231 breast cancer cells. Our i*n vitro* data is further supported by preclinical studies where administration of Antp-DN-MAML1 halted MDA-MB-231 tumour growth. The second strategy of Notch signalling inhibition presented here attempts the intranuclear delivery of single-chain variable-fragment (scFv) antibodies fused to Antp. Suitable scFvs were selected from a phage display library for their ability to bind residues 13–74 of MAML-1. This constitutes the minimal portion of MAML-1 necessary to form the active tripartite complex, therefore we expect any scFvs that bind this portion to inhibit downstream signalling. Our study illustrates two novel strategies for inhibition of Notch signalling at the transcriptional level which represent potential future therapeutic alternatives.

Acknowledgements

I would like to thank Prof. Dallman and Dr. Byrne for adopting me half way through the project, always making me feel welcome. Your guidance and support have been invaluable. A special acknowledgement to Dr. Deonarain for his supervision and help in shaping the project. I also thank Prof. Lamb and all the members of the Dallman lab. In particular, Dr. Bugeon for being my 'Notch' partner in the lab, no one understands the difficulty of working on this pathway like you do. Thank you to all the members of the, now extinct, RAT lab and Bijal for always being there, you are a good friend. On a personal note, thank you to all my family, my parents Rocco and Lorella, my sister Laura and Joe for their love and encouragement. Thank you to all my friends for convincing me that it was all worth it. I would like to thank my external supervisor Agamemnon Epenetos for introducing me to the concept of targeting the Notch pathway using Antenapedia based fusion proteins. Finally, I would like to thank the BBSRC for funding this work and Trojantec for allowing me to use their technology in my research.

Table of contents

List of Figures

Chapter 1: Introduction

Chapter 2: Materials and Methods

Chapter 3: Production and characterisation of the Antp-DN-MAML1 fusion

Chapter 4: Phage display selection of a scFv against DN-MAML1 and its fusion to Antp

List of Tables

Chapter 1: Introduction

Chapter 2: Materials and Methods

Chapter 3: Production and characterisation of the Antp-DN-MAML1 fusion

Chapter 4: Phage display selection of a scFv against DN-MAML1 and its fusion to Antp

List of abbreviations

Antp	Antennapedia
bp	Base pairs
BMDC	Bone marrow dendritic cells
BSA	Bovine serum albumin
BTD	β trefoil domain
cDNA	Complimentary DNA
CDR	Complimentary determining region
CH	Constant heavy chain
CHO	Chinese hamster ovary
CL	Constant light chain
CPP	Cell penetrating peptide
Ct	Cross threshold
CTD	C-terminal Rel homology domains
DMEM	Dulbecco's modified Eagle's medium
DMSO	Dimethyl sulfoxide
DNA	Deoxyribonucleic acid
DN	Dominant negative
dNTP	Deoxyribonucleotide triphosphate
DTE	Dithioerythritol
ECL	Enhanced chemi-luminescence
E.coli	Escherichia coli
EDTA	Ethylenediaminetetraacetic acid
ELISA	Enzyme-linked immunosorbent assay
FAB	Fragment of antigen binding
FACS	Fluorescence activated cell sorting
FBS	Fetal bovine serum
Fc	Fragment crystallizable
DNA	Deoxyribonucleic acid
GM-CSF	Granulocyte-macrophage colony-stimulating factor
GSI	γ-secretase inhibitor
h	Hours
HAMA	Human anti-mouse antibody
Hes	hairy/enhancer of split
HRP	Horse radish peroxidase
Ig	Immunoglobulin
IMAC	Immobilised Metal Affinity Chromatography
IPTG	Isopropyl β-D-1-thiogalactopyranoside
K_d	Dissociation equilibrium constant
kDa	Kilo Daltons
LB	Luria-Bertani
LPS	Lipopolysaccharide
M	Molar
mAb	Monoclonal antibody
MAML	Mastermind-like
mRNA	Messenger RNA
MW	Molecular weight

MWCO	Molecular weight cut-off
N^{IC}	Notch intracellular domain
NTD	N-terminal Rel homology domains
OD	Optical density
PBS	Phosphate buffered saline
PCR	Polymerase chain reaction
pI	Isoelectric point
PEG	Polyethylene glycol
*pel*B	Pectate lyase
qRT-PCR	Quantitative reserve transcription-PCR
RNA	Ribonucleic acid
scFv	Single chain variable fragment
SDS-PAGE	Sodium dodecyl sulphate poly acrylamide gel electrophoresis
TAE	Tris-acetate EDTA
TT-Hc	Tetanus toxin heavy chain
VH	Variable heavy chain
VL	Variable light chain

Chapter 1

Introduction

1.1 Notch signalling

1.1.1 The Notch signalling pathway

Over 90 years ago, the observation of notches at the wing margin in *Drosophila melanogaster* by the Morgan group lead to the discovery of the Notch gene (Morgan 1917). Subsequently, loss of function experiments revealed a "neurogenic" phenotype caused by Notch. In particular, cells programmed to become epidermis form neural tissue instead. At the start of the 1980's, it was found that the Notch gene encodes a 300 kDa single-pass transmembrane receptor.

The highly conserved Notch signalling pathway plays a major role both in metazoan development and adult tissue renewal. Transmission of Notch signals, which requires cell to cell contact, can influence cell proliferation, cell death and cell differentiation. Drosophila have a single Notch receptor and two Notch ligands, Delta and Serrate. In mammals, four single-pass transmembrane Notch receptors (Notch 1-4) and five ligands (Delta-like 1, 3, 4 and Serrate-like Jagged 1, 2) have been identified so far.

1.1.2 Notch receptors

Receptor synthesis involves the proteolytic cleavage at site 1 (S1) of large single polypeptide precursors by a Furin-like convertase in the Golgi (Logeat et al., 1998) resulting in the release of two receptor fragments which re-assemble non-covalently on the cell surface (Blaumueller et al., 1997). While transiting through the Golgi, Notch receptors can be glycosylated by glycosyl-transferases such as Fringe (Haines and Irvine, 2003). This post-translational modification affects the response to different ligand subfamilies. As illustrated in Figure 1.1, the Notch extracellular portion includes 29-36 tandem epidermal growth factor (EGF)-like repeats, some of which are involved in interactions with the Notch ligands. In particular, repeats 11-12 are required for trans interactions with ligands displayed on adjacent cells. In contrast, EGF repeats 24-29 are involved in cis inhibition by ligands expressed in the same cell. The ability of certain EGF repeats to bind calcium ions influences the structure and affinity of Notch in ligand binding and can affect signalling efficiency (Cordle et al., 2008). The extracellular portion of the receptor also contains a unique negative regulatory region (NRR), composed of three cysteine-rich Lin12-Notch repeats (LNR)

and a heterodimerisation domain. The NRR functions to prevent receptor activation in the absence of ligands.

The end of the receptor single transmembrane domain contains a C-terminal "stop translocation" signal composed of 3-4 arginine/lysine residues. In the intracellular portion we find a RAM (RBP-J associated module) domain which forms a high-affinity binding module of 12-20 amino acids centered on a conserved WxP motif. The RAM domain is linked to seven ankyrin repeats (ANK domain) by a long, unstructured linker comprising a nuclear localisation sequence. The ANK domain is made up of two α helices linked by a short turn followed by a β-hairpin motif. After the ANK domain, we find a bipartite nuclear localisation sequence and a transactivation domain. The C-terminal end of the receptor contains conserved proline/glutamic acid/serine/threonine-rich motifs (PEST) that include degradation signals (degrons) to regulate the stability of N^{IC}. Phosphorylation of PEST results in proteolytic degradation of N^{IC} via E3 ligase recognition and ubiquitination (Fryer et al., 2004).

1.1.3 Notch ligands

Canonical Notch ligands in mammals are type I transmembrane proteins (reviewed in (D'Souza et al., 2008), characterised by three related structural motifs: an N-terminal DSL (Delta/Serrate/LAG-2) motif and 6-16 EGF-like repeats (including both calcium and non-calcium binding). DSL ligands are classified depending on the presence/absence of a cysteine-rich domain (Jagged/Serrate or Delta, respectively). It is interesting to note that recent work by our laboratory led to the identification of Jagged 1 as a ligand for CD46 in humans (Le Friec et al., 2012).

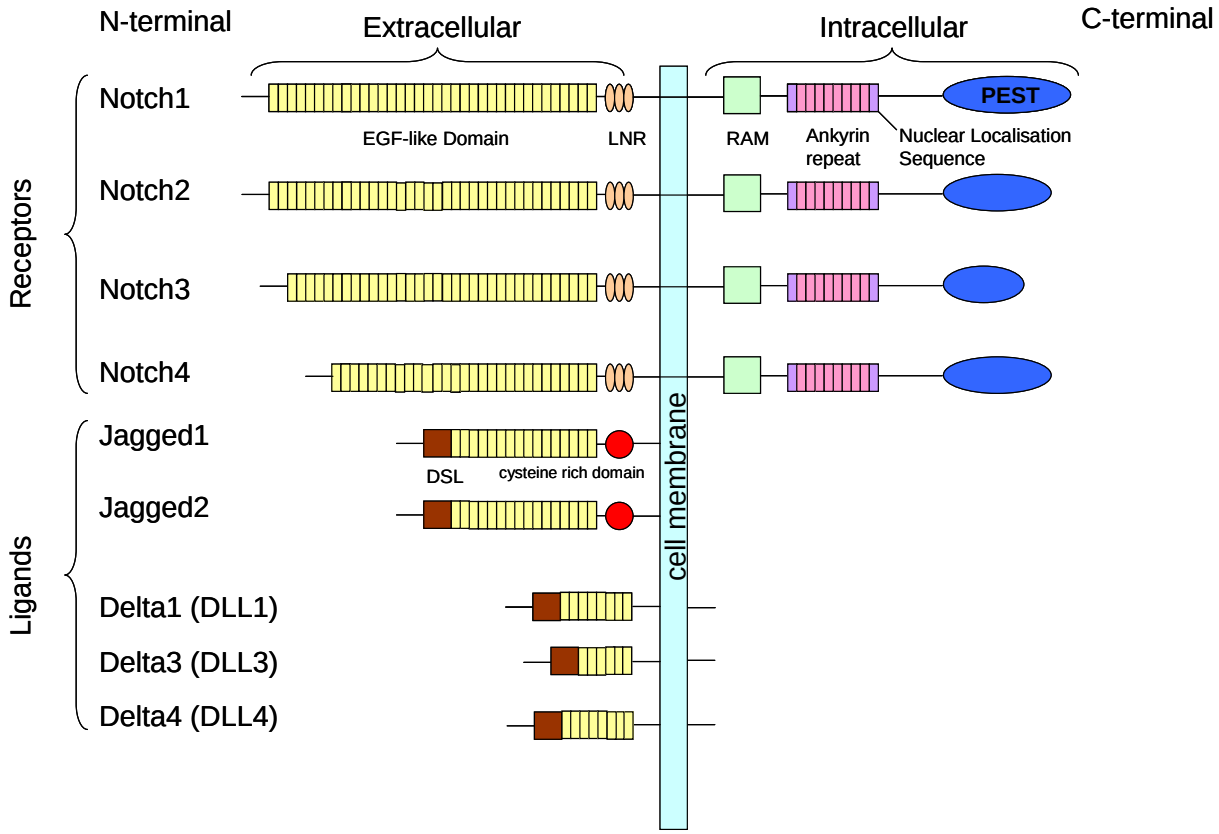

Figure 1.1: The structure of mammalian Notch receptors and ligands. All proteins are type I transmembrane and contain EGF-like domains. Extracellularly, the Notch receptors contain LIN-12-Notch repeats (LNR) close to the cell membrane and Notch ligands are characterised by DSL domains at the N-terminus. The ligands intracellular domains are very short in contrast with Notch receptors that present large modular intracellular domains (N^{IC}).

1.1.4 The canonical pathway

Receptor activation results in its cleavage by the TNF-alpha converting enzyme (TACE), a member of the 'a disintegrin and metalloprotease' (ADAM) family (Brou et al., 2000; Mumm et al., 2000). Cleavage at site 2 (S2) occurs circa 12 amino acids before the transmembrane domain in a site deeply buried within the negative regulatory region. The release of the Notch ectodomain results in the formation of a membrane-tethered intermediate called Notch extracellular truncation (NEXT). This is a substrate for the protease, γ-secretase, an enzyme complex containing presenilin, nicastrin, PEN2 and APH1 (Saxena et al., 2001). This second cleavage (S3-S4) releases the Notch intracellular domain (N^{IC}) which translocates to the nucleus to bind CSL (also called RBP-J, **C**BF1, **S**u(H) in flies and **L**AG-1 in *C.elegans*) (Tamura et al., 1995) (Figure 1.2). This DNA binding protein can normally be found in a complex with ubiquitous corepressor (CoR) proteins and histone deacetylases (HDACs) (Kao et al., 1998) (see Section 1.1.5). In these conditions CSL acts as a transcription repressor. However, the binding of N^{IC} to CSL displaces this inhibitory complex and coactivators such as Mastermind-like (MAML) are then recruited (Petcherski and Kimble, 2000; Wu et al., 2000).

1.1.4.1 Mastermind

Three MAML members (MAML 1-3) have been described in mammals (Lin et al., 2002; Wu et al., 2002). Wu et al. found that the three MAML genes are widely expressed in adult tissues whereas different expression patterns are observed in mouse early spinal cord development. The three MAML proteins include an N-terminal basic domain for binding to the Notch ankyrin repeat portion. They also share a C-terminal transcriptional activation domain. Co-immunoprecipitation experiments confirmed that each MAML protein is able to form a complex with the N^{IC} of each Notch receptor and CSL. Some differences were observed between the three MAML. For example, MAML-3 binds less efficiently to the N^{IC} derived from Notch-1. In addition, MAML-3 functions more efficiently as a coactivator with the Notch4 N^{IC} to transactivate a Notch target Hes1 promoter construct. Also, MAML3 does not significantly amplify transcription of the Hes1 gene upon induction with Jagged2 and Delta1 Notch ligands. In the context of human malignancies, genetic rearrangements of MAML-2 were first identified in a subset of salivary gland tumours (Tonon et al., 2003). Abnormal expression of MAML-2 also contributes to the activation of Notch

signalling in human lymphomas. In recent years, research efforts have focused mainly on MAML-1. This protein is also the main focus of this study. However, it is important to keep in mind that the difference between the three MAML proteins may partly be responsible for the diversity of biological effects observed upon Notch activation.

Mastermind proteins are approximately 1000 amino acids long but only a minor portion is involved in interactions with CSL and N^{IC} (Petcherski and Kimble, 2000; Nam et al., 2003). The importance of Mastermind as a whole is highlighted by studies employing truncated versions of Mastermind which act in a dominant-negative fashion, completely blocking all Notch target expression. Wu et al. showed that both MAML-1 (1-302) and MAML-1 (124-1016) reduce activation of Hes1 *in vitro* (Wu et al., 2000). The mutants are defective in transactivation and Notch binding, respectively. The dominant-negative effect of MAML-1 (1-302) observed by Wu et al., confirms the observations of Helms et al. in *Drosophila* where C-terminal truncations of Mastermind affect Notch pathway function in eye and wing development (Helms et al., 1999). A study in Xenopus embryos, showed that the C-terminal portion of Mastermind is crucial for contacts with CBP/p300 and transcriptional activation (Fryer et al., 2002). In fact, mutant Mastermind lacking the p300 interaction domain (amino acids 75-301) acts as a dominant-negative inhibitor (Fryer et al., 2002). A subsequent study demonstrated that MAML-1 (13-74) was the minimal domain necessary for the formation of a tripartite complex with N^{IC} and CSL on DNA (Weng et al., 2003). In fact, shorter MAML truncations (22-74, 13-63 and 13-52) showed weak association with binding partners. MAML (13-74) was also the minimal portion required for strong dominant-negative activity which suppressed growth and survival of T-ALL cells. This study provides the proof-of-concept for Notch inhibition by disruption of MAML for a therapeutic benefit.

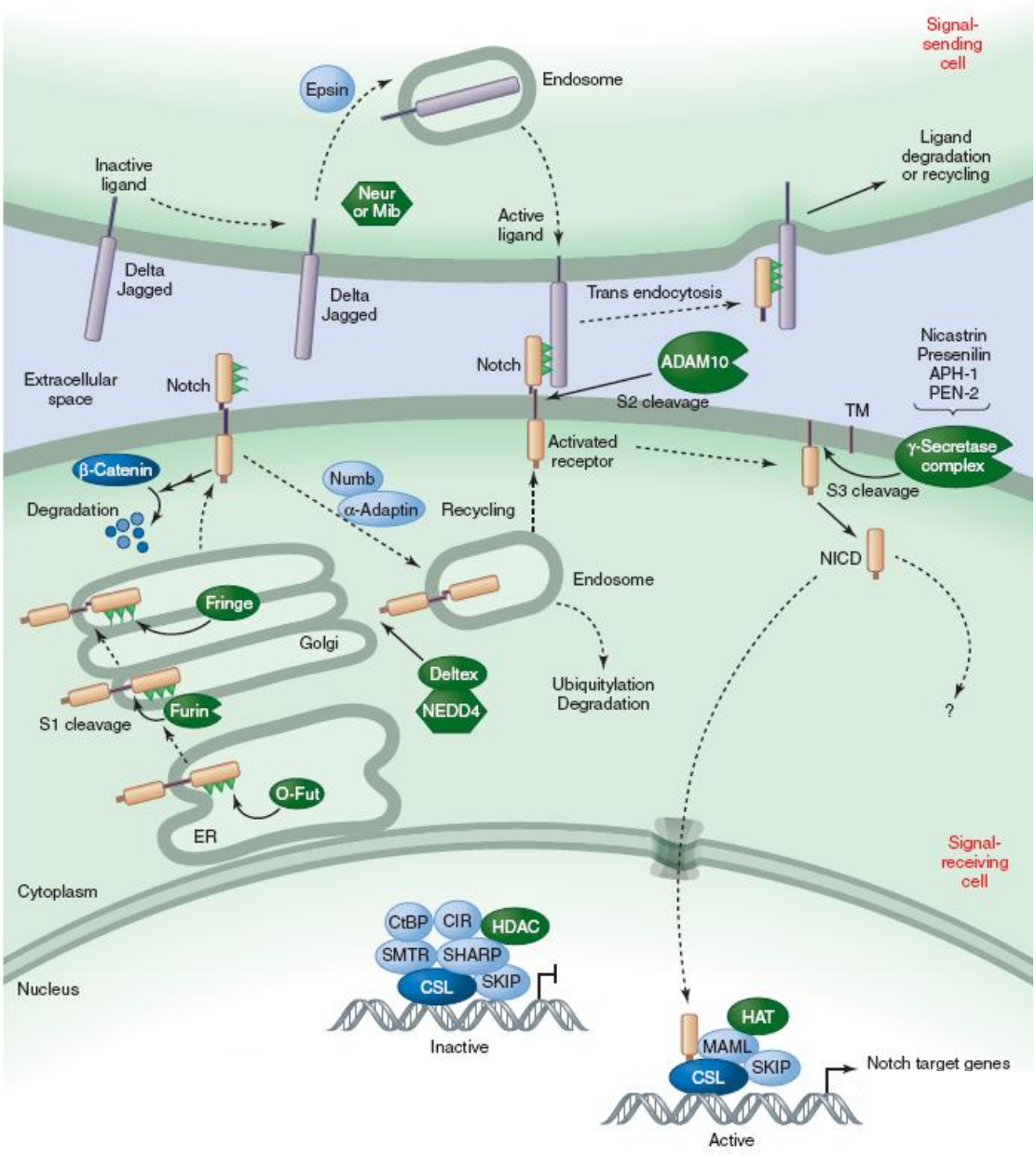

Figure 1.2: The Notch signalling pathway. Taken from (Kopan, 2012).

Formation of the CSL- N^{IC}-MAML ternary complex, shown in Figure 1.3, is mandatory to activate transcription of Notch target genes. Understanding how the complex is assembled at the molecular level is crucial for the design of an inhibitory strategy. CSL consists of N-terminal and C-terminal Rel homology domains (NTD and CTD) with a central β trefoil domain (BTD) (Kovall and Hendrickson, 2004). NTD and CTD have β sheet secondary structure with folding into immunoglobulin-like domains. The NTD and BTD function together to recognise and bind specific

DNA sequences, interacting with the major and minor groove, respectively (Kovall and Hendrickson, 2004). N^{IC} is composed of multiple domains of which only the RAM and ANK domains are involved in the interactions within the tripartite complex (Nam et al., 2003). The RAM domain of N^{IC} binds with high affinity (K_d in nanomolar range) to the BTD of CSL (Wilson and Kovall, 2006; Nam et al., 2006). ANK and CTD come together forming a binding groove for the N-terminal helical region of the MAML-1 polypeptide. MAML-1 also interacts with the NTD through its C-terminal. In particular, a β-hairpin loop structure in NTD (NTD-loop) assumes an open conformation induced by RAM binding to BTD. This conformational change allows binding of the C-terminal Mastermind helix. It is important to note that residues 13–74 constitute the minimal MAML-1 region necessary to form complexes with N^{IC} and CSL (Weng et al., 2003).

Recent studies suggest that aside from the canonical pathway, CSL-independent signalling also occurs (reviewed in (Andersen et al., 2012). The non-canonical Notch pathway interacts with the Wnt pathway by regulating active β-catenin levels. In order to control cellular activity outside the nucleus, Notch is proposed to interact with other protein such as Numb and Numblike. Non-canonical Notch signalling has been reported to be particularly important in the immune system as illustrated by studies in our laboratory (Gentle et al., 2012).

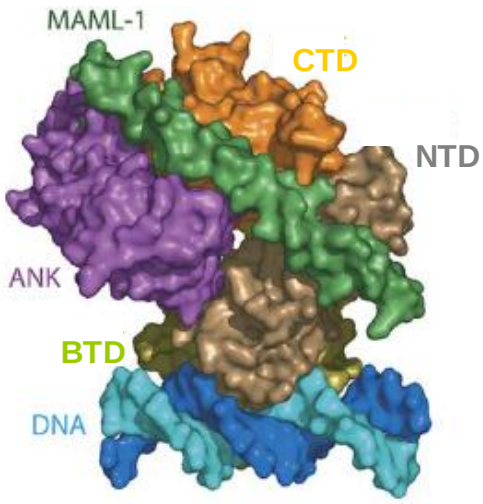

Figure 1.3: The CSL- N^{IC}-MAML-1 ternary complex. CSL is composed of the NTD (brown) and CTD (orange) (N-terminal and C-terminal Rel homology domains) plus the BTD (light green) (β trefoil domain). ANK (purple) = N^{IC} ankyrin domain. MAML-1 (dark green) and DNA (blue) are also shown. Figure adapted from Nam et al. (2006).

1.1.5 The CSL repressor complex

The CSL repressor complex is composed of various elements (reviewed in (Borggrefe and Oswald, 2009) (Figure 1.2). Firstly, the SHARP/MINT protein (Oswald et al., 2002; VanderWielen et al., 2011) was characterised *in vivo* during B- and T-cell development (Tsuji et al., 2007; Yabe et al., 2007; Kuroda et al., 2003). The evolutionary conserved SPOC domain at the C-terminal of SHARP can recruit various corepressor proteins such as CtIP/CtBP, ETPO and SMRT (Oswald et al., 2005; Salat et al., 2008; Shi et al., 2001). Other elements of the repressor complex include KyoT2 which is proposed to recruit Ring1 and other polycomb group (PcG) proteins (Taniguchi et al., 1998; Qin et al., 2004; Qin et al., 2005). Another protein CIR is thought to establish a HDAC-containing complex via SAP30 or NKAP (Hsieh et al., 1999; Pajerowski et al., 2009).

1.1.6 Regulation of Notch signalling

It is important to understand the mechanisms that regulate the amplitude and timing of Notch signalling since these are the basis for the cellular context dependency of the Notch response. Figure 1.2 illustrates the complexity of this system which affects many downstream processes. The E3 ubiquitin ligases Deltex and Nedd4 in addition to Numb and α-adaptin regulate the levels of Notch receptors on the cell membrane. Nedd4 is thought to modify Notch to target it for degradation and is therefore considered as a negative regulator of signalling. Studies in Drosophila showed that Deltex was able to antagonise the negative effect of Nedd4 thus promoting Notch signalling (Matsuno et al., 1995; Hori et al., 2004). Interestingly, studies in mammalian cells (lymphoid cells and neurons) showed the opposite effect with Deltex antagonising Notch (Itoh et al., 2003; Sestan et al., 1999). Numb, a negative regulator of Notch signalling, interacts with the ear domain of α-adaptin, a member of the adaptor protein-2 (AP2) complex which connects cargoes (Numb-Notch) to the clathrin coat of endocytic vesicles (Berdnik et al., 2002). Regulation of ligand activation involves E3 ubiquitin ligases such as Neur and Mindbomb (Mib) that process the ligand intracellular portion to induce epsin-mediated endocytosis (Chitnis, 2006; Le Borgne et al., 2005).

1.1.7 Epigenetic regulation of Notch target genes

Epigenetics is the study of changes in gene expression by modifications that do not involve any change in the underlying DNA sequence. These modifications are for example the acetylation and methylation of histone tails. The mechanisms of Notch epigenetic regulation are still unclear but several histone-modifying enzymes are involved in the regulation of Notch target genes. For example, the histone acetyltransferase (HAT) p300 is found in complex with CSL/N^{IC} acting as a positive co-factor (Oswald et al., 2001; Wallberg et al., 2002). Functional interactions between Notch and PCAF and GCN5 have also been described (Kurooka and Honjo, 2000). On the other hand, histone deacetylases were found to be involved in the repression of Notch signalling by the SHARP complex (Kao et al., 1998; Oswald et al., 2002).

1.1.8 Notch target genes

Despite the variety of outcomes observed upon activation of the Notch receptors, only a limited number of Notch target genes have been identified. The hairy/enhancer of split (Hes) genes are highly conserved proteins, regulated by Notch in various cellular contexts (Jarriault et al., 1995). Hes proteins are helix-loop-helix transcription factors that act as transcriptional repressors (Fischer and Gessler, 2007). Evidence supporting the direct link between Notch and Hes genes includes: a) The Hes1, Hes5 and Hes7 promoters can be activated by a constitutively active mutant of the Notch1 receptor. The Hey1, Hey2 and HeyL promoters (Hes subfamily, YRPW common motif) are also activated (Jarriault et al., 1995; Nishimura et al., 1998; Maier and Gessler, 2000; Iso et al., 2003) b) endogenous Hey1 and Hey2 are upregulated by N^{IC} in a variety of cell lines (Iso et al., 2001). These results were confirmed in experiments using Notch-ligand expressing cells to achieve more physiological levels of Notch signalling activation (Shawber et al., 1996; Jarriault et al., 1998). Treatment with the protein synthesis inhibitor cyclo-hexamide excludes any secondary effects. c) When T-cell leukemia cell lines, characterised by constitutively active Notch signalling, were treated with the γ-secretase inhibitor DAPT, microarray analysis identified Hes genes as direct targets (Weng et al., 2006).

Overall, Hes genes are considered to be the best characterised Notch target genes. NRARP and Deltex-1 have also been characterised as Notch target genes and they function as potent negative regulators of Notch signalling (Izon et al., 2002; Lamar et al., 2001). A variety of Notch target genes were identified for their involvement in

cancer such as c-Myc (Weng et al., 2006; Satoh et al., 2004; Palomero et al., 2006) and cyclin D1 (Ronchini and Capobianco, 2001). Other target genes include: NFκB2 (Oswald et al., 1998), Ifi-202, Ifi-204, Ifi-D3, ADAM19 (Deftos et al., 2000), Notch1, Notch3 (Weng et al., 2006), bcl-2 (Deftos et al., 1998), E2A (Ordentlich et al., 1998) and HoxA 5,9 and 10 (Weerkamp et al., 2006).

1.1.8.1 Hes1

Hes1 is the best-characterised Notch target gene. This transcriptional repressor contains a basic-helix-loop-helix (bHLH) DNA binding domain which interacts with conserved N-box sites (CACNAG). Hes1 recruits co-repressors such as TLE1-4 and histone deacetylases to repress expression of target genes including Hes1 itself (Fischer and Gessler, 2007; Iso et al., 2003). This negative feedback loop regulation explains the oscillatory expression of Hes1 mRNA and protein observed both *in vitro* and *in vivo* (Hirata et al., 2002; Iso et al., 2003; William et al., 2007).

1.1.9 Notch and cancer

The first link between Notch and cancer was unveiled in patients affected by T-cell acute lymphoblastic leukemias (T-ALL) where a 9:7 chromosomal translocation results in the production of human Notch1 receptors defective in their extracellular portion and therefore constitutively active (Ellisen et al., 1991). Although this translocation was only found in approximately 10% of T-ALL cases, it was later discovered that most patients present activating mutations in the Notch1 locus. These mutations cause ligand-independent activation of Notch1 and increased stability of the N^{IC}. In humans, abnormal expression levels of Notch receptors and their ligands has now been reported in a vast number of solid tumours (Table 1.1). Nevertheless, a causative role for Notch signalling in tumorigenesis is yet elusive. In contrast with T-ALL, no convincing evidence is available for genetic alterations in Notch genes in solid cancers. It is interesting to note that a tumour suppressor function has also been reported for Notch signalling in mouse keratinocytes, pancreatic and hepalocellular carcinoma, and small-cell lung cancer (Koch and Radtke, 2007). This suggests a strong dependence on the cellular, temporal and spatial context and crosstalk with other signalling pathways.

Table 1.1: Accumulated evidence of Notch involvement in cancer

Tumour type	Notch signalling component involved	Role of Notch	Reference
Breast cancer	Increased expression of Notch receptors and Hes1, Hes5	Tumour progression	(Mittal et al., 2009)
	Notch1 activation	Drug resistance and tumor progression	(Lee et al., 2008)
	N^{IC} accumulation	Tumour progression	(Stylianou et al., 2006)
Colorectal cancer	Notch1 activation	Chemoresistance	(Meng et al., 2009)
	Increased expression Jgd1, Notch1, Hes1	Tumour progression	(Reedijk et al., 2008)
	Increased Jgd1	Oncogenic	(Guilmeau et al., 2010)
Prostate cancer	Increased Jgd1	Tumour progression (metastases and recurrence)	(Santagata et al., 2004)
Liver cancer	Notch3	Drug resistance	(Giovannini et al., 2009)
	Increased expression of Notch3, Jgd1, DLL1, Hes1	Tumour progression	(Giovannini et al., 2006)
Pancreatic cancer	Notch3	Drug resistance	(Yao and Qian, 2010)
	Overexpression of Notch1,2; Jgd2;DLL3,4	Oncogenic and tumour progression	(Mullendore et al., 2009)
Glioblastoma	Notch1,2	Radioresistance	(Wang et al., 2010)
	Increased expression of Notch1,3; Hes1,2; Hey1	Tumour progression	(Hulleman et al., 2009)
	DLL1, Jgd1	Tumour progression	(Purow et al., 2005)
Cervical cancer	Notch	Drug resistance	(Song et al., 2008)
Squamous cell carcinoma	Notch1	Tumour progression (metastasis)	(Joo et al., 2009)
	Amplification and overexpression of Jgd1, DLL1, Notch4	Tumour progression	(Snijders et al., 2005)
Head and neck	Notch1	Drug resistance	(Gu et al., 2010)
Medulloblastoma	Notch2, Hes1	Tumour progression	(Fan et al., 2004)
Melanoma	Notch1	Tumour maintenance and progression	(Liu et al., 2006)
Lung cancer	Numb	Oncogenic/tumour progression	(Westhoff et al., 2009)
	Notch3, Jgd1 interactions	Tumour progression	(Lin et al., 2010)

1.1.9.1 Notch and angiogenesis

The importance of the Notch signalling pathway in angiogenesis is reflected by the common expression of Notch receptors and ligands in the vasculature. During the angiogenesis process in a normal context, vascular endothelial growth factor (VEGF) stimulates the formation of new vessels by increasing the presence of DLL4-expressing tip cells that originate from a pre-existing vessel (Claxton and Fruttiger, 2004). These cells are followed by Notch expressing motile and proliferative endothelial tube cells that form the lumen of the new vessel. In order to decrease vessel sprouting and branching, DLL4 expressed on the tip cells, binds and activates Notch on the tube cells resulting in a downregulation of the VEGF receptor 2 (VEGFR2) (Hellstrom et al., 2007; Suchting et al., 2007). Tumour cells are known to secrete high levels of VEGF which results in increased expression of DLL4 by endothelial cells in the stroma (Mailhos et al., 2001; Patel et al., 2006). When VEGF activity is blocked, DLL4 expression decreases (Thurston et al., 2007; Patel et al., 2005). Inhibition of DLL4 dependent Notch signalling on neighbouring endothelial cells, leads to a considerable reduction in tumour growth accompanied by increased formation of non-functional vessels (Noguera-Troise et al., 2006). The latter effect might be explained by the disruption of the DLL4 negative feedback loop. This is encouraging for the use of VEGF inhibitors in combination with Notch signalling inhibitors for a successful anti-angiogenic therapy.

1.1.9.2 Notch and breast cancer

The first evidence of the oncogenic consequences of de-regulated Notch signalling in solid tumours comes from studies on the mouse mammary tumour virus (MMTV). MMTV does not carry oncogenes like retroviruses, but its insertion into the genome interferes with normal gene expression leading to the formation of mammary tumours. A particular insertion site was identified as the Notch4 locus with resulting expression of a truncated version of the Notch4 receptor missing the majority of the extracellular portion (Gallahan and Callahan, 1987; Uyttendaele et al., 1996; Gallahan and Callahan, 1997). *In vivo* experiments with transgenic mice expressing the truncated Notch4 confirmed a direct link between de-regulated Notch signalling and the development of mammary tumours (Jhappan et al., 1992; Gallahan et al., 1996; Raafat et al., 2004; Dievart et al., 1999). MMTV insertions have also been observed in the Notch1 locus but with a reduced frequency (Dievart et al., 1999). This insertion

results in the expression of a truncated version of the receptor. Microarray studies identified the proto-oncogene c-Myc as a direct target gene of Notch1-induced mammary tumours (Klinakis et al., 2006). When examining human breast cancer samples, coexpression of Notch1 and c-Myc was observed reinforcing the idea that c-Myc is a direct Notch1 target gene (Efstratiadis et al., 2007). In addition elevated Notch1 and Jagged1 expression levels correlate with poor prognosis of breast cancer patients (Reedijk et al., 2005).

Studies on a negative regulator of Notch signalling named Numb, highlighted the importance of aberrant Notch signalling in human breast cancer (Jafar-Nejad et al., 2002; Roegiers and Jan, 2004). Loss of Numb expression was observed in most breast cancer cell lines and in approximately half of the tumours examined in the clinic including many aggressive forms (Pece et al., 2004). Interestingly, increased levels of N^{IC} were detected in 20 breast cancer samples from which Numb was absent (Stylianou et al., 2006).

1.1.9.3 Notch and drug resistance – Rationale for combinatorial therapies

Acquiring resistance to chemotherapeutic drugs is a crucial advantage to cancer cells for their survival. Resistance is usually achieved by the activation of survival pathways or the inhibition of apoptotic pathways. As Notch plays a key role in cell survival, this pathway is proposed to be involved in drug resistance. Upon treatment of colorectal cancer with platinum-based antineoplastic agent oxaliplatin, Notch and other survival pathways (PI3K-AKT) are activated. Blocking Notch signalling using γ-secretase inhibitors (GSIs) sensitises cells to oxaliplatin (Meng et al., 2009). Combination of taxanes and GSIs has been proposed for colon cancer therapy after observation of mitotic arrest in resistant cancer cells upon inhibition of Notch (Akiyoshi et al., 2008). In pancreatic cancer, synergistic anti-tumour effects were observed for GSI in combination with rapamycin due to increased inhibition of the PI3K/AKT/mTOR pathway (Vo et al., 2011). In ErbB2-positive breast cancer cells, Notch signalling is inactive and tumours are not sensitive to GSI treatment. Treatment with trastuzumab (Herceptin®) was shown to induce upregulation of Notch activity as cells become resistant to the treatment. However, combination treatment with trastuzumab and GSI led to apoptosis of the cells (Osipo et al., 2008). In another model, oestrogen receptor (ER)-negative breast cancer cells show elevated expression of survivin, increased proliferation and reduced apoptosis. Upon GSI treatment,

growth of these tumours is reduced suggesting a role for the Notch pathway in maintaining these tumours (Lee et al., 2008).

The Notch pathway has also been implicated in resistance to radiation. Wang et al. showed that Notch inhibition using GSIs makes glioma stem cells more radiosensitive by reducing AKT activity (Wang et al., 2010). Overall, accumulated evidence suggests a role for Notch signalling in drug resistance, hence the use of GSIs as combination therapies. Further research on the cross talk between Notch signalling and other signalling pathways is pivotal to the design of successful therapies.

1.1.10 Therapeutic targeting of the Notch pathway

As evidence accumulates for the implication of Notch in a variety of cancers (Table 1.1), there has been an equal effort to generate inhibitors of this pathway for tumour therapy (Table 1.2). *In vitro*, a variety of strategies have been employed to inhibit Notch signalling. These include antisense Notch (Garces et al., 1997), RNA interference (Fan et al., 2004; Purow et al., 2005), soluble receptor decoys that sequester Notch ligands to prevent receptor binding (Garces et al., 1997; Nickoloff et al., 2002) and dominant negative versions of MAML of CSL that affect transcriptional activation of Notch target genes (Weng et al., 2003; Duncan et al., 2005). The best described strategy for inhibition of Notch signalling is the use of γ-secretase inhibitors. This consists in inhibiting the S3-S4 cleavage to prevent release of the N^{IC}. One of these inhibitors, referred to as MK0752 (Merck) (Figure 1.4), showed severe intestinal toxicity when tested in a phase I clinical trial for T-cell acute lymphoblastic leukemia. These 'off target' effects can be explained by the fact that γ-secretase has many substrates other than the Notch receptor. In addition, the inhibitors may target other proteases which are involved in a multitude of cellular functions. Interestingly, in a mouse model of T-ALL, a reduction of toxic effects is observed when administering GSI in parallel with gluco-corticoids. This combination therapy is as effective as GSI alone. GSIs have also been proposed as a therapeutic agent for estrogen receptor-positive breast cancer. In fact, in this type of cancer, initial therapy with anti-estrogens or aromatase inhibitors results in a dependence on Notch signalling. GSI has also been proposed as a potential therapy for triple-negative breast cancer cells due to their cancer stem cell characteristics.

Table 1.2: Preclinical and Clinical trials of therapeutic agents targeting Notch signalling in cancer

Type	Compound	Condition	Progress	References
γ-secretase inhibitor	R04929097 (Roche)	Breast cancer Brain and CNS tumours Colorectal cancer Melanoma Solid Tumours T-cell leukemia	Phase I clinical trials	(Gounder and Schwartz, 2012)
	MRK-003 (Merck & Co)	Breast cancer T-cell leukemia tumour xenografts	Preclinical studies	(Tammam et al., 2009; Pandya et al., 2011)
	MK-0752 (Merck & Co)	Brain and CNS tumours Breast cancer Neoplasms Pancreatic cancer T-cell leukemia	Phase I clinical trials	(Gounder and Schwartz, 2012)
	PF-03084014 (Pfizer)	Neoplasms Lymphoid leukemia Solid tumours T-cell leukemia	Phase I clinical trial	(Wei et al., 2010)
Immunotherapy	OMP-59R5 α-Notch mAb (OncoMed Pharmaceutics)	Solid tumours	Phase I clinical trial	
	OMP-21M18 α-DLL4 mAb (OncoMed Pharmaceutics)	Colorectal cancer Pancreatic cancer Small cell lung cancer Solid tumours	Phase I clinical trials	(Fischer et al., 2011)
	NRR1 and NRR2 α -Notch1 mAbs (Genentech and Elelixis)	Anaplastic carcinoma Breast carcinoma Colon carcinoma tumour xenografts	Preclinical study	(Wu et al.)
	NRR1 α-Notch1 mAb (Merck & Co)	T-cell leukemia T-ALL cell line	*In vitro* study	(Aste-Amezaga et al., 2010)
	NRR3 α-Notch3 mAb	HEK293T cell line	*In vitro* study	(Li et al., 2008)
	A5226A Anti-Nicastrin mAb	T-cell leukemia T-ALL tumour xenografts	Preclinical study	(Hayashi et al., 2012)
Peptide inhibitor	stapled peptide (Aileron Therapeutics)	T-cell leukemia T-ALL tumour xenografts	Preclinical study	(Moellering et al., 2009)

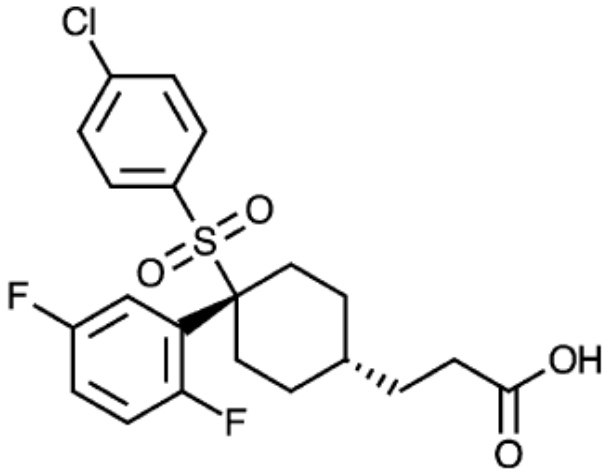

MK-0752

Figure 1.4: Structure of the MK-0752 γ-secretase inhibitor.

Another target for cancer therapy is the Notch ligand DLL4 because of its involvement in the process of angiogenesis (section 1.1.9.1). *In vivo* studies showed severe disruption of the vasculature following DLL4 mutation (Duarte et al., 2004) whereas heterozygous deletion of DLL4 is mostly lethal (Suchting et al., 2007). Anti-DLL4 antibodies have been generated and *in vitro* studies demonstrated their anti-tumour activities (Hoey et al., 2009). Anti-DLL4 antibodies are currently in phase I clinical trials where development of angiomas and neo-vascular tuft formation were reported in patients (Ridgway et al., 2006; Yan et al., 2010). Antibodies have also been used to modulate Notch signalling by targeting individual Notch receptors. In contrast to pan-Notch inhibitors, the advantages of a targeted strategy include potential reduction in side effects. Gastrointestinal toxicity is potentially minimised also because therapeutic antibodies can be delivered through the bloodstream in contrast with GSIs that were designed to be administered orally. In some cancers, oncogenicity can be related to a particular Notch paralogue, found to be mutated or deregulated. For example, abnormal Notch1 activity is implicated in T-ALL whereas Notch3 is implicated in certain lung cancers. These conditions are best suited for a targeted inhibition of Notch signalling. Antibodies have been developed that modulate Notch signalling by the extracellular negative regulatory region (NRR) of Notch 1, 2 and 3 (Li et al., 2008). Upon ligand binding, the NRR of Notch normally undergoes a conformation change to facilitate ADAM protease cleavage (Wu et al., 2010; Li et al., 2008; Aste-Amezaga et al., 2010). These antibodies successfully inhibit Notch

signalling at low concentrations. Wu et al. (2010) employed phage display to select antibodies that inhibit Notch1 only or Notch2 only. They emphasise that inhibition of either receptor alone reduces or avoids intestinal toxicity. Aste-Amezaga et al. (2010) showed how antibodies directed at the Notch1 NRR successfully inhibited signalling from Notch1 receptors with characteristic NRR mutations observed in T-ALL.

The ligand-binding site of Notch1 and Notch3 is also the target of specific antibodies to inhibit Notch downstream signalling. However, higher antibody concentrations are necessary for a successful inhibition effect. Several antibodies targeted at Notch are now undergoing preclinical development with one anti-Notch mAb in Phase I clinical trials (OMP-59R5 OncoMed Pharmaceuticals).

Antibodies could also be targeted to the γ-secretase complex. A recent study described the use of an antibody against the extracellular domain of Nicastrin, a component of γ-secretase. They showed how the antibody was able to inhibit γ-secretase activity by competing with substrate binding. The antibody affected proliferation of T-ALL cells *in vitro* and *in vivo* (Hayashi et al., 2012). Targeting γ-secretase with antibodies remains challenging due to the heterogeneity of the complex. In fact, permutation of the members means that six different complexes are possible depending on the involvement of Presenilin-1 or -2, Aph-$1A_S$, Aph-$1A_L$ or Aph-1B.

When designing a strategy for inhibition of Notch signalling it is important to keep in mind the possible disruption of other pathways. For example, one could target other components of the Notch pathway such as ADAM10/17 proteases or Notch glycosylation enzymes but these are also key components of other signalling pathways.

In the nuclear setting, inhibition of the tripartite complex formation (CSL- N^{IC}-MAML) has also been attempted. Moellering et al. (Moellering et al., 2009) engineered a membrane permeable MAML-1 peptide by chemical modification and cross-linking of two residues. This stapled peptide interferes with endogenous MAML-1 to inhibit assembly of the active transcriptional complex resulting in global repression of Notch1 signalling. Blocking formation of the CSL-N^{IC}-MAML1 complex inhibits proliferation of T-cell acute lymphoblastic leukemia cells *in vitro* and *in vivo*. The 'stapled peptide' technology is now being developed by AILERON therapeutics.

1.1.11 Mastermind-like: transcriptional co-activator in other signal transduction pathways

There is emerging evidence for Notch-independent functions of MAML proteins. The most relevant to this study is the interaction between MAML-1 and p53 (Zhao et al., 2007). p53 is a tumour suppressor that induces cell-cycle arrest and apoptosis in response to cellular stresses such as DNA damage, hypoxia and oncogene activation (Lakin and Jackson, 1999). Mutations in p53 are observed in approximately half of cancer patients. A recent study by Zhao et al., illustrates how MAML-1 co-activates p53-dependent gene expression. Immunoprecipitation studies showed that MAML-1 interacts with p53. In addition, MAML-1 was identified in activator complexes bound to the native promoter of the p53 target genes p21, Bax and GADD45. The p21 protein, able to block cell cycle progression at G1, is an intermediate by which p53 inhibits cellular proliferation. MAML-1 overexpression enhanced p53-dependent gene induction. In contrast, MAML-1 knockdown resulted in a decrease in p53-dependent gene expression. MAML-1 overexpression leads to an accumulation of p53 protein. This is not due to an increase in mRNA levels but to the ability of MAML-1 to stabilise the p53 protein thus increasing its half-life. More specifically, MAML-1 increases the levels of p53 phosphorylation and acetylation upon DNA damage.

Several studies have focused on increasing tumour suppression as a strategy for cancer therapy. Delivery of p53 in tumours has been achieved with both retroviral and adenoviral vectors, resulting in a significant reduction of growth (reviewed in (Roth et al., 1999)). Delivery of p21 by adenovirus resulted in significant inhibition of tumour growth by cell cycle arrest at G0/G1 (Katayose et al., 1995; Prabhu et al., 1996). However, viral delivery is limited in its applications and safety concerns have been raised (Somia and Verma, 2000).

1.2 Antibodies as "magic bullets"

1.2.1 Antibody structure

Antibodies are essential components of the mammalian immune system, produced by B lymphocytes, which allow the initiation of an adaptive response upon specific recognition of a foreign substance such as pathogenic organisms and toxins (Reichert, 2001). Antibodies are classified into five groups: IgG, IgD, IgE, IgA and IgM. The first type, IgG, is the most relevant to this study for its use as a therapeutic agent (Weiner et al., 2010). The IgG family is divided into four subgroups (IgG1 to IgG4) with IgG1 being the preferred format for therapeutic use (Isaacs, 2009).

Immunoglobulin G (IgG) is a 150 kDa glycoprotein composed of four chains connected through disulphide bonds (Porter, 1973) (Figure 1.5). In particular, IgG is composed of two identical light chains (25 kDa each) and two heavy chains (50 kDa each). Treatment with the papain enzyme cleaves above the hinge region to separate the 50kDa Fab (fragment antigen-binding) fragment and the 50kDa Fc (fragment crystallisable) domain. The light chain is composed of the variable light (V_L) domain at the N-terminal end and the constant light (C_L) domain at the C-terminal end. The heavy chain is composed of two constant (C_H) domains in the Fc portion and a constant and a N-terminal variable (V_H) domain in the Fab portion. The variable domains V_H and V_L are responsible for recognition and binding of a specific antigen through the complimentary determining regions (CDRs). The binding of IgG is bivalent as it targets the same epitope using each Fab arm. The Fc domain translates binding into a biological response by activating complement, inducing phagocytosis or triggering antibody-dependent cellular cytotoxicity.

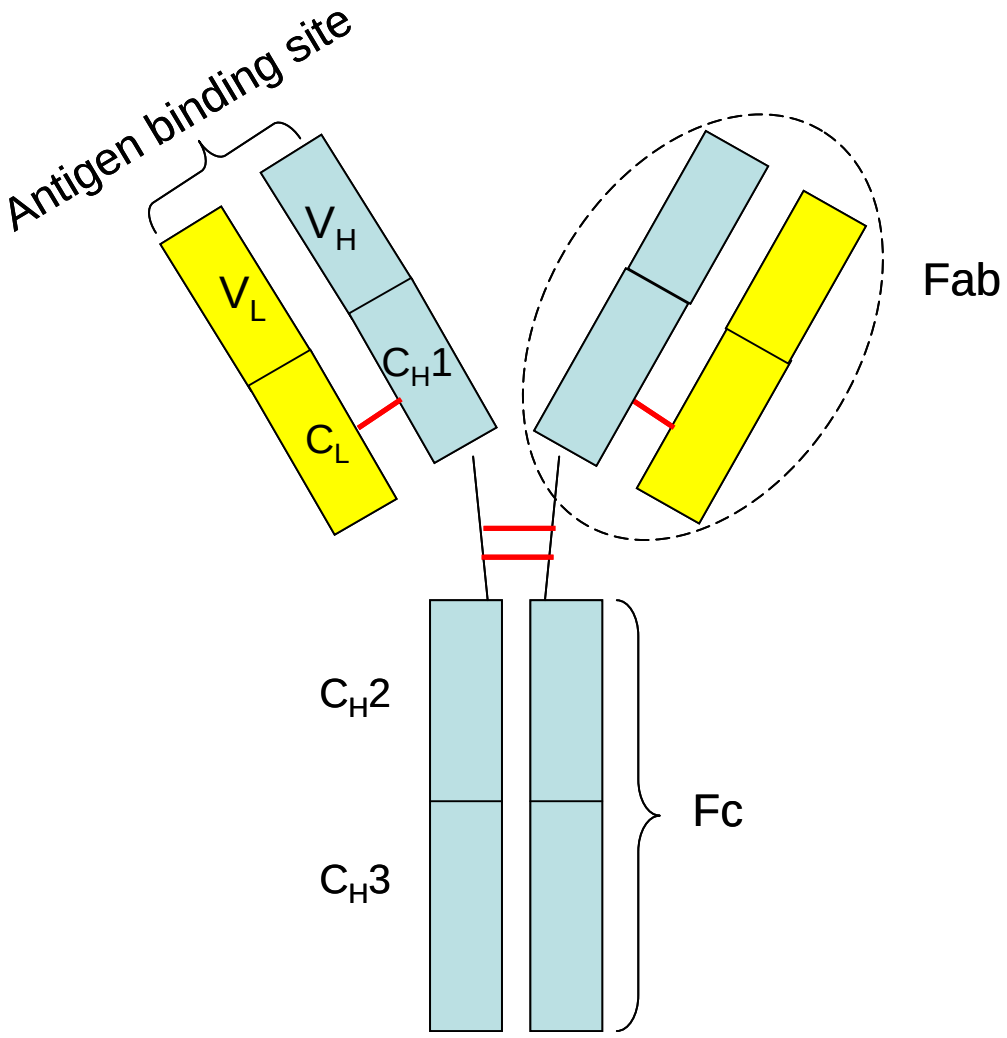

Figure 1.5: The IgG molecule at a glance: The IgG antibody is composed of two heavy chains (blue) and two light chains (yellow), connected through disulphide bonds (red). Each chain is divided into variable and constant domains. The Fab fragment is involved in binding whereas the Fc elicits effector functions.

1.2.2 Monoclonal antibodies

The first monoclonal antibodies were produced from mouse hybridomas generated by the fusion of B-lymphocytes with myeloma cells (Kohler and Milstein, 1975). The use of mouse monoclonal antibodies in the clinic revealed patients' immunogenic responses with release of human anti-mouse antibodies (HAMA) (Schroeder et al., 1990). These side effects triggered the development of chimeric (human constant domains) (Morrison et al., 1984), humanised (mouse CDRs only) (Jones et al., 1986) and then fully human mAbs (Figure 1.6). The first humanised mAb approved in 1997 for use in the clinic is Daclizumab (Zenapax®) which is directed at CD25 to ameliorate acute organ rejection (Ekberg et al., 1999). The generation of fully human mAbs was possible thanks to transgenic mice and phage display technologies. Adalimumab (Humira®) targeting TNF-α for the treatment of rheumatoid arthritis was originally derived from phage display and approved in 2002 (Scheinfeld, 2003). Panitumumab (Vectibix®) targeting EGFR for treatment of colon cancer was developed using transgenic mice and approved in 2006 (Chu, 2006).

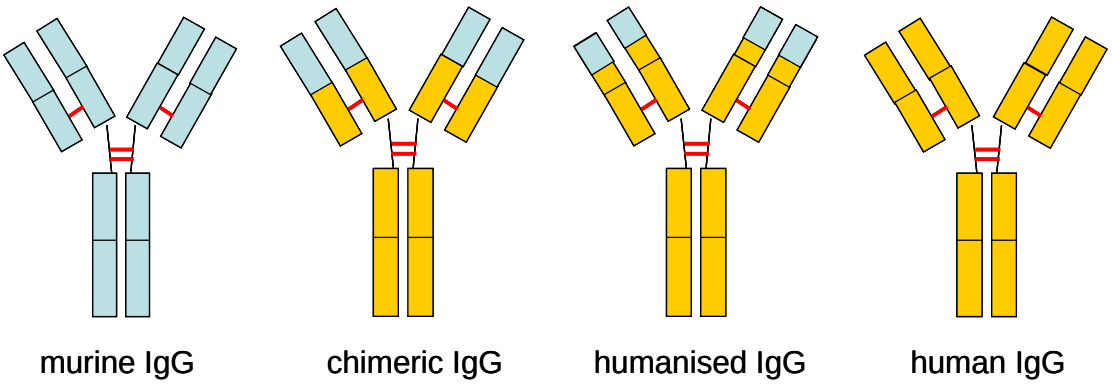

Figure 1.6: The evolution of monoclonal antibodies: from murine (blue) to fully human (orange).

1.2.3 Antibody formats

A variety of recombinant antibody fragments have now been generated as alternatives to the whole IgG format (Figure 1.7). Examples of these include the monovalent single chain variable fragment (scFv), the monovalent Fab fragment and other variants such as diabodies, triabodies and minibodies. These fragments are generated by combining critical V-domains of the parental IgG antibody, chosen on the basis of their final use. For example, the scFv consists in the combination of the variable regions of the IgG heavy and light chains linked together with a short linker. Thus, the scFv is still able to specifically recognise the antigen but it can not recruit cytotoxic effector functions due to the lack of the Fc region. If the linker between the two scFv domains is short (3 residues), this construct associates with another scFv molecule to form a diabody. The combination of two different scFvs allows the formation of bi-specific diabodies. If the linker is less than three residues long, scFvs associate into triabodies. Another variant of scFvs are minibodies in which the heavy- and light-chain variable regions are part of the same polypeptide chain including the heavy-chain hinge region and one heavy-chain constant domain. scFvs can also be linked to a multitude of molecules such as radionuclides for radioimmunotherapy (Davies, 2007), photosensitisers for photodynamic therapy (Bhatti et al., 2008), toxins (Chaudhary et al., 1989), and cytokines (Trachsel et al., 2007). The advantages of a smaller antibody construct are varied and include the lower cost of production and advantageous bio-distribution and blood pharmacokinetic properties. Lower costs of production are achieved as scFvs and fusions can be expressed in *E.coli* and yeast systems.

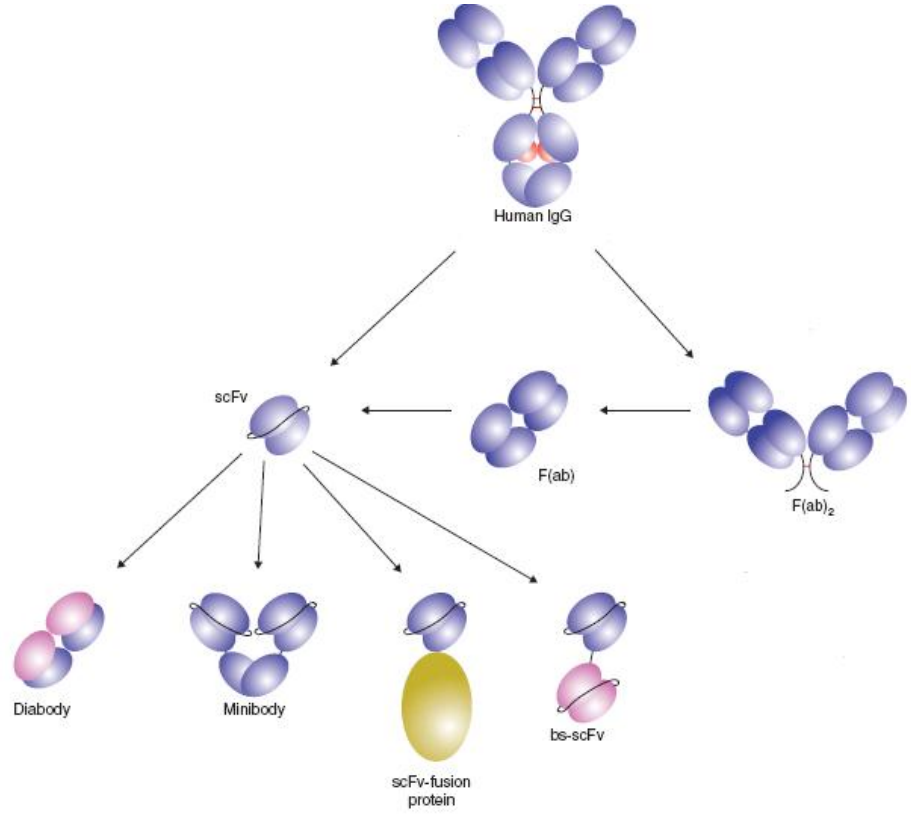

Figure 1.7: Dissection of the naturally occurring antibody into a large variety of recombinant antibody fragments. bs: bi-specific; dAb: single domain antibody; ds: disulphide; scFv: single-chain antibody fragment. Adapted from Deonarain (2008).

1.2.4 Immunotherapy

The high antigen binding affinity, specificity and modular structure that characterise antibodies, make them an excellent tool for immunotherapy. The term immunotherapy includes classical treatments such as vaccination and passive immunisation using serum, but also the use of monoclonal antibodies of which 34 were approved for therapeutic use as of March 2012 (Reichert, 2012). Out of these, 10 are for cancer therapy including rituximab (Rituxan®) (Coiffier, 2007), trastuzumab (Herceptin®) (Vogel et al., 2002) and bevacizumab (Avastin®) (Panares and Garcia, 2007) which have all reached sales of over 1 billion US dollars. Rituximab is a chimeric whole monoclonal IgG molecule and was the first of its kind to be approved for treatment of non-Hodgkins lymphoma targeting CD20 in 1997 (McLaughlin et al., 1998). CD20 is a receptor found on the cell surface in 99% of B-cell lymphomas and leukemias. Its biology is not well understood but binding of Rituximab to CD20 results in accelerated calcium ion flux rate and inhibition of anti-apoptotic survival pathways (Ben-Kasus et al., 2007). Trastuzumab is a humanised mAb targeting human epidermal growth factor receptor 2 (HER2). Early evidence suggested that HER2 is over-expressed in a variety of adenocarcinomas including breast, ovary, prostate, lung and gastrointestinal cancers (Slamon, 1987). HER2 over-expression leads to accelerated homodimer formation, deregulating signalling pathways involved in tumour cell survival, growth, metastasis and transformation (Wang and Greene, 2008). Bevacizumab was designed as a treatment of metastatic colorectal cancer with VEGF as its target. The mechanism of action of this humanised mAb is to block the interaction of the tumour associated cytokine VEGF with its receptor VEGFR, ultimately inhibiting angiogenesis (Dvorak, 2002). The main disadvantages of IgG mAbs are the slow perfusion into tumours reflected by low tumour to normal tissue ratios (Jain, 1990) in addition to Fc-domain mediated cross reactivity with associated side effects. In contrast, fragments such as scFvs have shown better increased tumour penetration but faster clearance due to their reduced size and the lack of a Fc region (Schier et al., 1996).

So far, all antibodies, in development or approved, bind to extracellular targets primarily to modulate/inhibit cell signalling (Chames et al., 2009). Engineering a cell-permeable antibody format would enable the exploitation of a multitude of intracellular signalling pathways to affect cancer cells (section 1.4.4).

1.3 Phage display

Phage display is a technique for high-throughput screening of molecular interactions using bacteriophage to connect genotype to phenotype. Practically, one of the binding partners is fused to a surface protein of a viral particle. The corresponding gene is found within the same virus. The high-throughput aspect of this technique consists of generating combinatorial libraries of such fusions and exposing them to a selected target molecule for the isolation of specific binders. The binders are amplified by a growth/infective stage to then isolate the gene corresponding to the positive binders.

A variety of molecules can be displayed on phage but antibody derivates are most common and relevant to this study. McCafferty et al. (McCafferty et al., 1990) first described the display of antibodies on phage and subsequent selection. Clackson et al. followed by constructing a combinatorial phage display library (Clackson et al., 1991). Other than scFv clones, other antibody derivatives have since been displayed on phage including Fab fragments (de Haard et al., 1999), disulphide stabilised scFvs (Bera et al., 1998), diabodies (McGuinness et al., 1996), tandem-scFvs (Wright and Deonarain, 2007) and single domain antibodies (Holt et al., 2008).

The most common viruses used in phage display are the non-lytic filamentous bacteriophage f1, M13 and fd (Marvin, 1998; Paschke, 2006). Their 6.5 kbp ssDNA genome includes nine genes encoding 11 proteins named pI to pXI. Proteins pIII and pVI are found at one end of the virus whereas pVII and pIX are found at the opposite end. pVIII is the major coat protein, present all around the surface (Figure 1.8). The other proteins are involved in the replication and control apparatus. The pIII coat protein specifically binds to the *E.coli* F-pilus, inducing its retraction and translocation of the phage genetic material in the bacterium. Once inside the host, genome replication is initiated followed by gene expression and assembly of the phage components at the inner membrane and periplasmic space of *E.coli*. Finally, the phage exits through the outer membrane. pIII is the most common fusion partner for phage antibody libraries although pVI (Hufton et al., 1999), pVII (Gao et al., 1999), pVIII (Felici et al., 1991) and pIX (Gao et al., 1999) have also been utilised.

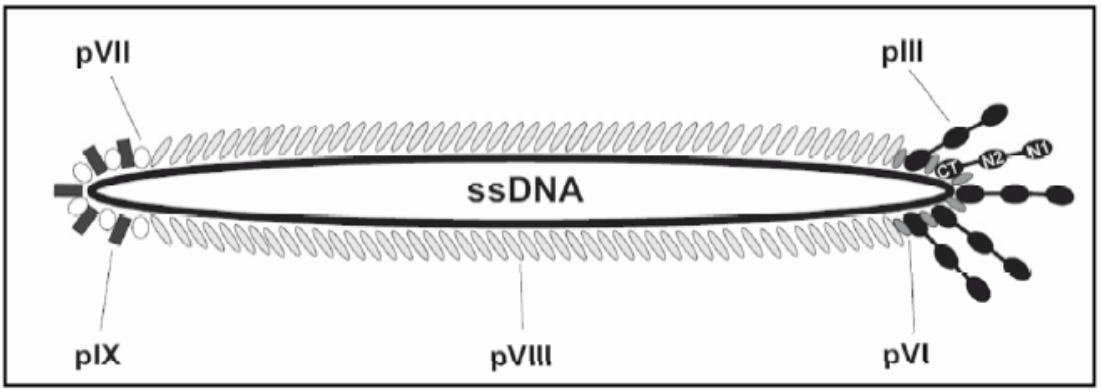

Figure 1.8: Spatial distribution of coat proteins on filamentous phage. The commonly used pIII is composed of three domains (CT: C-terminal; N1 and N2: N-terminal). Taken from (Paschke, 2006).

Both phage vectors and phagemid vectors are used in phage diplay (O'Connell et al., 2002). In the phage vector system, the protein of interest is cloned next to a phage coat protein on the phage genome itself. Therefore, every copy of the phage coat protein displays the protein of interest on all progeny phage particles. This results in polyvalent display. This system is best suited for low affinity interactions allowing rapid and successful enrichment with increased diversity amongst output clones. However, the polyvalency aspect of this technique means that clones with poor intrinsic affinity may be selected and enriched. Generally, lower phage titers (smaller library diversity) have been observed when using the phage vector system.

Phagemid libraries are the preferred system for antibody selection by phage display. In this set-up, the protein of interest is cloned next to a phage coat protein in a vector where no other phage component is present (Barbas et al., 1991). The vector contains an origin of replication for *E.coli* and a phage packaging signal. *E.coli* cells containing the phagemid vector are super-infected with helper phage which provides all the genetic material required for the production of functional phage particles. The characteristic of this system is that, due to competition between wild type coat proteins and fusion proteins, only 1-10% of progeny phage particles display the protein of interest. In addition, only 1 out of the 3-5 copies of pIII protein is fused with the protein of interest. This results in monovalent display, increasing the probability of isolating a high intrinsic affinity antibody fragment. On a practical level, the phagemid system allows for expression of the antibody portion alone thanks to the amber stop codon that precedes the coat protein gene. This allows read through

in amber suppressor strain *E.coli* XL1-blue but not in non-suppressing *E.coli* HB2151 (McCafferty et al., 1990).

Antibody display libraries

There is a large diversity of antibody libraries described in various reviews (Benhar, 2007; Marks and Bradbury, 2004; Hoogenboom, 2005; Mondon et al., 2008). Most of these libraries are for use in filamentous phage display selections using phagemid vectors. The preferred antibody format is the scFv, fused to coat protein pIII. One of the early phagemid vectors pHEN1 (Marks et al., 1991) is the base for subsequent constructs such as the pCANTAB6 vector used in this study (McCafferty et al., 1990). Antibody libraries are defined as either immunised or naive. In immunised libraries, the V gene diversity is derived from humans (Zebedee et al., 1992) or mice (Ames et al., 1995) immunised against the target antigen. Consequently, target specific enrichment and affinity maturation have already occurred *in vivo*. Higher affinity antibodies are usually isolated from immunised libraries versus naive libraries of the same size. The library employed here is of human origin and naïve. Therefore, we expect isolation of low to medium affinity antibodies.

1.4 Strategies for crossing the cell membrane

1.4.1 Cell-penetrating peptides

The hydrophobic nature of the cell membrane constitutes a major obstacle for drug delivery. In fact, many drugs, peptides, proteins and the majority of hydrophilic macromolecules are excluded by the membrane phospholipid bilayer. Only molecules that fit within a particular size range, charge and polarity can cross the membrane directly. Consequently, various strategies have been developed for successful transport of drugs inside the cell. In the past, techniques such as electroporation, microinjection and liposome encapsulation were attempted (Luo and Saltzman, 2000). The drawbacks of these approaches included inefficient drug delivery, cellular damage and toxicity. Another strategy is based on the use of vector molecules (antibodies, peptides and sugar moieties) for transport via receptor-mediated endocytosis. The main disadvantage of highjacking the endocytic pathway is the lack of escape routes from the endosomal compartment in addition to limited diffusion, degradation and lack of nuclear uptake.

Membrane translocating proteins present a promising tool for drug delivery across membrane barriers. The first naturally-occurring, shuttling protein to be described was the HIV-1 transactivating (Tat) protein which can translocate into cells and penetrate into the nucleus (Frankel and Pabo, 1988; Green and Loewenstein, 1988). Subsequent studies showed that when Tat protein was shortened to a few amino acids (^{47}YGRKKRRQRRR^{57}), now known as the Tat peptide, this retained its translocation activity (Vives et al., 1997). In this study, a 60 amino acid residue, polycationic protein called Antennapedia (Antp) is used (Figure 1.9). Antp, a portion of the *Drosophila* transcription homeoprotein, was initially shown to be internalised by neuronal cells (Joliot et al., 1991). Following internalisation, Antp is directed to the cell nucleus. Early data also demonstrated that Antp can promote the internalisation of a peptide cargo when expressed as a fusion (Perez et al., 1992; Schutze-Redelmeier et al., 1996). The characterisation of Antp led to the discovery of the first cell penetrating peptide (CPP) named penetratin (Derossi et al., 1994). This corresponds to a 16 amino acid portion of the third helix of the Antp homeodomain (see arrow in Figure 1.9A and red sequence in Figure 1.9B). Penetratin can deliver molecules, such as doxorubicin (anti-cancer agent targeting brain tumours) (Rousselle et al., 2001) and

p16 (tumour suppressor protein) peptides, into tumour cells. Internalisation of p16 results in decreased cancer growth and induction of apoptosis in cancer cells (Hosotani et al., 2002). Penetratin has also been used to deliver a p53 derived peptide which activates p53-mediated transcription ultimately blocking tumour growth (Tang et al., 2007).

A

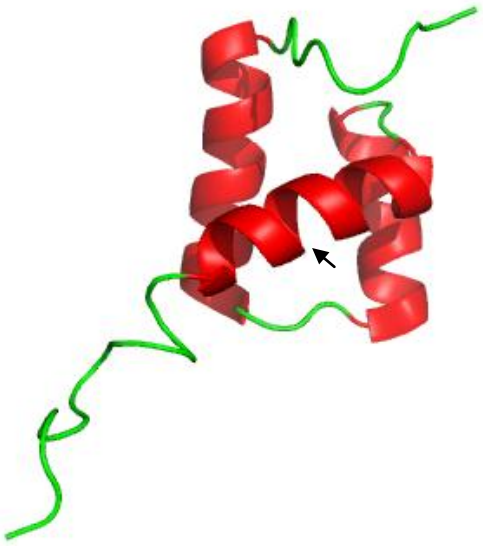

B

```
cgcaaacgcggaaggcagacatacacccggtaccagactctagagctagagaaagagttt
 R  K  R  G  R  Q  T  Y  T  R  Y  Q  T  L  E  L  E  K  E  F
cacttcaatcgctacttgacccgtcggcgaaggatcgagatcgcccacgccctgtgcctc
 H  F  N  R  Y  L  T  R  R  R  R  I  E  I  A  H  A  L  C  L
acggagcgccagataaagatttggttccagaatcggcgcatgaagtggaagaaggagaac
 T  E  R  Q  I  K  I  W  F  Q  N  R  R  M  K  W  K  K  E  N
```

Figure 1.9: A) Antennapedia helical structure. The third helix containing penetratin is highlighted by the arrow. B) Antennapedia DNA and protein sequence. The sequence corresponding to penetratin is highlighted in red.

1.4.2 Classification of CPPs

Over the past 20 years, more than 100 CPPs (5-40 amino acids long) have been reported for transport into mammalian, plant and bacterial cells (Lindgren and Langel, 2011; Hudecz et al., 2005; Stewart et al., 2008). Key CPPs are described in Table 1.3. CPPs can be classified according to their structure as either cationic or amphipathic. The first group is characterised by abundance of positively charged amino acids (mostly arginine and lysine) at physiological pH. These are thought to be involved in

electrostatic interactions with negatively charged glycoproteins on the extracellular side of the cell membrane. The guanidine head group of arginine is able to form hydrogen bonds with phosphates and sulfates, facilitating internalisation. Lysines, lacking the guanidine head group, are less effective at membrane penetration. The importance of the presence and distribution of arginine residues has been described (Lindgren and Langel, 2011). In addition, cationisation of macromolecules has been used as a strategy to improve cellular uptake (reviewed in (Blau et al., 2000). The Tat peptide, penetratin and polyarginines (Futaki et al., 2001) are part of this subclass of CPPs.

The second group, comprised of amphipathic CPPs, includes model amphipathic peptide (MAP) (Oehlke et al., 1998), transportan (Pooga et al., 1998) and Pep-1 (Henriques and Castanho, 2008). The chimeric peptide transportan is composed of the N-terminal fragment of the neuropeptide galanin fused to the wasp venom peptide mastoparan. Transportan was used for proof of concept of the application of CPPs *in vivo*. In particular, transportan was used to deliver peptide nucleic acids (PNAs). Delivery of small peptides and large proteins *in vivo* was demonstrated by the Dowdy group (Schwarze et al., 1999). Pep-1 and MPG were the first non-covalent CPP for delivery of proteins/peptides and nucleic acids, respectively (Morris et al., 1997; Morris et al., 2001).

Peptides	Origin	Sequences	Cargo type	References
Tat	HIV-Tat protein	PGRKKRRQRRPPQ	protein, peptide, siRNA, liposome, nanoparticle	(Snyder and Dowdy, 2005; Schwarze et al., 1999)
Penetratin	Homeodomain	RQIKIWFQNRRMKWKK	peptide, siRNA, liposome	(Joliot and Prochiantz, 2004)
Transportan	Galanin-mastoparan	GWTLNSAGYLLGKINLKALAALAKKIL	protein, peptide nucleic acids, siRNA	(Pooga et al., 1998)
MPG	HIV Gp41-SV40 nuclear localisation sequence	GALFLGFLGAAGSTMGAWSQPKKKRKV	siRNA, plasmid	(Morris et al., 2008)
Pep-1	Trp-rich motif-SV40 nuclear localisation sequence	KETWWETWWTEWSQPKKKRKV	protein, peptide	(Gros et al., 2006)
MAP	Chimeric	KALAKALAKALA	small molecule, plasmid	(Oehlke et al., 1998)
Oligoarginine	Chimeric	Arg8 or Arg9	protein, peptide, siRNA	(Futaki et al., 2001)

Table 1.3: Examples of CPPs

1.4.3 Mechanisms of CPPs internalisation

Despite major research efforts, the mechanisms that govern CPPs internalisation are still not clear. The controversy in the field is partly due to research groups using different models and techniques in their studies. Research into CPPs also suffers from experimental artefacts due to the attachment of fluorescent labels to CPPs to follow their uptake into cells.

It is generally believed that several factors influence the mechanism of uptake across the membrane including the properties of the CPP, such as length and charge distribution, as well as the characteristics of the cargo molecule such as size and charge. It has also become apparent that each CPP may employ a different entry route depending on the experimental context (choice of cell line, incubation conditions, cell stress environment). The mechanisms of cellular uptake can be classified into two groups: direct translocation across the cell membrane (energy-independent) and endocytosis (energy dependent) (Figure 1.10).

A recent study by Duchardt et al. examined the cellular uptake of three CPPs: the antennapedia/penetratin peptide, Tat and nona-arginine (R9) (Duchardt et al., 2007). The aim of this study was to clarify the role of the endocytic pathway in the CPP uptake process. Their main conclusion was that the processes of macropinocytosis, clathrin-mediated endocytosis and caveloae/lipid raft mediated endocytosis all played a role in CPP cellular uptake, in contrast with the idea of a single pathway being involved. In general, the main difference between the three endocytic pathways is the size of the vesicles together with their regulation and intracellular trafficking route. This suggests that cargo size might impact the choice of internalisation mechanism. For example, macropinosomes (1-5 μm) are best suited for transport of large CPP conjugates rather than other vesicle types (<150 nm). The scale of importance of each pathway in the uptake of a particular CPP was dictated by the CPP's sequence as well as its concentration. Tat and R9 are the peptides with most delocalised charge and share similarities on the pattern of both endocytic and direct uptake. At low CPP concentration, internalisation was not affected by inhibitors of clathrin-mediated endocytosis suggesting a main role for macropinocytosis and caveloae/lipid raft mediated endocytosis in this process. In contrast, at high Tat and R9 concentrations, peptide internalisation occurred independently of endocytic pathways, via direct uptake through specific nucleation zones. This effect was not observed for penetratin. Direct uptake of penetratin only occurred when macropynocytosis and caveloae/lipid

raft-mediated endocytosis were inhibited. Surprisingly, inhibition of clathrin-mediated endocytosis suppressed this effect. Another difference between penetratin and Tat/R9 is that cellular uptake of the first CPP increases linearly with peptide concentration whereas cellular fluorescence is not proportional to the concentration of Tat/R9 in the media.

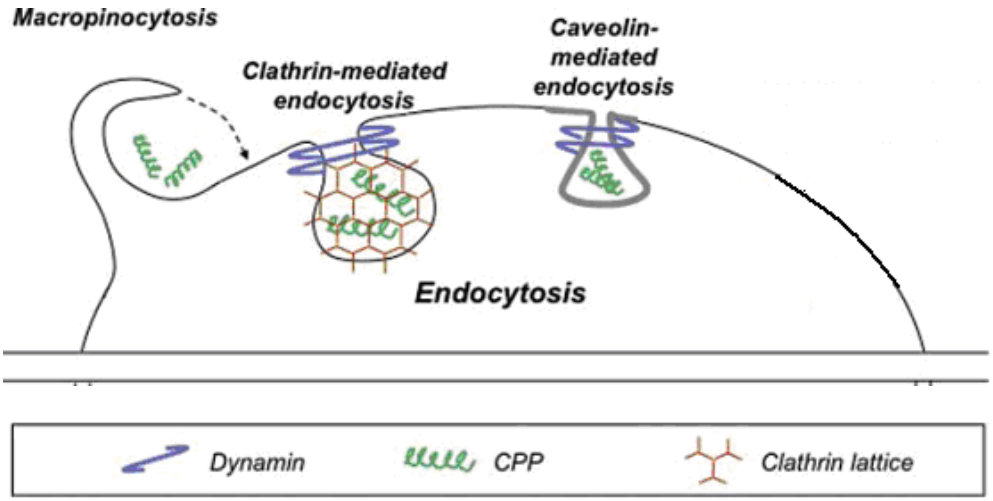

Figure 1.10: Crossing the plasma membrane. The mechanisms of CPP entry into the cell are classified into endocytosis (macropynocytosis, clathrin-mediated, caveolin-mediated) and direct translocation (carpet and barrel-stave models). Adapted from (Stewart et al., 2008).

1.4.4 Targeting antibodies to the cytoplasm

CPPs are a successful tool for the transport of a variety of cargoes including: nucleic acids (plasmid DNA, siRNA, oligonucleotides), proteins and peptides, contrast agents (MRI), drugs and nanoparticulate pharmaceutical carriers (liposomes, micelles). Some examples of these are included in Table 1.4.

Table 1.4: Examples of delivery of cargo by cell-penetrating peptides

Category	Cargo	CPP	Reference
Nucleic acids	siRNA	penetratin	(Davidson et al., 2004)
	siRNA	Tat	(Chiu et al., 2004)
	plasmid	Tat	(Ignatovich et al., 2003)
Protein	GFP	Tat	(Silhol et al., 2002)
	p21	Antp	(Kousparou et al., 2012)
Peptide	5-amino-acid peptide	Tat	(Hallbrink et al., 2001)
Contrast agent	Magnetic nanoparticles	Tat	(Lewin et al., 2000)
Quantum dots	CdS:Mn/ZnS	Tat	(Lagerholm, 2007)
	Liposomes	Tat	(Kale and Torchilin, 2007)
	Micelles	Tat	(Sawant et al., 2006)

This study focuses on the transport of proteins including antibody fragments (scFvs). Historically, the *in vivo* potency of CPPs was illustrated by the fusion of Tat to β-galactosidase (Schwarze et al., 1999). Following intra-peritoneal injection in mice, successful delivery was observed in most tissues including the brain. Other CPPs have since been employed for delivery of proteins including penetratin and synthetic polyarginines. CPPs can be covalently linked to the cargo or expressed as a CPP fusion protein. It is interesting to note that derivatives of antibodies have themselves been used as carriers. In particular, the Fc portion of an antibody has previously been used to deliver p53, preventing liver metastasis *in vivo* (Hansen et al., 2007).

The successful delivery of antibodies and antibody fragments into the cytoplasm would allow to fully exploit their potential, reaching a multitude of novel targets. Several strategies to achieve this are being investigated including intrabodies and transmabs/transbodies.

1.4.4.1 Intrabodies

Intrabodies describe antibodies that are expressed in the cytosol. Antibodies are extracellular proteins capable of surviving harsh conditions thanks to their rigid antiparallel β sheet core stabilised by disulphide bonds (Stocks, 2005). Antibody folding and disulphide bond occurs in the endoplasmic reticulum with the help of resident chaperones such as BiP and protein disulfide isomerase (PDI) (Kirkpatrick et al., 1995; Mayer et al., 2000). Intracellularly expressed antibodies were most successful when targeting antigens that follow the same secretory pathway (IL2 receptor, ErbB-2 receptor, β-amyloid precursor protein and VCAM1) (Boldicke, 2007; Beerli et al., 1994; Richardson et al., 1995; Kontermann, 2004; Paganetti et al., 2005; Strebe et al., 2009). Retention of the complex in the ER is achieved by the presence of an ER retention sequence (e.g. KDEL peptide) at the C-terminal of the intrabody.

The main challenge remains the direct expression of antibody fragments in the cytoplasm due to the reducing environment unfavourable for disulphide bond formation and lack of chaperones for folding (Biocca et al., 1994). Only in 1% of cases has the stability of an scFv being sufficient for its use as an intrabody (Auf der Maur et al., 2004; Visintin et al., 2004). Several strategies for improving cytosolic expression have been examined. These include the screening of antibodies for pre-determined properties (e.g. no requirement for intra-domain disulphide bonds) that make cytosolic functioning favourable. This is illustrated by the crystallisation and functional characterisation of cysteine-deleted mutants of an anti-RAS intrabody (Tanaka and Rabbitts, 2008). Other strategies include fusing antibodies to a Cκ domain (Cohen et al., 1998; Mhashilkar et al., 1995) or N utilisation substance A (NusA) (Zheng et al., 2003) to enhance cytosolic expression.

1.4.4.2 Transmabs/transbodies

Various antibody formats have been fused to CPPs for intracellular delivery including scFvs, Fabs and whole IgGs. Most commonly, Tat and Antennapedia derivatives are used for transport (Anderson et al., 1993; Zhao et al., 2001; Niesner et al., 2002). Despite some encouraging attempts, this strategy of delivery is still challenging due to production problems. For example, when secretion of Tat-fusion proteins was attempted, the majority of fusion protein was in the cell lysate rather than in the supernatant fraction (Koutsokeras and Kabouridis, 2009). It was also shown that

secretion levels decreased with greater cationic charge, a characteristic of most CPPs including Antp (Shaw et al., 2008). Most of the fusions are expressed as inclusion bodies and refolded (Theisen et al., 2006). Classic chemical conjugation methods are also used to link the antibody format to CPPs despite numerous disadvantages including no control over stoichiometry or the site of linkage. In order to address these limitations, research is now focused on site specific coupling and native chemical ligation strategies.

1.4.4.3 Penetratin-scFv fusions

The genetic fusion of scFvs to Antp derivatives for their successful delivery across membrane barriers is most relevant to this study. At least two previous publications describe the use of this strategy. Avignolo et al. successfully delivered a scFv that recognises the transactivation domain of c-Myc (Avignolo et al., 2008). Successful internalisation of a fluoresceinated fusion was confirmed by confocal microscopy. The fusion was detected in both the cytoplasm and the cell nucleus. The study confirmed that cell membrane integrity was not affected during the experiment. A mutated (constitutively active) version of c-Myc is observed in a variety of cancers, making this protein a target for cancer therapy. Mutations of c-Myc result in deregulated expression of genes involved in cell proliferation, a situation favourable to the cancer cell. By successful delivery of an anti-c-Myc scFv, Avignolo et al. observed growth inhibition of HCT116 cells (human colon cancer line).

The second study aimed to deliver a scFv specific to the matrix protein (M1) of the influenza A virus using penetratin (Poungpair et al., 2010). Internalisation of the genetic fusion was verified by immunofluorescent confocal microscopy and only negligible cytotoxic effects were observed on MDCK cells. On a functional level, the scFv-penetratin fusion reduced the number of viruses released from the cells.

1.5 Aims and Objectives

The aim of this project is to study two novel strategies for inhibition of Notch signalling that target MAML using Antp as a delivery method. The first tool is a fusion protein composed of Antp fused to a dominant negative version of MAML-1 (DN-MAML1). The second strategy of Notch signalling inhibition is the intranuclear delivery of scFv antibody fragments fused to Antp.

The research objectives included:

- Production of Antp (negative control), evaluating the use of a secretion system.
- Production of Antp-DN-MAML1 followed by i*n vitro* characterisation to determine its effect on Notch signalling and proliferation of MDA-MB-231.
- *In vivo* characterisation of Antp-DN-MAML1 using a MDA-MB-231 xenograft model in mice.

- Production of DN-MAML1 as the antigen for phage display selection.
- Undergo three rounds of phage display selection followed by screening of anti-DN-MAML1 scFv-phagemid by ELISA.
- Production of candidate scFvs in order to perform binding studies by ELISA.
- Production of Antp-scFv fusions, evaluating the use of a secretion system.
- Determine the capability of Antp-scFv fusions to interact with DN-MAML1.

Chapter 2

Materials and Methods

2.1 Materials

2.1.1 Solutions and buffers

As necessary, solutions were degassed using nitrogen gas exchange and filtered with a 0.2µm vacuum filtration apparatus. The optimal pH for buffers was obtained with gradual addition of HCl (VWR) or NaOH (VWR). When required, sodium azide (Sigma) was added to a final concentration of 0.05%. Sterilisation was achieved by autoclaving. Deionised water (dH_2O) was obtained from a Purite Select system. VWR Nuclease Free and DEPC-treated water was used for molecular biology applications.

Table 2.1: Composition of solutions and buffers

Solutions and Buffers	**Composition**
10x Phosphate buffered saline (PBS)	80g NaCl, 2g KCl, 2.4g KH_2PO_4, 14.4g Na_2HPO_4 in 1L dH_2O
Tris-acetate EDTA buffer (TAE)	242g TRIS base, 37.2g $Na_2EDTA.2H_2O$, 57.1 ml glacial acetic acid in 1L dH_2O
PAGE Running Buffer	3.03g TRIS base, 14.4g Glycine, 1g Sodium dodecyl sulphate (SDS) in 1L dH_2O
6x Sample loading buffer (DTT based)	360 mM Tris-HCl pH 6.8, 36% Glycerol, 600 mM DTT, 12% SDS, Bromophenol blue
Stacking gel	1.5 ml dH_2O, 0.25 ml 1.5 M Tris-HCl pH 6.8, 300 µl 30% Bis/Acrylamide, 20 µl 10% SDS, 20 µl ammonium persulfate (APS), 2 µl *N,N,N',N'*-Tetramethylethylenediamine (TEMED)
12% Resolving gel	1.7 ml dH_2O, 1.25 ml 1.5 M Tris-HCl pH 8.8, 2 ml 30% Bis/Acrylamide, 50 µl 10% SDS, 50 µl ammonium persulfate (APS), 2 µl *N,N,N',N'*-Tetramethylethylenediamine (TEMED)
Semi-dry PAGE transfer buffer	5.8g TRIS, 3g glycine, 0.4g SDS, 200 ml methanol in 1L dH_2O

2.1.2 Bacterial strains and growth conditions

The bacterial strains used in this project are listed in Table 2.2. The appropriate antibiotic concentration was added to the culture media from stock solutions (Carbenicillin: 100µg/µl; Chloramphenicol: 25 µg/µl; Tetracycline: 15 µg/µl; Kanamycin: 50 µg/µl).

Table 2.2: List of *E.coli* strains

Strain	Genotype	Source
XL1-Blue	F'::Tn10 *pro*A^+B^+ *lac*I^q D(*lac*Z) M15/*rec*A1 *end*A1 *gyr*A96 (Nal^r) *thi* *hsd*R17 ($r_K^-m_K^+$) *sup*E44 *rel*A1 *lac*	Stratagene
HB2151	*nalr thi-1 ara ((lac-proAB [F' proAB+ laciq lacZ(M15])*	GE Heathcare
TUNER (DE3)	F^- *ompT hsdS*$_B$($r_B^-m_B^-$) *gal dcm lacY1* (DE3)	Novagen
JM109 (DE3)	*end*A1, *rec*A1, *gyr*A96, *thi*, *hsd*R17 (r_k^-, m_k^+), *rel*A1, *sup*E44, Δ(*lac-pro*AB), [F´ *tra*D36, *pro*AB, *laq*I^qZΔM15].	Promega
BLR (DE3)	F^- *ompT hsd*S_B(r_B^- m_B^-) *gal dcm lacY1* (DE3) Δ (*srl-recA*)*306*::Tn*10* (Tet^R)	Novagen
BLR (DE3) pLysS	F^- *ompT hsd*S_B(r_B^- m_B^-) *gal dcm lacY1* (DE3) Δ (*srl-recA*)*306*::Tn*10* pLysS (Cam^R, Tet^R)	Novagen
B21 (DE3)	F^- *omp*T *hsd*S_B (r_B^- m_B^-) *gal dcm* (DE3)	Novagen
BL21 (DE3) pLysS	F^- *omp*T *hsd*S_B (r_B^- m_B^-) *gal dcm* (DE3) pLysS (Cam^R)	Novagen
BL21 (DE3) pLysE	F^- *omp*T *hsd*S_B (r_B^- m_B^-) *gal dcm* (DE3) pLysE (Cam^R)	Novagen

Table 2.3: Culture media composition

Culture media	**Composition in 1L dH_2O**
2TY	16g bacto tryptone, 10g bacto yeast, 5g NaCl
2TY agar	16g bacto tryptone, 10g bacto yeast, 5g NaCl, 15g bacto agar
LB	10g bacto tryptone, 5g bacto yeast, 5g NaCl
LB agar	10g bacto tryptone, 5g bacto yeast, 5g NaCl, 15g bacto agar
10x M9 Salt Solution	60g Na_2HPO_4, 30g KH_2PO_4, 10g NH_4Cl, 5g NaCl
M9 minimal agar	100 ml of 10x M9 salt solution, 1ml 1M MgSO4, 100µl 1M $CaCl_2$, 5mg Vitamin B1, 10 ml 20% glucose solution

2.1.3 Plasmids and molecular techniques

The list of plasmids used in this study can be found in Table 2.4. The gene encoding the Antp protein was amplified by PCR from the pds56 vector using primer pairs 1-2 and 3-4 (Table 2.5) which allow the addition of essential restriction sites. For the future addition of a single chain variable fragment (scFv) gene upstream of the Antp gene, this was cloned into pET20b in-between the *Nco* I/*Xho* I sites (Figure 2.1A). To obtain the reverse order (Antp-scFv), the Antp gene was cloned into the same vector using the *Pci* I/*Not* I sites on the insert and the compatible *Nco* I/*Not* I sites on the vector (Figure 2.1B). Primer pair 2-5 (Table 2.5) was used to amplify Antp allowing the addition of *Nde* I and *Xho* I sites for subsequent cloning into the pET23b vector. *Bam*HI was used to excise Antp from the pRSET A vector containing Antp-DN-MAML1, leaving DN-MAML1 only. Primer 9 and FDSEQ1 were used to eliminate the accidental stop codon in the E7P3 scFv clone (t to c point mutation). Primer pair and 6-7 and 6-8 were used to amplify the Antp-scFv fusion and Antp, respectively. This allows the addition of the *Pci*I and *Age*I sites for subsequent cloning into the pcDNA4a vector for mammalian expression. Ligation reactions included T4 ligase and buffer (Fermentas) with vector and insert at a 1:3 molecular ratio. All ligations reactions consisted of incubation at 22℃ and 16℃ for 30 minutes, respectively, followed by 15 minutes at 65℃. This was followed by transformation into XL1-Blue chemo-competent cells. All constructs were verified by DNA sequencing (MWG) (data not shown). The LMB3 and FDSEQ1 primers were used to sequence the phage display derived scFvs. The BGH and CMV primers allowed the sequencing of pcDNA4a constructs.

Table 2.4: List of plasmids

Plasmid	**Description**	**Source**
pds56	Amp^R, N-term His tag, Antp	Trojantec
pRSET A	T7 promoter, Amp^R, N-term His tag, Antp-DN-MAML1	Trojantec
pET20b	T7 promoter, Amp^R, C-term His tag, *pel*B	Novagen
pET23b	T7 promoter, Amp^R, C-term His tag	Novagen
pcDNA4a	CMV promoter, Amp^R, C-term His tag, N-term leader sequence (Δ *Pci* I)	Dr. Constantinou, ICL
pds56	Amp^R, N-term His tag, Antp-DN-MAML1	Trojantec
pCANTAB6	Lac promoter, Amp^R, C-term His and *myc* tag, ScFv-pIII	Cambridge Antibody Technology

Table 2.5: List of primers (5' to 3' orientation)

Number	**Sequence**
1	ATCCATGGTCATAGCGGCCGCACGCAAACGCGGA
2	ATCTCGAGGTTCTCCTTCTTCCACTTCATGCGCCG
3	TAATACATGTTACGCAAACGCGGAAGGCAGACATA
4	TAATGCGGCCGCTATGACCATGGGGTTCTCCTTCTTC
5	CTAATCCATATGCGCAAACGCGGAAGGCAG
6	TAATACATGTCTCGCAAACGCGGAAGGCAGACATACACCCGG
7	GGTCCACCGGTTGCGGCCGCACGTTTGATCTCCAGCTTGGTC
8	GGTCCACCGGTGTTCTCCTTCTTCCACTTCATGCGCCGATTCTGGA
9	CGGCCATGGCCCAGGTGCAGC
LMB3	CAGGAAACAGCTATGAC
FDSEQ1	GAATTTTCTGTATGAGG
BGH	AAG GCA CAG TCG AGG
CMV	CGC AAA TGG GCG GTA GGC GTG

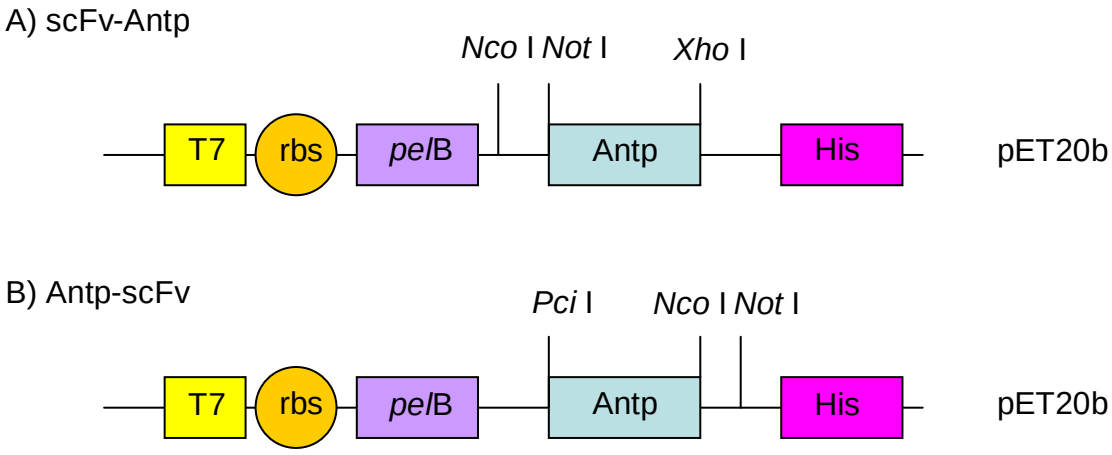

Figure 2.1: strategy for cloning Antp in pET20b allowing for the subsequent addition of an scFv gene upstream (A) or downstream (B).T7: promoter, rbs: ribosome binding site, pelB:leader sequence, His: tag.

Table 2.6: Antibodies

Antibody	**Species**	**Antigen**	**Working dilution**	**Source**
9E10 IgG	murine	c-Myc epitope (EQKLISEEDL)	1:5000	Sigma
αMouse HRPO IgG	goat	murine Fc domain	1:10000	Sigma
αHis HRPO IgG	murine	penta-histidine peptide tag	1:4000	Sigma
αM13 HRPO IgG	murine	phage major coat protein PVIII	1:5000	GE Healthcare

Table 2.7: Speciality reagents

Reagent	**Use**	**Source**
extravidin peroxidase HRPO	HRPO conjugated avidin, use 1:1000	Sigma
Milk powder	blocking nitrocellulose and ELISA plates	Marvel®
BM-Blue POD	chromogenic substrate for Peroxidase	Roche
ECL kit	enhanced chemiluminescence detection kit	GE Healthcare
EZ-link® Sulfo-NHS-LC-LC-Biotin	biotinylation reagent	Pierce
BSA	ELISA blocking	Sigma

Table 2.8: Cell lines

Cell line	Description	Origin
MDA-MB-231	human breast adenocarcinoma	Prof. Djamgoz
CHO Δ	chinese hamster ovary cells transfected with the delta-like ligand 1	Celldex therapeutics
CHO N2	chinese hamster ovary cells transfected with the Notch receptor 2	Celldex therapeutics
CHO K	chinese hamster ovary	Celldex therapeutics

Small molecule inhibitors:

- DAPT: N-[N-(3,5-difluorophenacetyl)-L-alanyl]-S-phenylglycine t-butyl ester, inhibits γ-secretase activity (Calbiochem)
- GSI-1: Z-Leu-Leu-Nle-CHO, inhibits γ-secretase activity (Calbiochem)
- LiCl: Lithium chloride, inhibits GSK3β activity (Sigma)

Kits:

- Fugene® HD transfection reagent (Promega)
- ONE-Glo® Luciferase assay system (Promega)
- CellTiter 96® AQueous Non-Radioactive Cell Proliferation Assay (MTS) (Promega)
- MagMAX™ 96 total RNA isolation kit (Invitrogen)
- High capacity cDNA Reverse Transcription kit (Applied Biosystems)
- Taqman® Fast Real-Time PCR Universal Mastermix (2x)

Taqman® gene expression assays:

Hes1 – Hs00172878_m1

Hes1 – Mm00468601_m1

18S rRNA – 4319413E

p21 – Hs00355782_m1

Table 2.9 : Tissue culture reagents

Tissue culture reagent	**Origin**
DMEM	PAA Laboratories
sterile PBS without Ca and Mg ions	PAA Laboratories
trypsin-EDTA	Invitrogen
geneticin	Invitrogen
hygromycin B	Invitrogen
zeocin	Invitrogen
FBS	Invitrogen
Jagged1-Fc	R&D systems
Human IgG1	Sigma
phycoerythrin (PE) Annexin V	BD Biosciences
10x Annexin V binding buffer	0.1 M Hepes (pH 7.4), 1.4 M NaCl, 25 mM $CaCl_2$ in dH_2O
DAPI	Sigma
sodium pyruvate	Sigma
DMSO	Sigma

2.2 Methods

2.2.1 Bacterial culture

2.2.1.1 Preparation of chemically competent *E.coli* cells

A single colony was picked from a freshly streaked plate for overnight growth in 5 ml of media at 37°C with shaking (250 rpm). The culture was subsequently diluted 100 fold and grown up to an OD_{600} of 0.6. At this point, the culture was placed on ice for 15 minutes before centrifugation at 1500 g for 5 minutes at 4°C. Pellets were resuspended in half the culture volume of ice-cold sterile 0.1M $CaCl_2$ and incubated for 30 minutes on ice. Following a centrifugation step, the pellet was resuspended in 0.1M $CaCl_2$ including 10% glycerol and aliquots were stored at -80°C.

2.2.1.2 Tranformation of chemically competent *E.coli* by heat shock method

Cells were placed on ice and incubated with plasmid DNA for 30 minutes. Heat shock was performed at 42°C for 45 seconds. One ml of growth media was added to the cells followed by incubation at 37°C with shaking (250 rpm) for one hour. A portion of the cell suspension was then plated and left growing overnight at 37°C.

2.2.2 Expression, purification, labelling and analysis of recombinant proteins

2.2.2.1 Expression of Antp as a secreted protein

Antp in pET20b (section 2.1.3) was transformed in *E.coli* TUNER (DE3), JM109 (DE3), BLR (DE3), BLR (DE3) pLysS, BL21 (DE3), BL21 (DE3) pLysS and BL21 (DE3) pLysE cells. A single colony of each transformation was grown in 5 ml of 2TY including the appropriate antibiotic(s), shaking overnight at 37°C. The bacterial culture was diluted 1:100 in 5 ml of 2TY supplemented with the suitable antibiotic(s) and grown shaking at 37°C up to an OD_{600} of 0.8. The culture was then induced using either 0.1 mM or 1 mM isopropyl-1-thyo-β-D-galactopyranoside (IPTG) for 4 hours. The culture was centrifuged at 2000 g for 5 minutes before analysis of the supernatant and pellet fractions by Western blot using HRPO conjugated murine α-His antibody.

2.2.2.2 Expression of Antp in the cytosolic fraction of *E.coli* BL21 (DE3) plysS and its purification

This method was adapted from Joliot et al. 1991. A single *E.coli* BL21 (DE3) plysS colony transformed with Antp in pET23b (section 2.1.3) was grown in 5 ml of LB including carbenicillin and chloramphenicol, shaking overnight at 37°C. The bacterial culture was diluted 1:100 in 500 ml of LB media containing carbenicillin and chloramphenicol and grown shaking at 37°C up to an OD_{600} of 1.2. The culture was then induced using 1 mM IPTG for 5 hours. The culture was centrifuged at 2000 g for 30 minutes. The cell pellet was freeze-thawed and resuspended in 20 ml of 50 mM sodium phosphate (pH 7.5), 2 mM EDTA, 1 mM DTE with the inclusion of a protease inhibitor tablet (Roche). Sonication was used to further lyse the cells before centrifuging at 25,000 g for 30 minutes at 4°C. The soluble fraction was applied to a pre-equilibrated SP sepharose fast flow (GE healthcare) ion exchange column (5 ml slurry). Antp was washed and eluted using increasing concentrations of NaCl (50mM-1M) (25 ml each). The sample was concentrated 5 fold using a 3,000 kDa MWCO spin concentrator (Vivaspin, Generon) before being applied to a size exclusion chromatography column (Superdex-75) and eluted in PBS. The absorbance of fractions was measured at 214 nm and 280 nm using the QuadTec™ detector in combination with the Bio-Rad BioLogic Duo-Flow™ system. The collected fractions are named according to the fraction collector used. The first rack collected fractions A1 to A90; the second rack collected fraction B1 to B64 which corresponds to the run end.

2.2.2.3 Expression of Antp-DN-MAML1 in the cytosolic fraction of BL21 (DE3) plysS

A single *E.coli* BL21 (DE3) plysS colony transformed with Antp-DN-MAML1 in pRSET A (or pET23) was grown in 5 ml of LB including carbenicillin and chloramphenicol, shaking overnight at 37°C. The bacterial culture was diluted 1:100 in 500 ml of LB media containing carbenicillin and chloramphenicol and grown shaking at 37°C up to an OD_{600} of approximately 0.8. The culture was then induced using 1 mM IPTG overnight. The culture was centrifuged at 2000 g for 30 minutes. The pellet was lysed using of ice cold B-PER® reagent (Pierce) with the addition of a protease inhibitor tablet (Roche) before spinning at 15000 g for 1 hour at 4°C. The resulting pellet was resuspended in 6 M guanidinium chloride in phosphate buffered

saline (PBS) and left incubating overnight before a final spin at 40000 g for 1 hour at 15°C. At this stage Antp-DN-MAML1 is present as a solubilised, denatured inclusion body.

2.2.2.4 Purification of Antp-DN-MAML1 using Immobilised Metal Affinity Chromatography (IMAC)

Chelating sepharose (Fast Flow, GE Healthcare) was charged with nickel ions by applying two bed volumes of 500 mM $NiCl_2$ to the column. The resin was washed with distilled water and equilibrated with PBS-8 M Urea. The soluble protein fraction was applied to the resin to allow Antp-DN-MAML1 binding. The column was washed extensively with PBS-8 M Urea. Increasing concentrations of imidazole were used to further wash and finally elute the protein. The elution samples were analysed by reducing 12% SDS-PAGE and stained using Coomassie Blue. A Western blot was also performed using HRPO conjugated murine α-His antibody. Antp-DN-MAML1 refolding was attempted by dialysis in PBS with different combinations of L-Arginine (mediator of refolding) and Urea concentrations. Finally, the samples were concentrated using a 5000 kDa cut-off ultrafiltration column.

2.2.2.5 Expression trial for Antp-DN-MAML1

Expression was based on a method provided by Prof. Cole (University of Birmingham, personal communication). Antp-DN-MAML1 in pRSET A was transformed into the *E.coli* BL21 (DE3) plysS strain, plated on 2TY plates with 80 μg/ml carbenicillin and grown overnight at 37°C. The following day, colonies were replated to purify them and grown at 37°C. Later the same day, single colonies were grown overnight in 20 ml of LB supplemented with carbenicillin at 30°C. All flasks and media were pre-warmed to 30°C before culturing to avoid a cold shock. The overnight starter culture was used to provide a 2% inocula for six flasks containing 50 ml of LB medium/carbenicillin and shaken at 30°C. When the OD (650 nm) reached 0.5, IPTG was added to the following μM concentrations: 0, 5, 10, 20, 50 and 100. Samples were collected after 1, 2, 3, 4 and 20 h for measuring the soluble and insoluble protein content by SDS-PAGE and Western blotting.

2.2.2.6 Expression of MAML-1 (13-74) in the cytosolic fraction of *E.coli* BL21 (DE3) plysS and its purification/refolding

This method was adapted from Nam et al., (2003). A single *E.coli* BL21 (DE3) plysS colony transformed with MAML-1 (13-74) in pRSET A was grown in 5 ml of LB including carbenicillin and chloramphenicol, shaking overnight at 37°C. The bacterial culture was diluted 1:100 in 500 ml of LB media supplemented with antibiotics and grown shaking at 37°C up to an OD_{600} of approximately 0.8. The culture was then induced using 1 mM IPTG, overnight. The culture was centrifuged at 2000 g for 30 minutes. The resulting pellet was resuspended in 15 ml of 50 mM Tris (pH 8), 150 mM NaCl, 6 M guanidinium-HCl, 5 mM β-mercaptoethanol, including a protease inhibitor tablet. Following sonication, the mixture was centrifuged at 18,000 g for 30 minutes. The resulting supernatant was applied for 1 hour at 4°C to pre-equilibrated chelating sepharose charged with nickel ions (5ml slurry). The column was washed with 10 column volumes of 50 mM Tris (pH 8), 150 mM NaCl, 6 M guanidinium-HCl, 5 mM β-mercaptoethanol, 10 mM imidazole. One column volume of 50 mM Tris (pH 8), 150 mM NaCl, 6 M guanidinium-HCl, 5 mM β-mercaptoethanol, 250 mM imidazole was added to elute the protein. This was dialysed against 5% acetic acid for 24 hours, lyophilised overnight and re-dissolved in dH_2O.

2.2.2.7 Expression of secreted scFv proteins in *E.coli* HB2151

A single HB2151 colony transformed with scFv genes in the phagemid vector pCANTAB6 was grown in 5 ml of 2TY including carbenicillin, shaking overnight at 37°C. The bacterial culture was diluted 1:100 in 500 ml of LB media supplemented with antibiotics and grown shaking at 37°C up to an OD_{600} of approximately 0.8. The culture was then induced using 1 mM IPTG, overnight at 30°C. The culture was centrifuged at 2000 g for 30 minutes. Protease inhibitors were used throughout the purification steps. The supernatant was concentrated to one tenth of its original volume using a Vivaflow 200 10kDa MWCO peristaltic pump driven dia-filtration cassette (Vivascience) and then exhaustively dialysed into PBS pH 7.4. The supernatant was then applied to pre-equilibrated chelating sepharose charged with nickel ions (5 ml slurry), overnight at 4°C. The scFvs were washed and eluted using increasing concentrations of imidazole (10mM-250mM) (25 ml each). Finally, the

sample was dialysed into PBS pH 7.4 and concentrated using a 5,000 kDa MWCO spin concentrator.

2.2.2.8 Antp-ScFv small scale expression trials

Antp-N4

A single *E.coli* BL21 (DE3) plysS colony transformed with Antp-N4 (anti TT-Hc scFv) in pET20b was grown in 5 ml of 2TY or LB including carbenicillin and chloramphenicol, shaking overnight at 37°C. The bacterial culture was diluted 1:100 in 5 ml of 2TY/LB media containing carbenicillin and chloramphenicol and grown shaking at 37°C up to an OD_{600} of 0.8. The culture was then induced using 0.1 mM or 1 mM IPTG for 4 hours at 37°C/30°C and centrifuged at 2000 g for 10 minutes. Pellets were resuspended in ice cold PBS containing 0.1% Igepal (Sigma) and sonicated on ice. Samples were spun at 2000 g for 15 minutes at 4°C before analysis of the soluble and insoluble fractions.

Antp-E7P3

A single *E.coli* BL21 (DE3) plysS colony transformed with Antp-E7P3 in pET20b was grown in 5 ml of 2TY including carbenicillin and chloramphenicol, shaking overnight at 37°C. The bacterial culture was diluted 1:100 in 5 ml of 2TY media containing carbenicillin and chloramphenicol and grown shaking at 37°C up to an OD_{600} of 0.8. The culture was then induced using 0.1 mM or 1 mM IPTG for 1, 2 or 4 hours at 25°C/18°C and centrifuged at 2000 g for 10 minutes.

Antp-E7P3 autoinduction

A single *E.coli* BL21 (DE3) plysS colony transformed with Antp-E7P3 in pET20b was grown in 10 ml of LB including carbenicillin and chloramphenicol, shaking overnight at 37°C. The bacterial culture was diluted 1:100 in 1L of autoinduction media containing carbenicillin and chloramphenicol and grown shaking at 37°C for 2 hours. The culture was transferred at 20°C shaking overnight. Finally, the culture was centrifuged at 2000 g for 30 minutes before analysis of the supernatant and cell pellet fractions.

2.2.2.9 Antp-ScFv large scale expression

A single *E.coli* BL21 (DE3) plysS colony transformed with Antp-Scfv (scFv: G7P4, H8P5) in pET20b was grown in 10 ml of 2TY including carbenicillin and chloramphenicol, shaking overnight at 37°C. The bacterial culture was diluted 1:100 in 1 L of 2TY media containing carbenicillin and chloramphenicol and grown shaking at 37°C up to an OD_{600} of 0.8. The culture was then induced using 1 mM IPTG for 5 hours at 25°C and centrifuged at 2000 g for 30 minutes. Pellets were resuspended in 25 ml of ice cold PBS containing 0.1% Igepal and sonicated on ice. The samples were spun at 2000 g for 15 minutes at 4°C before proceeding with the refolding protocol.

2.2.2.10 Antp-ScFv refolding

Inclusion bodies were resuspended in 25 ml of 50 mM Tris-HCl (pH 8), 20 mM EDTA before adding Triton X-100 to 2% and NaCl to 0.5 M final. This was centrifuged for 1 hour at 25,000 g before repeating the procedure twice. The final pellet was denatured in 10 ml of 100 mM Tris-HCl (pH 8), 2 mM EDTA, 6 M guanidinium-HCl before addition of DTE 0.3 M final. After rotating for 1 hour at room temperature, the mixture was centrifuged at 30,000 g for 30 minutes at room temperature. Five ml of the denatured inclusion bodies were added to a 500 ml solution of 100 mM Tris-HCl (pH 8), 0.4 M L-Arginine, 8 mM GSSG (oxidised glutathione), 2 mM EDTA chilled to exactly 10°C. The remaining 5 ml were then added in 0.5 ml aliquots. Refolding occurred overnight at 10°C. Any precipitate was removed by centrifugation and the soluble fraction was dialysed in PBS buffer and concentrated using a 5000 kDa spin concentrator.

2.2.2.11 Protein analysis by sodium dodecyl sulphate polyacrylamide gel electrophoresis (PAGE) and Western blotting

Each test sample was mixed with loading buffer and boiled for 5 minutes. Typically 10 µl of sample was loaded per well on duplicate gels (for Coomassie blue staining and Western blotting). A constant voltage of 200V was applied for 30 minutes. The gels included a pre-stained molecular weight marker as reference ladder (PageRuler™ (Plus), Fermentas). For Western blotting, protein gels were transblotted onto a nitrocellulose membrane using a Bio-Rad Trans-Blot® SD Semi-dry transblotter. All components, including a pair of thick Whatman® filter paper slices, were briefly pre-soaked in transfer buffer. Transfer occurred for 30 minutes under a constant voltage of

10V. The membrane was blocked for 1 hour at room temperature or overnight at 4°C with 3% milk powder in PBS pH 7.4. Antibody detection was performed in 1% milk powder for an hour per step. Washes consisted of 2x 10 minutes incubation with PBS pH 7.4 0.1% Tween-20 detergent followed by a 10 minutes PBS pH 7.4 wash. The ECL kit was used for detection and the chemiluminescent signal was imaged with the FujiFilm LAS-3000 laser scanning densitometer. The resulting image was later overlapped with the corresponding ladder picture. Protein concentration was determined by absorption at 280 nm using a NanoDrop® Micro-Volume UV-Vis spectrophotometer (Thermo Scientific).

2.2.2.12 Chemical biotinylation

Thermo Scientific EZ-Link® Sulfo-NHS-LC-LC-Biotin reagent (sulfosuccinimidyl-6-[biotinamido]-6-hexanamido hexanoate), is a *N*-Hydroxysuccinimide (NHS) ester of biotin which reacts efficiently with primary amino groups (i.e. lysine side chain). In order to minimise epitope masking, we chose the 30.5Å spacer arm length and a reagent to protein molar coupling ratio of 1:10 (minimal ratio). One ml of DN-MAML1 protein at a 0.15 mg/ml concentration was mixed with 2 µl of 1 mM biotin solution in dH_2O. The mixture was incubated at room temperature for 1 hour. Free biotin was removed using a PD10 desalting column and eluted in PBS pH 7.4.

2.2.2.13 Circular dichroism

Circular dichroism was performed using a Chirascan™ CD Spectrometer (Applied Photophysics) and a 1mm path quartz cuvette. The sample analysed was at a concentration of 0.1 mg/ml and the machine was set with the following conditions:

Temperature: 20°C

Wavelength: 190-260 nm

Step: 0.5 nm intervals

Band width: 1nm

Time per sec: 1 sec

Characteristic CD spectra for α helix, β sheet and random coil are shown in Figure 2.2

Data analysis was perfomed using the DichroWeb online software, with either the SELCON3 or K2D analysis programme (Whitmore and Wallace, 2008). Data was compared to values obtained using the CFSSP protein secondary structure prediction tool (ExPASy).

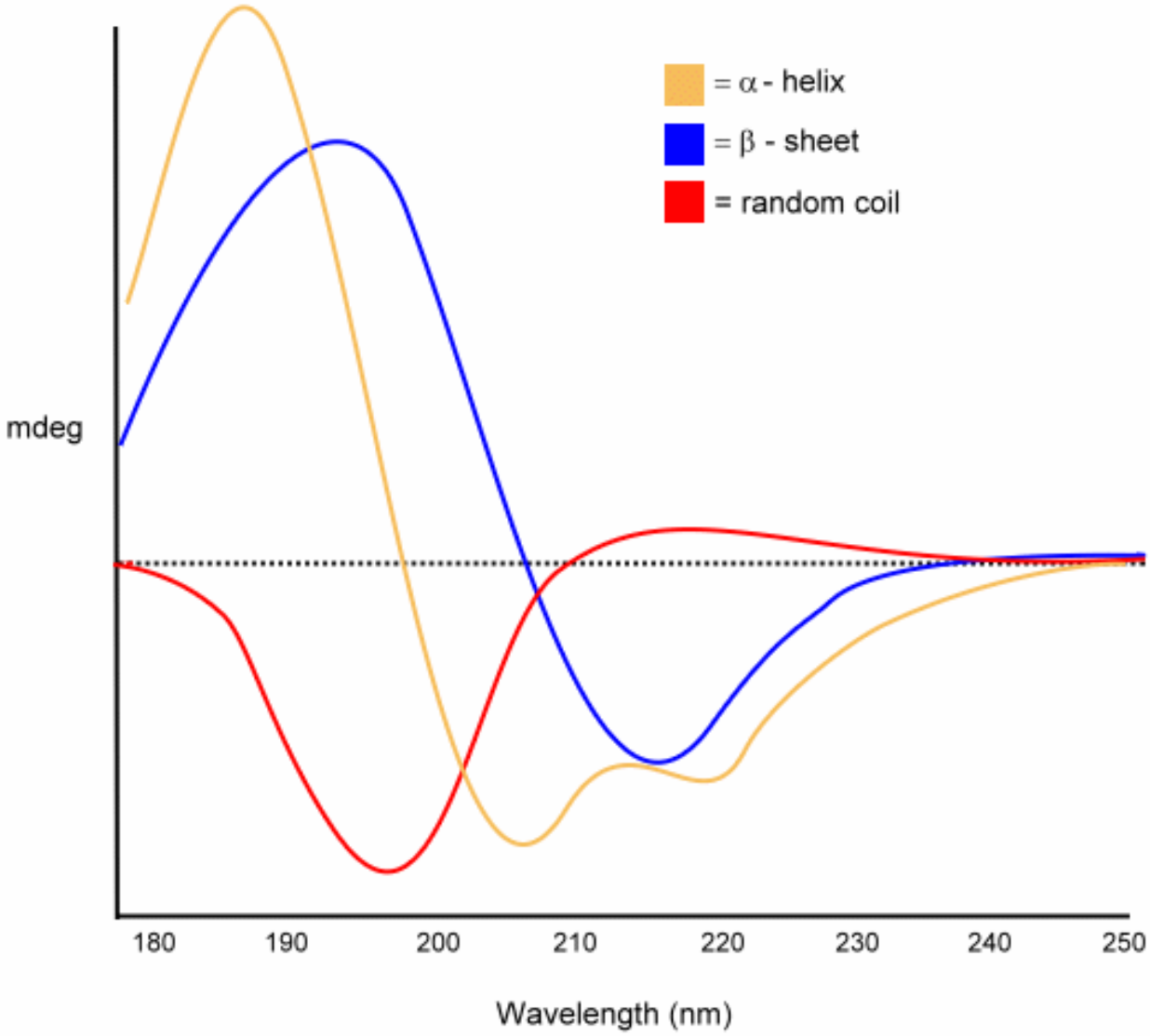

Figure 2.2: Theoretical circular dichroism profiles

2.2.3 Enzyme-Linked Immunosorbent Assay (ELISA)

A MaxiSorp® 96 well ELISA plate (Nunc) was coated overnight at 4°C with 100 µl of antigen in PBS pH 7.4 (DN-MAML1: 20 µg/ml; Antp-DN-MAML1: 50 µg/ml or 5 µg/ml ; TT-Hc: 200 µg/ml). No antigen was coated when testing for plastic binders. The following day, ELISA plates were washed three times with PBS and blocked using 250 µl of 3% Milk/PBS for 2 hours at 37°C. Different dilutions of scFv in 3% milk/PBS were added to the ELISA plate in triplicate and incubated for one hour at room temperature. Addition of 3% milk/PBS only was a control for cross reactivity between the antibodies and the coated antigen. Plates were washed three times with PBS-Tween and three times with PBS. Next, 9E10 IgG was added 1/5000 in 3% milk/PBS (100 µl per well), incubated and washed as before. Plates were then incubated with 100 µl of goat α-mouse HRPO conjugate diluted 1/10000 in 3% milk/PBS. One hundred µl of BM-Blue POD substrate were added and incubated for 10-30 minutes at room temperature. The reaction was quenched using 50 µl of 1M HCl before measuring the OD at 450nm. The curve was fitted using SigmaPlot® software to a sigmoidal, four parameter logistic equation.

Variations of this protocol include coating tests in which different concentrations of antigen were coated overnight. Following blocking, the coated protein was detected in a one step reaction using α-His HRPO IgG.

To test fusion protein binding, half of a 96 well ELISA plate was coated overnight at 4°C with 100 µl of 200 µg/ml fusion in PBS pH 7.4. The other half was left empty to include negative controls. After blocking the whole plate, serial dilutions of biotinylated DN-MAML1 in 3% milk/PBS were added to the plate in triplicate and incubated for one hour at room temperature. Other controls included: addition of 3% milk/PBS only and addition of DN-MAML1 (no biotin) both on the coated and uncoated portion of the ELISA plate. After washing, extravidin peroxidase HRPO was added 1/1000 in 3% milk/PBS (100 µl per well), incubated, washed and developed as before.

2.2.4 Phage display

2.2.4.1 Affinity selection (biopanning) on immunotubes

Nunc-Immuno tubes were coated overnight at 4°C with 1 ml of 20 µg/ml DN-MAML1 in PBS pH 7.4. The tubes were washed with PBS three times before blocking with 3% BSA/PBS for 2 hours at 37°C. After three PBS washes, 10^{12} library phage particles in 1 ml of 3% BSA/3% Milk/PBS were added and mixed for 2 hours at room temperature, rotating continuously. The tube was washed 10 times with PBS-Tween and 10 times with PBS (increased to 20 times in the second and third round of selection). Any liquid was removed before the addition of 1 ml 100mM HCl, incubated at room temperature for 10 minutes with constant rotation. The resulting eluate was added to 1 ml of 1M Tris-HCl pH 7.4. One ml of eluate was then added to 20 ml of exponentially growing (OD_{600} 0.6-0.8) XL1-blue cells, previously maintained on minimal media plates. The culture was left at 37°C for one hour with no shaking. Dilute the culture 1/10, 1/100 and 1/1000 and plate 10 µl of each mixture in duplicate onto 2TY agar 1% glucose plates, supplemented with carbonicillin. This titration is necessary to determine the panning output. The leftover culture was spun at 2000 g for 10 minutes at room temperature, resuspended in 500 µl of 2TY and split between two 150mm 2TY agar plates with 1% glucose and carbonicillin. All plates were incubated overnight at 37°C.

2.2.4.2 Further cycles

Five ml of 2TY media including 15% glycerol were added to the 150mm plate to retrieve the output colonies. Fifty µl of this mixture was diluted 1/1000 in 2TY 1% glucose, supplemented with carbonicillin (2TYGC). The remaining bacteria were stored at -80°C. The culture was grown at 37°C with shaking (250 rpm) until an OD_{600} of 0.5. Ten ml of culture were then infected with helper phage (VCSM13, prepared by Dr. Scott, ICL) in the ratio of 1:20. Infection took place at 30°C without shaking followed by 30 minutes shaking at 37°C. Cells were centrifuged at 2000 g for 10 minutes at room temperature. The pellet was finally resuspended in 50 ml of 2TY supplemented with carbonicillin and kanamycin and incubated overnight at 30°C with shaking.

The culture supernatant was isolated by centrifugation at 10,000 g for 10 minutes at 4°C. Ten ml of ice-cold 10% PEG-8000 containing 2.5M NaCl were added to the

supernatant and left for 2 hours on ice. Rescued phages were pelleted at 10,000 g for 10 minutes and resuspended in 2 ml of ice cold, sterile PBS pH 7.4. Any bacterial debris was removed by centrifugation at 10,000 g for 10 minutes at 4℃. To titre the resulting phage preparation, serial ten-fold dilutions were made in sterile PBS to infect XL1-blue cells, as previously described. The selection was repeated for a further two cycles.

2.2.4.3 Identification of monoclonal phage by ELISA

Individual colonies from the output plate of the final cycle (approximately 500 colonies screened) were inoculated into 200 µl 2TYGC media in sterile 96 well plates (round bottom) and grown overnight at 37℃ with shaking (200 rpm). Ten µl from each well were subcultured into 200 µl of fresh 2TYGC media in a 96 well format. These were grown for 2 hours at 37℃ with shaking. The original overnight plate was stored after addition of 15% glycerol (final concentration). Following the 2 hour incubation, 25 µl of 2TYGC media containing 10^9 PFU of helper phage were added per well. Infection occurred at 37°C for 30 minutes without shaking followed by 30 minutes with shaking. The plate was centrifuged at 1000 g for 10 minutes at room temperature. The cell pellets were resuspended in fresh 2TY supplemented with carbonicillin and kanamycin and incubated overnight at 30℃ with shaking. A 96 well ELISA plate was coated overnight at 4°C with 100 µl of 20 µg/ml DN-MAML1 in PBS pH 7.4. The following day, ELISA plates were washed three times with PBS and blocked using 250 µl of 3% Milk/PBS for 2 hours at 37°C. The culture plates were centrifuged at 1000 g for 10 minutes at room temperature. The supernatant in 3% BSA/3%milk/PBS was added to the ELISA plate and incubated for one hour at room temperature. Addition of 3% BSA/3%milk/PBS only was a control for cross reactivity between the antibodies and the coated antigen. Plates were washed three times with PBS-Tween and three times with PBS. HRP-Anti-M13 was added 1/5000 in 3% milk/PBS (100 µl per well), incubated and washed as before. One hundred µl of BM-Blue POD substrate were added and incubated for 10-30 minutes at room temperature. The reaction was quenched using 50 µl of 1M HCl before measuring the OD at 450nm. Promising candidates were screened again on a 5 ml culture format with recovery of rescued phages by PEG/NaCl precipitation, added to the ELISA plate in triplicate. Plastic binders were eliminated at this stage (binding to uncoated ELISA plates).

2.2.5 Molecular biology techniques

2.2.5.1 Isolation and purification of DNA

DNA was isolated using the QIAquick® Spin range of DNA isolation and purification kits (QIAGEN). The miniprep, PCR purification and gel extraction kits were used to isolate and purify DNA from bacterial cultures, PCR/digest reaction mixtures and agarose gels, respectively. DNA concentration was determined by absorption at 260 nm using a NanoDrop® Micro-Volume UV-Vis spectrophotometer.

2.2.5.2 Agarose gel electrophoresis

Gels consisted of 1% agarose in TAE buffer with 1µg/ml ethidium bromide. DNA samples, mixed with loading buffer, were electrophoresed at 120V and bands were visualised using a UV transilluminator. Molecular weight markers were Hyperladder I (10kbp to 200bp) and IV (1000bp to 100bp).

2.2.5.3 Restriction enzyme digests

All restriction enzymes were purchased from Fermentas. Reactions were carried out at 37°C for 2 hours, including 10 units of each enzyme.

Table 2.10: Restriction enzymes and corresponding buffer

Enzyme combination	**Buffer**
NcoI XhoI	1x Tango
PciI NotI	G
NcoI NotI	O
NdeI XhoI	Fast digest
BamHI	1x Tango
PciI	1x Tango
AgeI	O

2.2.5.4 Polymerase chain reaction (PCR)

Generally, *pfu* DNA polymerase (Fermentas) was used to amplify DNA under the following cycling conditions:

Step 1: 94°C for 3 minutes

Step 2: 94°C for 45 seconds

Step 3: 70°C for 45 seconds

Step 4: 72°C for 45 seconds

Repeat steps 2-4 35 times

Step 5: 72°C for 10 minutes

2.2.5.5 RNA extraction and cDNA synthesis

Total cellular RNA was extracted using the MagMAX™ 96 total RNA isolation kit (Invitrogen) as per manufacturer's instructions. Isolated RNA was quantified by absorbance at 260 nm using a NanoDrop® Micro-Volume UV-Vis spectrophotometer. The 260/280 nm absorbance ratio was also monitored to assess purity and was expected to fall between the value of 1.9 to 2.3. Total cDNA was synthesised from 85 ng of RNA using the high capacity cDNA reverse transcription kit. Synthesis was carried out at 25℃ for 10 minutes (hybridisation), 37℃ for 2 hours and 85℃ for 10 minutes (enzyme degradation). The resulting cDNA was stored at -20℃.

2.2.5.6 Quantitative real-time PCR

qRT-PCR allows to determine the relative expression of a gene between DNA samples based on the fluorescence emission during the amplification cycles of a PCR reaction. All reactions were performed in a volume of 10 µl consisting of 5 µl of Taqman® Fast Real-Time PCR Universal PCR 2x Mastermix (buffer, polymerase and dNTPs included), 1 µl of cDNA sample, 0.5 µl of the relevant 20x primer and probe mix (Taqman® gene expression assays) and 3.5 µl of molecular biology grade water. qRT-PCR was performed using an Applied Biosystems 7500 Fast Real-Time PCR system with a program of 95℃ for 20 seconds followed by 40 cycles at 95℃ for 3 seconds and 60°C for 30 seconds. All samples were loaded in triplicate on a 96 well optical plate. The threshold value was set to 0.2 for all probes. Analysis of relative gene expression data was performed using the $2^{-\Delta\Delta Ct}$ method. The house-keeping gene 18s rRNA was used to normalize the expression levels of target genes. This controls for potential discrepancies of cDNA content between samples. All samples are then

compared to an internal calibrator sample (ex. untreated control). The standard deviation of the difference between the average sample value and the average 18s rRNA value was calculated as follows: stdev = $((\text{stdev sample})^2 + (\text{stdev 18s rRNA})^2)^{1/2}$. Error in fold change was then calculated from this.

2.2.6 Mammalian cell culture

All procedures were carried out aseptically in laminar flow tissue culture hoods. All cell lines were cultured in a 37°C humidified incubator with 5% CO_2 and passaged using trypsin-EDTA digestion. The Chinese hamster ovary (CHO) cell line was cultured in Dulbecco's modified eagles medium (DMEM) and 10% Fetal Bovine Serum (FBS). CHO cells transfected with either the delta-like ligand 1 (CHO Δ) or the Notch receptor 2 (CHO N2) required addition of 0.5 mg/ml geneticin and 0.2 mg/ml hygromycin (CHO N2 only). The MDA-MB-231 cell line was cultured in DMEM phenol red free media with 5% FBS and 1 mM pyruvate. Cells were stored in 10% DMSO 90% FBS at -80°C.

2.2.6.1 Luciferase reporter gene assay

This assay requires the use of white 96 well plates (Nunc) for luminescent readings. All conditions are present as triplicates on duplicate (identical) plates. Ten thousand CHO N2 cells and 5,000 CHO Δ cells were plated together in a final volume of 180 µl of media per well with 10 mM LiCl. To test inhibition of Notch signalling, 20 µl of the appropriate drug concentration were added. The following controls were also included: Antp, 1% DMSO, CHO N2 only and combination of CHO N2 and CHO Δ in media only. After 24 hours, 100 µl of ONE-Glo™ reagent (Promega) was added to the wells and left for at least 3 minutes before measuring luminescence in a plate reader. The second identical plate was used for a parallel MTS assay where 20 µl of the MTS reagent were added per well. Following 2 hour incubation at 37°C, the absorbance was read at 490 nm on a plate reader.

2.2.6.2 MDA-MB-231 treatment for qRT-PCR

MDA-MB-231 cells were plated in a 48 well plate at 50,000 cells/ well in 250 µl of media. The following day, 20 µl of drug/control were added to 180 µl of cells in fresh media. Cells were incubated for 24 hours at 37°C, 5% CO_2 before being harvested for qRT-PCR.

2.2.6.3 Generation and maintenance of mouse bone marrow-derived dendritic cells

This procedure was carried out by Dr. Bugeon (ICL). The mice used for this procedure were wild-type C57BL/6 male, aged between 8 and 12 weeks. The femurs, tibias and humeri were removed from the mouse, sterilised and transferred into DMEM. The bone marrow was flushed out with a thin gauge needle (26G) connected to a syringe filled with media. The collected cells were washed and harvested by centrifugation at 500 g for 5 minutes. Cells were resuspended in complete DMEM (10% FBS, 50 units/ml penicillin, 50 µg/ml streptomycin and 2 nM glutamine) and passed through a 70µm cell strainer (VWR). 1×10^7 cells were plated in a T25 flask (25 cm^2) in DMEM supplemented with 20 ng/ml GM-CSF. After 3 days, half the media was replaced with fresh media supplemented with GM-CSF. A media change was performed on day 6 and the cells were ready to use on day 8.

2.2.6.4 Stimulation of BMDC with recombinant Notch ligand

This procedure was carried out by Dr. Bugeon (ICL). Recombinant rat Jagged1-human IgG1 constant region fusion protein (Jagged1-Fc) was used to activate the Notch pathway. Human IgG1 (Sigma) was used in parallel to control for Fc-mediated effects. These lyophilised proteins were dissolved in 0.1% BSA-PBS, aliquoted and stored at -80°C.

Jagged1-Fc was coated at 4°C overnight onto polysterene tissue culture plates at 10 µg/ml, diluted in PBS. The next day, wells were washed twice with PBS. Twenty µl of drug/control were added to 180 µl of cells in media and incubated for 30 minutes at 37°C, 5% CO_2 prior plating. Following 4 hours incubation, cells were harvested for qRT-PCR.

2.2.6.5 MTS cell proliferation assay

The MTS cell proliferation assay consists in measuring the amount of formazan converted from the MTS reagent by dehydrogenase enzymes found in metabolically active cells. MDA-MB-231 cells were plated in a 96 well plate at a density of 5,000 cells per well in 100 µl media. All conditions are present as triplicates. After 48 hours, 100 µl of varying concentrations of Antp-DN-MAML1 in media were added to the appropriate wells. The following controls were also included: Antp, γ-secretase inhibitor 1 (GSI-1, Merck) diluted in dimethyl sulfoxide (DMSO)-media, cells in

media and cells in 1% DMSO-media. After 72 hours, 20 µl of the MTS reagent were added per well. Following 2 hour incubation at 37°C, the absorbance was read at 490 nm on a plate reader.

2.2.6.6 Flow cytometry

MDA-MB-231 cells were plated in a 48 well plate at a density of 15,000 cells per well in 200 µl media. After 48 hours, 200 µl of varying concentrations (10 µM, 5 µM, 2 µM) of Antp-DN-MAML1 or Antp were added to the appropriate wells, in quadruplicate. The following controls were also included: doxorubicin (2 µM and 0.2 µM) and media only. After 24 hours, one sample of cells per treatment was harvested for p21 mRNA expression analysis by qRT-PCR. After 72 hours, cells were harvested and washed twice before incubation with 2.5 µl Annexin V PE in 250 µl of Annexin V binding buffer (1x) per sample. The incubation lasted 20 minutes at room temperature, in the dark. Samples were transferred on ice until analysis. DAPI stain was added to each sample at 200 ng/ml final concentration. Flow cytometry was carried out on a FACSCalibur™ and analysed using Flowjo® software. Debris were excluded based on the forward and side scatter (FSC/SSC) profile; duplets were excluded based on the side scatter width and side scatter area (SSCW/SSCA) profile. Data was recorded for 5000 events per sample.

2.2.6.7 Transient transfection

CHO cells were cultured onto 100 mm Petri dishes until they reached a confluence of 50%. Cells were transfected with pcDNA4a encoding Antp and Antp-Scfv using Fugene® HD transfection reagent (Roche), according to the manufacturer's protocol. Cells were also transfected with pcDNA vector and no DNA as controls. Expression was monitored at 24, 48 and 72 hours post transfection. Media (concentrated x10) and lysed cell pellet samples were collected in order to analyse protein expression by Western blot.

2.2.6.8 Polyclonal stable transfection

Same as transient transfection until one day after transfection when zeocin™ (Melford) was added to the media at a final concentration of 1mg/ml. In the following days, media was replaced when needed.

2.2.7 *In vivo* mouse models

All procedures were carried out by Mr. Daniel Wells of the CBS (ICL) under Dr. Deonarain's Home Office Licence 70/6982. Eighteen female BALB/c nude mice (6-8 weeks old) were inoculated with 2 million MDA-MB-231 tumour cells in ice-cold 50% DMEM media/FBS and 50% matrigel, subcutaneously. The tumours were monitored until they reached a size of 32-126 mm^3 (around 4-5 mm diameter). The mice were randomised and grouped as follows.

Group 1: Antp-DN-MAML1, 4mg/kg, 3 times per week, 11 doses (approx. 0.1mg/mouse)

Group 2: paclitaxel, 10mg/kg, 3 times per week, 6 doses

Group 3: Saline only, 0.1 ml, 3 times per week, 6 doses

All administrations were blind and performed via the tail vein intravenous route in a volume of 0.2 ml. The animals were culled and dissected after three and a half weeks or when tumours were greater than 15 mm diameter. Tumour sizes were calculated as (LxWxW)/2 and plotted as a percentage change from the day treatment started.

2.2.8 Statistical analysis

Statistical analysis was carried out using Excel. One-way ANOVA (analysis of variance) was employed to compare data sets. Two-way ANOVA was used to compare differences in response between two factors – i.e. to compare differences between cells stimulated with Jagged1-Fc in the presence or absence of an inhibitor.

Chapter 3

Production and characterisation of the Antp-DN-MAML1 fusion

3.1 Introduction

The first strategy to inhibit Notch signalling consisted of blocking transcription activation using a dominant-negative MAML1 delivered by Antp. A study by Weng et al. (Weng et al., 2003), described the 13-74 truncated MAML-1 as a strong dominant negative construct. MAML-1 (13-74) is still able to form the tripartite transcription activation complex but cannot recruit co-activators such as p300 (see Figure 1.3). In the same study, delivery of MAML (13-74) causes growth arrest and death of T-ALL cells. A similar strategy has since been employed by Moellering et al. (2010). They engineered a MAML-1 stapled peptide which interferes with endogenous MAML-1 to inhibit assembly of the active transcriptional complex. Thus, disruption of MAML function is considered a viable method for Notch inhibition, resulting in a therapeutic benefit.

The first goal is to produce Antp-DN-MAML1 and Antp proteins. The helical structure of both constructs make soluble expression the preferred method of production. In order to achieve soluble expression, both cytosolic expression and secretion were attempted. Expression through the secretory pathway is the method of choice for proteins that require formation of disulphide bonds. The methods available for protein purification are based on charge (ion exchange), size (exclusion chromatography) or tag affinity (IMAC). In the case of insoluble expression, inclusion bodies need to be isolated, solubilised and refolded, each step requiring considerable optimisation.

Circular dichroism was the preferred method to establish the secondary structure of Antp following expression and purification due to its strong and characteristic profile. It is important to confirm a strong helical content for Antp which is thought to be crucial for its function. Circular dichroism (CD) spectroscopy measures differences in the absorption of left-handed polarised light versus right-handed polarised light that relate to structural differences. The presence of alpha helices results in a distinct circular dichroism spectra.

The first experiment chosen to assess Antp-DN-MAML1 potency *in vitro* is a luciferase reporter gene assay. In this established method, firefly luciferase is transcriptionally regulated by activated Notch 2 receptor (Figure 3.1). The luminescence signal is amplified due to the presence of ten CSL binding sites relying on endogenous CSL for transcriptional activation. Signalling is initiated by mixing

CHO cells transfected with the Notch receptor 2 (CHO N2) with CHO cells transfected with the delta-like ligand 1 (CHO Δ).

The γ-secretase inhibitor DAPT (Figure 3.2A), is used as a positive reference in *in vitro* studies. This dipeptide analog has been shown to inhibit Notch signalling by acting on the γ-secretase complex (Morohashi et al., 2006). DAPT is considered a much cleaner inhibitor compared to GSI-1 (Z-LLNle-CHO) (Figure 3.2B), with decreased effects on other signalling pathways.

The MDA-MB-231 cell line is used in this study as a model to examine the effects of Notch inhibition in human breast cancer. Stylianou et al. (Stylianou et al., 2006) showed that Notch signalling is increased in MDA-MB-231 cells and Western blot analysis revealed an upregulation of N^{IC} and Hey1. Rizzo et al. (2008) also employed MDA-MB-231 cells to study the cross talk between Notch and the estrogen receptor pathway in breast cancer.

The expression of Hes1 is also evaluated in parallel in BMDC. These primary cells are an established model to study Notch signalling in our laboratory (Gentle et al., 2012). Notch signalling can be stimulated by addition of Notch ligands to then examine inhibition by several compounds examined.

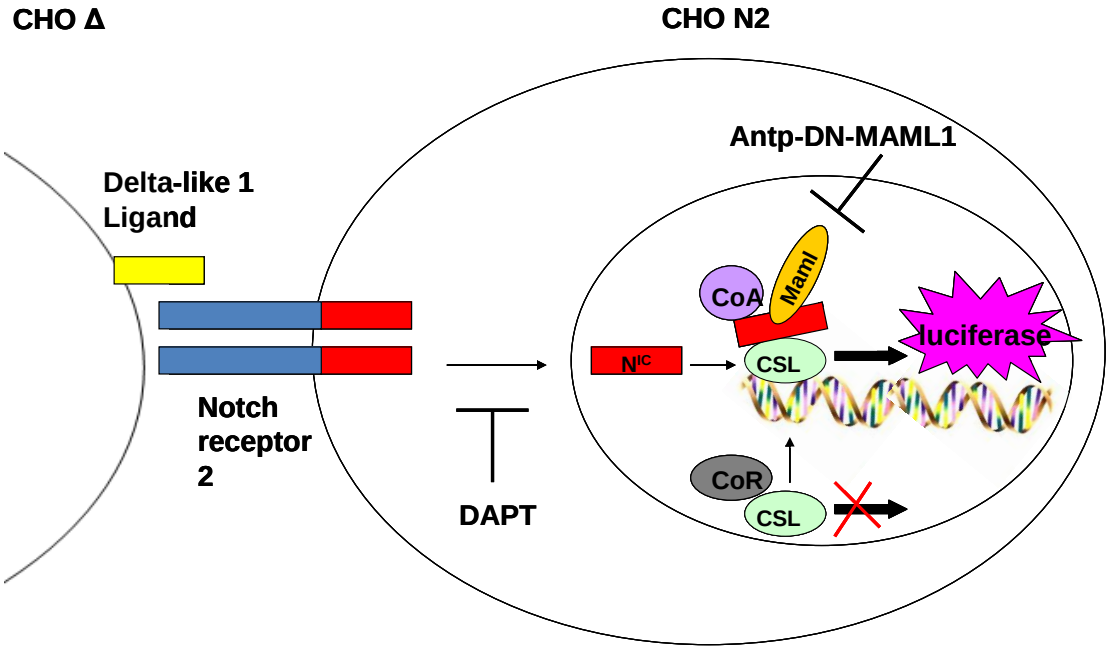

Figure 3.1: Schematic illustration of the luciferase reporter gene assay. Notch signaling is initiated by mixing CHO cells transfected with the delta-like ligand 1 (CHO Δ) with CHO cells transfected with the Notch receptor 2 (CHO N2) in which firefly luciferase is transcriptionally regulated by the activated receptor. This signaling cascade is affected at different levels by addition of DAPT or Antp-DN-MAML1.

A

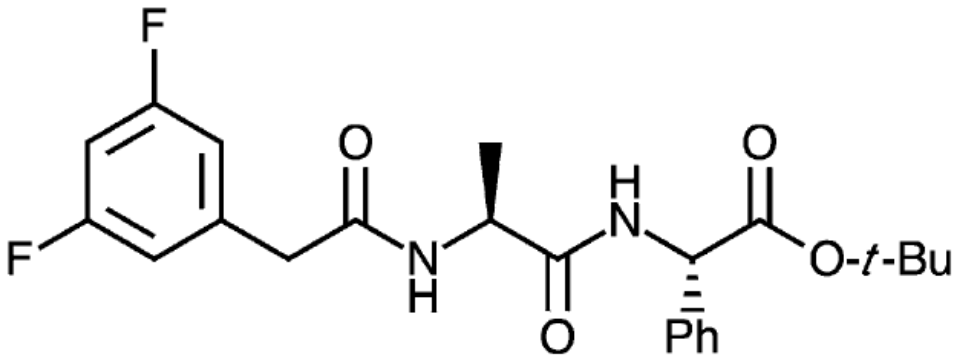

B

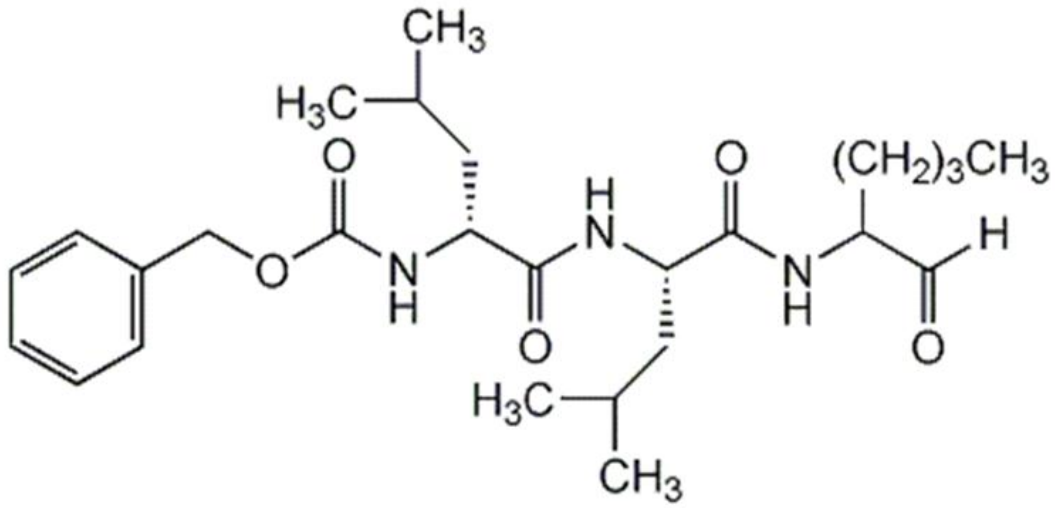

Figure 3.2: Structures of the γ-secretase inhibitors DAPT (A) and GSI-1 (B) (taken from (Groth and Fortini, 2012)).

3.2 Aims and objectives

The aim of this project is to study the potential as a Notch inhibitor of a dominant negative version of MAML-1 fused to Antp for intracellular delivery.

The objectives at a practical level are to:

- Evaluate the possibility of expressing Antp as a secreted protein by cloning into the appropriate vector and using a panel of bacterial expression systems.
- As an alternative, establish a protocol for expression of Antp as a soluble protein following cloning into a vector for cytoplasmic expression.
- Attempt purification of Antp by exploiting the strong positive charge on this protein and its small size.
- Carry out a circular dichroism analysis of the Antp protein to confirm its correct refolding.

- Optimise the expression and purification protocol for production of Antp-DN-MAML1 as an insoluble protein.
- Evaluate various methods for refolding of the fusion protein.
- Attempt soluble expression of Antp-DN-MAML1 by matrix expression trials and use of alternative vectors.

- *In vitro* characterisation of Antp-DN-MAML1 to establish the effects of the fusion protein on Notch signalling. Perform luciferase reporter gene assays for a direct assessment of Notch signalling levels. Carry out qRT-PCR studies to examine the expression level of the Hes1 Notch target gene, both in the MDA-MB-231 cancer cell line and the BMDC model primary cells.
- *In vitro* characterisation of Antp-DN-MAML1 to establish the effects of the fusion protein on proliferation of MDA-MB-231 cells upon inhibition of Notch signalling.
- *In vivo* studies using a MDA-MB-231 mice xenograft model to establish the effect of Antp-DN-MAML1 on tumour growth.

3.3 Results

3.3.1 Expression, purification and characterisation of Antp

The cell penetrating protein Antp is the platform for the construction of all fusion proteins in this study. Therefore, its expression and purification is essential for its use as a negative control in functional assays of Notch signalling. The protocol for the production of Antp, previously used by Trojantec, consisted of expressing this protein in inclusion bodies, followed by refolding. This approach required optimisation because of poor yields and concerns about the correct folding of helical Antp.

Table 3.1: Antp characteristics derived from ProtParam on the ExPASy Server

parameter	**value**
Theoretical pI	11.18
Molecular weight (Da)	7826.1
Amino acid residues	60
Extinction coefficient (M^{-1} cm^{-1})	15470

The first strategy to improve production of Antp consisted of expressing it as a secreted protein. In this approach, the Antp gene, cloned in pET20b (see section 2.1.3), is controlled by the T7 expression system which in turn is regulated by the lac operon/promoter system induced using IPTG. The pET20b vector allows fusion of Antp to a signal sequence which facilitates export into the periplasmic space. This vector also carries a C-terminal His tag sequence which enables purification.

Small scale expression trials were carried out in a variety of *E.coli* host strains including TUNER (DE3), JM109 (DE3), BLR (DE3), BLR (DE3) pLysS, BL21 (DE3) pLysE, BL21 (DE3) and BL21 (DE3) pLysS cells. BL21 (DE3) and JM109 (DE3) are used for general protein expression. Expression in BLR (DE3) helps stabilising target plasmids. TUNER (DE3) cells allow control over protein expression levels throughout the cell culture to prevent protein misfolding and reduce toxicity effects. pLysS and pLysE hosts suppress basal protein expression facilitating expression of toxic proteins. Unfortunately, no or extremely low expression was obtained using the first five strains (data not shown).

Figure 3.3 illustrates the expression levels obtained when the Antp construct was transformed in BL21 (DE3) and BL21 (DE3) pLysS. Unexpectedly, expression is mostly cytoplasmic, with increased yields in the pLysS host. When BL21 (DE3) pLysS cells were induced using 0.1 mM IPTG, a portion of Antp is found in the supernatant. However, secretion could not be confirmed due to the observation of bacterial lysis during expression. Altogether, expression trials of Antp as a secreted protein suggest Antp toxicity to host cells.

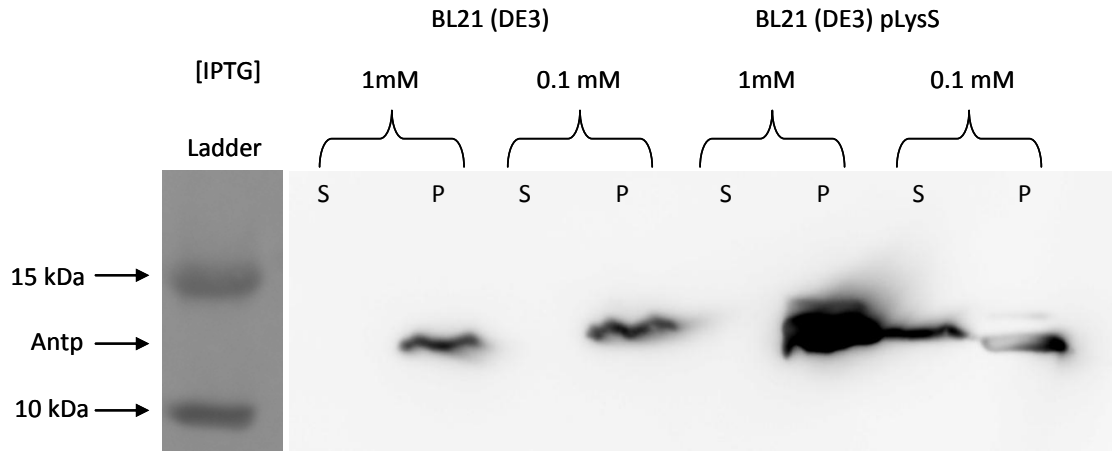

Figure 3.3: Small scale expression trials of Antp in pET20b transformed in BL21 (DE3) and BL21 (DE3) pLysS cells. The bacterial culture was grown in 5 ml of 2TY up to an OD_{600} of 0.8 before induction with either 0.1 mM or 1 mM IPTG for 4 hours. The culture was centrifuged at 2000 g for 5 minutes before analysis of the secreted (S) and total cell pellet (P) fractions by α-His Western blot. Antp is present as a band migrating between 15 kDa and 10 kDa.

In order to overcome the toxicity effects observed upon Antp expression as a secreted protein, Antp was re-cloned into pET23b for cytoplasmic expression in BL21 (DE3) pLysS cells (see section 2.1.3). Antp was successfully expressed as a soluble protein (Figure 3.4).

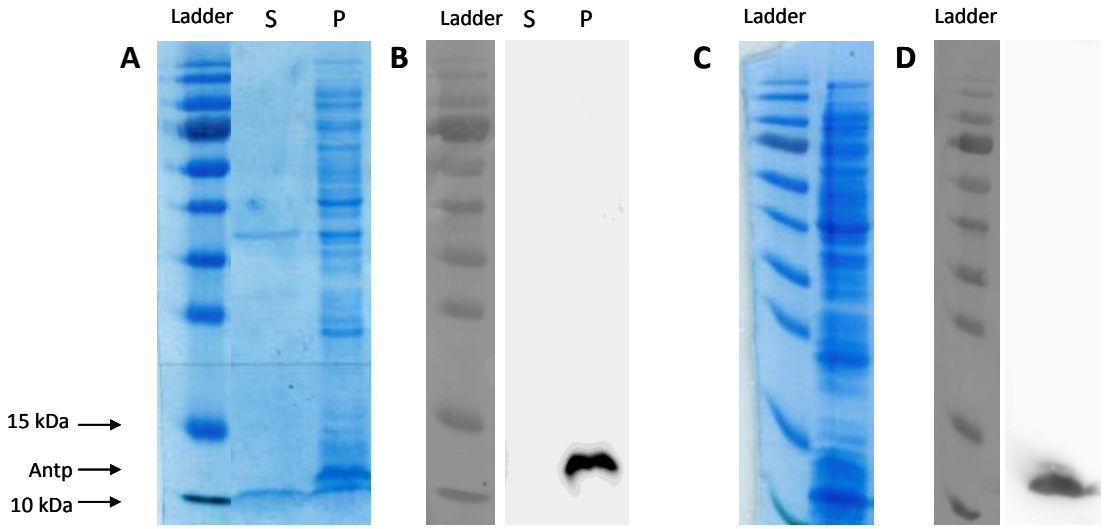

Figure 3.4: Cytoplasmic expression of Antp in pET23b transformed in BL21 (DE3) pLysS cells. The bacterial culture was grown in 500 ml of LB up to an OD_{600} of 1.2 before inducing with 1 mM IPTG for 5 hours at 37°C. The supernatant (S) and cell pellet (P) fractions were analysed by reducing 12% SDS-PAGE, stained using Coomassie Blue (A). Antp is present as a band migrating between 15 kDa and 10 kDa. The corresponding α-His Western blot is also shown (B). The cell pellet was resuspended in 15 ml of 50 mM sodium phosphate (pH 7.5), 2 mM EDTA, 1 mM DTE with the inclusion of a protease inhibitor tablet. Cells were lysed by sonication before centrifuging at 25,000 g for 30 minutes at 4°C. The soluble fraction was analysed by reducing 12% SDS-PAGE, stained using Coomassie Blue (C). The corresponding Western blot is also shown (D).

Ion exchange was the chosen method for Antp purification due to the protein's high positive charge. The column fractions were analysed by reducing 12% SDS-PAGE and stained using Coomassie Blue (Figure 3.5A). As the vector carries a C-terminal His tag sequence, a Western blot using HRPO conjugated murine α-His antibody was also performed to confirm the identity of the purified protein (Figure 3.5B). It is important to note how the high salt interferes with gel electrophoresis. Antp migrates as a band between 15 kDa and 10 kDa which is greater than its predicted molecular weight of 7.8 kDa and could be due to its high positive charge (Table 3.1). A similar migration pattern was observed by (Muller et al., 1988). Antp is present in the last elution fraction (1M NaCl) although a considerable portion is lost in the flow-through and wash steps. This could be due to saturation of nickel on the column or poor affinity binding. It is interesting to note that Antp migrates as a band of different size between the wash, flow-through and elution fractions. This is thought to be due to the gel not running uniformly. The wash and flow-through fractions were subsequently reapplied to the resin to retrieve additional protein (data not shown).

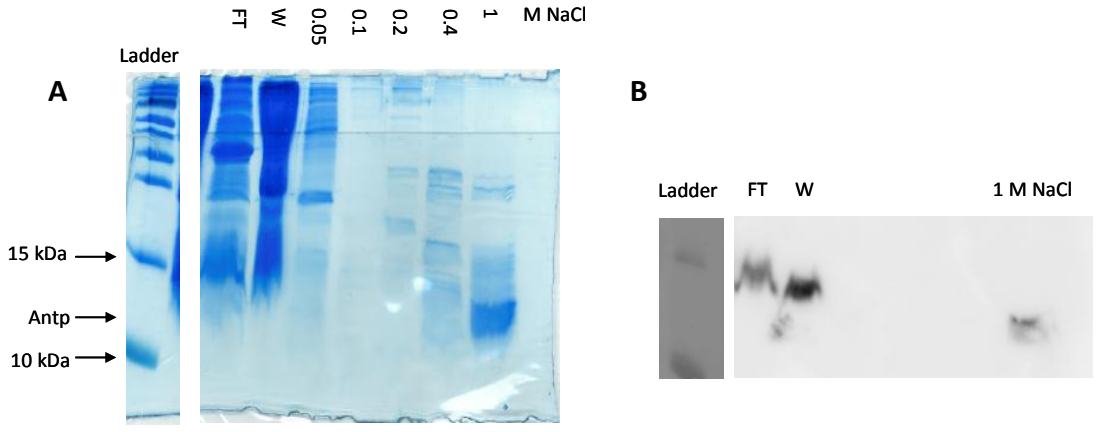

Figure 3.5: Purification of Antp by ion exchange chromatography. Ion exchange flow-through, wash and elution fractions were analysed by reducing 18% SDS-PAGE and stained using Coomassie Blue (A). The corresponding α-His Western blot is also shown (B). Antp is present as a band migrating between 15 kDa and 10 kDa in the flow-through (FT), wash (W) and 1M NaCl elution fractions.

The ion exchange elution fractions containing Antp, were pooled and loaded onto a calibrated Superdex-75 gel filtration column. A peak of absorbance was observed at 75 minutes, followed by two peaks at 100 and 105 minutes (Figure 3.6). According to the column equilibration (Figure 3.7) using cytochrome c (12 kDa) and aprotinin (6 kDa), the peak at 75 minutes should correspond to Antp. Surprisingly, gel analysis showed Antp present in the fractions corresponding to the later peaks (Figure 3.8). In particular, fractions B54 and B61 (Figure 3.8A), representing the top absorbance values, show the highest Antp protein content. Antp is over 95% pure.

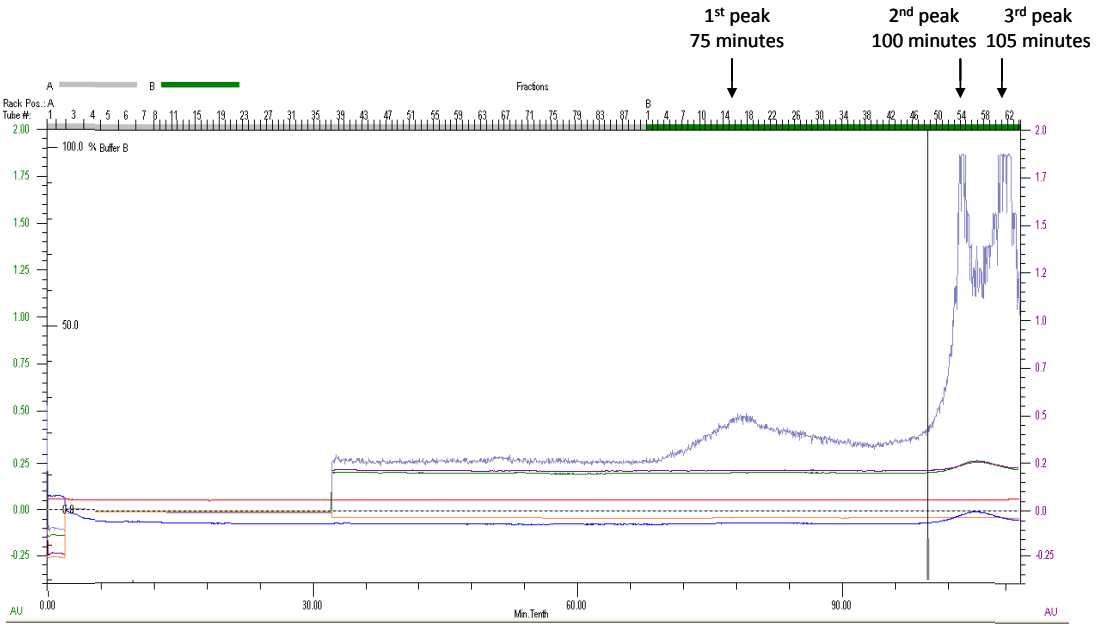

Figure 3.6: Size exclusion chromatography of recombinant Antp. Antp was fractionated on a Superdex-75 gel filtration column. The absorbance was monitored at 214 nm and 280 nm. Every third fraction between B4 and B28 was analysed to examine the first peak at 75 minutes (see arrow). All fractions between B50 and B64 were analysed to examine the second (100 minutes) and third peak (105 minutes).

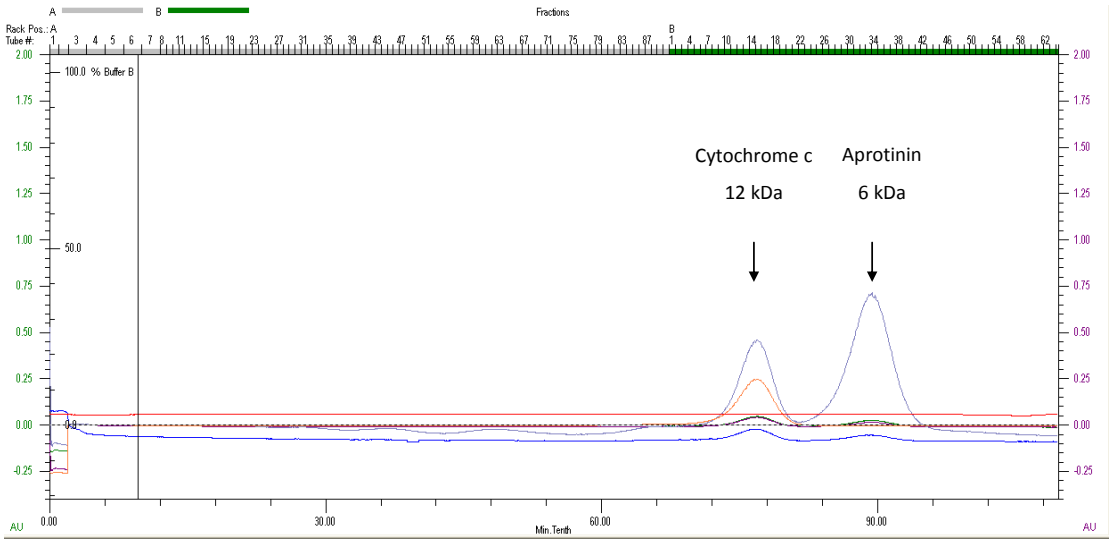

Figure 3.7: Calibration of a Superdex-75 gel filtration column. Cytochrome c and aprotinin were analysed using a Superdex-75 gel filtration column in order to verify its calibration prior to a sample run.

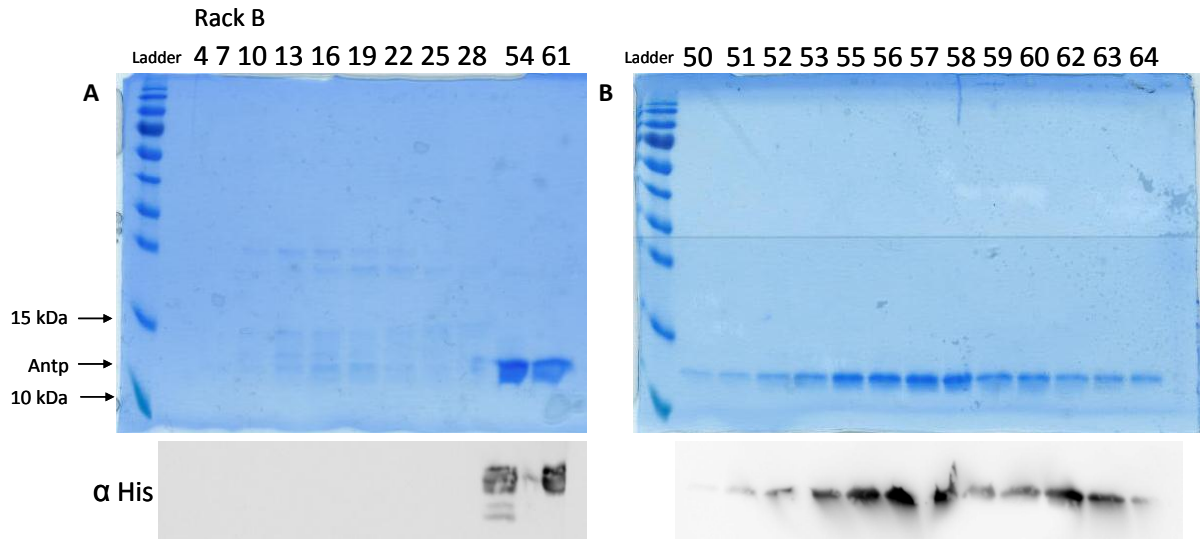

Figure 3.8: Analysis of size exclusion chromatography fractions from Antp fractionation. Antp was fractionated on a Superdex-75 gel filtration column and a selection of peak fractions analysed by reducing SDS-PAGE (stained using Coomassie) and corresponding α-His Western blot below. Fractions from B4 to B28 (A) represent the first peak at 75 minutes, fractions between B50 and B64 (A and B) correspond to the second and third peak (at 100 and 105 minutes).

In order to confirm the secondary structure and folding properties of Antp, a circular dichroism analysis was performed on the purified protein. Different structural elements have characteristic CD spectra. For example, α-helical proteins have a minima at 222 nm and 208 nm and a maxima at 193 nm (Figure 2.2). As shown in Figure 3.9, the CD spectra of Antp confirms a strong α-helical content estimated to be between 42% and 57% depending on the algorithm used. This data is consistent with the predicted α-helical content of 60% assigned to Antp *in silico*.

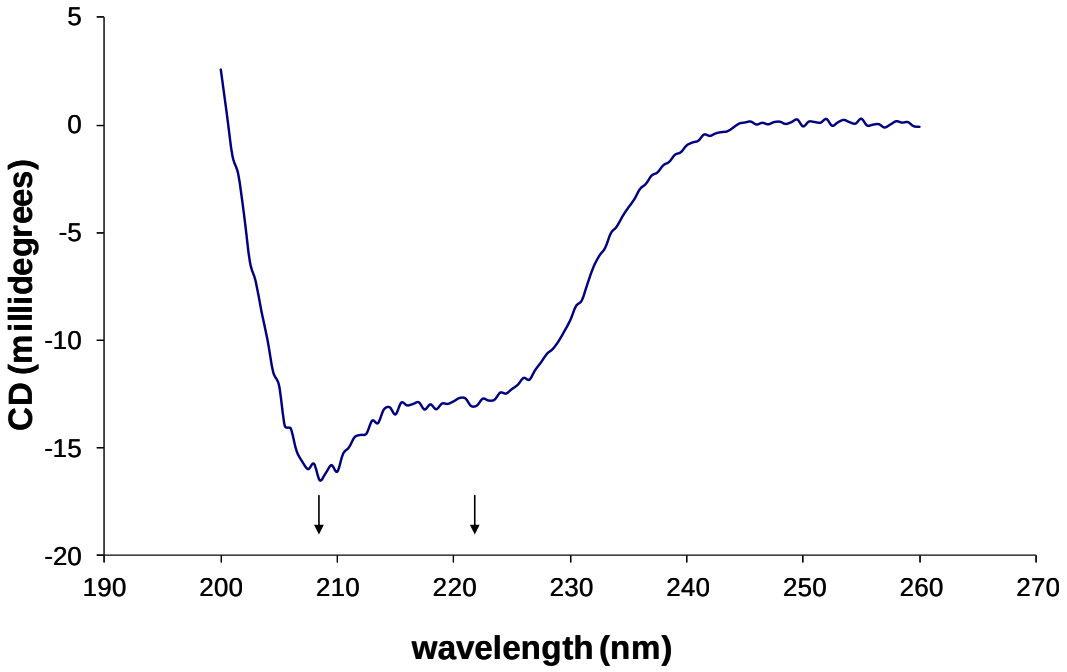

Figure 3.9: Circular dichroism spectra of Antp at 100 µg/ml in PBS using a 1mm path cuvette.

3.3.2 Antp-DN-MAML1 expression and purification trials

The Antp-DN-MAML1 gene was previously cloned by Trojantec in pRSET A (T7 promoter) which is designed for cytoplasmic expression and carries a N-terminal His tag sequence for purification. The construct was transformed in the BL21 (DE3) plysS strain for expression. As illustrated in Figure 3.10A, Antp-DN-MAML1 is expressed as an insoluble form, therefore 6 M guanidinium chloride was used to solubilise the protein from the inclusion body pellet (Figure 3.10B).

Table 3.2: Antp-DN-MAML1 characteristics derived from ProtParam on the ExPASy Server

parameter	**value**
Theoretical pI	10.85
Molecular weight (Da)	16352.9
Amino acid residues	132
Extinction coefficient (M^{-1} cm^{-1})	16960

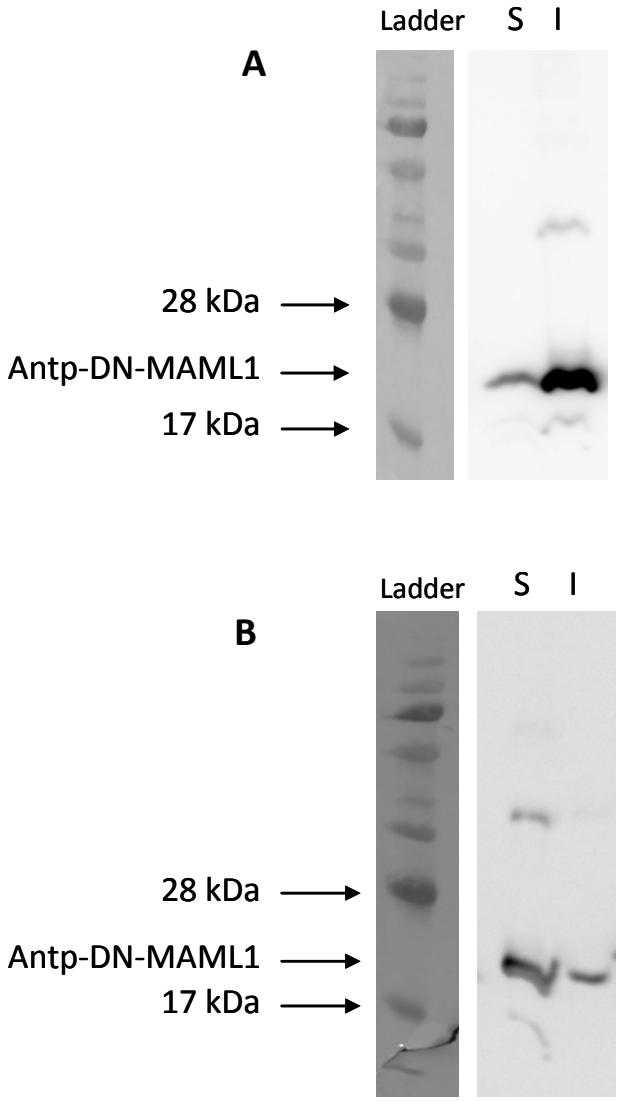

Figure 3.10: Cytoplasmic expression of Antp-DN-MAML1 in pRSET A transformed in BL21 (DE3) pLysS cells. A) Western blot analysis of the soluble (S) and insoluble fractions (I) following B-PER® treatment of the expression cell pellet. Antp-DN-MAML1 is present as a band migrating between 28 kDa and 17 kDa. B) Western blot analysis of the soluble (S) and insoluble (P) fractions following treatment with 6 M guanidinium chloride of the expression pellet.

Antp-DN-MAML1 was purified under denaturing conditions by affinity chromatography. IMAC elution fractions were analysed by reducing 12% SDS-PAGE and stained using Coomassie Blue (Figure 3.11). A Western blot using HRPO conjugated murine α-His antibody was also performed to confirm the identity of the purified protein. The flow-through and wash samples were also included. Antp-DN-MAML1 was present in the all elution fractions, starting from the addition of 20 mM imidazole, as a band migrating between 26 kDa and 17 kDa. This is greater than its predicted molecular weight of 16.35 kDa and could be due to the high positive charge of Antp-DN-MAML1 (Table 3.2). Overall, the (insoluble) expression yields and purification outcome (>50% pure) for this protein were satisfactory.

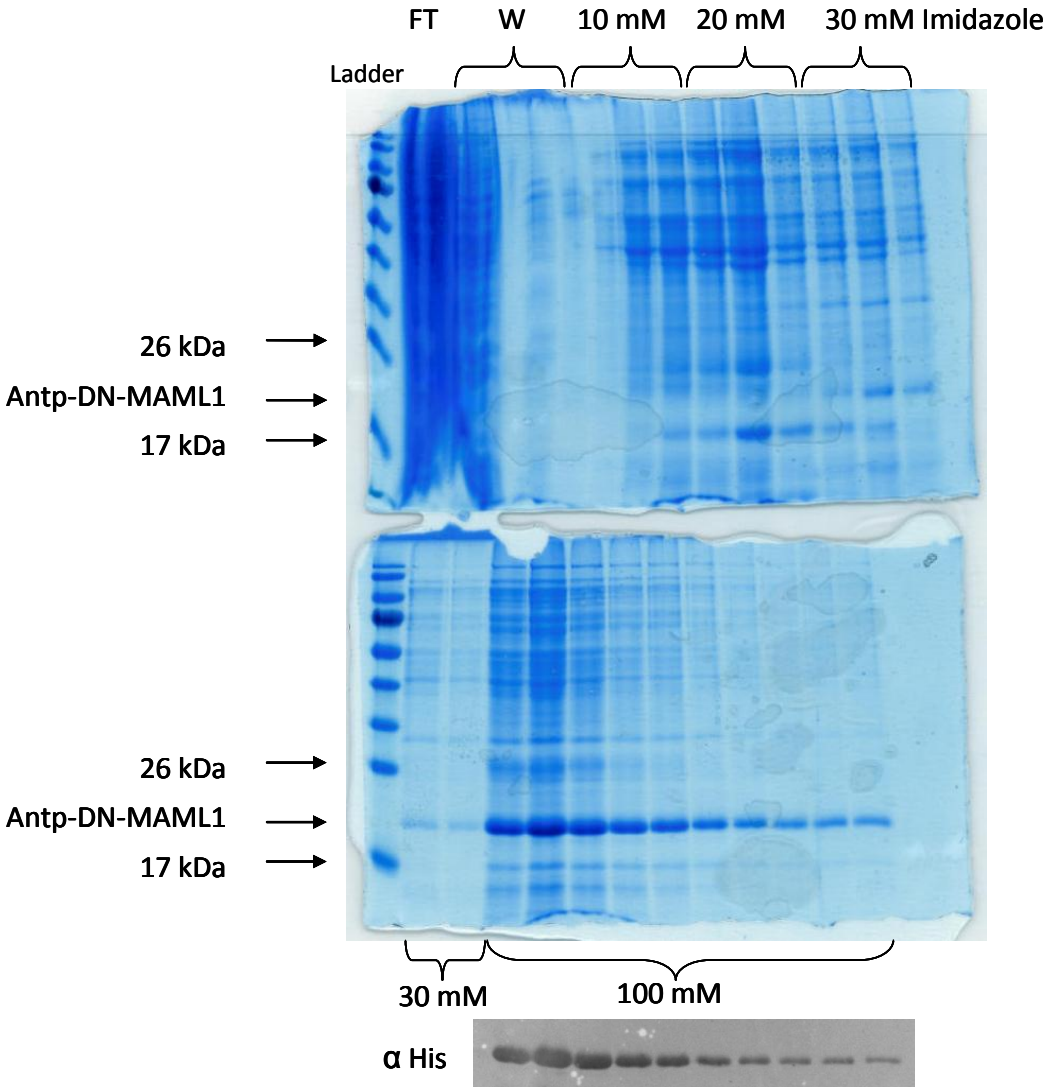

Figure 3.11: Purification of Antp-DN-MAML1 by affinity chromatography. IMAC flow-through (FT), wash (W) and elution fractions analysed by reducing 12% SDS-PAGE and stained using Coomassie Blue. The corresponding α-His blot is also shown for the elution fractions. Antp-DN-MAML1 is present as a band migrating between 26 kDa and 17 kDa in all elution fractions, starting from the addition of 20 mM imidazole (labelled).

Following purification, denatured Antp-DN-MAML1 was refolded in order to obtain the functional protein. Two refolding strategies were considered based on the assumption that Antp-DN-MAML1 does not form any disulphide bonds. The first strategy consisted of dialysis overnight at 4° C in PBS with the addition of 0.4 M L-Arginine followed by dialysis in PBS over 1 day (Figure 3.12A). The second strategy consisted of serial dialyses over 4 days at 4° C using 6 M Urea, 4 M Urea, 2 M Urea with 0.4 M L-Arginine,1 M Urea with 0.2 M L-Arginine, 0.5 M Urea and 0.1 M L-Arg and finally PBS (Figure 3.12B). In this method, the Antp-DN-MAML1 sample was centrifuged after each of the last four dialysis rounds in order to minimise precipitation. As illustrated in Figure 3.12, both strategies resulted in a minority of Antp-DN-MAML1 being present in the soluble fraction as a refolded protein. The majority of the sample precipitated due to the incorrect refolding. This represented a major hurdle in the production of functional and correctly folded Antp-DN-MAML1.

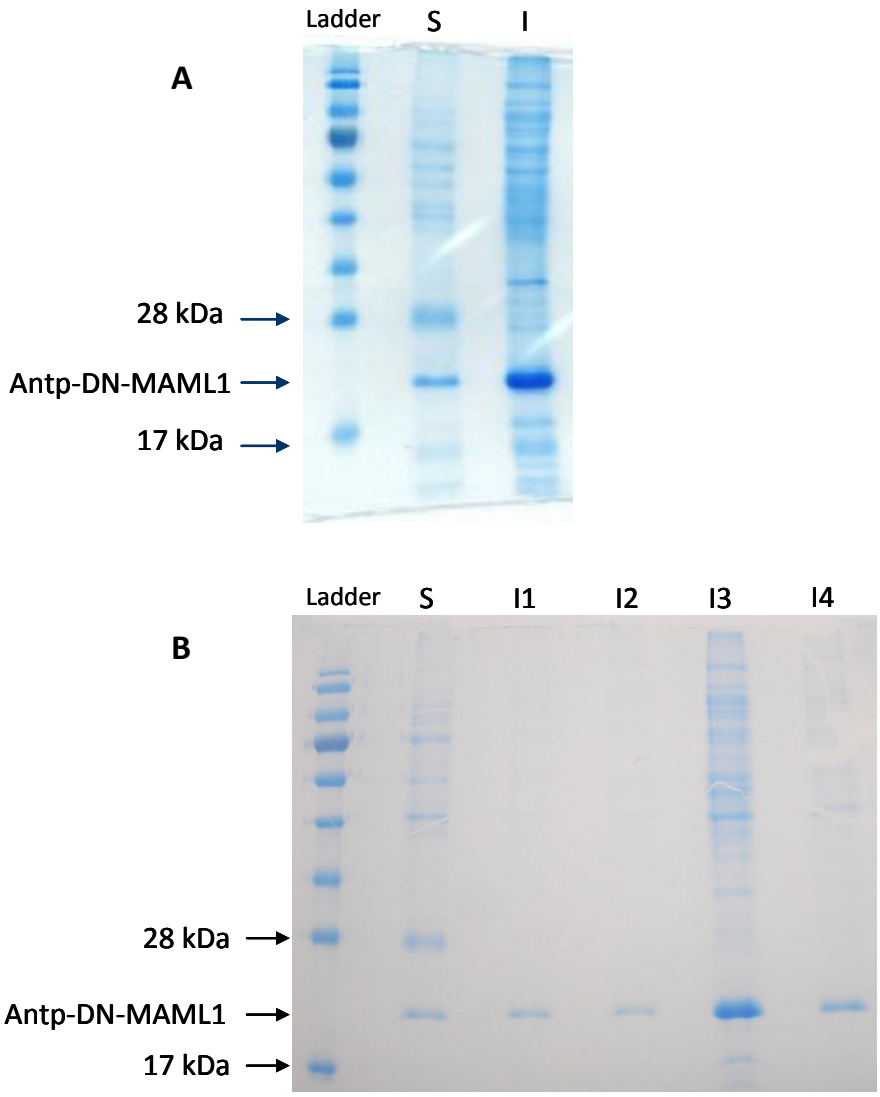

Figure 3.12: Antp-DN-MAML1 refolding trials. Analysis of the soluble (S) and insoluble (I) refolding fractions by reducing 12% SDS-PAGE, stained using Coomassie Blue. Antp-DN-MAML1 is present as a band migrating between 28 kDa and 17 kDa. A) First refolding strategy: dialysis overnight at 4° C in PBS with the addition of 0.4 M L-Arginine followed by dialysis in PBS over 1 day. B) Second refolding strategy: serial dialysis over 4 days at 4° C using 6 M Urea, 4 M Urea, 2 M Urea with 0.4 M L-Arginine,1 M Urea with 0.2 M L-Arginine, 0.5 M Urea and 0.1 M L-Arg and finally PBS. I1= spin after dialysis in 2 M Urea with 0.4 M L-Arginine, I2= spin after dialysis in 1 M Urea with 0.2 M L-Arginine, I3= spin after dialysis in 0.5 M Urea and 0.1 M L-Arg, I4= spin after final dialysis in PBS.

An attempt to express Antp-DN-MAML1 as a soluble protein consisted of monitoring the soluble/insoluble protein content of cultures induced with increasing IPTG concentrations, over time. Overall, greater yields were observed with increased IPTG concentrations (Figure 3.13A-E). The results collected an hour post induction, suggested that, even at the highest IPTG concentration, a considerable portion of Antp-DN-MAML1 is expressed as a soluble protein (3.13A). In contrast, overnight expression results in all Antp-DN-MAML1 being insoluble (3.13E). This suggests a limited time frame for soluble expression of Antp-DN-MAML1.

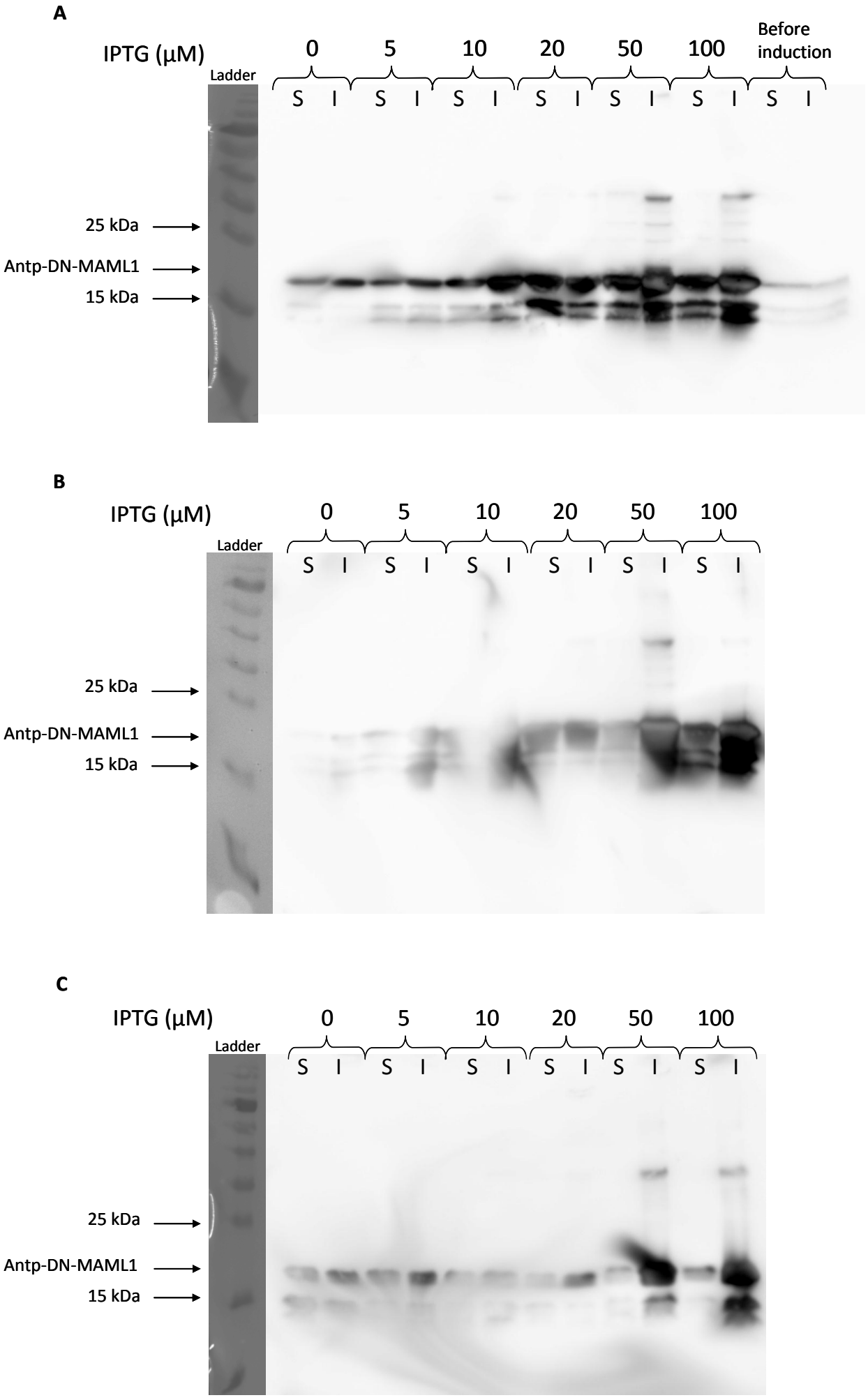
A
IPTG (μM)
0
5
10
20
50
100
Before induction
Ladder
S I S I S I S I S I S I S I
25 kDa
Antp-DN-MAML1
15 kDa
B
IPTG (μM)
0
5
10
20
50
100
Ladder
S I S I S I S I S I S I
25 kDa
Antp-DN-MAML1
15 kDa
C
IPTG (μM)
0
5
10
20
50
100
Ladder
S I S I S I S I S I S I
25 kDa
Antp-DN-MAML1
15 kDa

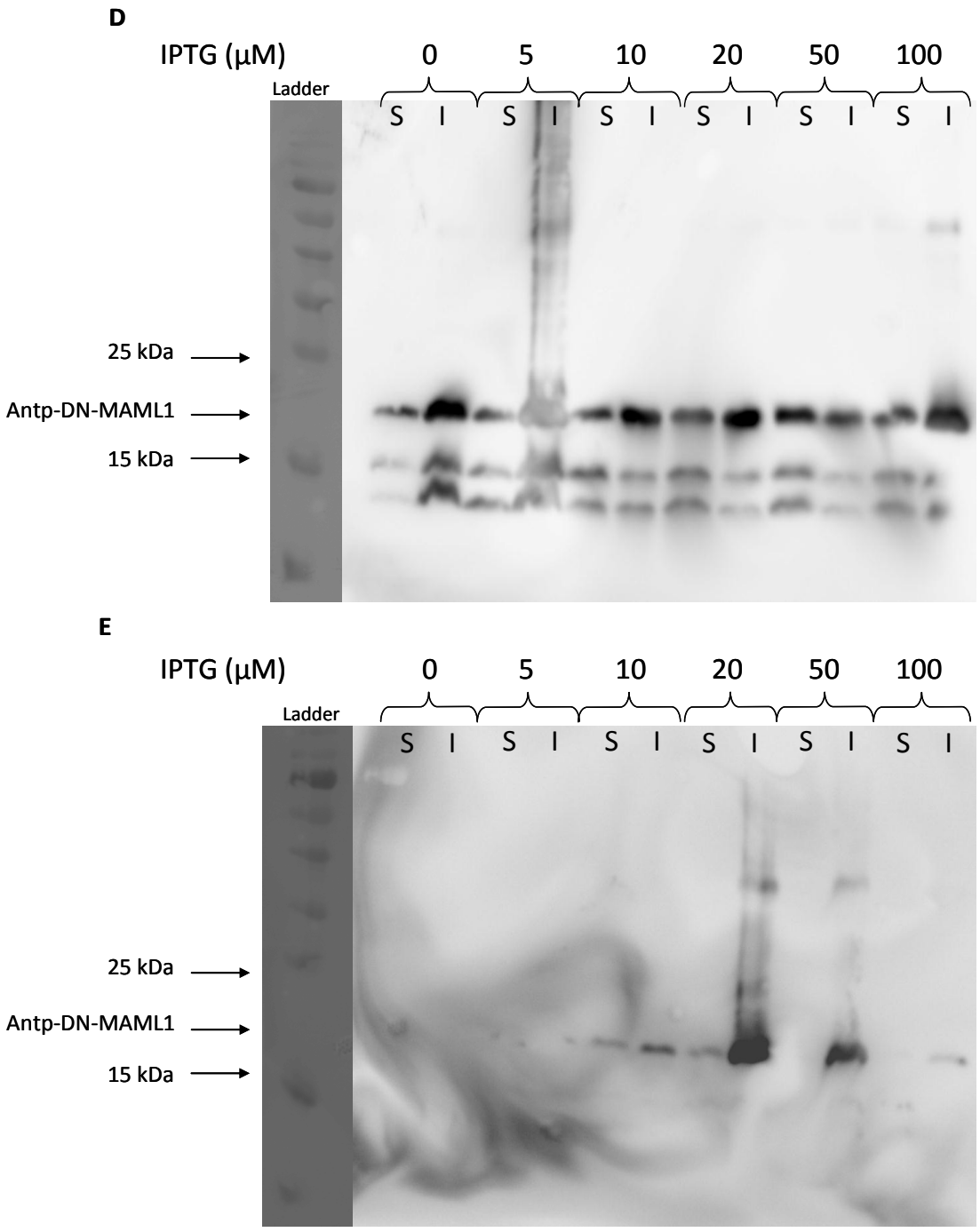

Figure 3.13: Cytoplasmic expression of Antp-DN-MAML1 in pRSET A transformed in BL21 (DE3) pLysS cells, induced with increasing concentrations of IPTG. Western blot analysis of the soluble (S) and insoluble (I) fractions following B-PER® treatment of six expression pellets. Antp-DN-MAML1 is present as a band migrating between 25 kDa and 15 kDa. A) 1 hour induction B) 2 hour induction C) 3 hour induction D) 4 hour induction E) 20 hour induction.

Based on the results obtained in the small scale expression trial with one hour induction, the protocol was scaled up to a 1 litre culture. As shown in Figure 3.14, the protocol was reproducible and Antp-DN-MAML1 was expressed as a soluble protein in the cytoplasm. The chemiluminescent signal on the first blot (Figure 3.14B) was bleached due to protein overload on the gel (Figure 3.14A); the signal is much clearer on the second blot with lower loading (Figure 3.14C). Interestingly, the α-His Western blot flags up several bands other than the one corresponding to Antp-DN-MAML1, both of higher and lower molecular weight. This was also observed in the small scale expression trials. The lower bands might be due to partial degradation of the expressed protein. Further efforts to pursue this strategy were discouraged when all attempts at purification of the protein by both affinity and ion exchange chromatography failed (data not shown).

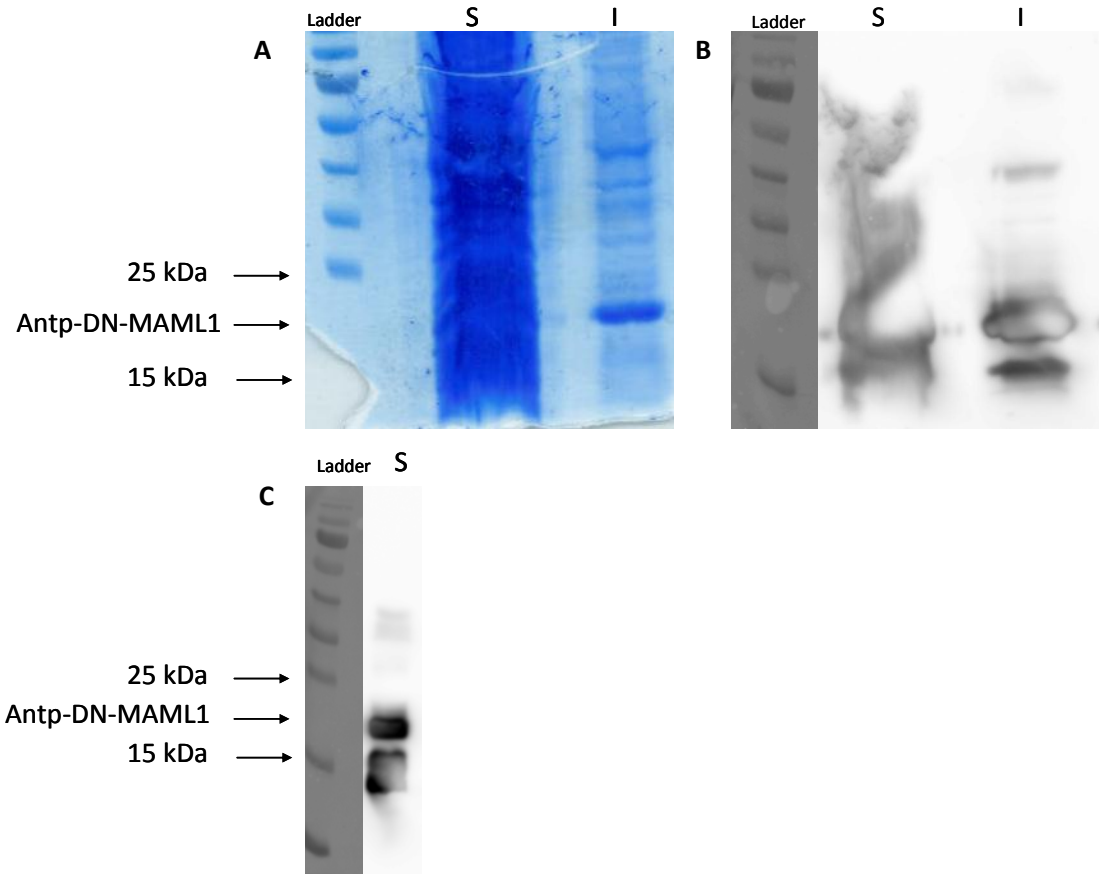

Figure 3.14: Large scale cytoplasmic expression of Antp-DN-MAML1 in pRSET A transformed in BL21 (DE3) pLysS cells. The bacterial culture was grown in 1L of LB up to an OD_{650} of 0.5 before inducing with 100 μM IPTG for 1 hour at 30°C. The soluble (S) and insoluble (I) fractions, following B-PER® treatment of the expression pellet, were analysed by reducing 12% SDS-PAGE, stained using Coomassie Blue (A). Antp-DN-MAML1 is present as a band migrating between 25 kDa and 15 kDa. The corresponding α-His Western blot is also shown (B) with a clearer blot of the soluble fraction in C.

Further trials of Antp-DN-MAML1 production are summarised in Table 3.3. Different aspects of the expression, purification and refolding protocols were tackled without success. In particular, expression trials of a codon optimised Antp-DN-MAML1 construct in pET23 also resulted in inclusion body formation (Figure 3.15). Antp-DN-MAML1 was finally manufactured as a custom peptide by Almac Ltd.

Table 3.3: Summary of Antp-DN-MAML1 production trials

Strategy	People Involved	Detailed Method	Outcome	Decision
SDS-Dialysis	Dr Stylianou	Boil expression pellet in SDS to lyse and solubilise then dialyse SDS out	Not reproducible, poor yields and purity. Unable to carry out IMAC in the presence of SDS	Abandon and follow standard protein refolding methods
Urea-Dialysis	Ms Colucci	Solubilise inclusion body pellet in 6M GuHCl, purify by IMAC under denaturing (8M Urea) conditions and step-wise dialysis into PBS	Pure Antp-DN-MAML1 at IMAC stage, but poor yields due to multiple precipitation steps	Try adding a redox couple to help with potential disulphides
Codon optimised construct	Ms Colucci	Codon optimised construct with C-terminal His tag, process as above	Still insoluble expression and lower yields compared to original construct	Abandon
Urea-Dialysis with glutathione	Ms Colucci & Dr Constantinou	As above but include GSSG/GSH couple in the latter dialysis stages	No real improvement over that seen above	Hand over to Fusion Antibodies (Contract Manufacturer) to optimise
Urea-Dialysis (Contract)	Fusion Antibodies Ltd	As above but with minor refinements	Still low yields and non-reproducible	Try and express it solubly
Soluble expression	Ms Colucci	Identify time window when Antp-DN-MAML1 is in the soluble phase and correlate with plasmid instability.	Some soluble Antp-DN-MAML1 seen within 1 hr of expression	Hand over to Prof. Cole
Soluble expression in Fermentor	Prof J. Cole (Univ. of Birmingham)	Use stress-resistant strains, fermentation and identify nature of soluble protein	Antp-DN-MAML1 found to be associated with the membrane. Small amount of soluble material isolated but hard to purify and needed detergent extraction	Project on hold
Pichia Pastoris	Prof K. Chester (UCL)	Re-clone into Pichia vectors, express using standard methods as a secreted protein	Antp-DN-MAML1 found to be mostly insoluble but some soluble secreted and pure. Yields are low	Project on hold
Peptide synthesis	Almac Ltd	Synthesise the Antp-DN-MAML1 peptide and test if it behaves like the recombinant protein	Synthesis successful with high degree of purity. Expensive but reliable. Antp-DN-MAML1 peptide refolds upon dissolving in PBS and has biological activity	Use this version of Antp-DN-MAML1 until recombinant methods are fully developed

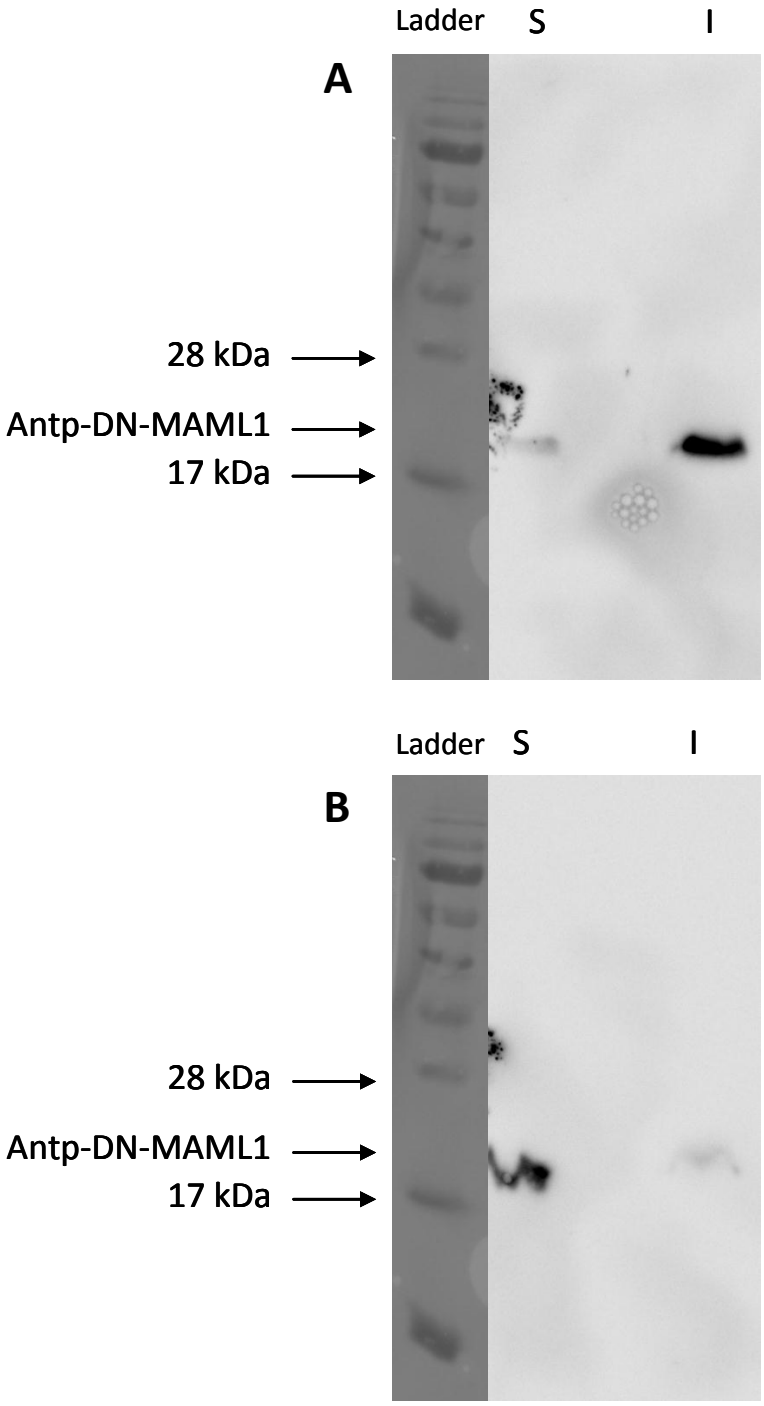

Figure 3.15: Cytoplasmic expression of Antp-DN-MAML1 in pET23 transformed in BL21 (DE3) pLysS cells. Western blot analysis of the soluble (S) and insoluble fractions (I) following B-PER® treatment (A) and 6 M guanidinium chloride denaturation (B) of the lysed expression cell pellet. Antp-DN-MAML1 is present as a band migrating between 28 kDa and 17 kDa.

3.3.3 *In vitro* characterisation of Antp-DN-MAML1

In order to assess whether Antp-DN-MAML1 can repress Notch target gene expression, a luciferase reporter assay was used. In order to initiate signalling, CHO cells transfected with the Notch receptor 2 (CHO N2) were mixed with CHO cells transfected with the delta-like ligand 1 (CHO Δ) (Figure 3.16). Activation was minimal when CHO N2 are mixed with CHO K (wild type) due to the presence of endogenous ligand. Activation did not occur in the three cell types in isolation. A calibration curve (Figure 3.17A) showed a linear increase in luminescence signal with increasing CHO Δ cell numbers. A ratio between CHO N2 and CHO Δ of 1:0.5 was chosen as activation is significant (see enlarged Figure 3.17B) and there is no over stimulation of the system such that inhibition of Notch signalling could be readily observed in subsequent experiments.

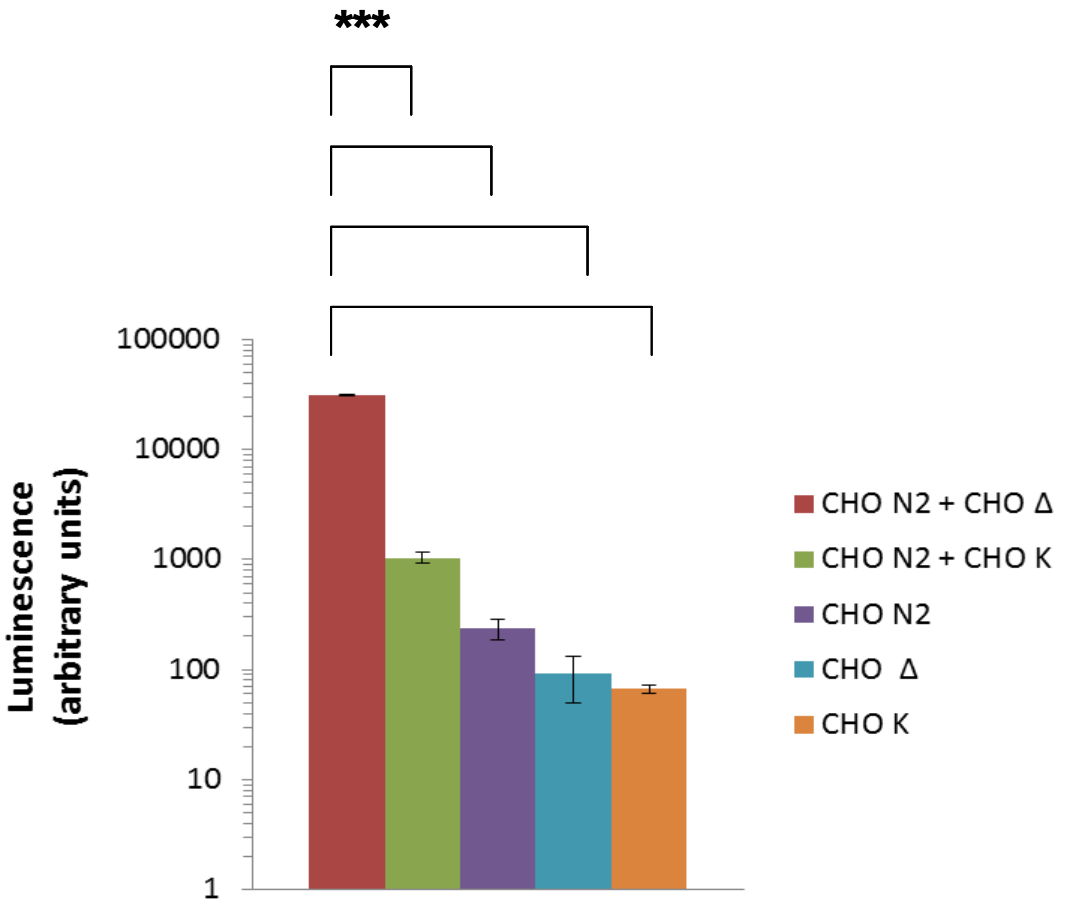

Figure 3.16: Establishment of the CHO luciferase report-gene assay system. CHO N2, CHO Δ and CHO K are plated alone or in combination (CHO N2 + CHO Δ, CHO N2 + CHO K). Luminescence is read after a 24 hour incubation. Error bars represent the standard deviation between triplicates. One-way ANOVA was used to statistically compare conditions; $p \leq 0.05$ was considered significant. ***$p \leq 0.001$.

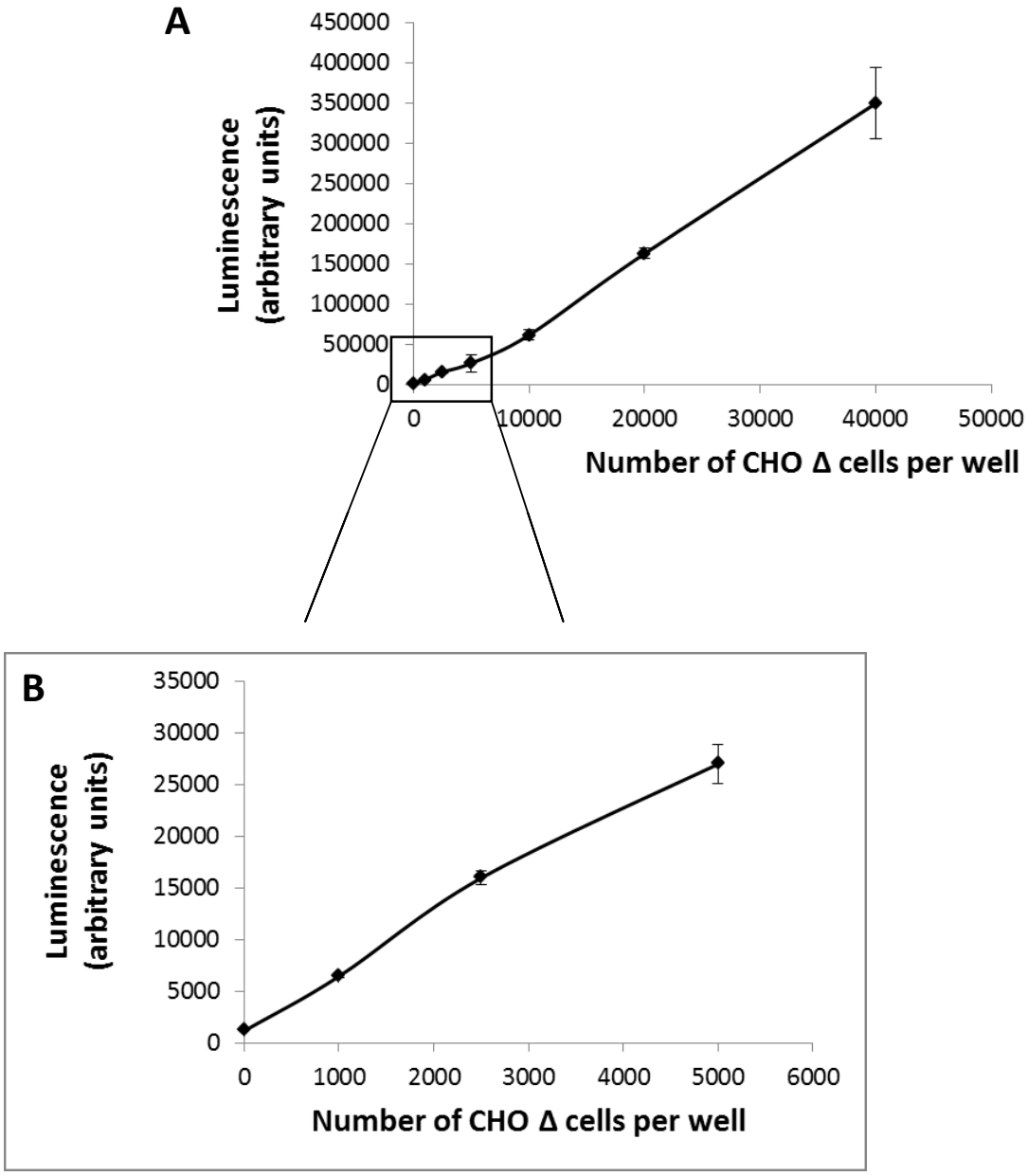

Figure 3.17: Calibration curve to determine the optimal ratio of CHO Δ to CHO N2 cells in the luciferase reporter-gene assay. 10,000 CHO N2 cells were plated with CHO Δ cells in the ratios of: 1:0.125, 1:0.25, 1:0.5, 1:1, 1:2 and 1:4 (A) with lower range expanded in (B). Luminescence was measured 24 hours after plating. Error bars represent the standard deviation between triplicates.

Antp-DN-MAML1 was then tested in the luciferase reporter-gene assay. The data shown is from a single representative experiment out of three repeats which showed the same trend. As expected, treatment with Antp-DN-MAML1 resulted in a dose-dependent decrease in luminescence compared to the Antp and cells in media controls (Figure 3.18A). This corresponds to an inhibition of Notch signalling. A strong decrease in luminescence was also observed with the γ-secretase inhibitor DAPT compared to 1% DMSO (vehicle control). Basal levels of luminescence in the CHO N2 alone control are due to lack of activation of the Notch 2 receptor. Altogether, this suggests that Antp-DN-MAML1 is able to translocate into cells and inhibit Notch signalling specifically. An MTS assay, set up in parallel, confirmed that decrease in luminescence was not due to Antp-DN-MAML1 cytotoxicity (Figure 3.18B). Addition of Antp-DN-MAML1 at 30 μM, resulted in an unexpected increase in absorbance. As expected, a lower absorbance is observed in the CHO N2 alone control.

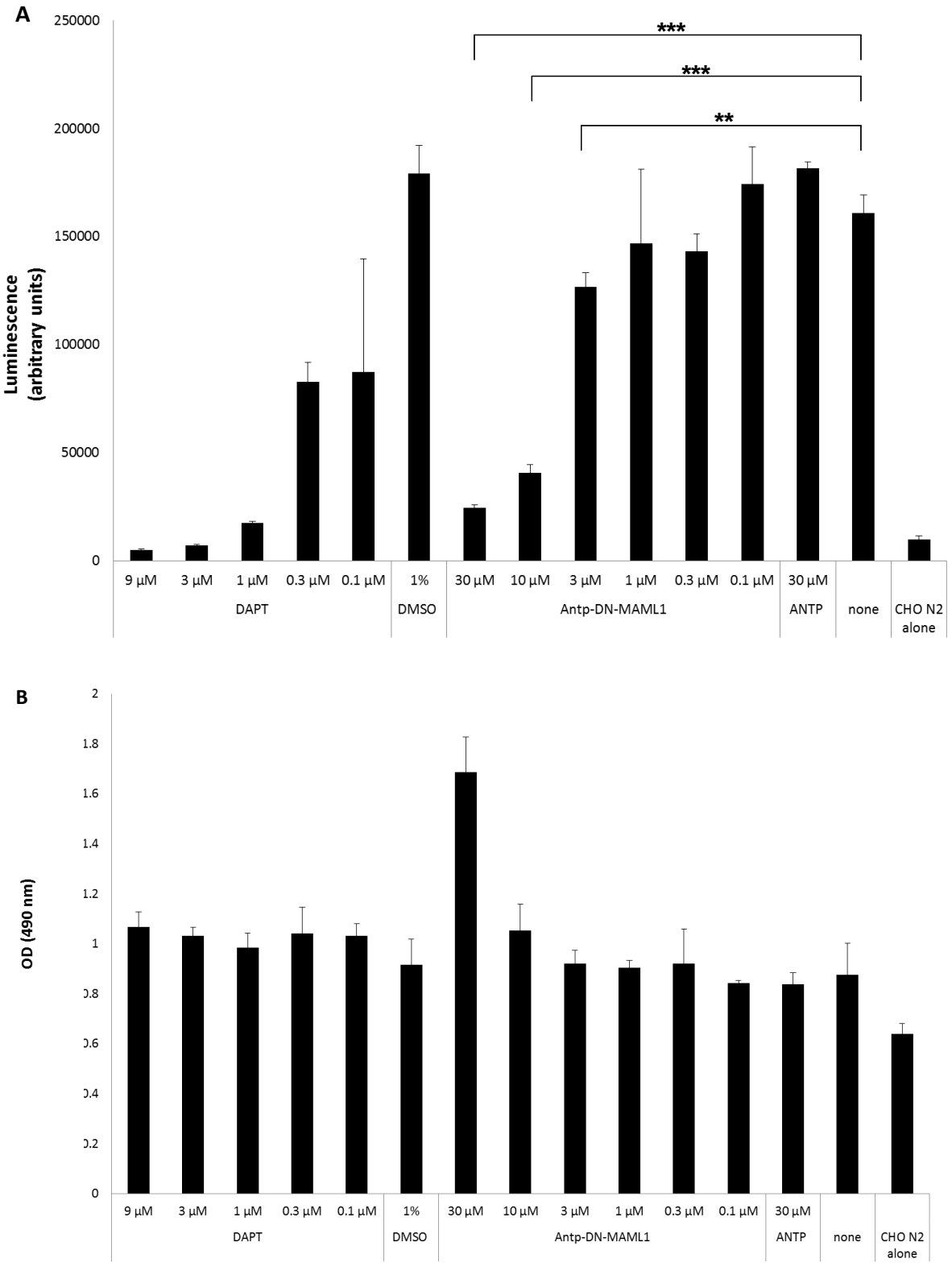

Figure 3.18: Inhibition of Notch signalling by Antp-DN-MAML1 in the luciferase reporter-gene assay. CHO-N2 and CHO-Δ cells were plated at a 1:0.5 ratio in the presence of drug/controls. Each bar represents the mean + standard deviation of 3 replicates. A) Luminescence was measured after 24 hours. One-way ANOVA was used to statistically compare conditions; $p \leq 0.05$ was considered significant. $^{**}p \leq 0.01$, $^{***}p \leq 0.001$. B) The MTS reagent was added after 24 hours to account for cell death and plot shows absorbance at 490 nm.

In order to support the results obtained in the luciferase assay, the effect of Antp-DN-MAML1 on the expression of Notch target genes in MDA-MB-231 was investigated by qRT–PCR. MDA-MB-231 cells were plated and treated the following day with two doses of Antp-DN-MAML1 and Antp for 24 hours. Cells were also treated with DAPT and 1% DMSO vehicle control.

A dose-dependent decrease in expression of the Notch target gene Hes1 was observed after treatment with Antp-DN-MAML1 relative to controls (Antp and cells only) (Figure 3.19). As expected, Hes1 expression was also downregulated with DAPT treatment.

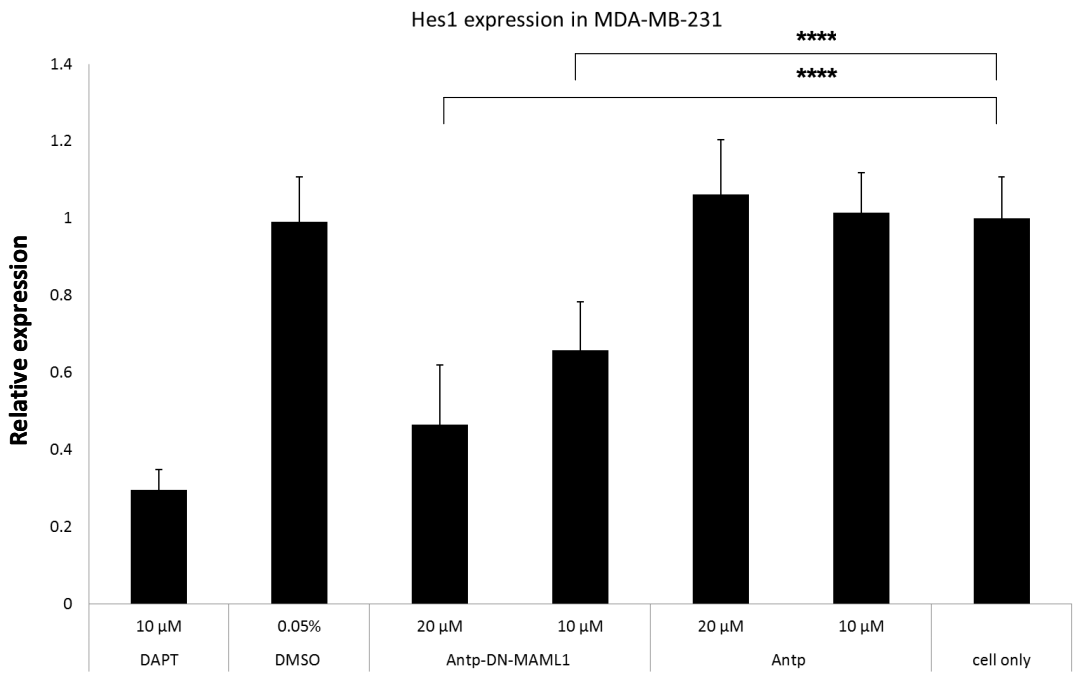

Figure 3.19: Assessment of Notch target gene expression in MDA-MB-231 cells treated with Antp-DN-MAML1. MDA-MB-231 cells were plated in a 48 well plate at a density of 50,000 cells per well. The following day, cells were treated with varying concentrations of Antp-DN-MAML-1/Antp and DAPT/DMSO as controls. After 24 hours, cells were harvested and Hes1 mRNA expression analysed by qRT-PCR. Ct were normalized to 18s mRNA and relative expression compared to a cell-only control. Data are mean + standard deviation of triplicate experiments. One-way ANOVA was used to statistically compare conditions; $p \leq 0.05$ was considered significant. ****$p \leq 0.0001$ (n=9).

Antp-DN-MAML1 effects on Notch signalling were further investigated in BMDC. Hes1 expression was induced in these primary cells by culture with immobilised Jagged1-Fc. The Jagged1-Fc protein used was a fusion between rat Jagged1 and the Fc portion of IgG1 and therefore immobilised IgG1 was used as a control in these experiments. Cells stimulated by the Notch ligand show a significant increase in Hes1 expression corresponding to activation of Notch signalling (Figure 3.20). This increase was reduced in the presence of either Antp-DN-MAML1 or DAPT compared to controls (Figure 3.20).

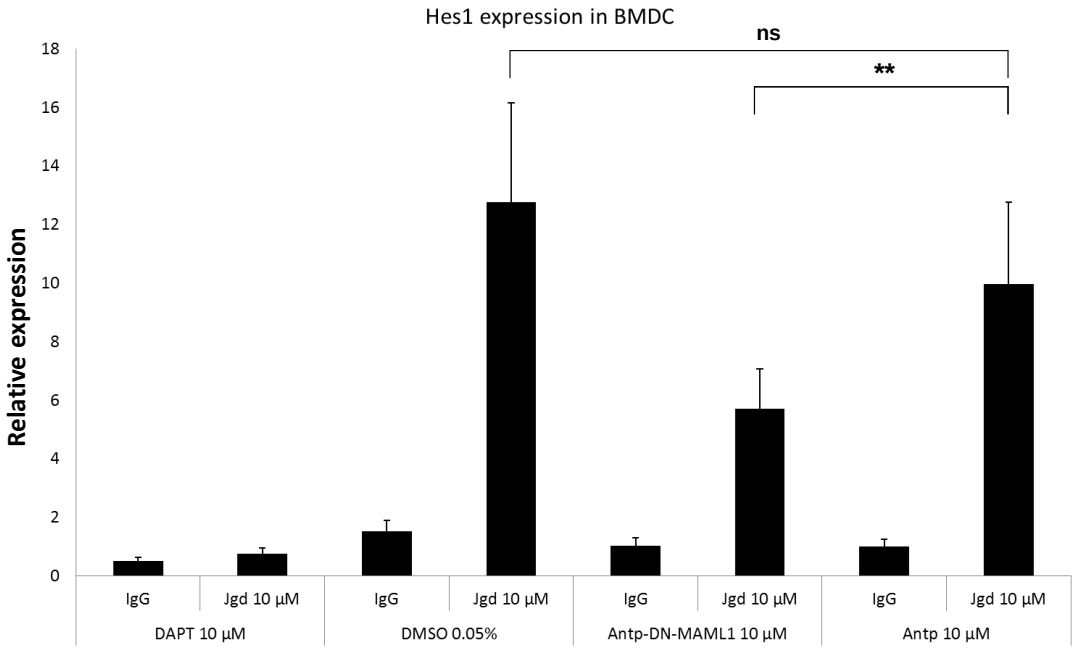

Figure 3.20: Assessment of Hes1 expression in BMDC cells treated with Antp-DN-MAML1. BMDC, pre-treated with Antp-DN-MAML1 and controls, were stimulated with plate-bound Jagged1-Fc (Jgd) or IgG1 (Fc control). After 4 hours, cells were harvested and Hes1 mRNA expression analysed by qRT-PCR. Ct were normalized to 18s mRNA and relative expression compared to Antp + IgG control. Data are mean + standard deviation of triplicate experiments. Two-way ANOVA with replicates was used to statistically compare conditions; $p \leq 0.05$ was considered significant.
**$p \leq 0.01$ (n=9), ns: not significant.

At this point of the study, different experiments suggested that Antp-DN-MAML1 could repress Notch target gene expression. The following experiment was designed to examine whether Antp-DN-MAML1 had any effect on the proliferation of MDA-MB-231 cells. In order to determine the optimal number of MDA-MB-231 cells for an MTS assay, a calibration curve was generated (Figure 3.21) and 5000 cells/well was chosen for all future assays to ensure sufficient sensitivity. Addition of Antp-DN-MAML-1 to MDA-MB-231 cells had a growth-inhibitory effect compared to Antp at intermediate concentrations (Figure 3.22). Addition of the commercial γ-secretase inhibitor 1, GSI-1, also had a strong inhibitory effect on cell proliferation. As the GSI-1 was diluted in DMSO, 1% DMSO was also added to the cells as a vehicle control and this had no effect on cell proliferation compared to untreated control. Using SigmaPlot® fitted curves, calculated IC_{50} values were 0.55 μM, 1.61 μM and 7.03 μM for GSI-1, Antp-DN-MAML1 and Antp, respectively.

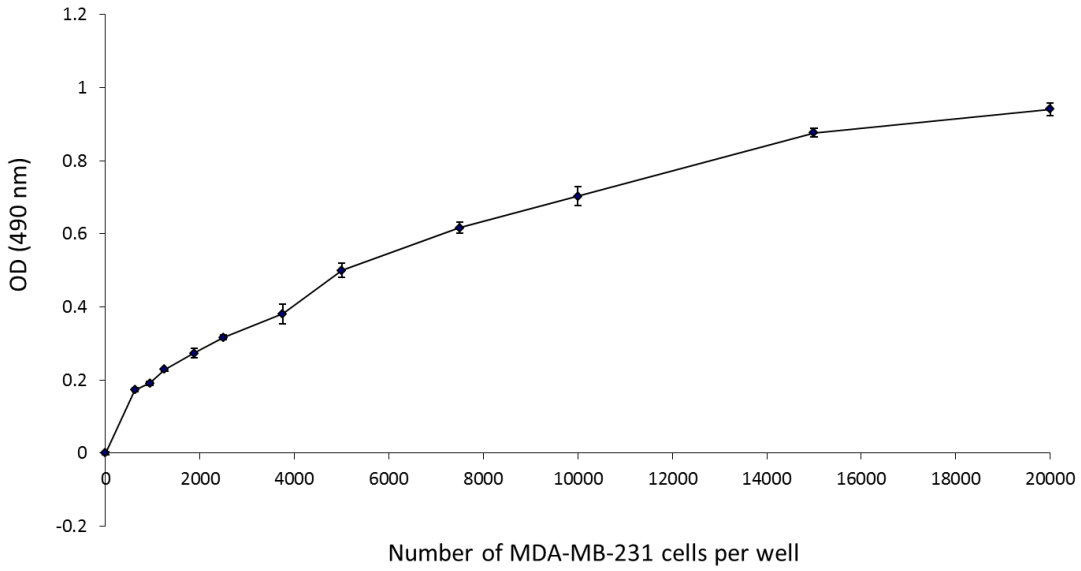

Figure 3.21: Effect of cell number on absorbance at 490 nm measured using the MTS Assay. Various numbers of MDA-MB-231 cells were added to the wells of a 96 well plate. The MTS reagent was added after 120 hours and plot shows absorbance at 490 nm. Each point represents the mean ± standard error of 8 replicates.

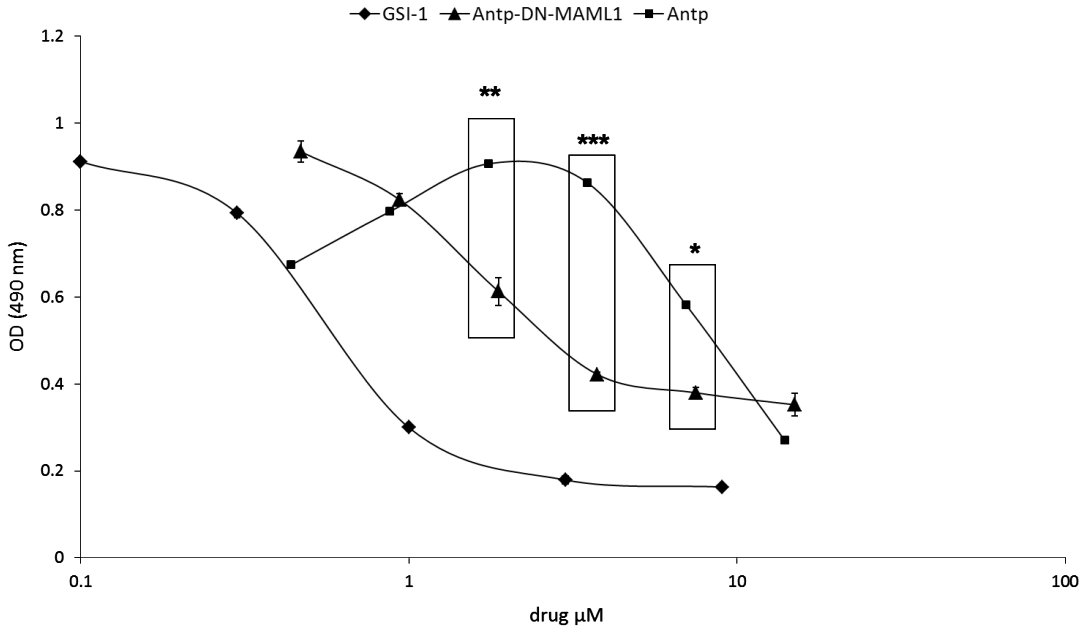

Figure 3.22: Proliferation of MDA-MB-231 cells upon exposure to Antp-DN-MAML1. Cells were plated in a 96 well plate at a density of 5,000 cells per well. Cells were treated 48 hours after plating. The MTS reagent was added following a further 72 hours incubation. Each point represents the mean ± standard deviation of triplicates. 1% DMSO (OD_{490}= 0.85) does not affect cell proliferation compared to the untreated control (OD_{490}= 0.89). One-way ANOVA was used to statistically compare conditions; $p \leq 0.05$ was considered significant. *$p \leq 0.05$, **$p \leq 0.01$, ***$p \leq 0.001$.

A further experiment was performed using the alternative γ-secretase inhibitor DAPT because GSI-1 has previously been shown to inhibit a variety of other signalling pathways in addition to Notch. DAPT did not affect proliferation of MDA-MB-231 at any concentration tested and even with repeated dosing (data not shown). Since DAPT had previously been shown to inhibit Hes1 transcription following the activation of Notch signalling in both MDA-MB-231 cells and BMDC it seems probable that the inhibitory effects of GSI-1 on MDA-MB-231 cell proliferation were unrelated to an effect on Notch signalling. As inhibition of Notch signalling by DAPT did not result in inhibition in MDA-MB-231 cell growth, a question was raised about whether the effects of Antp-DN-MAML1 on MDA-MB-231 cell proliferation were related to inhibition of Notch signalling.

This possibility led to the investigation of other effects that Antp-DN-MAML1 could have on MDA-MB-231 to induce a slow down in growth. MAML1 has been described to interact with p53 through its N-terminal region (1-302) and function as a co-activator (Zhao et al., 2007). In addition, the same study demonstrated that MAML-1 is part of the activator complex that binds to the native promoter of p21. Crucially, MAML-1 increases p53-mediated trans-activation of its target gene p21.

It was hypothesised that the N-terminal portion of MAML-1 (13-74) could still bind to and stabilise p53, increasing p21 expression, resulting in cell death via apoptosis. In order to assess this, the effect of Antp-DN-MAML1 on the expression of p21 in MDA-MB-231 was investigated by qRT–PCR (Figure 3.23). Treatment with Antp-DN-MAML1 shows a strong dose-dependent increase in expression of the p21 gene relative to controls.

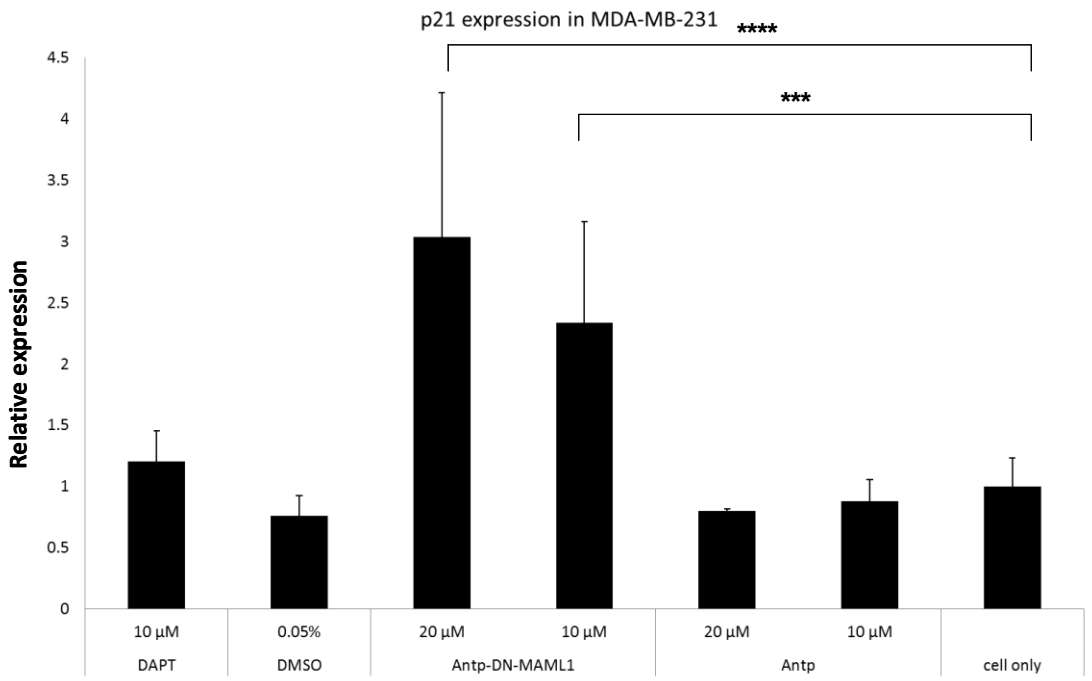

Figure 3.23: Assessment of Notch target gene expression in MDA-MB-231 cells treated with Antp-DN-MAML1. MDA-MB-231 cells were plated in a 48 well plate at a density of 50,000 cells per well. The following day, cells were treated with varying concentrations of Antp-DN-MAML1/Antp and DAPT/DMSO as controls. After 24 hours, cells were harvested for p21 mRNA expression analysis by qRT-PCR. Results were normalized to 18s mRNA and relative expression compared to a cell-only control. Data are mean + standard deviation of multiple independent experiments. One-way ANOVA was used to statistically compare conditions; $p \leq 0.05$ was considered significant. ***$p \leq 0.001$ (n=9) ****$p \leq 0.0001$ (n=9).

Consequently, we also assessed if MDA-MB-231 cells treated with Antp-DN-MAML1 were undergoing apoptosis. For this purpose, treated cells were stained with Annexin V. The human vascular anticoagulant Annexin V is a Ca^{2+} dependent phospholipid binding protein that binds phosphatidylserine with high affinity. This phospholipid is located on the cytoplasmic side of the cellular membrane. When a cell undergoes apoptosis, phosphatidylserine flips to the outside where it can be detected by Annexin V conjugates. This staining is specific for early apoptosis when dyes such as DAPI are still excluded by the plasma membrane. In this experiment, different doses of doxorubicin were used a control for early and late apoptosis based on a calibration curve (Figure 3.24). Doxorubicin IC_{50} was determined to be 0.16 μM (72 hour treatment). An IC_{50} value of 1.26 ± 0.39 is reported in the literature for doxorubicin treatment of MDA-MB-231 cells for 24 hours.

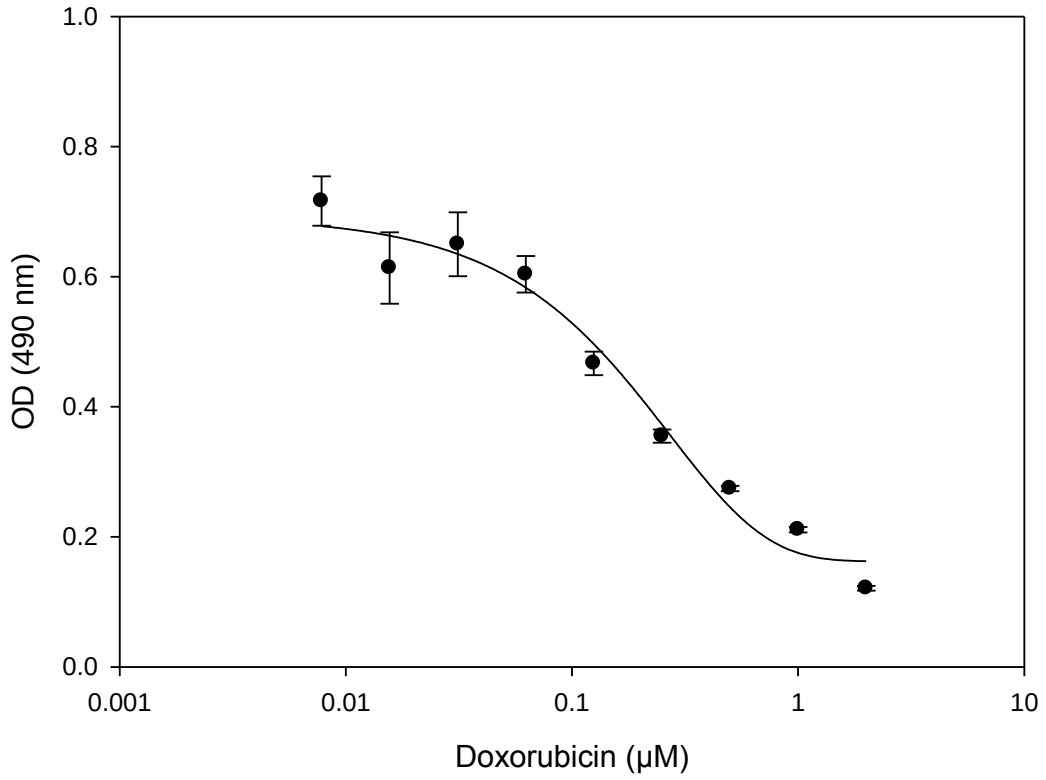

Figure 3.24: Proliferation of MDA-MB-231 cells upon exposure to doxorubicin. Cells were plated in a 96 well plate at a density of 5,000 cells per well. Cells were treated with doxorubicin at the concentrations shown 48 hours after plating. The MTS reagent was added following a further 72 hours incubation. Each point represents the mean ± standard deviation of triplicates. Curve fitted using SigmaPlot® software. 1% DMSO (OD_{490}= 0.79) does not affect cell proliferation compared to the untreated control (OD_{490}= 0.7).

MDA-MB-231 cells treated with Antp-DN-MAML1 show a dose dependent increase in Annexin V (early apoptosis) and Annexin V/DAPI positive cells (late apoptosis) compared to Antp (Figure 3.25). The cell population shifts from the bottom left quadrant towards the right (Annexin V positive) and up (Annexin V and DAPI positive) with increasing drug concentration. A similar pattern is observed in the positive control doxorubicin where cells treated with the low dose are undergoing early apoptosis whereas those treated with a high concentration are in the late apoptosis phase. Data collected from three independent experiments was combined and plotted in Figure 3.26. In parallel, cells were also collected for qRT-PCR analysis of p21 gene expression levels (Figure 3.27). As expected, p21 expression in MDA-MB-231 cells was increased in a dose-dependent manner upon exposure to Antp-DN-MAML1 compared to controls. The dose response curves for p21 and induction of apoptosis were very similar.

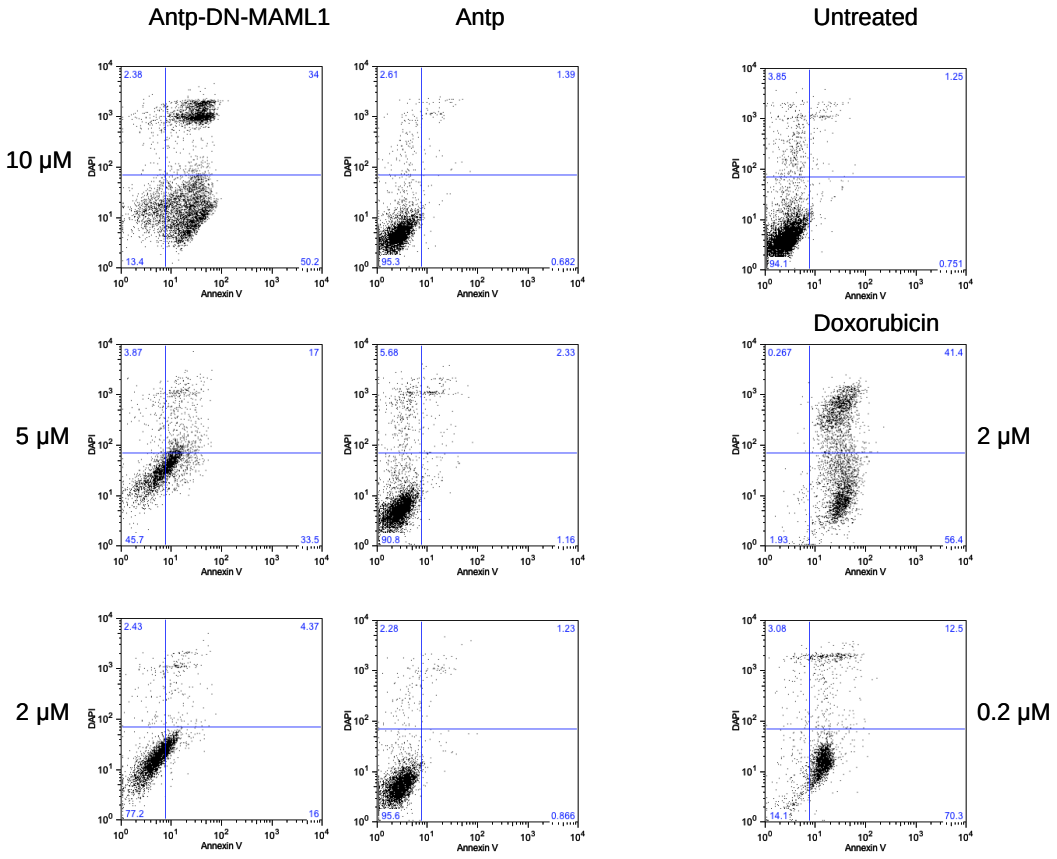

Figure 3.25: Apoptotic cells determined with Annexin V-DAPI staining followed by flow cytometry. MDA-MB-231 cells were plated in a 48 well plate at a density of 15,000 cells per well. After 48 hours, cells were treated with varying concentrations of Antp-DN-MAML1 or Antp, in triplicate (a singe plot representative of the triplicates is shown). The following controls were also included: doxorubicin (2 µM and 0.2 µM) and media only. After 72 hours, cells were stained with Annexin V PE and DAPI. Bottom left quadrant: live cells, bottom right: early apoptosis, top right: late apoptosis, top left: dead cells.

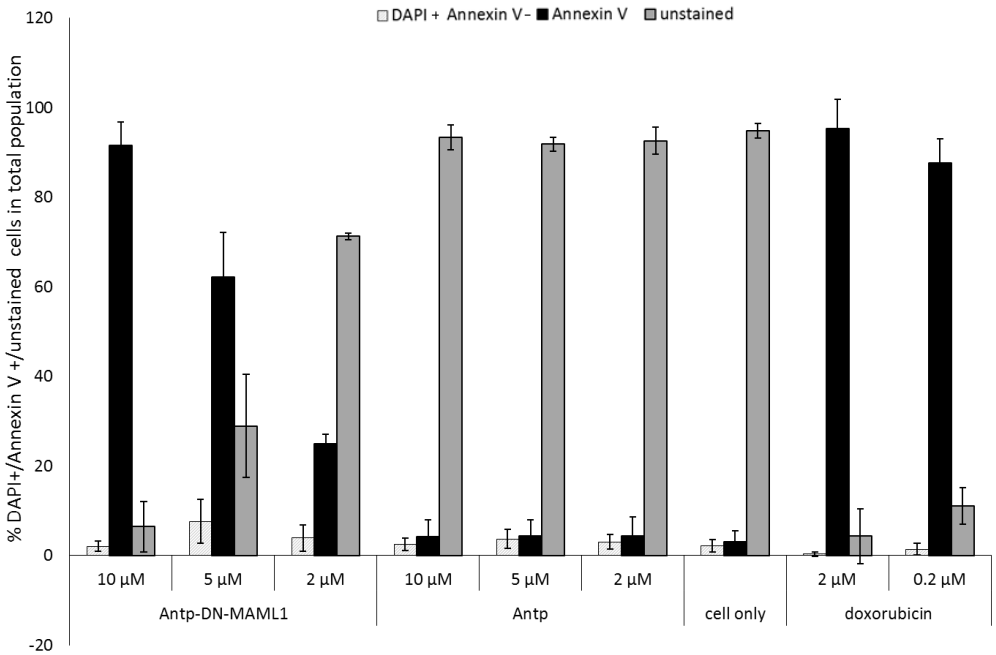

Figure 3.26: Induction of apoptosis by Antp-DN-MAML1 shown by Annexin V-DAPI staining. Error bars represent the standard deviation between triplicates from three independent flow cytometry experiments. Data for the bottom right and top right quadrants of Figure 3.25 was combined as annexin V positive.

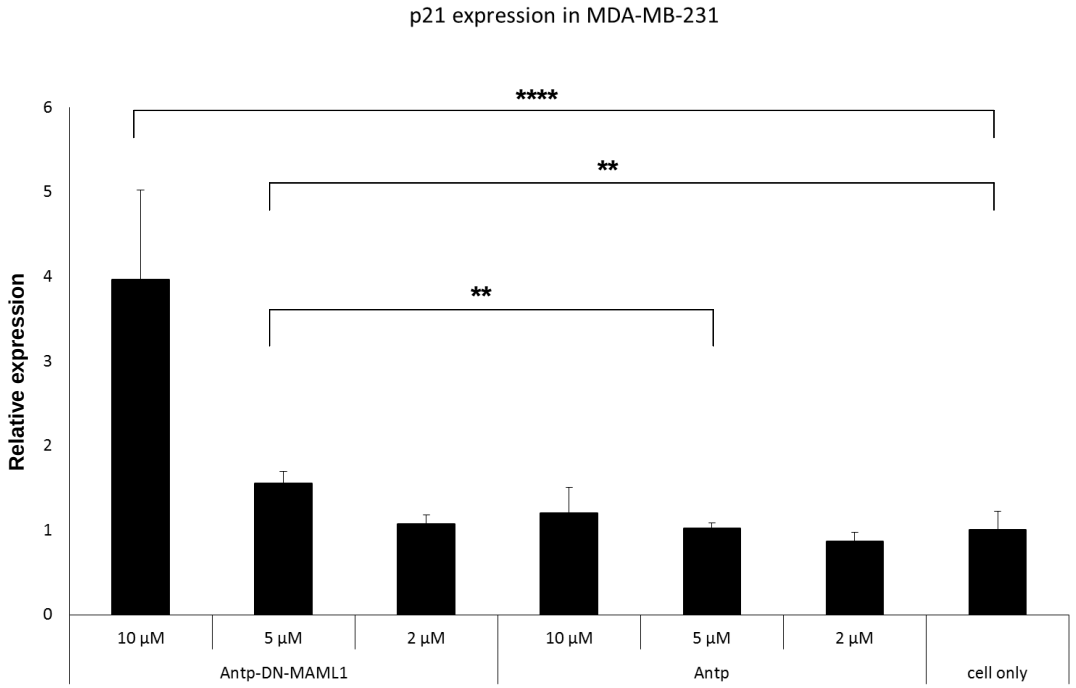

Figure 3.27: p21 expression in MDA-MB-231 cells treated with Antp-DN-MAML1. MDA-MB-231 cells were plated in a 48 well plate at a density of 15,000 cells per well. After 48 hours, cells were treated with varying concentrations of Antp-DN-MAML-1 or Antp. After 24 hours, cells were harvested and p21 mRNA expression analysed by qRT-PCR. Ct were normalized to 18s mRNA and relative expression compared to cell only control. Data are mean + standard of multiple independent experiments. One-way ANOVA was used to statistically compare conditions; $p \leq 0.05$ was considered significant. **$p \leq 0.01$ (n=6), ****$p \leq 0.0001$ (n=9).

3.3.4 *In vivo* characterisation of Antp-DN-MAML1

The effects of Antp-DN-MAML1 on MDA-MB-231 proliferation were assessed in *in vitro* models. It was also necessary to assess the compound's efficiency *in vivo*. For this, BALB/c nude mice were inoculated with MDA-MB-231 cells subcutaneously. The tumours were left to grow to an appropriate size before the start of treatment. Antp-DN-MAML1 was injected at 4mg/kg, 3 times per week for a total of 11 doses. Control groups consisted of paclitaxel treatment at 10mg/kg and saline only (0.1 ml). Tumour sizes were calculated as (LxWxW)/2 and plotted as a percentage change from the day treatment started (Figure 3.28). The data shown is from a single representative experiment out of three repeats. Tumours treated with Antp-DN-MAML1 only marginally increased in size compared to controls. In fact, the animals in both control groups had to be culled before the end of Antp-DN-MAML1 treatment for humane reasons. In conclusion, Antp-DN-MAML1 inhibits MDA-MB-231 tumour growth *in vivo*.

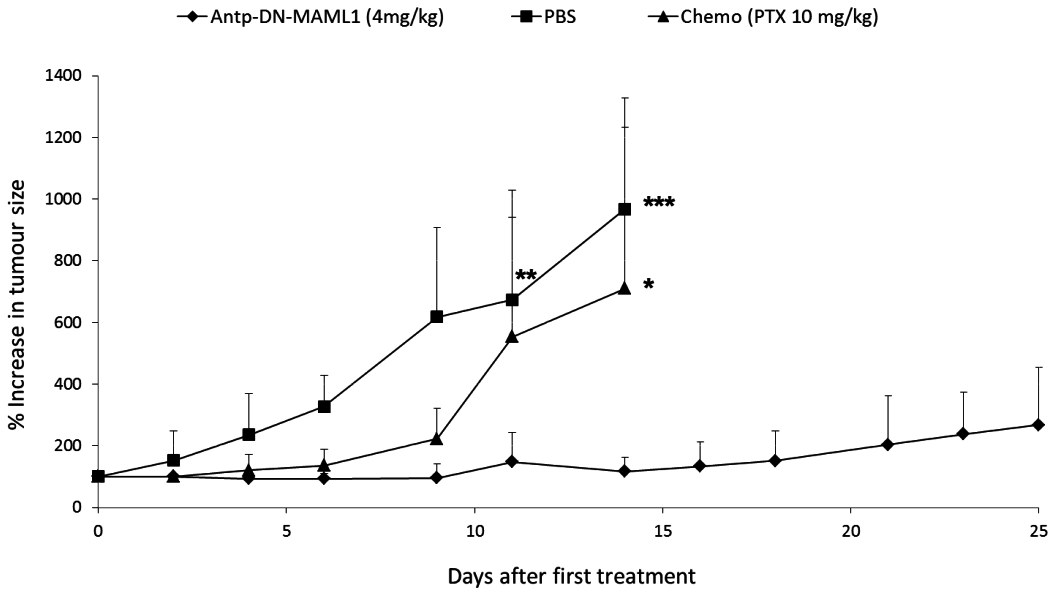

Figure 3.28: Antp-DN-MAML1 therapy of MDA-MB-231 tumours in BALB/c nude mice. Control animals (PTX: paclitaxel and PBS) had to be culled early for humane reasons. Tumour sizes were calculated as (LxWxW)/2 and plotted as a percentage change from the day treatment started. One-way ANOVA was used to statistically compare conditions; $p \leq 0.05$ was considered significant. *$p \leq 0.05$, **$p \leq 0.01$, ***$p \leq 0.001$. All procedures were carried out by Mr. Daniel Wells of the CBS (ICL).

Discussion

In order to test the effects of the Antp-DN-MAML1 fusion protein as a Notch inhibitor, it was necessary to produce this protein and the negative control Antp. It was important to assess Antp in parallel due to its interactions with the membrane and possible disruption of cellular functions. The effects of DN-MAML1 alone were not assessed as this protein can not cross the membrane or disrupt cellular signalling. The aim for the production of Antp was to express it as a soluble protein. Refolding of Antp is not advisable due to its strong α-helical content and previous experience at Trojantec. Expression of Antp as a secreted protein was attempted as this strategy is best suited for expression of Antp-scFv fusions, to allow the formation of disulphide bonds. Despite numerous attempts, Antp expression as a secreted protein was unsuccessful. The observation of bacterial lysis upon addition of IPTG suggested severe toxicity of Antp to the host cells. Interestingly, Palm et al. describe the internalisation of penetratin into *E.coli* with an associated antimicrobial effect (Palm et al., 2006). Antp was finally produced by cytoplasmic expression and purified based on its high positive charge and small size. Circular dichroism analysis of Antp confirmed the correct folding of this protein. Future studies involving the use of more elaborate methods such as NMR could provide more detailed structural information about recombinant proteins produced.

The initial attempts of Antp-DN-MAML1 production showed expression of this protein in inclusion bodies. The purification of Antp-DN-MAML1 was carried out under denaturing conditions, making use of the N-terminal His tag. Despite encouraging expression yields and successful purification, refolding of denatured Antp-DN-MAML1 was unsuccessful. Improvement of the expression and purification protocols was attempted in this study and by several collaborators and contractors. It is important to note that protocols in the literature for production of DN-MAML1 involve refolding (Nam et al., 2003). Thus, it is possible that the insolubility of DN-MAML1 underlies the production problems encountered for the fusion protein. Expression of Antp-DN-MAML1 as a soluble protein was achieved in an expression trial where different IPTG concentrations and induction times were evaluated. Soluble expression was dependent on the length of induction. Whereas a portion of Antp-DN-MAML1 is soluble in the first hours following induction, the same protein is insoluble following an overnight incubation. This suggests a strain on the host cells in producing soluble protein resulting in loss of plasmid and cell death. Interestingly,

further studies by Prof. Cole (University of Birmingham) found Antp-DN-MAML1 to be associated with membranes rather than in inclusion bodies (personal communication). This highlights the difficulty of producing a protein that interacts with membranes by a mechanism that is not well understood. Several attempts to purify soluble Antp-DN-MAML1 by both affinity and ion exchange chromatography were unsuccessful. The inability of the His tag to bind the resin under native conditions was also observed by our collaborators. This suggests that Antp-DN-MAML1 folds in such a way to render the tag inaccessible. It is important to note that the positive charge on Antp might also interfere with the affinity binding. Affinity chromatography is a powerful tool especially for the isolation of small amounts of recombinant protein from complex mixtures. Consequently, future studies should attempt the use of different tags (GST, FLAG or other) and/or alternative positions (C-terminal, different linker lengths). In particular, epitope based tags such as FLAG have been shown to yield comparatively higher purity protein but require expensive, low capacity resins. In the future, one could also explore the use of antibodies against the His tag in order to successfully isolate the protein of interest. Finally, Antp-DN-MAML1 was produced as a synthetic peptide. The relatively small size of the fusion is at the limit of what synthesis can achieve. Despite this, synthesis was successful producing a protein with high degree of purity.

The luciferase reporter-gene assay allows for a direct assessment of Notch signalling as activation of Notch2 receptor leads to quantifiable luciferase readouts. Consequently, this method can provide information about the mode of Antp-DN-MAML1 action, specifically related to Notch signalling. We observed a significant inhibition of luminescence compared to controls induced by Antp-DN-MAML1. This was not due to cytotoxicity as CHO cell viability was unaltered. These results suggest that Antp-DN-Maml-1 is able to translocate into cells and inhibit Notch-mediated transcriptional activation.

Inhibition of Notch signalling and Antp-DN-MAML1 functionality was further assessed by analysing expression levels of the Hes1 gene as it is known to be a target gene of Notch signalling. Hes1 expression was assessed in both MDA-MB-231 and BMDC models. It is important to note that basal levels of Hes1 expression are considerably elevated in the cancer cell line compared to the primary cells. This supports the observation that Notch signalling is deregulated in MDA-MB-231 cells. By contrast, there is low constitutive expression of Hes1 in BMDC and therefore

Notch signalling was stimulated in these cells with immobilised Jagged1. It is interesting to note that TNF-α cytokine expression levels, examined in parallel with Hes1 expression, were elevated upon addition of Antp-DN-MAML1, compared to controls (data not shown). This is unlikely to be due to bacterial products such as lipopolysaccharide in the protein as it had been produced by peptide synthesis. However, the fusion of the *Drosophila* protein Antp and a truncated MAML1 might create new epitopes recognised by the TLR/NLR receptors.

Several lines of evidence suggest that Antp-DN-MAML1 can repress Notch target gene expression. However, it is unclear whether Antp-DN-MAML1 affects proliferation of MDA-MB-231 cells through inhibition of Notch signalling. The MTS cell proliferation assay revealed that Antp-DN-MAML1 had a strong growth-inhibitory effect (IC_{50}: 1.61μM) when added to MDA-MB-231 cells for 72h. The commercial GSI-1, used as a positive control, showed an IC_{50} of approximately 0.55 μM, consistent with the value of 1.3 μM obtained by (Rizzo et al., 2008) at 48 hours. The difference between Antp-DN-MAML1 and the GSI-1 could be explained by the ability of GSIs to inhibit a variety of other signalling pathways in addition to Notch (Beel and Sanders, 2008). In the same experiment, addition of a different GSI, DAPT, did not have any effect on MDA-MB-231 cell proliferation, despite its effect on Hes1 expression. This is consistent with the findings of a study by Han et al. They argue that the observed cytotoxicity of GSI-1 on breast cancer cells in not due to disruption of γ-secretase activity but to proteasome inhibition (Han et al., 2009). Therefore, the MTS experiment does not demonstrate a direct link between inhibition of Notch signalling and inhibition of proliferation of the MDA-MB-231 breast cancer cell line. A previous study by Moellering et al., showed inhibition of Notch signalling using stapled MAML-1 peptides (Moellering et al., 2009). This inhibition resulted in the arrest of T-ALL cell proliferation. As a causative role for deregulated Notch in T-ALL is well established, this model is best suited to study the consequences of Notch inhibition on cell proliferation. In this study, the T-ALL model could have been useful to study the biological effects of Antp-DN-MAML1 and should be considered for future studies.

In order to understand the anti-proliferative effect of Antp-DN-MAML1 on MDA-MB-231, it was important to consider other functions of MAML-1 aside from its effects on the Notch pathway. A study by Zhao et al. revealed that MAML-1 can interact with p53 via its N-terminal region (1-302), increasing transactivation of the

target gene p21 (Zhao et al., 2007). Therefore, it was possible that MAML-1 (13-74) could bind and stabilise p53, increasing p21 expression and leading to cell death by apoptosis (see section 1.1.11). In future studies, binding of MAML-1 (13-74) to p53 should be assessed. Assessment of p21 expression levels by qRT-PCR revealed an increase upon treatment of MDA-MB-231 cells with Antp-DN-MAML1 but not with controls. Experiments using flow cytometry confirmed that MDA-MB-231 cells died by apoptosis rather than necrosis. p21 expression showed an increase when assessed in parallel. Doxorubicin was used as a positive control, showing an IC_{50} value of 0.16 μM (72 hour treatment). An IC_{50} value of 1.26 ± 0.39 is reported for doxorubicin treatment of MDA-MB-231 cells for 24 hours (Costantini et al., 2010).

Based on the results obtained in the *in vitro* studies using Antp-DN-MAML1 to inhibit MDA-MB-231 cell proliferation, an *in vivo* study was designed to test the effect of this drug on tumour growth in mice. Mice were xenografted with the same cells, MDA-MB-231, the choice of doses and therapy schedule being based on previous experience in the laboratory. Antp-DN-MAML1 was injected in parallel with PBS and paclitaxel as controls. Paclitaxel (Taxol) is a mitotic inhibitior used as a standard for chemotherapy of breast cancers. Antp-DN-MAML1 treatment resulted in tumours only marginally increasing in size compared to controls. In these experiments, the reasons for inhibition of tumour growth were not assessed but, given the *in vitro* data, it is possible that they are unrelated to the inhibitory effect of Antp-DN-MAML1 on Notch signalling but related to its effects on promoting apoptosis.

Concluding remarks

This study showed successful production of the control protein Antp confirming soluble expression as the preferred method of expression for the correct folding of this protein. Native folding with the characteristic triple helix is believed to be a key factor in the function of this protein as a carrier for intracellular delivery.

Fusion of the Antp protein to its cargo DN-MAML1 increased the difficulty in the production of this fusion. Despite several attempts to optimise the expression and refolding protocols, Antp-DN-MAML1 was finally obtained through peptide synthesis.

In vitro studies demonstrated the ability of Antp-DN-MAML1 to inhibit the Notch pathway although it was also shown to affect p53 target gene expression. The fusion protein affects proliferation of MDA-MB-231 cells *in vitro* and *in vivo*. The study

suggests that this effect might be due to concurrent modulation of cellular pathways including Notch and p53 signalling.

CHAPTER 4

Phage display selection of a scFv against DN-MAML1 and its fusion to Antp

4.1 Introduction

The aim of this part of the project was to inhibit Notch signalling using antibody fragments fused to Antp to enable their successful intracellular delivery. Once internalised, the fusion should block tripartite complex formation by targeting MAML-1 interactions with N^{IC} and CSL. As residues 13–74 constitute the minimal MAML-1 portion necessary to form the active complex, we expected any scFv that binds this portion to inhibit downstream signalling. As a scFv binding to MAML-1 (13-74) is not readily available, the technique of phage display was employed to select such scFv from an ample library.

Several factors affect the successful outcome of a phage display selection (Figure 4.1) including:

Antigen utility

The quality and condition of the target antigen are of extreme importance for a successful selection. Two strategies of antigen exposure are widely used: direct immobilisation of the antigen on microtitre plates (Marks et al., 1991) or solution capture with biotinylated antigen (Hawkins et al., 1992; Sawyer et al., 1997). In the latter, isolation of the biotinylated antigen following binding is achieved using paramagnetic beads coupled to avidin.

Selection strategy

When the phage library is exposed to the antigen, there are various variables to take into account including: the length of binding time, pH and ionic strength, temperature, coated antigen levels and the stringency of washes. In the first round of selection, washes are less stringent to account for the low presence of individual clones (Schier and Marks, 1996). Washes become more stringent in subsequent rounds to select high affinity binders. In an industrial setting, multiple combinations of different settings would be assessed using a robotic system.

Elution

Various methods are used to elute the bound phages: alterations in pH using glycine or TEA based buffers (Griffiths et al., 1993), elution with excess antigen (Clackson et al., 1991), proteolytic/chemical cleavage between the coat protein and antibody

fragment (Goletz et al., 2002). Following elution, output phages are amplified by infection of *E.coli* before a second round of selection. In most cases, 3-4 rounds of phage display are sufficient for successful enrichment of high-affinity antigen binding clones.

Screening

Screening of output clones can occur at various stages of the phage display selection. This consists of phage-ELISAs to assess antigen specificity and ELISAs with soluble scFvs to check for functional expression levels. Further analysis includes DNA sequencing.

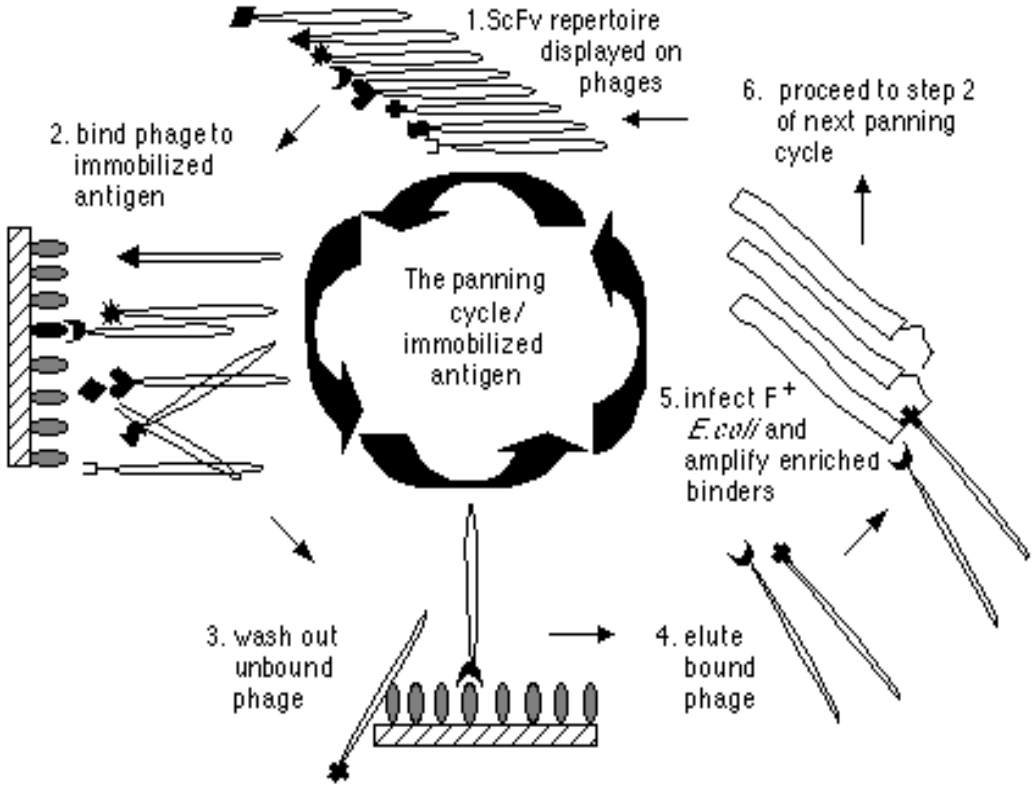

Figure 4.1: The phage display selection cycle. Taken from *Current Protocols in Immunology* (2002) Unit 10.19B.

The phage display vector system allows for expression of scFvs fused to pIII and scFvs alone without the need for re-cloning. Expression is switched between the two types depending on which bacterial strain is employed. In the amber suppressor strain XL1-blue, the amber stop codon present between the scFv and pIII is read through as

a Glu residue. In non-suppressing *E.coli* HB2151 the presence of the stop codon halts transcription.

Binding of the scFv-phagemid or purified scFv candidates to MAML-1 (13-74) is verified by ELISA binding studies. This colorimetric assay allows the detection of protein binding to a coated antigen. Measurement of binding relies on substrate conversion by an enzyme conjugated onto a primary or secondary antibody.

4.2 Aims and objectives

- Following a cloning step, express, purify and refold DN-MAML1 according to an established protocol. Carry out a circular dichroism analysis of the DN-MAML1 protein to confirm its correct refolding.
- Verify successful coating of DN-MAML1 onto the surface of phage display tubes and undergo three rounds of phage display selection.
- High through put screening of anti-DN-MAML1 scFv-phagemid by ELISA followed by selective screening on a bigger production scale.
- Sequencing analysis of the scFv candidates in order to eliminate any identical clones and to identify any stop codons.
- Carry out the expression of candidate scFvs as secreted proteins using the HB2151 *E.coli* strain and purify the proteins by affinity chromatography.
- scFv binding studies by ELISA to determine the individual K_d values.
- Following cloning, optimise the expression protocol for production of Antp-scFv fusions, evaluating the use of a secretion system.
- Determine the K_d value for Antp-scFv fusions binding to DN-MAML1.

4.3 Results

4.3.1 Expression, purification and characterisation of DN-MAML1

To our knowledge, a scFv binding MAML-1 (13-74) is not available. Therefore, it was necessary to express and purify this truncated version of MAML-1 as the antigen for a phage display selection. MAML-1 (13-74) corresponds to the DN-MAML1 portion of our fusion protein Antp-DN-MAML1. Following a cloning step to excise Antp from the pRSET A construct (see section 2.1.3), DN-MAML1 was successfully expressed intracellularly in BL21 (DE3) pLysS cells (Figure 4.2).

Table 4.1: DN-MAML1 characteristics derived from ProtParam on the ExPASy Server

parameter	**value**
Theoretical pI	10.76
Molecular weight (Da)	7454.6
Amino acid residues	62
Extinction coefficient (M^{-1} cm^{-1})	1490

However, solubilisation of DN-MAML1 from inclusion bodies was necessary (Figure 4.2). The denatured protein was purified by IMAC. All samples were analysed by reducing 12% SDS-PAGE and stained using Coomassie Blue (Figure 4.2A). A Western blot using HRPO conjugated murine α-His antibody was also performed to confirm the identity of the purified protein (Figure 4.2B). DN-MAML1 was present in the elution fractions as a band migrating between 15 kDa and 10 kDa. This is greater than its predicted molecular weight of 7.5 kDa and could be due to the high positive charge on DN-MAML1 (Table 4.1).

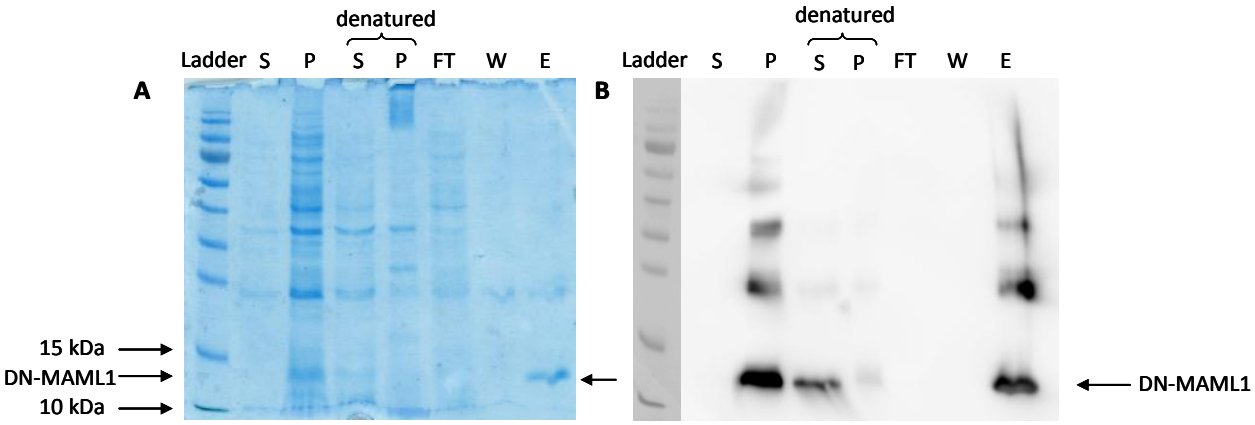

Figure 4.2: Expression and purification of DN-MAML1 in pRSET A transformed in BL21 (DE3) plysS cells. The bacterial culture was grown in 500 ml of LB media up to an OD_{600} of 0.8. The culture was then induced using 1 mM IPTG overnight at 37°C. The supernatant (S) and pellet (P) fractions of the expression culture were analysed by reducing 12% SDS-PAGE, stained using Coomassie Blue (A). The corresponding α-His Western blot is also shown (B). DN-MAML1 is present, as a band migrating between 15 kDa and 10 kDa. The cell pellet was lysed under denaturing conditions. DN-MAML1 is present exclusively in the soluble (S) fraction as a denatured protein. This was applied to an IMAC column. The column was washed (W) extensively before elution (E) of DN-MAML1.

DN-MAML1 was refolded by extensive dialysis against 5% acetic acid. As illustrated in Figure 4.3A, the majority of DN-MAML1 was recovered in the soluble phase whereas most contaminants precipitated upon refolding. Finally, DN-MAML1 was lyophilised overnight and re-dissolved in dH_2O (Figure 4.3B). The DN-MAML1 prep is over 90% pure.

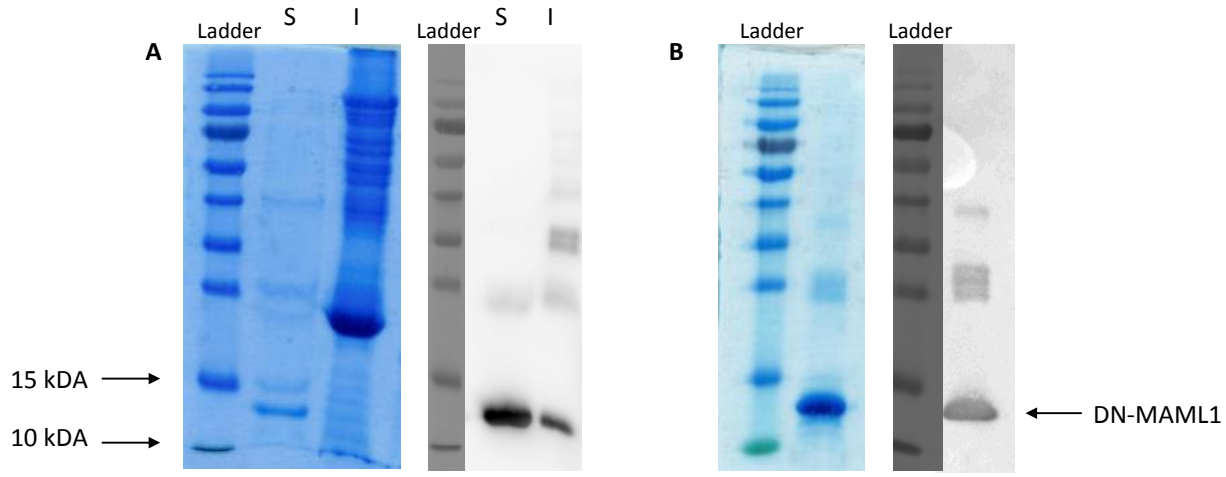

Figure 4.3: DN-MAML1 refolding. A) Following dialysis against 5% acetic acid for 24 hours, the insoluble (I) was separated from the soluble (S) material by centrifugation. Both fractions were analysed by reducing 12% SDS-PAGE, stained using Coomassie Blue. The corresponding α-His Western blot is also shown. B) DN-MAML1 was lyophilised overnight and re-dissolved in dH_2O.

In order to confirm the secondary structure and folding properties of DN-MAML1 following refolding, circular dichroism analysis was performed on the purified protein. Different structural elements have characteristic CD spectra (Figure 2.2). As shown in Figure 4.4, the CD spectra of DN-MAML1 suggests a strong α-helical content of 41%. This value is inferior to the predicted α-helical content of 63% assigned to DN-MAML1 *in silico*. This could be due to sub optimal refolding of the protein.

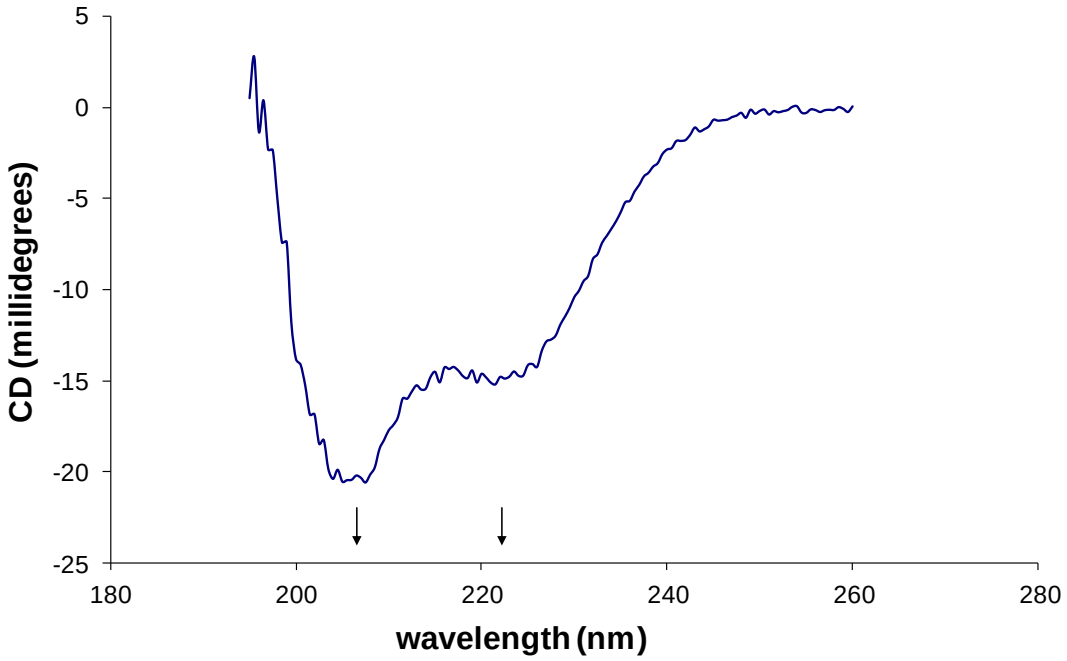

Figure 4.4: Circular dichroism spectra of DN-MAML1 at 100 µg/ml in dH_2O using a 1mm path cuvette.

In order to determine the coating efficiency of DN-MAML1 on ELISA plates, this protein was serially diluted in PBS pH 7.4 and coated overnight. Following blocking, coated protein was detected using α-His HRPO IgG (Figure 4.5). A concentration of 20 μg/ml was chosen for further experiments.

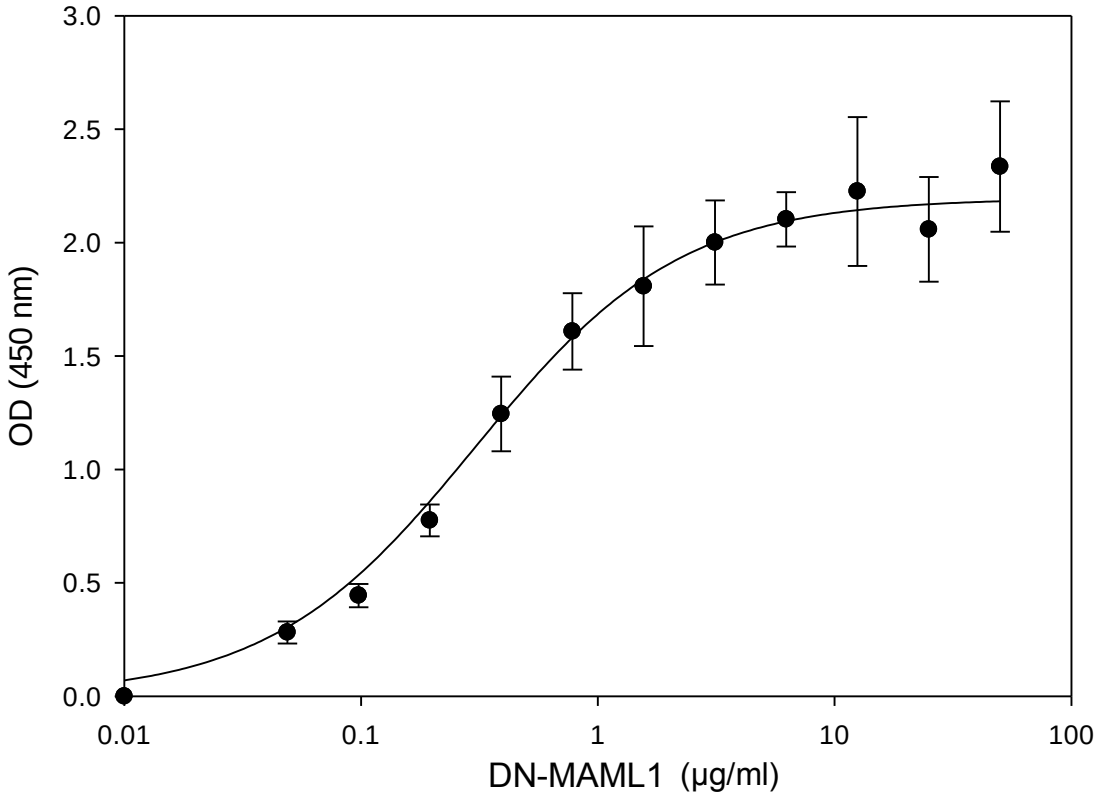

Figure 4.5: ELISA showing coating efficiency of DN-MAML1 on plastic plates. DN-MAML1 was serially diluted, coated onto an ELISA plate overnight and detected by α-His IgG. Absorbance values at 450 nm were measured and background signals (no coated protein) were deducted. Error bars represent the standard deviation between triplicates. Curve fitted using SigmaPlot® software.

4.3.2 Phage display

After three rounds of affinity selection (biopanning), approximately 500 colonies were screened on a 96 well plate format to identify antigen-binding scFv-displaying monoclonal phage. Briefly, single colonies were grown in order to rescue monoclonal phage and assess its binding on ELISA plates coated with 20 μg/ml of DN-MAML1. The results of this initial screening are shown in Figure 4.6, where ‘hits’ have been highlighted with arrows and colony reference name.

Plate 1

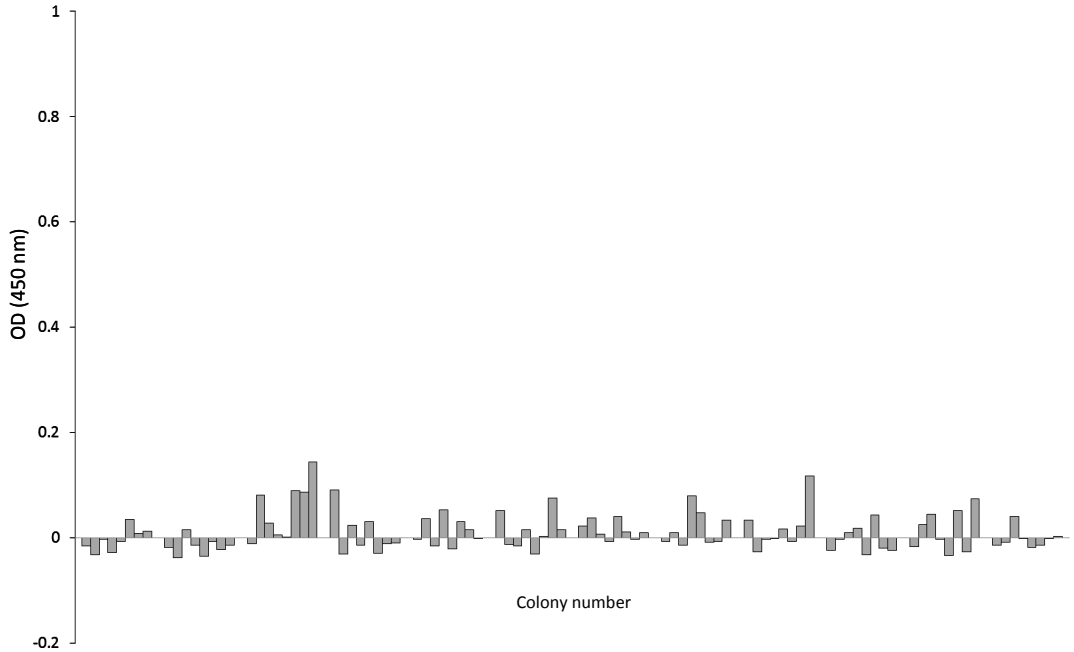

Plate 2

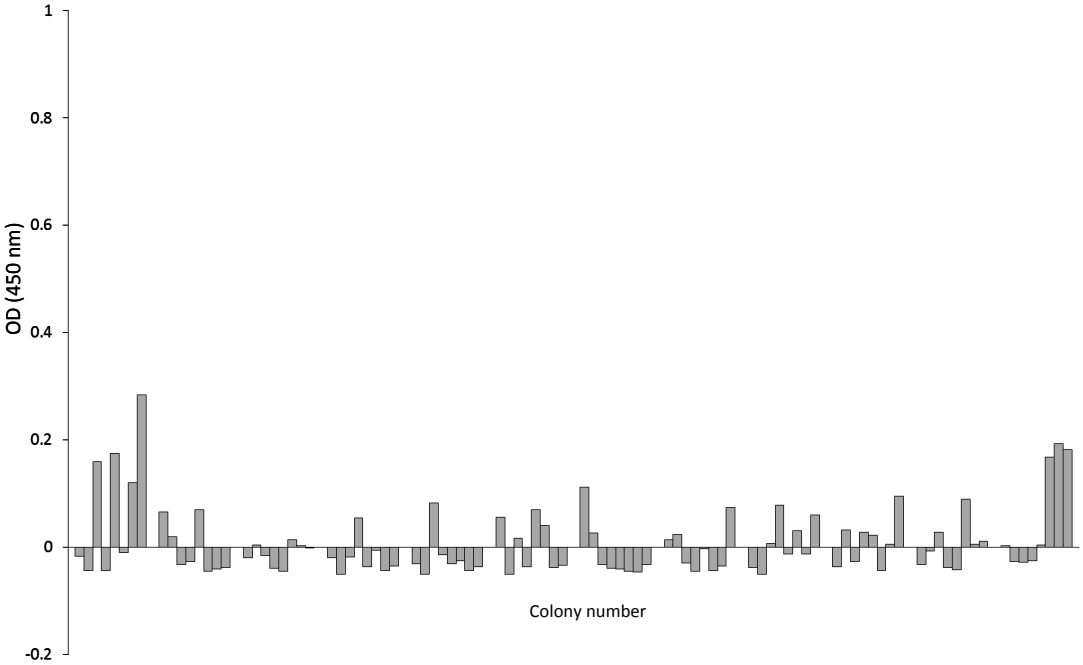

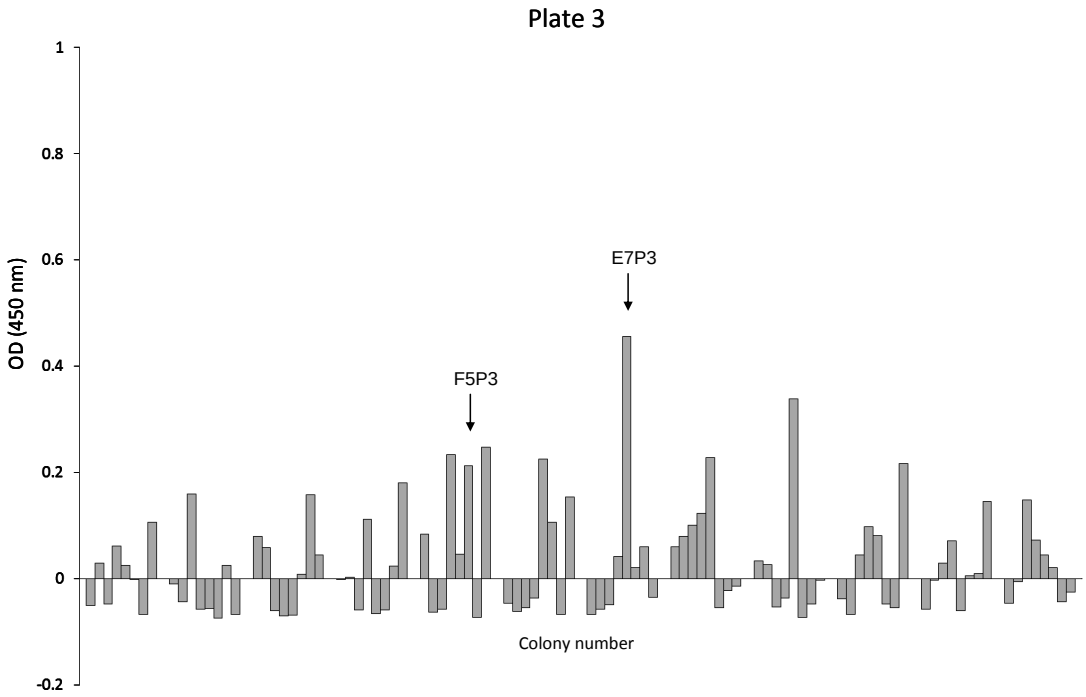
Plate 3
OD (450 nm)
1
0.8
0.6
0.4
0.2
0
-0.2
E7P3
F5P3
Colony number

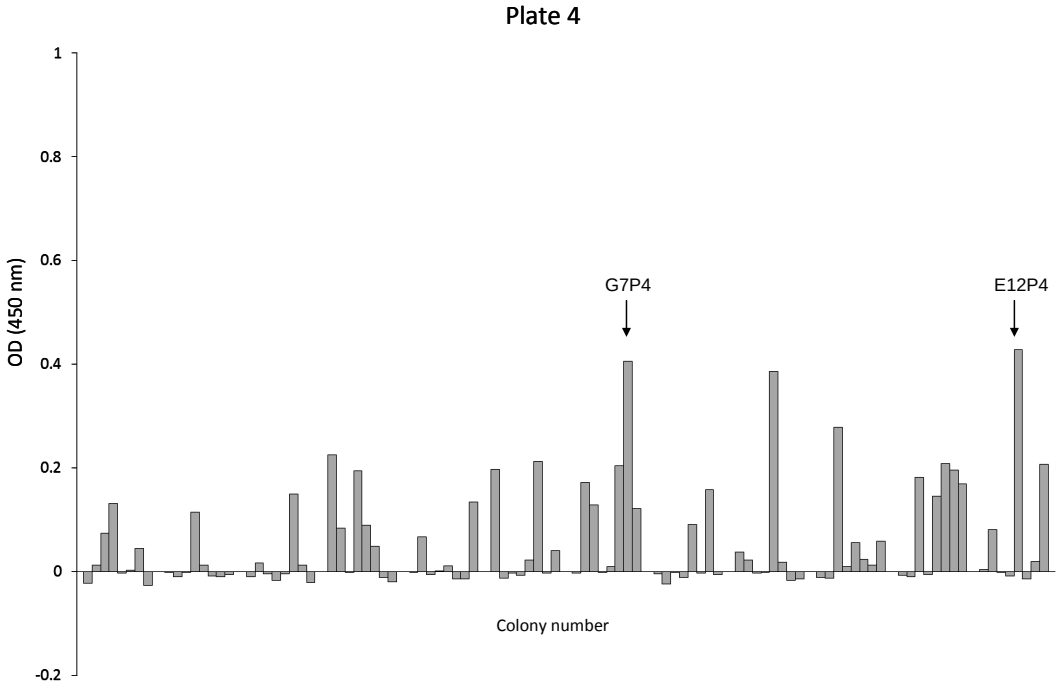
Plate 4
OD (450 nm)
1
0.8
0.6
0.4
0.2
0
-0.2
G7P4
E12P4
Colony number

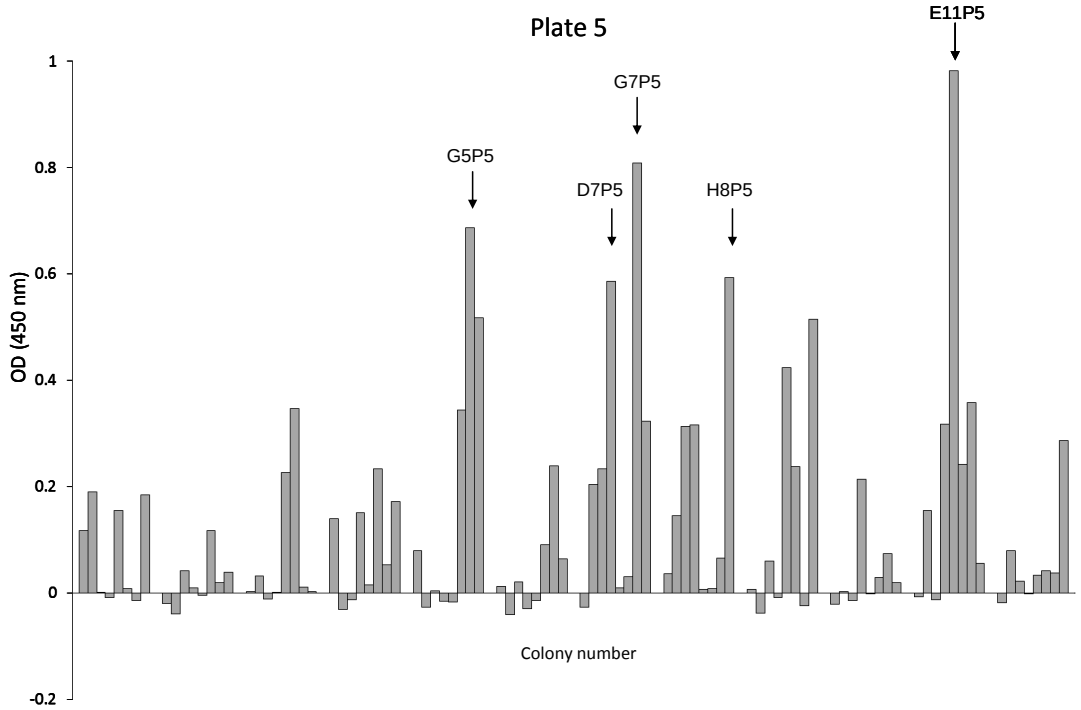

Figure 4.6: Screening of candidate monoclonal phage by ELISA (plates 1 to 5). Binding of the scFv-diplaying phage to DN-MAML1 was detected using Anti-M13 and is represented by high absorbance reading at 450 nm. The background absorbance value was deducted from all readings. Clones were selected based on high absorbance values relative to the corresponding plate and are indicated by an arrow.

Promising candidates were subsequently screened on a 5 ml culture format with recovery of rescued phages by PEG/NaCl precipitation. At this screening stage, E11P5 and G5P5 rescued phage did not show consistent strong binding to DN-MAML1 and was consequently discarded (Figure 4.7).

The remaining rescued phage candidates (excluding E12P4) showed strong binding to DN-MAML1 but not to uncoated ELISA plates, thus eliminating the possibility of having selected plastic surface binders (Figure 4.8). The reason for E12P4 not showing any binding, could be the unsuccessful precipitation of rescued phage or the instability of this clone.

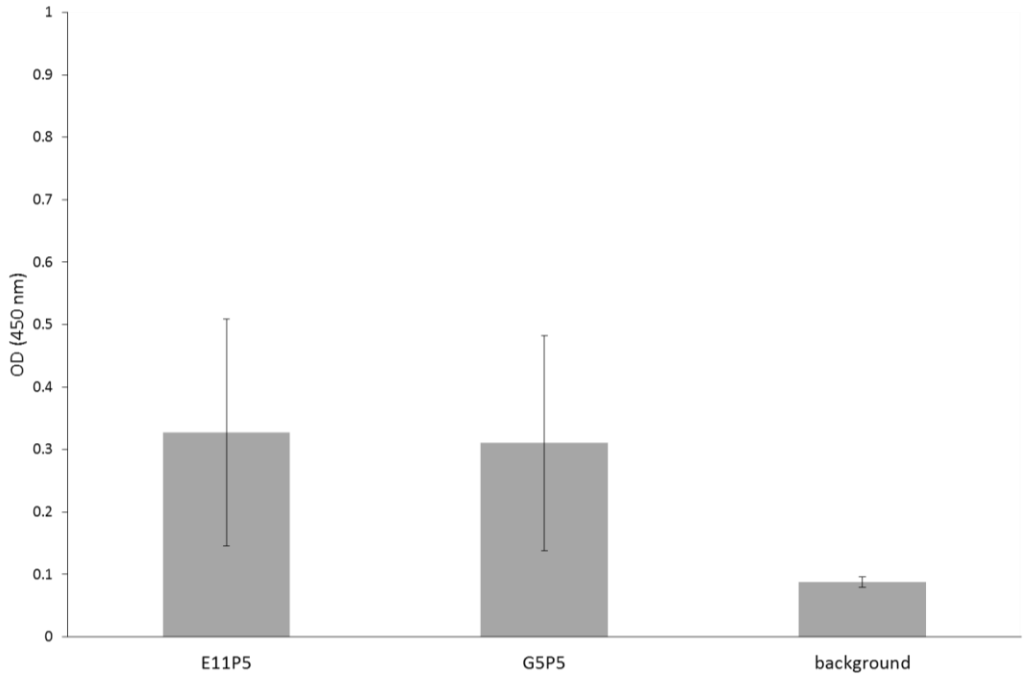

Figure 4.7: Binding of rescued E11P5 and G5P5 scFv-phagemid to DN-MAML1. Binding was detected using Anti-M13 and is measured by an absorbance reading at 450 nm. Error bars represent the standard deviation between triplicates.

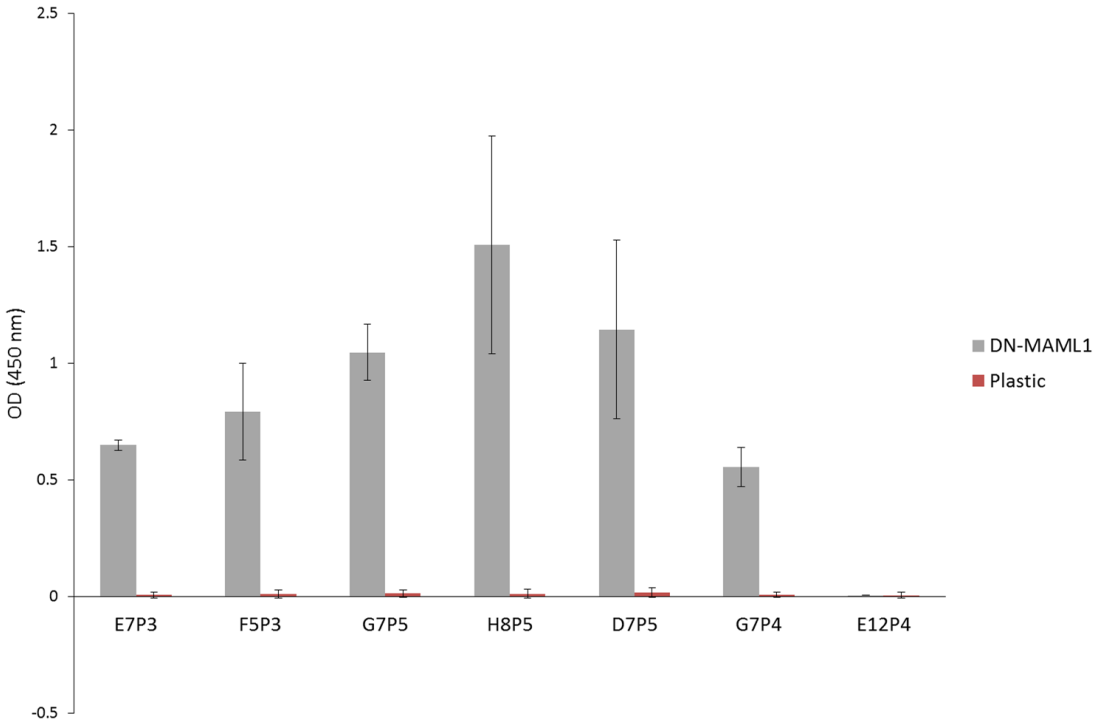

Figure 4.8: Screening of rescued monoclonal scFv-phagemid by ELISA. Binding of the scFv-displaying phage to DN-MAML1 (grey bars) was detected using Anti-M13 and is represented by high absorbance reading (>0.5) at 450 nm. The background absorbance value was deducted from all readings. Binding to uncoated ELISA plates was assessed in parallel to eliminate any plastic surface binders (red bars). Error bars represent the standard deviation between triplicates.

In order to distinguish between identical and unique clones amongst positive binders, their DNA was sequenced. As shown in Figure 4.9, the seven candidates resulted to be three unique clones. In particular, G7P4 = G7P5 = E12P4 = D7P5 and E7P3 = F5P3. Sequence analysis also revealed a stop codon at the start of the E7P3 (F5P3) open-reading frame which had to be removed by single point mutation (section 2.1.3) before expression in the HB2151 strain.

```
G7P4        PAMAQVQLLQSAGGLVQPGGSLRLSCAASGFNFNNYAMSWVRQAPGKGLEWVSDISGTGG
G7P5        PAMAQVQLLQSAGGLVQPGGSLRLSCAASGFNFNNYAMSWVRQAPGKGLEWVSDISGTGG
E12P4       PAMAQVQLLQSAGGLVQPGGSLRLSCAASGFNFNNYAMSWVRQAPGKGLEWVSDISGTGG
D7P5        PAMAQVQLLQSAGGLVQPGGSLRLSCAASGFNFNNYAMSWVRQAPGKGLEWVSDISGTGG
H8P5        PAMAQVQLLQSAGGLVQPGGSLRLSCTASGFIFN-YAMSWVRQAPGKGLEWISGISLGGD
E7P3        PAMA-VQLQESGPRLVKPSETVSLRCAVSGASVTSYSWNWIRQAPGKGLEWIGYFSKYG-
F5P3        PAMA-VQLQESGPRLVKPSETVSLRCAVSGASVTSYSWNWIRQAPGKGLEWIGYFSKYG-
                    x   ** ***  * ***** * **  ***** *** *          **** ** *
                                      #    #  #                  # #  ## #

G7P4        TTKYADSVKGRFTISRDNSKNTLYLQMNSLRAEDTAIYYCAKRYCSGGSCYSIDHWGQGT
G7P5        TTKYADSVKGRFTISRDNSKNTLYLQMNSLRAEDTAIYYCAKRYCSGGSCYSIDHWGQGT
E12P4       TTKYADSVKGRFTISRDNSKNTLYLQMNSLRAEDTAIYYCAKRYCSGGSCYSIDHWGQGT
D7P5        TTKYADSVKGRFTISRDNSKNTLYLQMNSLRAEDTAIYYCAKRYCSGGSCYSIDHWGQGT
H8P5        TTKYADSVKGRFTISRDTSKNTLYLQMSSLRAEDTAVYYCARRYCSGGSCYSIDHWGKGT
E7P3        NDRYNPSYKSRVTVSVDTSNNQFSLRLGSVTAADTAIYYCAK---WNDEFRAFDIWGQGT
F5P3        NDRYNPSYKSRVTVSVDTSNNQFSLRLGSVTAADTAIYYCAK---WNDEFRAFDIWGQGT
            *** ** * * * * * * * *** *** ** *   *    ************ *
                           #                 #    #              #

G7P4        LVTVSSGGGGSGGGGSGGGGSDIQMTQSPSTLSASIGDRVTITCRASEGIYHWLAWYQQK
G7P5        LVTVSSGGGGSGGGGSGGGGSDIQMTQSPSTLSASIGDRVTITCRASEGIYHWLAWYQQK
E12P4       LVTVSSGGGGSGGGGSGGGGSDIQMTQSPSTLSASIGDRVTITCRASEGIYHWLAWYQQK
D7P5        LVTVSSGGGGSGGGGSGGGGSDIQMTQSPSTLSASIGDRVTITCRASEGIYHWLAWYQQK
H8P5        MVTVSSGGGGSGGGGSGGGGSDIQMTQSPSTLSASIGDRVTITCRASEGIYHWLAWYQQK
E7P3        MVTVSSGGGGSGGGGSGGGGS-SELTQDP-AVSVALGQTVRITCQGDSLRSYYTNWFQQK
F5P3        MVTVSSGGGGSGGGGSGGGGS-SELTQDP-AVSVALGQTVRITCQGDSLRSYYTNWFQQK
            *                    ****  * *** *** ** *   *********** *
            #

G7P4        PGKAPKLLIYKASSLASGAPSRFSGSGSGTDFTLTISSLQPDDFATYYCQQY--SNYPLT
G7P5        PGKAPKLLIYKASSLASGAPSRFSGSGSGTDFTLTISSLQPDDFATYYCQQY--SNYPLT
E12P4       PGKAPKLLIYKASSLASGAPSRFSGSGSGTDFTLTISSLQPDDFATYYCQQY--SNYPLT
D7P5        PGKAPKLLIYKASSLASGAPSRFSGSGSGTDFTLTISSLQPDDFATYYCQQY--SNYPLT
H8P5        PGKAPKLLIYKASSLASGAPSRFSGSGSGTDFTLTISSLRPDDFATYYCQQY--SNYPLT
E7P3        PGQAPLLVVYAKNKRPSGIPDRFSGSSSGNTASLTITGAQAEDEADYYCHSRDSSGNHVL
F5P3        PGQAPLLVVYAKNKRPSGIPDRFSGSSSGNTASLTITGAQAEDEADYYCHSRDSSGNHVL
              *  **** ******  * *       ****   ******** *   ***** *****
                                              #

G7P4        FGGGTKLEIKRAAAHHHHHH
G7P5        FGGGTKLEIKRAAAHHHHHH
E12P4       FGGGTKLEIKRAAAHHHHHH
D7P5        FGGGTKLEIKRAAAHHHHHH
H8P5        FGGGTKLEIKRAAAHHHHHH
E7P3        FGGGTKLTVLGAAAHHHHHH
F5P3        FGGGTKLTVLGAAAHHHHHH
                ****
```

yellow: end of leader sequence blue: vH red: linker green: vL pink: His tag
x: stop codon
*: difference between G7P4 and E7P3 #: difference between G7P4 and H8P5

Figure 4.9: Amino acid sequence alignment for 7 α-DN-MAML1 scFv candidates. The amino acid sequences of 7 scFvs were aligned using ClustalW (Thomson et al. 1994).

4.3.3 Expression and purification of candidate α-DN-MAML1 scFvs

The DNA construct of each remaining candidate (G7P4, E7P3 and H8P5) was transformed in HB2151 cells for expression of secreted scFvs on a large scale. Each culture supernatant was concentrated, dialysed into PBS pH 7.4, and applied to an IMAC column (nickel). All samples were analysed by reducing 12% SDS-PAGE and stained using Coomassie Blue (Figure 4.10A, 4.11A, 4.12A). A Western blot using HRPO conjugated murine α-His antibody was also performed in parallel (Figure 4.10B, 4.11B, 4.12B). ScFvs run as a band migrating between 35 kDa and 25 kDa corresponding to their predicted molecular weight of 30 kDa and are present in the all elution fractions. Analysis of the flow-through sample reveals that not all the His-tagged protein is bound to the affinity column. This could be due to poor affinity binding or saturation of the nickel column. It is important to note the multiple bands detected by the Western blot. In the early elutions, there are two close bands on the blot. The second band is likely to correspond to scFv still attached to its leader sequence for secretion. In the latter elutions, a band corresponding to 15 kDa is also present. This suggests cleavage in the exposed linker region. The imidazole eluted protein samples were pooled together, concentrated and dialysed before final gel analysis (Figure 4.13). The final scFv preparations are over 90% pure.

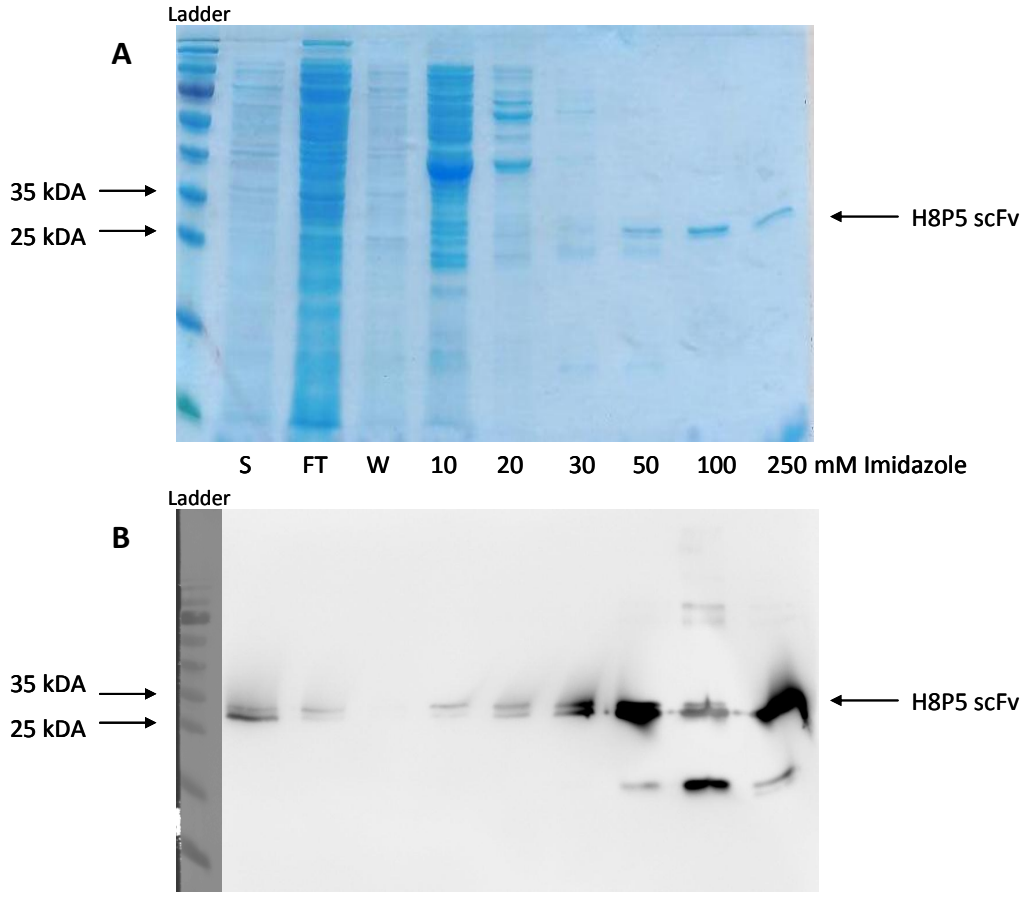

Figure 4.10: Purification of H8P5 scFv by affinity chromatography. IMAC flow-through (FT), wash (W) and elution fractions analysed by reducing 12% SDS-PAGE and stained using Coomassie Blue (A). The corresponding α-His Western blot is also shown (B). H8P5 scFv is present as a band migrating between 35 kDa and 25 kDa in the FT and all elution fractions, starting from the addition of 10 mM imidazole.
S= soluble fraction before column.

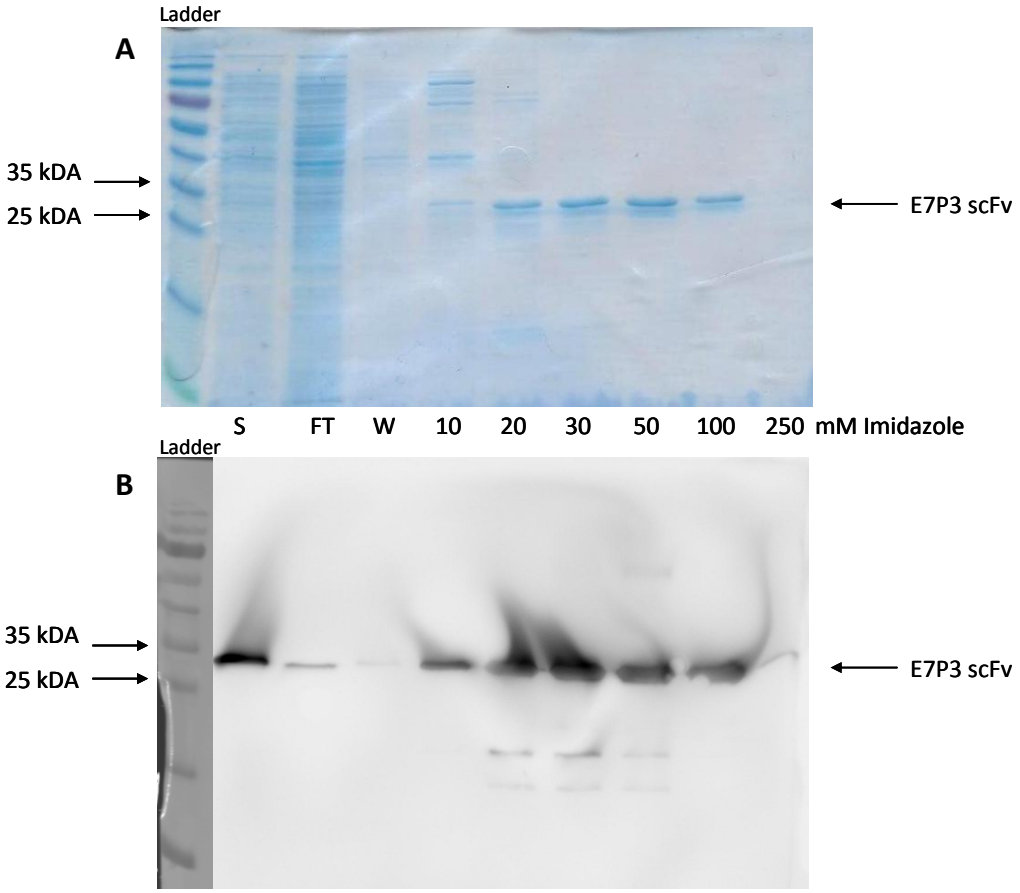

Figure 4.11: Purification of E7P3 scFv by affinity chromatography. IMAC flow-through (FT), wash (W) and elution fractions analysed by reducing 12% SDS-PAGE and stained using Coomassie Blue (A). The corresponding α-His Western blot is also shown (B). E7P3 scFv is present as a band migrating between 35 kDa and 25 kDa in the FT and all elution fractions up to 100 mM imidazole. S= soluble fraction before column.

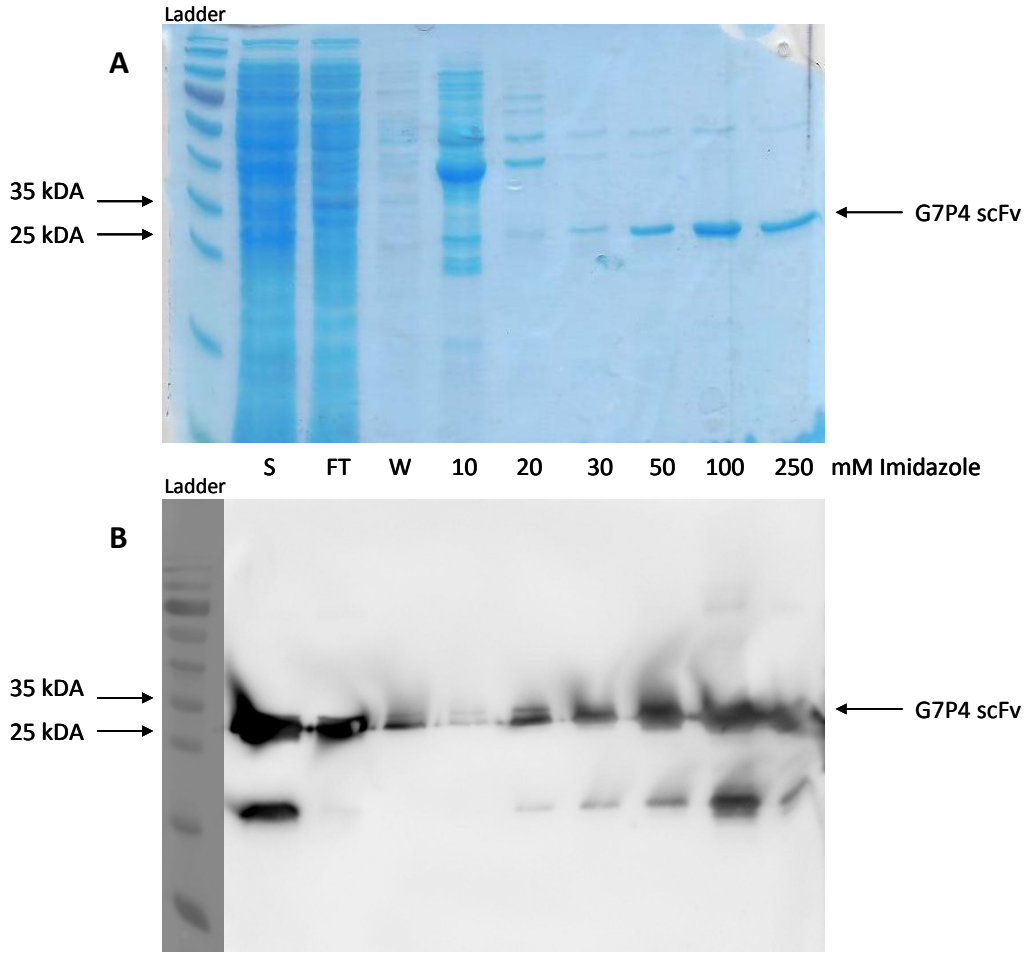

Figure 4.12: Purification of G7P4 scFv by affinity chromatography. IMAC flow-through (FT), wash (W) and elution fractions analysed by reducing 12% SDS-PAGE and stained using Coomassie Blue (A). The corresponding α-His Western blot is also shown (B). G7P4 scFv is present as a band migrating between 35 kDa and 25 kDa in the FT, wash and all elution fractions. S= soluble fraction before column.

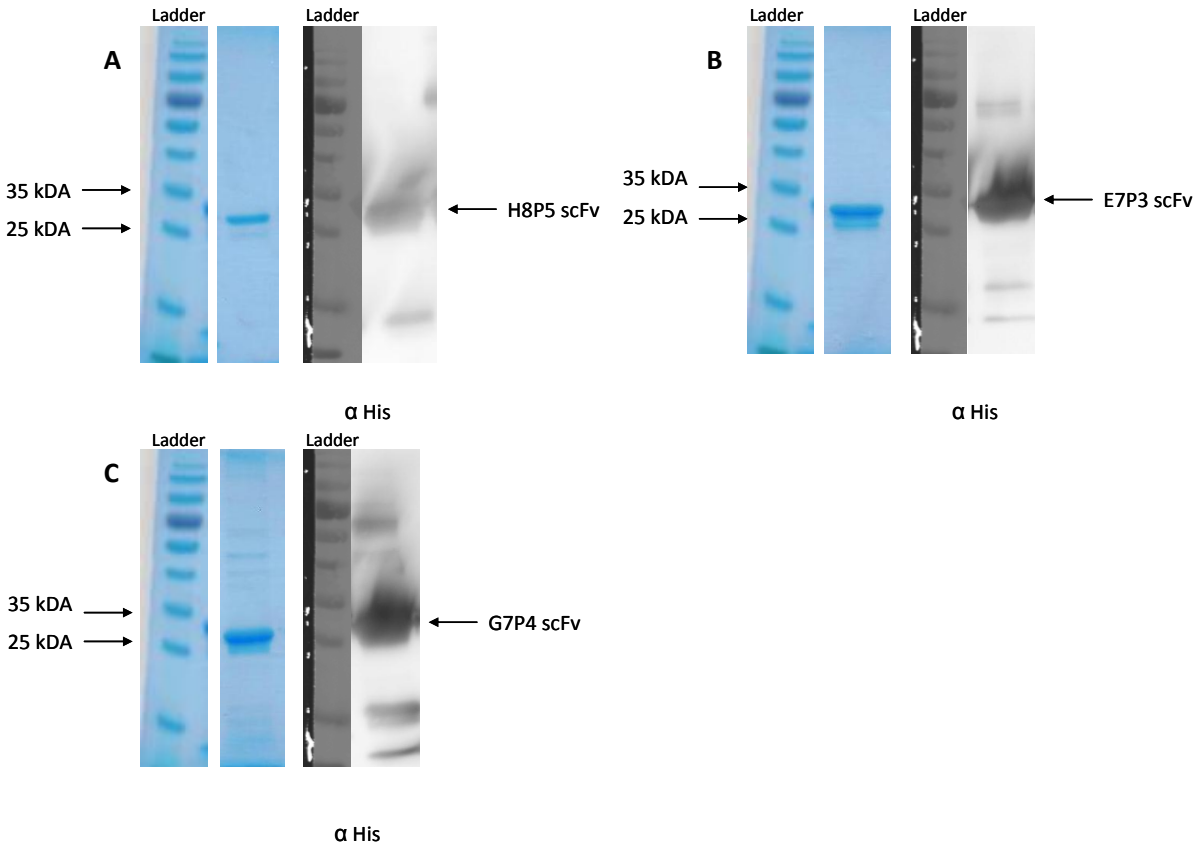

Figure 4.13: scFv samples following final concentration and dialysis. A) H8P5 B) E7P3 C) G7P4 analysed by reducing 12% SDS-PAGE and stained using Coomassie Blue. The corresponding α-His Western blot is also shown. scFvs are present as a band migrating between 35 kDa and 25 kDa.

4.3.4 ScFv binding studies

The antigen used in the phage display selection includes some extra sequence other than DN-MAML1: the vector encoded N-terminal His tag, the T7 gene 10 sequence and the N-terminal Xpress™ epitope tag. It was thus necessary to determine whether any of the binding scFv candidates recognised this extra sequence rather than the relevant antigen DN-MAML1. For this, scFvs were screened again for binding to synthetic Antp-DN-MAML1. This protein was coated at 50 μg/ml giving a similar coating efficiency to DN-MAML1 at 20 μg/ml (data not shown). Two concentrations of pure E7P3 scFv were added in triplicate to a plate coated with DN-MAML1 or Antp-DN-MAML1. Incubation with 9E10 IgG (α-c-Myc), followed by goat α-mouse HRPO, was used to detect binding. Background signals (antigen replaced by PBS) are plotted as a negative control. As shown in Figure 4.14, E7P3 did not bind to Antp-DN-MAML1 therefore this candidate was discarded. In contrast, binding to Antp-DN-MAML1 was confirmed for H8P5 and G7P4 (Figure 4.15).

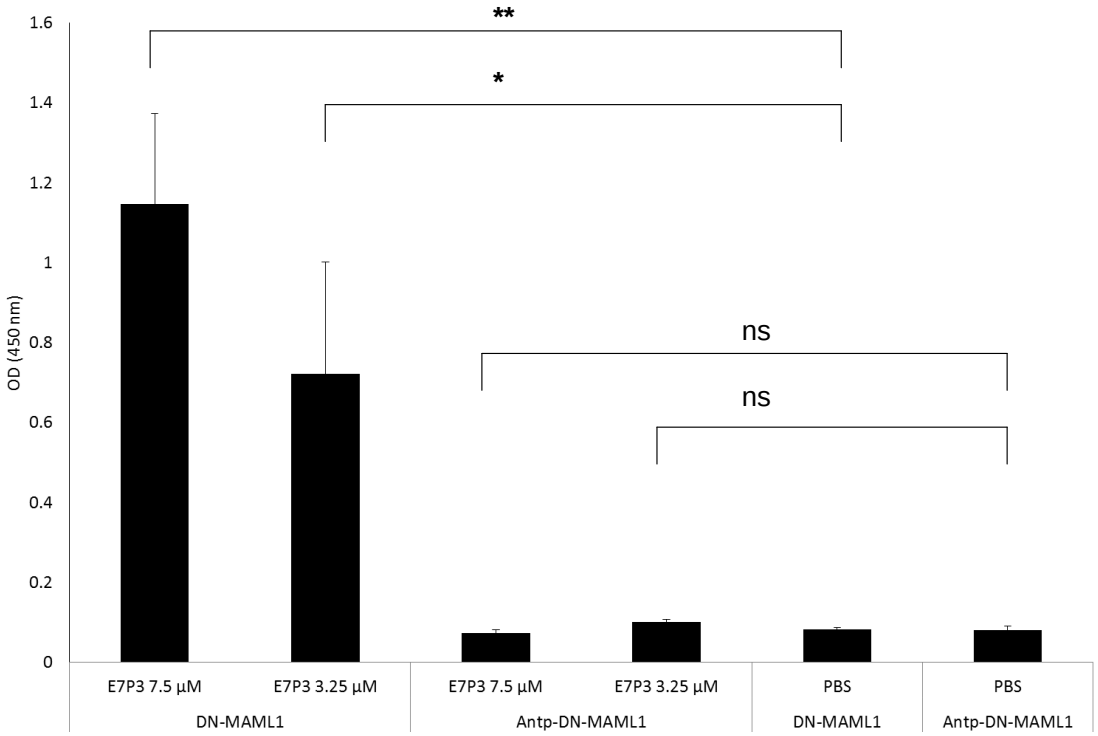

Figure 4.14: ELISA showing binding of E7P3 to DN-MAML1 but not to Antp-DN-MAML1. Two concentrations of E7P3 were added to a plate coated with DN-MAML1 (20 µg/ml) or Antp-DN-MAML1 (50 µg/ml) and detected by α-c-Myc. Absorbance values at 450 nm were measured and background signals (antigen replaced by PBS) are plotted as a negative control. Error bars represent the standard deviation between triplicates. One-way ANOVA was used to statistically compare conditions; $p \leq 0.05$ was considered significant. *$p \leq 0.05$, **$p \leq 0.01$; ns: not significant.

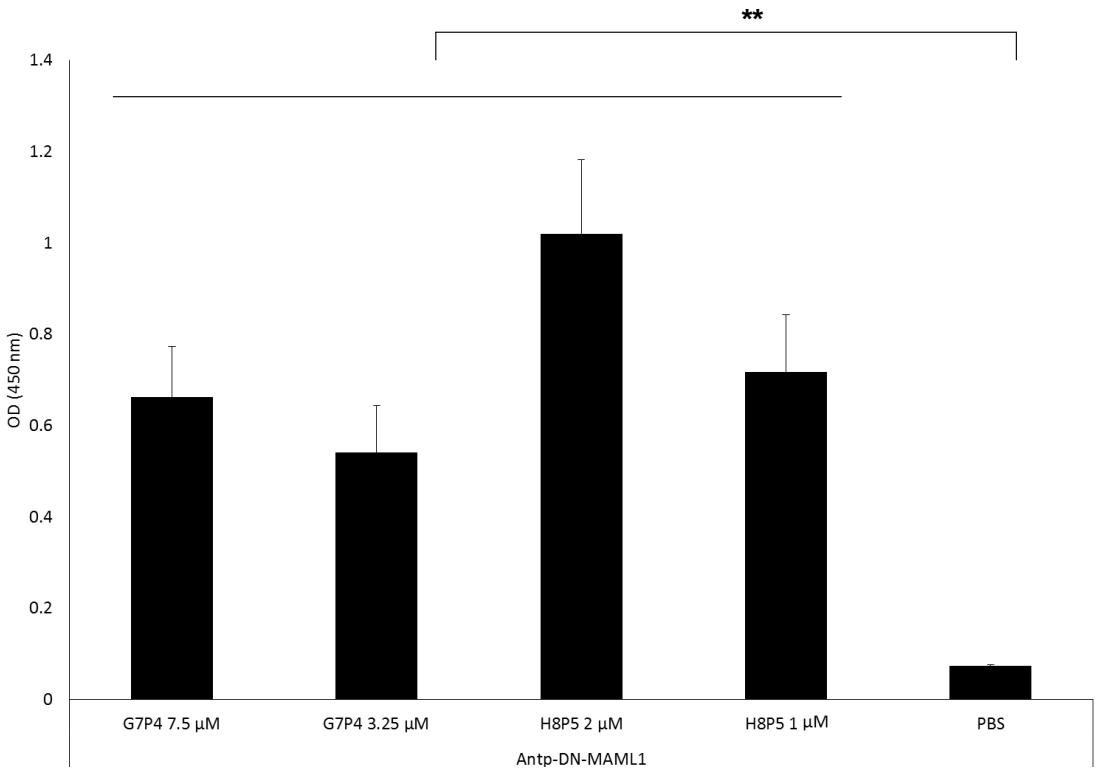

Figure 4.15: ELISA showing binding of G7P4 and H8P5 to immobilised Antp-DN-MAML1. Two concentrations of G7P4 and H8P5 were added to a plate coated with Antp-DN-MAML1 (50 µg/ml) and detected by α-c-Myc. Absorbance values at 450 nm were measured and background signals (antigen replaced by PBS) are plotted as a negative control. Error bars represent the standard deviation between triplicates. One-way ANOVA was used to statistically compare conditions; $p \leq 0.05$ was considered significant. **$p \leq 0.01$;

The only extra sequence in common between the synthetic Antp-DN-MAML1 construct and the vector encoded extra sequence is the His tag. In order to exclude binding of H8P5 and G7P4 to the tag, an irrelevant His-tagged protein (Tetanus toxin heavy chain: TT-Hc) was coated in parallel with Antp-DN-MAML1. Coating efficiency was very low for TT-Hc in both PBS pH 7.4 and carbonate buffer (data not shown) even when coated at a maximum of 200 µg/ml. Antp-DN-MAML1 was coated at 5 µg/ml to achieve comparable coating levels (similar α-His signals, data not shown). Due to the minimal coating, binding signals are lower than usual but it is clear that G7P4 and H8P5 bind to Antp-DN-MAML1 but not to His-tagged TT-Hc (Figure 4.16).

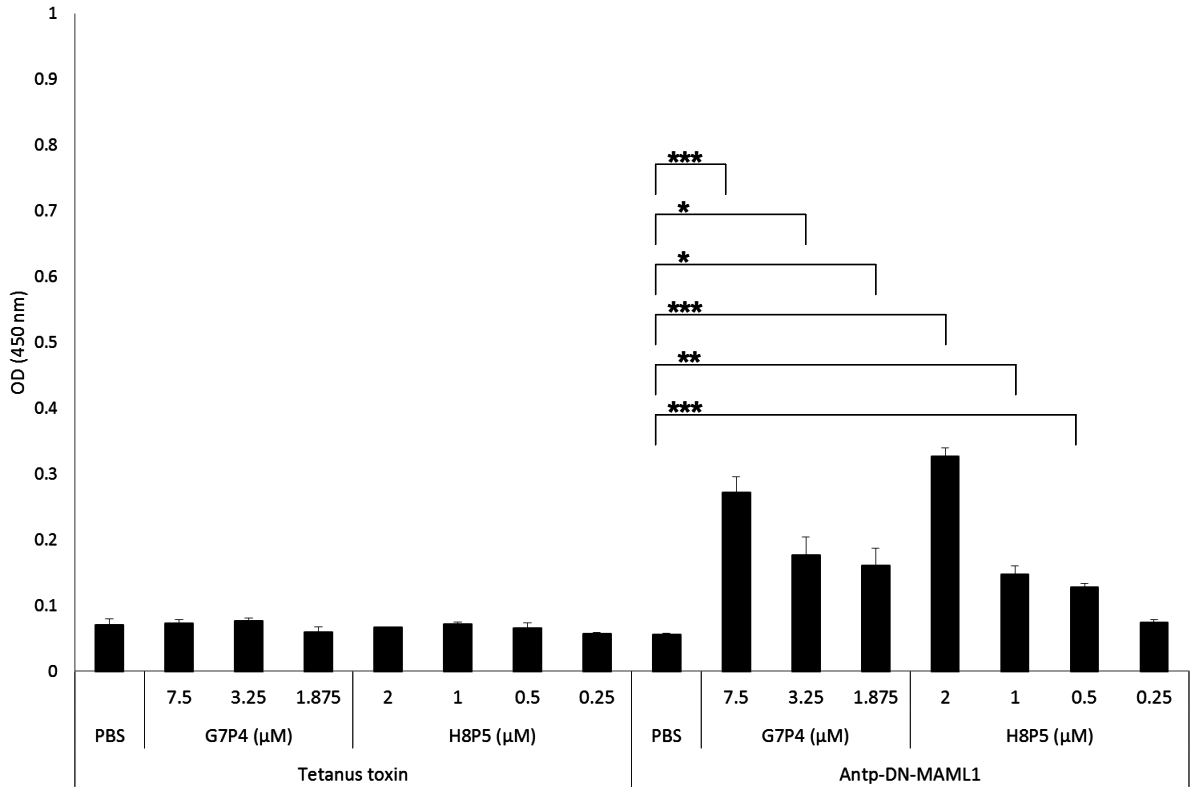

Figure 4.16: ELISA showing binding of G7P4 and H8P5 to Antp-DN-MAML1 but not to tetanus toxin heavy chain (TT-Hc). Several concentrations of G7P4 and H8P5 were added to a plate coated with Antp-DN-MAML1 (5 µg/ml) or tetanus toxin (200 µg/ml) and detected by α-c-Myc. Absorbance values at 450 nm were measured and background signals (antigen replaced by PBS) are plotted as a negative control. Error bars represent the standard deviation between triplicates. One-way ANOVA was used to statistically compare conditions; $p \leq 0.05$ was considered significant. *$p \leq 0.05$, **$p \leq 0.01$, ***$p \leq 0.001$.

The K_d for the H8P5 and G7P4 scFv was determined by ELISA on DN-MAML1 coated plates. Incubation with 9E10 IgG, followed by goat α-mouse HRPO, was used to detect binding. The calculated K_d value was 114 nM for G7P4 and 98 nM for H8P5 (Figures 4.17 and 4.18).

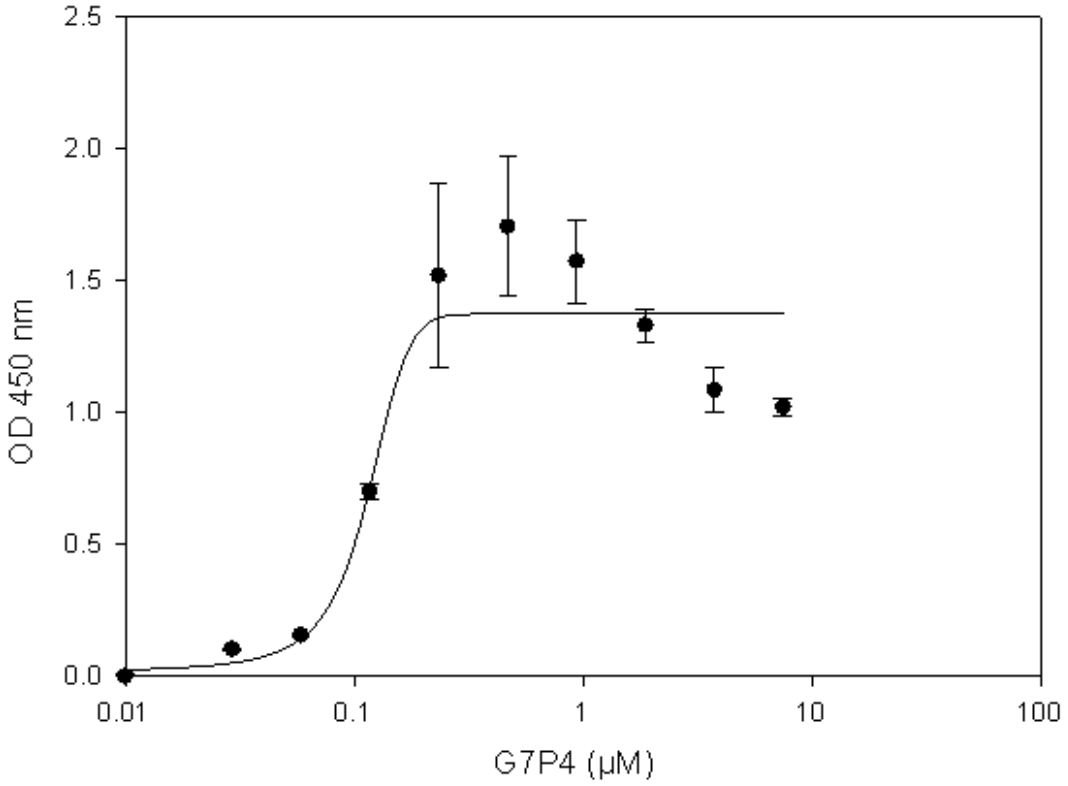

Figure 4.17: ELISA showing binding of G7P4 to immobilised DN-MAML1. G7P4 was serially diluted against a DN-MAML1 (20 μg/ml) coated plate and detected by α-c-Myc. Absorbance values at 450 nm were measured and background signals (no antigen) were deducted. Error bars represent the standard deviation between triplicates. Curve fitted using SigmaPlot® software.

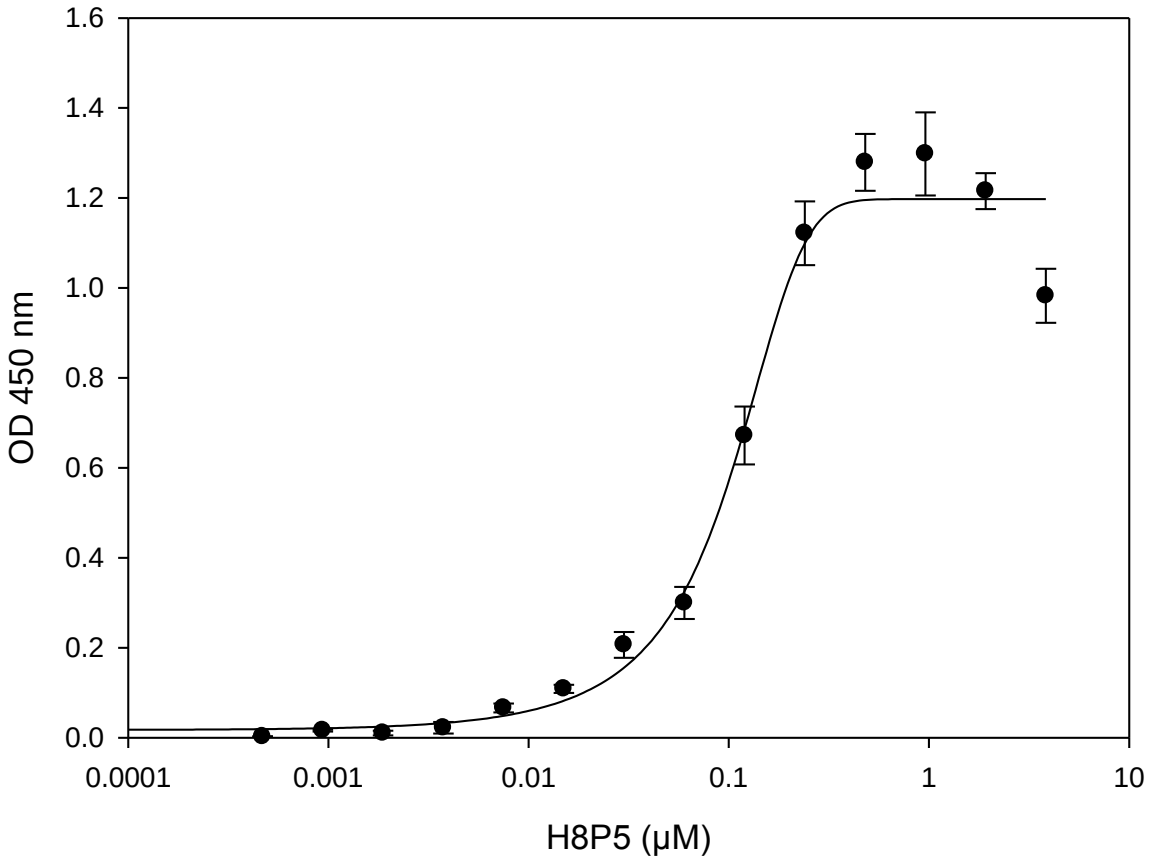

Figure 4.18: ELISA showing binding of H8P5 to immobilised DN-MAML1. H8P5 was serially diluted against a DN-MAML1 (20 µg/ml) coated plate and detected by α-c-Myc. Absorbance values at 450 nm were measured and background signals (no antigen) were deducted. Error bars represent the standard deviation between triplicates. Curve fitted using SigmaPlot® software.

.

4.3.5 Production of Antp-scFv fusions

Production of Antp fused to an irrelevant scFv (N4), in both orientations, was carried out in parallel with phage display selection in order to determine which expression and purification strategies are best suited for antibody-based fusion constructs.

N4 was subcloned upstream and downstream of Antp in the pET20b vector which includes a signal sequence, facilitating export into the periplasmic space (section 2.1.3). This strategy is best suited for expression of soluble fusions as it promotes correct folding and disulfide bond formation of the scFv portion.

Despite numerous trials, varying several conditions (media, IPTG concentration, temperature and OD_{600} value upon induction) no expression was obtained for the N4-Antp orientation in BL21 (DE3) pLysS cells (data not shown). Good expression levels were achieved for the Antp-N4 construct although this was not secreted (Figure 4.19). As illustrated in Figure 4.20, Antp-N4 is present in the pellet fraction of lysed cells suggesting that this protein is expressed insolubly.

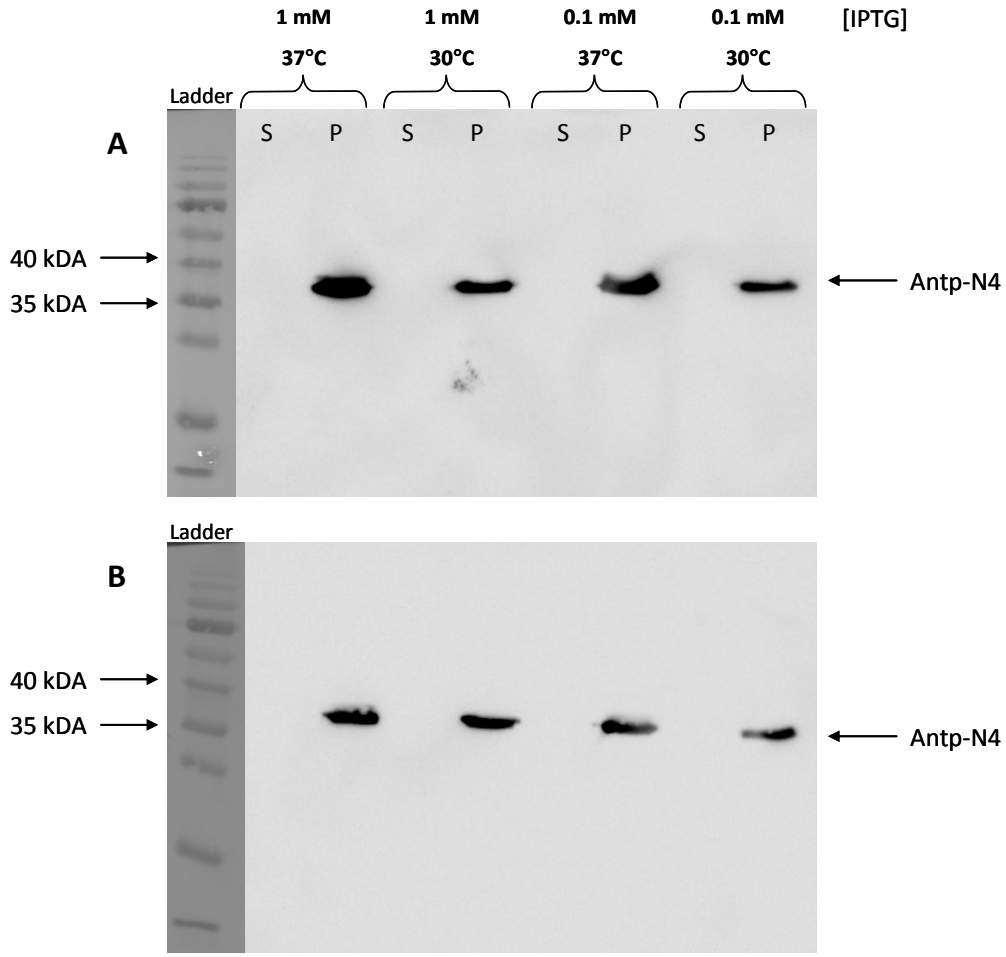

Figure 4.19: Small scale expression trials of Antp-N4 in pET20b transformed in BL21 (DE3) pLysS cells. The bacterial culture was grown in 5 ml of 2TY (A) or LB (B) up to an OD_{600} of 0.8 before induction with either 0.1 mM or 1 mM IPTG for 4 hours at 37°C/ 30°C. The culture was centrifuged before analysis of the secreted (S) and cell pellet (P) fractions by α-His Western blot. Antp-N4 is present as a band migrating between 40 kDa and 35 kDa.

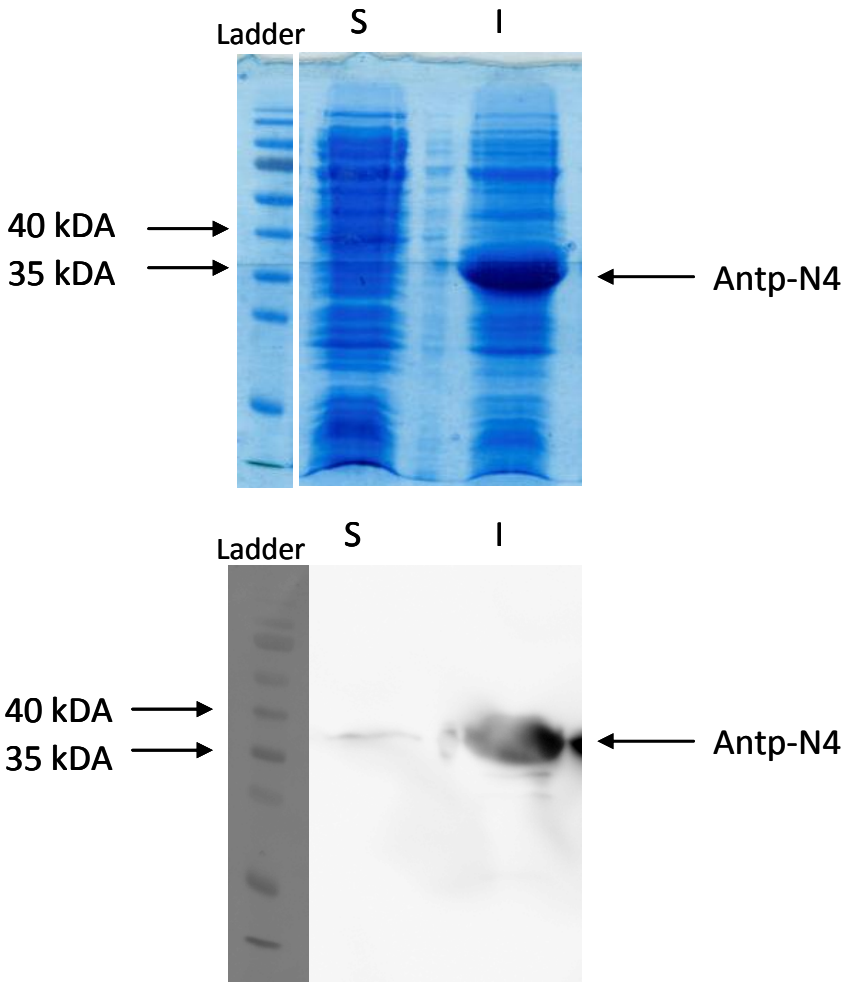

Figure 4.20: Antp-N4 is expressed in inclusion bodies. Gel and α-His Western blot analysis of the soluble (S) and insoluble fractions (I) following 0.1% Igepal treatment and sonication of the expression pellet.

Expression studies for the α-DN-MAML1 scFvs fused to Antp in both orientations, were carried out in parallel with binding studies for the scFv alone. Although E7P3 did not bind to DN-MAML1, it is still an acceptable model to study expression due to the similarity of the constructs. E7P3 was subcloned upstream and downstream of Antp in the pET20b vector (section 2.1.3). No expression was ever obtained for the E7P3-Antp orientation in BL21 (DE3) pLysS cells (data not shown). An expression trial for Antp-E7P3 at a lower temperature (25°C) using two IPTG concentrations was monitored at 1, 2 and 4 hours post-induction (Figure 4.21). Good expression levels with increased yield over time were achieved but the fusion was not secreted. Additional expression trials at 18°C (data not shown) or by autoinduction (Figure 4.22) did not improve on this approach.

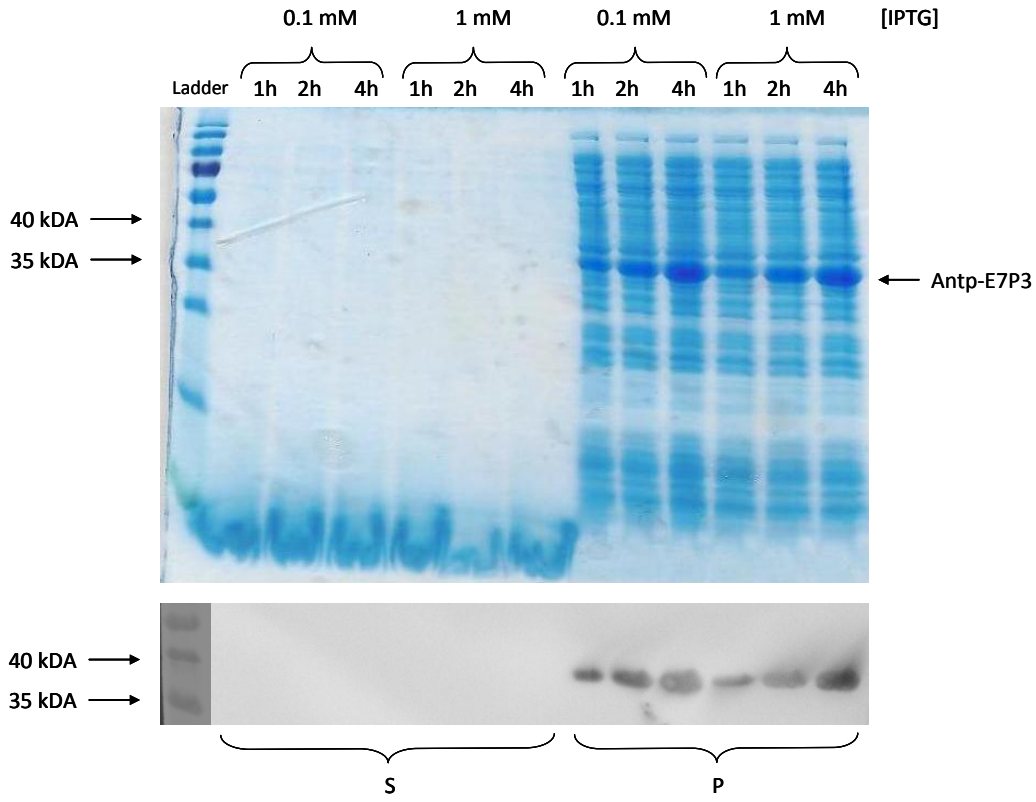

Figure 4.21: Small scale expression trials of Antp-E7P3 in pET20b transformed in BL21 (DE3) pLysS cells. The bacterial culture was grown in 5 ml of 2TY up to an OD_{600} of 0.8 before induction with either 0.1 mM or 1 mM IPTG for 1,2 and 4 hours at 25°C. The culture was centrifuged before analysis of the secreted (S) and cell pellet (P) fractions by reducing 12% SDS-PAGE stained using Coomassie Blue and α-His Western blot. Antp-E7P3 is present as a band migrating between 40 kDa and 35 kDa in the pellet fractions.

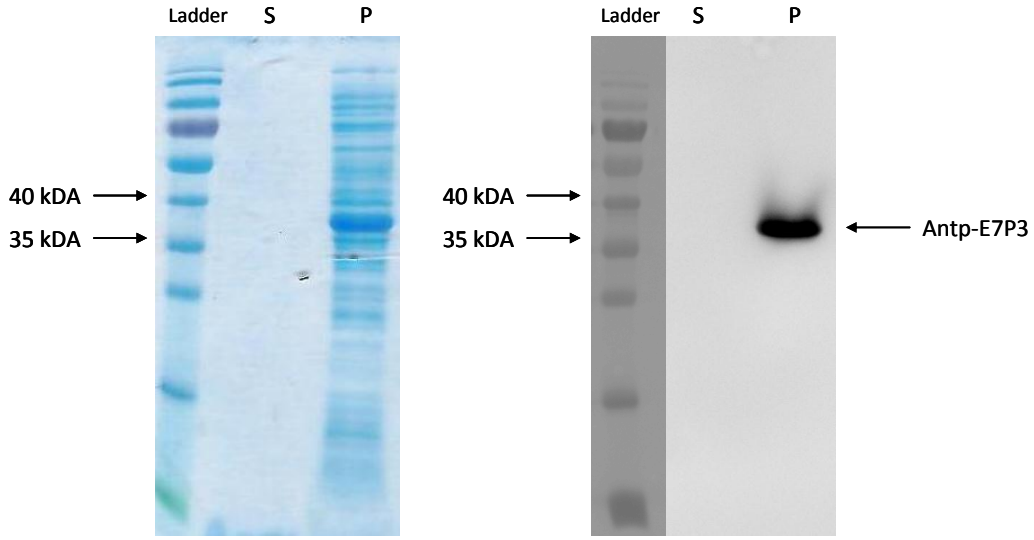

Figure 4.22: Expression of Antp-E7P3 in pET20b transformed in BL21 (DE3) pLysS cells by autoinduction. The overnight culture, grown in autoinduction media at 20°C overnight, was centrifuged before analysis of the secreted (S) and cell pellet (P) fractions by reducing 12% SDS-PAGE stained using Coomassie Blue and α-His Western blot. Antp-E7P3 is present as a band migrating between 40 kDa and 35 kDa in the pellet fraction.

Antp-G7P4 and Antp-H8P5 were expressed on a large scale with induction by 1 mM IPTG at 25°C (Figue 4.23). Both inclusion body pellets were processed and solubilised. A refolding strategy was attempted for Antp-H8P5 only, due to limitation of resources (Figure 4.24). The protocol, previously optimised for Antp-N4, is tailored to the refolding of antibody fragments by including the presence of a redox reagent. Refolding occurred overnight at 10°C. Overall, yields after refolding were low due to precipitation. The soluble fraction was dialysed in PBS buffer and concentrated using a 5000 kDa spin concentrator. Antp-H8P5 is over 85% pure (Figure 4.25).

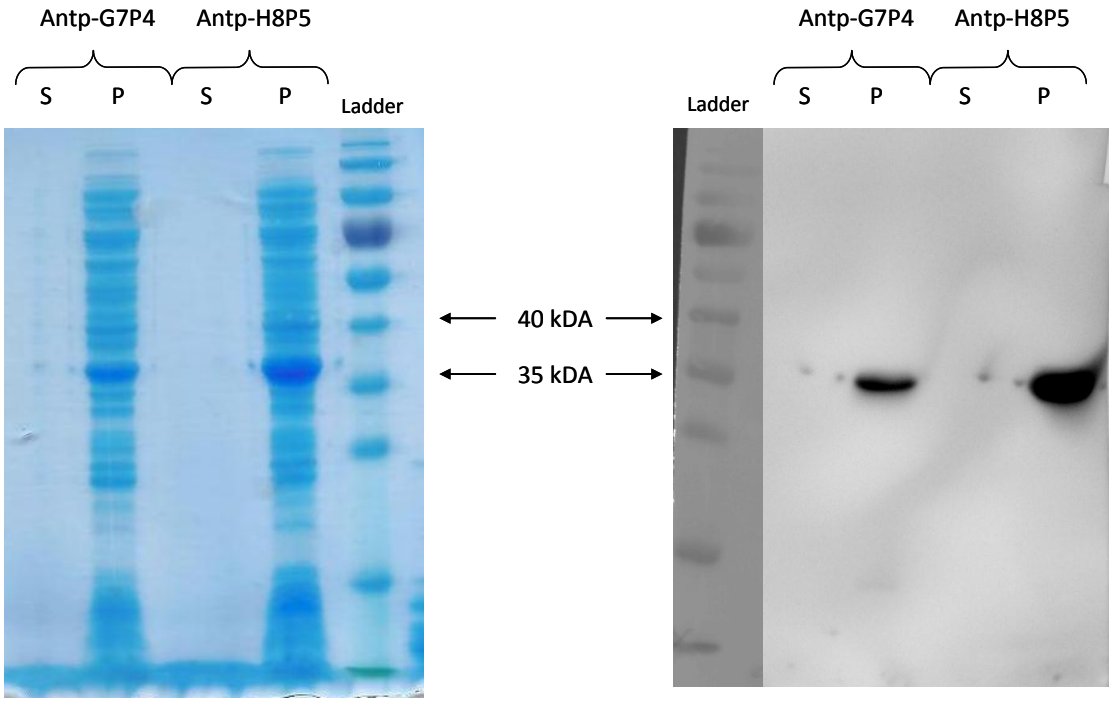

Figure 4.23: Expression of Antp-G7P4 and Antp-H8P5 in pET20b transformed in BL21 (DE3) pLysS cells. Each bacterial culture was grown in 1L of 2TY up to an OD_{600} of 0.8 before induction with 1 mM IPTG for 5 hours at 25°C. The culture was centrifuged before analysis of the secreted (S) and cell pellet (P) fractions by reducing 12% SDS-PAGE stained using Coomassie Blue and α-His Western blot. Antp-G7P4 and Antp-H8P5 are present as a band migrating between 40 kDa and 35 kDa in the pellet fractions.

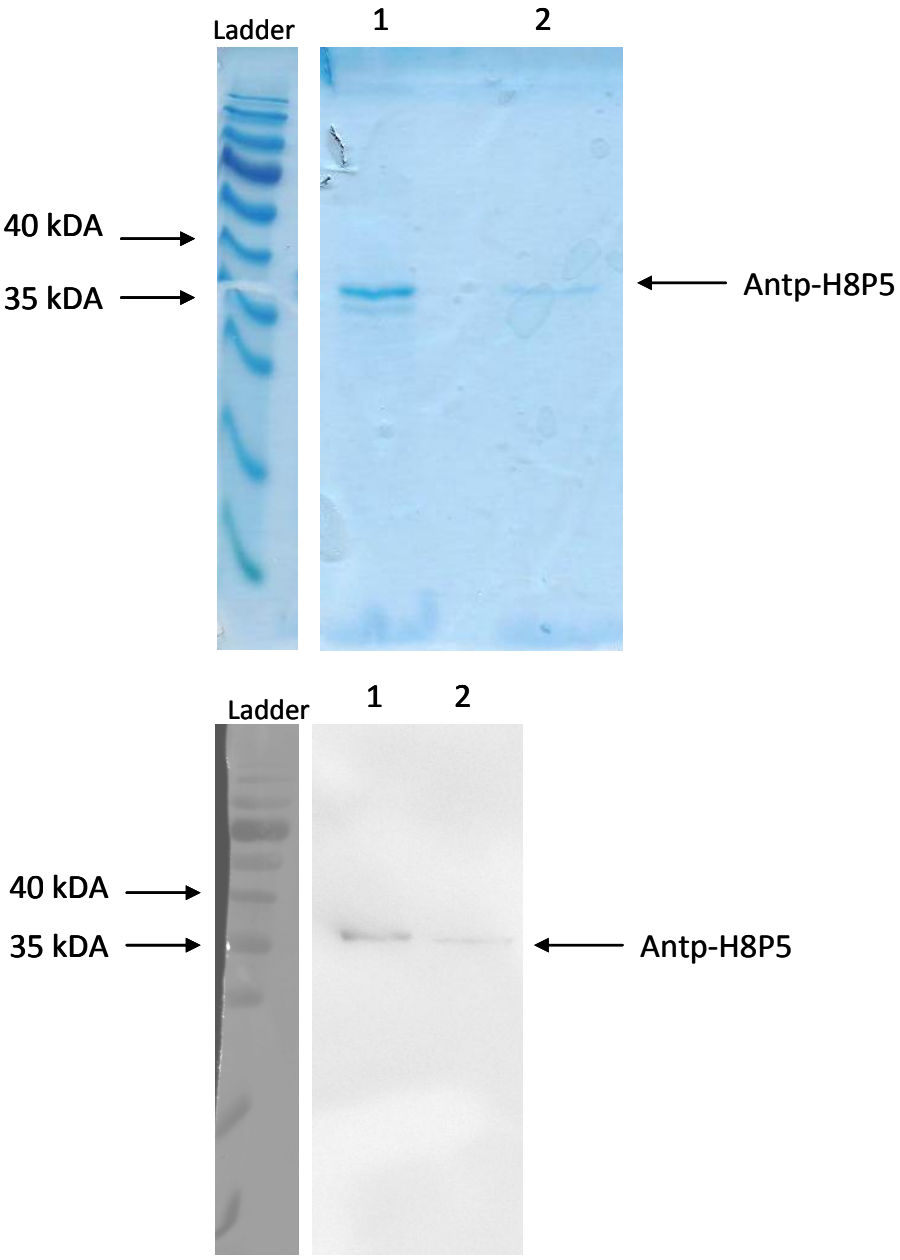

Figure 4.24: Analysis of the soluble fractions during denaturation and refolding of Antp-H8P5. Fractions were analysed by reducing 12% SDS-PAGE, stained using Coomassie Blue. Antp-H8P5 is present as a band migrating between 40 kDa and 35 kDa**.** The corresponding anti-his Western blot is also shown.
1= soluble fraction following denaturing of the inclusion body pellet using 6M guanidinium chloride. 2= soluble fraction following refolding at 10°C.

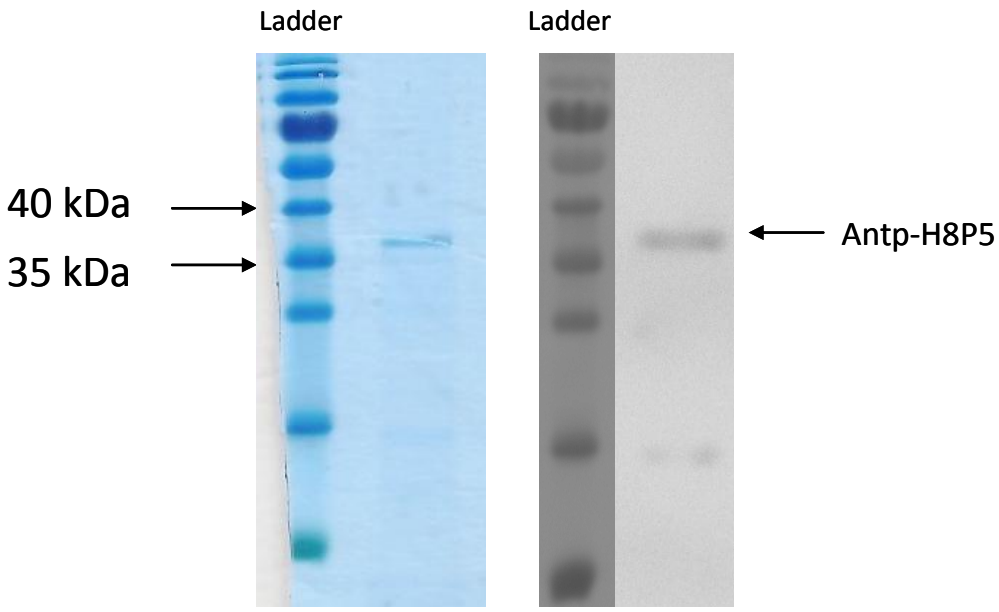

Figure 4.25: Soluble Antp-H8P5 following final dialysis and concentration. The sample was analysed by reducing 12% SDS-PAGE stained using Coomassie Blue and α-His Western blot. Antp-H8P5 is present as a band migrating between 40 kDa and 35 kDa in the pellet fractions.

Finally, it was necessary to determine whether H8P5 scFv retained its binding properties when fused to Antp, following refolding. The fusion protein did not contain a c-Myc tag for detection so another strategy was chosen. In this experiment, the fusion was coated onto ELISA plates. The antigen DN-MAML1 was biotinylated for detection using extravidin peroxidase HRPO (Figure 4.26). Binding to the plastic surface was assessed along with other controls including: PBS instead of antigen and addition of DN-MAML1 (no biotin) both on the coated and uncoated portion of the ELISA plate.

A K_d value of 438 nM was calculated for Antp-H8P5. This is not directly comparable to H8P5 scFv binding as the detection method is entirely different. Nevertheless, binding between the fusion and DN-MAML1 was confirmed.

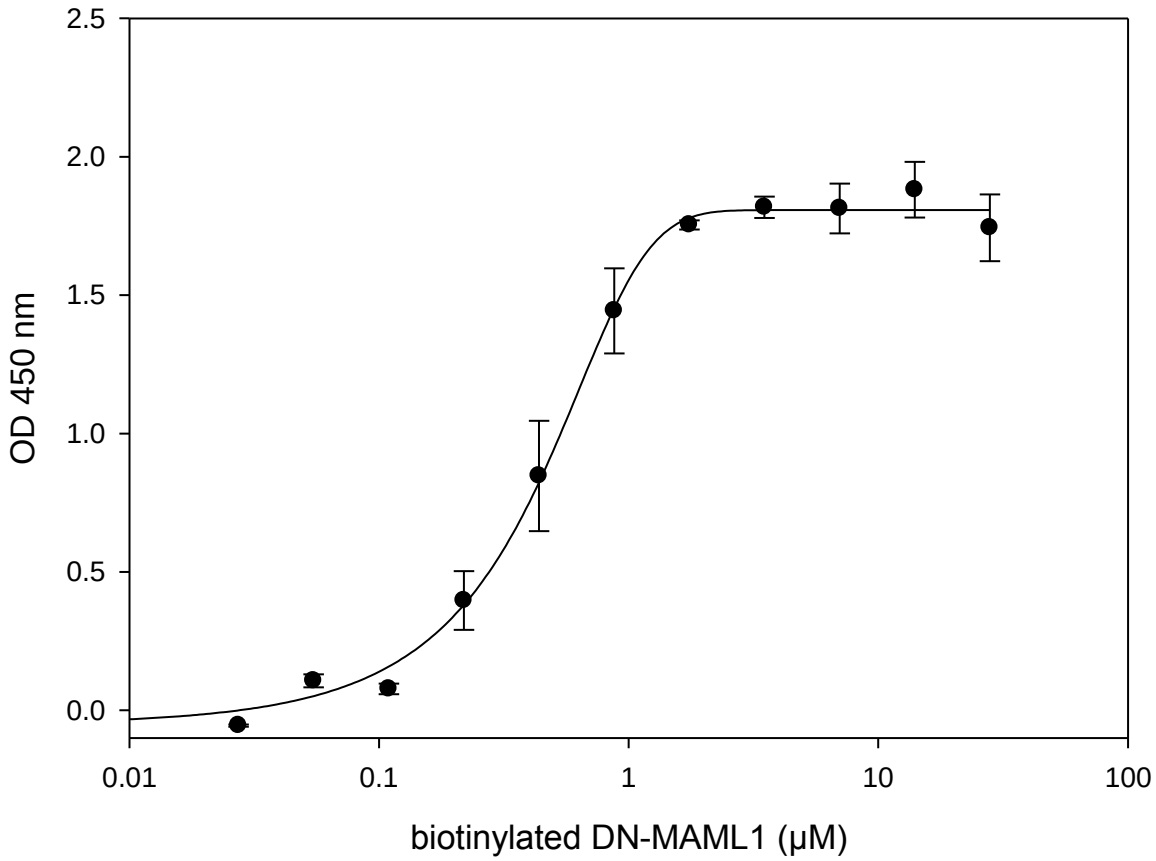

Figure 4.26: ELISA showing binding of biotinylated DN-MAML1 to immobilised Antp-H8P5. In triplicate, biotinylated DN-MAML1 was serially diluted against a Antp-H8P5 coated plate. Extravidin peroxidase HRPO was used to detect binding. Absorbance values at 450 nm were measured and background signals (no antigen) were deducted. Curve fitted using SigmaPlot® software.

4.3.6 Mammalian expression trials for Antp-H8P5

Testing of the Antp-H8P5 scFv fusion in the luciferase reporter-gene assay was necessary to verify whether delivery of a scFv against DN-MAML1 successfully inhibits Notch signalling. However, the refolding protocol did not scale enough to achieve the amount needed for addition of this potential drug at high doses. Next, we investigated whether mammalian expression in CHO cells could give better, soluble yields of fusion protein. The wild type CHO K cell line was used as the standard expression system. Transfection was also attempted in CHO N2 cells to explore the recombinant protein's action in the CHO luciferase system itself, without purification. For this, Antp-H8P5 and Antp were cloned into pcDNA4a (Δ Pci I) containing a leader sequence. Both transient and polyclonal stable expression were attempted. No fusion protein was ever detected by anti-His Western blot either in the concentrated supernatant or lysed cell pellet fractions. Antp was detected in the lysed cell pellet exclusively but this result was not reproducible. This suggests the protein is produced in an inactive form as it is unable to cross the cellular membrane. In the polyclonal stable expression system, zeocin selection confirmed that transfection was successful. It is important to note that detection relies on the presence of the His tag at the C-terminal end of the protein. If the His tag had been removed by proteolytic cleavage, the protein would not be detectable on the Western blot. A commercial anti-Antp is available although, when previously tested on Antp produced in-house, the Western blot had a negative outcome. Our collaborators also tested this antibody and binding was only observed to Pichia expressed Antp-DN-MAML1 protein. This suggests that the antibody binds to Antp after it has undergone some form of post-translational modification.

4.4 Discussion

The aim of this study was to select anti-MAML (13-74) scFvs and fuse them to Antp for inhibition of Notch signalling. The antigen MAML (13-74), also known as DN-MAML1 was produced following an established protocol involving refolding of the protein using acetic acid. The published structures of DN-MAML1 in complex with CSL and N^{IC} were also obtained using refolded protein (Nam et al., 2006). This is encouraging for recovery of the original fold of DN-MAML1. A circular dichroism analysis of DN-MAML1 showed a high helical content, confirming successful refolding. Three rounds of phage display selection on immobilised DN-MAML1 were carried out using a human naïve scFv library. In order to maximise the chances of selecting a high affinity antibody fragment, it would have been preferable to employ an immunised library. However, this was not readily available and would yield murine/rabbit scFvs to be subsequently humanised.

A first high-through put screening of colonies revealed a number of positive phagemid binding to DN-MAML1. Sequencing analysis of positive clones revealed the presence of duplicate phagemids, restricting the analysis to three clones: H8P5, G7P4 and E7P3. It is interesting to note the similarity between H8P5 and G7P4. The low number of different clones is expected as the library used is naïve and of human origin, like the antigen.

In order to further characterise the scFv candidates, these were expressed in the HB2151 strain which does not allow read-through to the pIII sequence. Expression was successful for all clones, with slight differences in yields. This observation could be related to the small variations in the genetic sequences and the presence of more/less favourable codons.

The antigen used in the phage display selection included some extra vector encoded sequence other than DN-MAML1. Binding studies revealed that E7P3 did not bind the relevant DN-MAML1 sequence and was discarded. The key point to study binding of scFv to different portions of the DN-MAML1 construct is to achieve similar binding onto the plastic surface. This is essential in order to obtain comparable and reliable results. Equal starting antigen concentrations do not guarantee similar coating. Coating efficiency varies for each protein depending on their hydrophobic/hydrophilic profile and can be improved by the use of different buffers. In this study, similar development values (absorbance at 450nm) were considered as the best read out for coating efficiency.

ELISA binding studies allowed the calculation of a K_d value of 114 nM and 98 nM for G7P4 and H8P5, respectively. These values are within the range expected from naïve library selections (Griffiths et al., 1993). Further studies should include the study of binding kinetics using surface plasmon resonance. This method is widely used in the field of antibody technology and provides additional information in order to compare one scFv to the other and perform competition studies.

In order to achieve cell penetration, scFvs were fused to Antp, considering both orientations (Antp-scFv and scFv-Antp). Expression trials revealed that only the Antp-scFv orientation was successfully produced. Therefore, scFv-Antp fusions were not characterised further. One possibility is that the scFv-Antp fusion was produced as a truncated protein lacking the C-terminal tags and therefore could not be detected by Western blot.

Despite employing a vector for secretion of the expressed protein to facilitate folding, Antp-scFv fusions were never detected in the culture supernatant. Initial studies using Antp-N4 as a model (N4 being an irrelevant scFv with expression yields of >20 mg/L) showed that the fusion was expressed insolubly in the cytoplasm. Further efforts to express the fusions solubly included the use of: different media (LB, 2TY, autoinduction), temperatures (18°C, 20°C, 25°C, 30°C, 37 °C), IPTG concentrations (0.1 mM and 1 mM), induction length (1h, 2h, 4h, 5h and overnight). Generally, alternative conditions such as different media, lower temperatures and lower IPTG concentrations were explored in order to attenuate the stress to cells during expression. In particular, the use of autoinduction media has proven successful for a variety of proteins that were otherwise produced insolubly (Studier, 2005). Exploring different induction times was related to the observations made during expression trials for Antp-DN-MAML1. There are various examples of scFv fusion proteins that fail to secrete and are insoluble even if the scFv alone was successfully secreted and soluble (Linardou et al., 2000; Kipriyanov et al., 1996; Cooke et al., 2002). The insoluble protein was refolded following a protocol optimised for the processing of antibody fragments. The yields for soluble, refolded protein were very low. Nevertheless, enough Antp-H8P5 protein was produced to characterise its binding to DN-MAML1. In this experiment, Antp-H8P5 was coated onto the plastic surface of ELISA plates. This alternative strategy is convenient because less protein is used but also necessary because of the lack of c-Myc tag in the fusion construct. Working in the context of cancer signalling pathways, it seemed inappropriate to include the sequence of a

previously described oncogene to be carried inside the cell. A K_d value of 438 nM was calculated for Antp-H8P5. This can not be directly comparable with H8P5 binding because of the different detection methods used. However, this bigger value suggests a detrimental effect of refolding on the binding capabilities of Antp-H8P5. Another possibility is a small interference of binding due to fusion with Antp. It is also important to note that coating protein onto the plate surface can change its conformation. Therefore, it is possible that coated DN-MAML1 differs slightly from its soluble version. The same consideration applies to the fusion Antp-H8P5 which is coated prior to assessing its binding to the antigen.

Mammalian expression was also investigated for production of Antp-scFv fusion proteins. Mammalian expression systems are usually preferred when working with larger and complex fusion proteins. Two strategies of expression were designed and attempted. Although zeocin selection suggested successful transfection, neither method resulted in the production of active Antp-H8P5 and Antp control proteins. Future studies should aim to detect the mRNA corresponding to each construct in order to confirm a problem at the protein expression level. The loss of tags is a common problem in recombinant expression systems. Therefore, this project would benefit from the availability of tools such as a reliable anti-Antp antibody to follow the fusion protein directly. The impossibility of producing substantial amounts of fusion protein meant that characterisation of this protein was halted. In the future, it will be necessary to confirm internalisation and successful inhibition of Notch signalling by the methods established in Chapter 3.

Concluding remarks

This study allowed the isolation of two candidate antibody fragments that successfully bind DN-MAML1 with affinities in the mid nanomolar range. This result is even more significant considering that the phage display selection was carried out using a naïve library. Expression trials of Antp fused to scFv in both orientations revealed a preference for the Antp-scFv constructs. Despite successful expression, fusion proteins were produced as inclusion bodies and yields were minimal. Binding of the Antp-H8P5 fusion to DN-MAML1 was mostly conserved upon refolding. No further characterisation was possible even when resorting to a mammalian system.

CHAPTER 5

General Discussion

The aim of this study was to evaluate novel strategies for Notch inhibition, targeting MAML. The choice of target was influenced by various considerations. Firstly, it is important to think about the difference between targeting a signalling pathway through extracellular versus intracellular components. Generally, antibodies and other protein inhibitors are designed to target the interactions between a receptor and its ligand(s) at the cell surface. The inhibition of the initiation of signalling itself is believed to be a powerful tool to modulate cellular pathways. However, this strategy does not take into account the overlap and redundancy of intracellular signalling modulators between different pathways. It is rational for the cell to evolve multiple and intricate mechanisms for tight regulation of crucial intracellular signalling molecules. In normal conditions this allows control of signalling in the event of 'misfiring' from a particular pathway. However, in the context of cancer, this same regulatory system can lead to drug resistant cancer cells. When a signalling pathway is inhibited, the cell can activate a parallel pathway that acts on the same modulators inside the cell or on different signalling molecules that have the same downstream effect (e.g. survival, proliferation). Targeting signalling inside the cell, aiming for the bottom of the signalling chain, is a viable option to consider. This strategy is better suited for 'funnel' pathways such as Notch, where multiple signalling routes through different receptors binding several ligands converge into a single event: the formation of the N^{IC}, CSL and MAML tripartite complex for transcriptional activation. In the context of Notch, this strategy also allows to differentiate between the canonical and non canonical Notch pathways. In fact, by targeting the tripartite complex, our molecules should not interfere with CSL-independent signalling. It follows that the fusion proteins examined in this study could potentially be used to better understand the Notch pathway as a whole.

In this study, two different strategies for inhibition of signalling were examined. The first includes the use of a dominant-negative version of MAML. Dominant-negative molecules outcompete the wild-type molecule for binding and act antagonistically, as they are not able to carry out the same function. Dominant-negative molecules have been commonly used as tools to better dissect and understand complex signalling pathways. However, the use of dominant-negative proteins as therapeutic agents has its limitations. In fact, only a minority of signalling molecules have a characterised dominant negative version. For other molecules, a dominant negative has yet to be identified. In contrast, our second strategy of delivering antibody fragments promises

to be suited to virtually any molecule in any pathway. Thanks to continuously evolving antibody isolation techniques, antibody and antibody fragments can be raised or selected from libraries against any antigen. Thus, this study provides a proof-of-concept applicable to other pathways or even to other molecules involved in Notch signalling.

The development of strategies for intracellular delivery is a vibrant field and several methods have been explored in the past years. The choice of using Antennapedia in this study is predicated on its ability to cross the cellular membrane as well as the nuclear membrane. This is crucial for reaching nuclear MAML. It is important to note that the full length Antennapedia protein is used in this study rather than the corresponding cell-penetrating peptide penetratin. The reasoning behind this choice is that the full-length Antennapedia is thought to be more suitable for the delivery of larger cargoes.

There is one main difference between the standard cancer therapy strategy and the approaches described in this study. Standard therapies are aimed to target cancer cells, specifically. Chemotherapy drugs affect rapidly dividing cells and antibody therapies target receptors/ligands overexpressed by cancer cells. In contrast to this, our cargoes DN-MAML1 and scFvs have the potential to be delivered to every cell in the body. This raises the question of the effect of inhibiting a crucial pathway such as Notch signalling in healthy cells alongside cancer cells. Studies in mice have highlighted the importance of Notch receptor and ligand genes for development. In fact, knock-out mice for Notch1, Notch2, DLL1 and Jagged-1 are embryonic lethal (Swiatek et al., 1994; Shimizu et al., 1999; Hrabe de Angelis et al., 1997; Xue et al., 1999). In addition, mice heterozygous for DLL4 inactivation also die before birth (Gale et al., 2004). Our *in vivo* study did not show obvious side effects in adult mice upon injection of Antp-DN-MAML1. This highlights the difference between tempering with Notch in the context of development versus altering its function in adult tissue renewal. Nevertheless, future studies should investigate potential side effects in more depth in order to confirm Notch as a viable target for the development of therapies in the adult.

This project involved production of Antp fusion proteins which was very challenging on a technical level. The presence of recombinant proteins in inclusion bodies is a well-known obstacle in protein production. Refolding protocols need to be tailored to each protein and thus require extensive optimisation. In addition, refolding is not

favoured in biopharmaceuticals due to inconsistency and production of mixtures. Thus, multiple attempts at producing Antp fusion proteins in a soluble form were performed before resorting to a refolding strategy. It is important to note that modification of the expression protocol for Antp was a successful strategy for production of this protein in the soluble phase. However, fusion of Antp to DN-MAML1 increased the difficulty of producing this protein. The expressed protein was insoluble in multiple experimental settings suggesting that there is an unavoidable biological or toxic constraint on bacterial expression of Antp-DN-MAML1. Expression using a mammalian system was considered as a portion of the fusion protein is of human origin, but was never attempted. However, CHO cells were used for expression trials of Antp-scFv and Antp, with no success. It is possible that interactions with the membrane impede the successful production of these proteins. Alternative host systems such as expression in yeast should be considered in future studies. It would also be interesting to explore whether the use of alternative cell-penetrating proteins or peptides would relieve the production problems observed when using Antp. Although satisfactory expression yields were obtained for expression of insoluble Antp-DN-MAML1, refolding was unsuccessful. Soluble expression of Antp-DN-MAML1 was achieved but its purification was not possible.

Increasing evidence is available supporting a role for Notch in cancer stem cells (CSC). It is believed that targeting Notch will enable manipulation of the elusive CSC population. CSC have been described as a small population within the cancer cell population (Al-Hajj et al., 2004; Donnenberg and Donnenberg, 2005; Kakarala and Wicha, 2007; Korkaya and Wicha, 2007; Yang and Wechsler-Reya, 2007). These ‘tumour initiating cells’ are hypothesised to possess some biological properties characteristic of normal stem cells such as unlimited self-replication, asymmetric cell division and resistance to toxic molecules through increased expression of ABC transporters amongst other mechanisms. The origin of CSC is the subject of continuing debate amongst scientists. Three hypotheses have been formulated. First, scientists believe that CSCs derive from normal tissue stem cells that have undergone some form of transformation. According to this model, the CSCs are proposed to generate other cancer cells by aberrant differentiation, evading normal regulatory mechanisms (Song and Miele, 2007). Supporting this hypothesis is the finding of stem cell markers in CSC from primary tumours such as, CD133 (promimin-1), nestin, c-kit, sox2, Oct4 and musashi-1 (Hemmati et al., 2003; Singh et al., 2003;

Singh et al., 2004; Eramo et al., 2008; Ricci-Vitiani et al., 2007; Collins et al., 2005). The second hypothesis states that stem cell characteristics can be acquired by any cell through transformation. For example, normal fibroblasts acquire stem cell qualities by expression of Oct4, Sox2, Nanog and LIN28 (Yu et al., 2007) or Oct3/4, sox2, Klf4 and c-Myc (Takahashi et al., 2007). In epithelial cancers, epithelial-mesenchymal transition (EMT) has been described as a process of partial dedifferentiation (Hugo et al., 2007). In this process, epithelial-specific cytokeratins and E-cadherin are lost and replaced by mesenchymal markers such as vimentin and N-cadherin. Transcription factors Twist, Snail or Slug and TGF-β have been implicated in the initiation of EMT. Recent publications by the Weinberg group support the idea that cancer cells can re-acquire stem cell characteristics as they undergo EMT, a process linked to invasive and metastatic tumour behaviour (Mani et al., 2008). A third hypothesis proposes an "intermediate" mechanism. In this model, CSCs are thought to originate from particular cell populations such as tissue stem cells and immature progenitors that have short-term self-replication capabilities. Research supporting this idea showed that estrogen receptor (ERα)-negative breast cancers and aggressive ERα-positive cancers originate from ERα-negative primitive mammary stem cells whereas less aggressive ERα-positive cancers originate form ERα-positive intermediate progenitors (Dontu et al., 2004). It is important to note that there three models are not necessarily mutually exclusive and may explain different stages of cancer or may underlie the differences observed between different types and different subtypes of cancer.

The study of CSCs has been limited so far by the lack of universal markers specific for these cells that would allow their isolation from the tumour mass. In addition, some of the markers identified so far are not found in different malignancies (O'Brien et al., 2010). Previous studies have also highlighted the importance of considering the cellular microenvironment and the role of the immune system when studying CSCs (LaBarge, 2010). Taking into account the cellular microenvironment is particularly crucial when studying Notch signals which are transmitted by cell to cell contact. The role of the immune system was highlighted by studies in mice, where tumorigenicity of CSCs in different mice models varied depending on the levels of immunodeficiency (Schatton et al., 2008; Quintana et al., 2008).

There is accumulated evidence for a role of Notch in CSC in breast cancer (Farnie and Clarke, 2007; Farnie et al., 2007; Sansone et al., 2007), embryonal brain tumours (Fan

et al., 2006) and gliomas (Fan et al., 2010; Wang et al., 2010). GSIs have been shown to inhibit formation of secondary mammospheres in multiple human breast cancer cell lines and primary patient samples (Grudzien et al., 2010). Mammospheres are considered as an indicator of stem-like cells. GSIs and a Notch4 monoclonal antibody also inhibited formation of mammospheres in breast ductal carcinoma, *in situ* (Farnie et al., 2007). A study by Sansone et al. highlighted a cross talk between IL6 and Notch in mammospheres from human breast cancers. IL6 is shown to induce Notch3 signalling specifically, increase Jagged-1 expression and promote resistance to hypoxic conditions through Notch3 (Sansone et al., 2007). Other studies showed that Notch inhibition results in the depletion of medulloblastoma and glioblastoma CSCs (Fan et al., 2010; Fan et al., 2006).

It is generally believed that current cancer therapeutics do not allow adequate targeting of CSCs. It is proposed that long-lasting remissions or cures will require the complete abolition of CSCs. Based on the evidence of a role for Notch in CSC, Notch inhibitors are considered promising tools to target CSCs for cancer therapy. In this study, the effect of novel Notch inhibitors was not investigated in the context of CSCs. Future studies should investigate the potential of the fusions as therapeutic agents in such a model. Also, the tools developed in this study can be employed to better understand the role of canonical Notch signalling in the context of CSCs.

The study of Notch signalling has led to the development of various inhibitors. These can be divided in two categories: pan-Notch inhibitors versus specific inhibitors. As previously described, Notch signalling can be initiated by binding to four different receptors in mammals. In the canonical pathway, signals from all receptors are believed to converge into a single event: the formation of the active tripartite transcription complex in the nucleus. The structure of the Notch pathway is such that depending at which level they target the pathway, inhibitors can affect Notch signalling as a whole or signalling originating from a single receptor only. At present, there is no clear advantage of one strategy versus the other. Both categories have their advantages and disadvantages and might be applicable to different biological scenarios. As inhibitors of γ-secretase activity, GSIs are pan-Notch inhibitors but also block the cleavage of other γ-secretase substrates. It is believed that off-target effects might be different depending on the inhibitor used. Developers of these drugs argue that inhibition of other γ-secretase targets might be beneficial in some cases, contributing to therapeutic efficacy. Advantages of GSIs include ease of

administration, oral bioavailability and low cost. Research by Moellering et al. has revolutionised the field of Notch inhibition by developing pan-Notch inhibitors without the off-target effects of GSIs (Moellering et al., 2009). Specificity to the Notch pathway is achieved by targeting formation of the CSL-N^{IC}-MAML complex. This study described the development of two alternative strategies that promise to be more suitable for use in the clinic. In particular, the delivery of antibody fragments means that higher binding affinities can potentially be obtained compared to peptide drugs (picomolar compared to micromolar). The scFv fusion developed in this study has affinity in the nanomolar range. This can be improved by random mutagenesis followed by additional rounds of phage display selection. This is a common strategy used in the development of antibodies, especially when the initial selection is performed using a naïve library (Pini et al., 1998). Another common practice to improve on affinity is to combine two scFvs in an IgG format. This is not applicable to this study as a high affinity monovalent binder is needed to block a single complex on DNA. Antibodies are also used for selective inhibition of Notch signalling, targeting single receptors/ligands. These tools are best suited where a specific Notch-ligand combination is involved in malignancy. For example, antibodies against DLL4 have been developed following the discovery of this ligand's specific involvement in angiogenesis. In the context of CSCs, Notch3 could be targeted to attain hypoxia-resistant cells specifically.

Future work

This study involved extensive work on expressing and purifying several protein constructs. The production of these proteins is crucial in order to test their effect *in vitro*. Therefore, future work should involve optimisation of these protocols in order to obtain improved protein yields and to ensure correct folding of these proteins. The first protein produced in this study is Antp. The protocol for isolation of this cell penetrating protein is satisfactory. However, since Antp is a *Drosophila* protein, the use of insect cells as a recombinant system is worth investigating in the future. Regarding Antp-DN-MAML1, extensive work has been carried out in this study and by our collaborators in order to determine a successful strategy for production of this fusion protein. Despite multiple efforts, currently production of Antp-DN-MAML1 relies on its synthesis as a custom peptide. This procedure is costly and could not be

applied to larger fusions. One strategy that was not attempted is the expression of Antp-DN-MAML1 using a mammalian expression system. This is worth considering in future studies as the DN-MAML1 portion of the protein is of mammalian origin. However, expression trials of Antp and Antp-scFv in CHO cells have shown that, even in this system, protein production is problematic. A second strategy for future production of Antp-DN-MAML1 is to further investigate its expression as a soluble protein within the first hour post induction and attempt its purification. As ion exchange and affinity chromatography showed disappointing results, successful isolation of this protein might rely on changing the position or the nature of the tag. The fusion between Antp and a scFv is the construct that requires most attention in future studies. Production of this fusion protein currently relies on expression in inclusion bodies followed by a refolding protocol. There is scope for improvement of the refolding method, but soluble expression should be the target in the future. Recently, a collaborator has successfully expressed scFv antibody fragments in the cytoplasm. This strategy requires the fusion of the scFv to an 'expression partner' and the use of a particular *E.coli* strain that presents the suitable conditions for formation of disulphide bonds in the cytoplasm (oxidising environment and presence of chaperones). Expression of the Antp-scFv fusions should be assessed in this novel system.

The novel tools employed in this study for the inhibition of Notch signalling, rely on the Antp protein for successful intracellular delivery. The study of the internalisation mechanism of Antp was beyond the scope of this study. However, further studies should aim at further investigating this system. In particular, it is of interest to determine whether the internalisation process is dependent on endocytosis and if there are any specific interactions with particular membrane components.

The study of Antp internalisation should include a direct comparison with its derivative penetratin including an evaluation of their respective toxic effects. Further studies should also evaluate the ability of Antp and penetratin to transport cargoes of different sizes. In order to avoid the artefacts observed when using fluorescence to track protein internalisation, the use of radioactivity constitutes a suitable alternative. Using a radioactive marker enables quantification of internalisation. One of the limitations of using this technique is the measure of particles stuck to the membrane as internalised protein. Extensive washing can minimise this artefact.

Hes1 gene expression levels were used as a read out of Notch activity in *in vitro* assays. Hes1 is a well-characterised Notch target gene and its expression levels can confidently be related to Notch signalling activation/inhibition. Future studies should explore the expression of alternative genes (i.e. Hey1) upon treatment with Notch inhibitors. It is important to verify that the genes analysed are in fact direct Notch target genes. Ideally, their expression should not be influenced by other systems of regulation.

The observations made in this study that point to a possible interaction of DN-MAML1 with p53 should be further investigated. It is important to verify binding of truncated MAML1 to p53 to support our model. This will involve production of the p53 protein to carry out binding studies by ELISA. It is important to note that increase in p21 might rely on a different mechanism related to inhibition of Notch. This possibility should be investigated in the future.

The inhibitors studies in this project should also be tested in alternative cancer models such as T-ALL cells and CSCs. In a T-ALL model, it is well established that inhibition of Notch results in cell death. Therefore, this model offers a clear readout for testing of the Notch inhibitors. The effect of Notch inhibitors in CSCs should be investigated to better understand the role of canonical Notch signalling in this context. Future studies should investigate the potential of the fusions as therapeutic agents in this model.

The *in vivo* experiments presented in this study provide initial evidence supporting the use of Antp-DN-MAML1 as a therapeutic agent. In the future, *in vivo* experiments should be carried out on a bigger scale with the addition of all relevant control groups. A range of dosages and different administration routines should be envisaged. In order to study a possible role for the immunise system in the effect of Antp-DN-MAML1 on tumour growth, it would be interesting to collect blood samples during the *in vivo* study to monitor the immune system's levels of activation. Tumour samples should also be collected to study the cellular composition and morphology in addition to gene expression profiles. In particular, Ki-67 staining is useful to determine the levels of cellular proliferation in the tumour and surrounding tissue. Staining for CD44, CD24 and ALDH1 is also of interest as this allows the identification of cancer stem cells within the breast cancer population. Analysis of tumour samples could also reveal the presence of apoptosis (cleaved caspase 3) and metastasis (uPA and PAI1) markers.

In relation to the work on the Antp-scFv fusions, additional time will allow to better characterise the pool of antibody fragments isolated by phage display selection. In this study, screening of candidate scFvs was based on the binding to DN-MAML1. Ideally, a functional screening should be carried out to determine successful inhibition of tripartite complex formation upon binding. This was not possible due to the unavailability of the CSL and N^{IC} proteins. By choosing the minimal portion of MAML required for complex formation as the antigen in our phage display selection, the chances of selecting an appropriate scFv are maximised. If future studies revealed that the affinity of selected scFvs is not sufficient to have an effect on initiation of signalling, it will be necessary to carry out random mutagenesis of the scFv pool followed by an additional phage display round. This is a common practice in the field of antibody engineering. Mutagenesis could also be employed to engineer the antibody fragment's linker region to prevent cleavage as observed during production.

In this study, ELISA was chosen as a technique to detect binding between two proteins. Other methods are available to study binding including surface plasmon resonance, isothermal titration calorimetry (ITC) and bandshift gel retardation assay on native gels. While ELISA allows end-point measurements, rate constants can be measured using surface plasmon resonance. An alternative method named ITC allows direct measurements of the heat absorbed or released during binding, providing a complete thermodynamic profile of molecular interactions. The limitation of ITC is the requirement for vast amounts of protein to perform the assay. Thus, ITC was not applicable to this study. The least sophisticated method is the use of native gels to observe bandshifts on gels upon binding. This method only allows the detection of strong interactions and requires considerable optimisation to achieve the optimal running conditions.

A critical tool that was missing from this study is a reliable antibody against Antp in order to track this protein and the corresponding fusions. It is desirable to be able to detect the proteins of interest directly rather than relying on tags. Future studies should include the development of such tool or the verification of the antibody available on the market.

Overall, future studies building on the results obtained during this project will provide interesting insights on the biology of Notch and help establish the intracellular inhibition of Notch as a valid strategy for cancer therapy.

BIBLIOGRAPHY

Akiyoshi, T., Nakamura, M., Yanai, K., Nagai, S., Wada, J., Koga, K., Nakashima, H., Sato, N., Tanaka, M., and Katano, M. (2008). Gamma-secretase inhibitors enhance taxane-induced mitotic arrest and apoptosis in colon cancer cells. Gastroenterology *134*, 131-144.
Al-Hajj, M., Becker, M.W., Wicha, M., Weissman, I., and Clarke, M.F. (2004). Therapeutic implications of cancer stem cells. Curr Opin Genet Dev *14*, 43-47.
Ames, R.S., Tornetta, M.A., McMillan, L.J., Kaiser, K.F., Holmes, S.D., Appelbaum, E., Cusimano, D.M., Theisen, T.W., Gross, M.S., Jones, C.S., *et al.* (1995). Neutralizing murine monoclonal antibodies to human IL-5 isolated from hybridomas and a filamentous phage Fab display library. J Immunol *154*, 6355-6364.
Andersen, P., Uosaki, H., Shenje, L.T., and Kwon, C. (2012). Non-canonical Notch signaling: emerging role and mechanism. Trends Cell Biol *22*, 257-265.
Anderson, D.C., Nichols, E., Manger, R., Woodle, D., Barry, M., and Fritzberg, A.R. (1993). Tumor cell retention of antibody Fab fragments is enhanced by an attached HIV TAT protein-derived peptide. Biochem Biophys Res Commun *194*, 876-884.
Aste-Amezaga, M., Zhang, N., Lineberger, J.E., Arnold, B.A., Toner, T.J., Gu, M., Huang, L., Vitelli, S., Vo, K.T., Haytko, P., *et al.* (2010). Characterization of Notch1 antibodies that inhibit signaling of both normal and mutated Notch1 receptors. PLoS One *5*, e9094.
Auf der Maur, A., Tissot, K., and Barberis, A. (2004). Antigen-independent selection of intracellular stable antibody frameworks. Methods *34*, 215-224.
Avignolo, C., Bagnasco, L., Biasotti, B., Melchiori, A., Tomati, V., Bauer, I., Salis, A., Chiossone, L., Mingari, M.C., Orecchia, P., *et al.* (2008). Internalization via Antennapedia protein transduction domain of an scFv antibody toward c-Myc protein. FASEB J *22*, 1237-1245.
Barbas, C.F., 3rd, Kang, A.S., Lerner, R.A., and Benkovic, S.J. (1991). Assembly of combinatorial antibody libraries on phage surfaces: the gene III site. Proc Natl Acad Sci U S A *88*, 7978-7982.
Beel, A.J., and Sanders, C.R. (2008). Substrate specificity of gamma-secretase and other intramembrane proteases. Cell Mol Life Sci *65*, 1311-1334.
Beerli, R.R., Wels, W., and Hynes, N.E. (1994). Intracellular expression of single chain antibodies reverts ErbB-2 transformation. J Biol Chem *269*, 23931-23936.
Ben-Kasus, T., Schechter, B., Sela, M., and Yarden, Y. (2007). Cancer therapeutic antibodies come of age: targeting minimal residual disease. Molecular oncology *1*, 42-54.
Benhar, I. (2007). Design of synthetic antibody libraries. Expert Opin Biol Ther *7*, 763-779.
Bera, T.K., Onda, M., Brinkmann, U., and Pastan, I. (1998). A bivalent disulfide-stabilized Fv with improved antigen binding to erbB2. J Mol Biol *281*, 475-483.
Berdnik, D., Torok, T., Gonzalez-Gaitan, M., and Knoblich, J.A. (2002). The endocytic protein alpha-Adaptin is required for numb-mediated asymmetric cell division in Drosophila. Dev Cell *3*, 221-231.
Bhatti, M., Yahioglu, G., Milgrom, L.R., Garcia-Maya, M., Chester, K.A., and Deonarain, M.P. (2008). Targeted photodynamic therapy with multiply-loaded recombinant antibody fragments. Int J Cancer *122*, 1155-1163.
Biocca, S., Pierandrei-Amaldi, P., Campioni, N., and Cattaneo, A. (1994). Intracellular immunization with cytosolic recombinant antibodies. Bio/technology *12*, 396-399.
Blau, S., Jubeh, T.T., Haupt, S.M., and Rubinstein, A. (2000). Drug targeting by surface cationization. Crit Rev Ther Drug Carrier Syst *17*, 425-465.

Blaumueller, C.M., Qi, H., Zagouras, P., and Artavanis-Tsakonas, S. (1997). Intracellular cleavage of Notch leads to a heterodimeric receptor on the plasma membrane. Cell *90*, 281-291.
Boldicke, T. (2007). Blocking translocation of cell surface molecules from the ER to the cell surface by intracellular antibodies targeted to the ER. Journal of cellular and molecular medicine *11*, 54-70.
Borggrefe, T., and Oswald, F. (2009). The Notch signaling pathway: transcriptional regulation at Notch target genes. Cell Mol Life Sci *66*, 1631-1646.
Brou, C., Logeat, F., Gupta, N., Bessia, C., LeBail, O., Doedens, J.R., Cumano, A., Roux, P., Black, R.A., and Israel, A. (2000). A novel proteolytic cleavage involved in Notch signaling: the role of the disintegrin-metalloprotease TACE. Mol Cell *5*, 207-216.
Chames, P., Van Regenmortel, M., Weiss, E., and Baty, D. (2009). Therapeutic antibodies: successes, limitations and hopes for the future. Br J Pharmacol *157*, 220-233.
Chaudhary, V.K., Queen, C., Junghans, R.P., Waldmann, T.A., FitzGerald, D.J., and Pastan, I. (1989). A recombinant immunotoxin consisting of two antibody variable domains fused to Pseudomonas exotoxin. Nature *339*, 394-397.
Chitnis, A. (2006). Why is delta endocytosis required for effective activation of notch? Dev Dyn *235*, 886-894.
Chiu, Y.L., Ali, A., Chu, C.Y., Cao, H., and Rana, T.M. (2004). Visualizing a correlation between siRNA localization, cellular uptake, and RNAi in living cells. Chem Biol *11*, 1165-1175.
Chu, E. (2006). Panitumumab: a new anti-EGFR antibody for the treatment of advanced colorectal cancer. Clin Colorectal Cancer *6*, 13.
Clackson, T., Hoogenboom, H.R., Griffiths, A.D., and Winter, G. (1991). Making antibody fragments using phage display libraries. Nature *352*, 624-628.
Claxton, S., and Fruttiger, M. (2004). Periodic Delta-like 4 expression in developing retinal arteries. Gene expression patterns : GEP *5*, 123-127.
Cohen, P.A., Mani, J.C., and Lane, D.P. (1998). Characterization of a new intrabody directed against the N-terminal region of human p53. Oncogene *17*, 2445-2456.
Coiffier, B. (2007). Rituximab therapy in malignant lymphoma. Oncogene *26*, 3603-3613.
Collins, A.T., Berry, P.A., Hyde, C., Stower, M.J., and Maitland, N.J. (2005). Prospective identification of tumorigenic prostate cancer stem cells. Cancer Res *65*, 10946-10951.
Cooke, S.P., Pedley, R.B., Boden, R., Begent, R.H., and Chester, K.A. (2002). In vivo tumor delivery of a recombinant single chain Fv::tumor necrosis factor-alpha fusion [correction of factor: a fusion] protein. Bioconjug Chem *13*, 7-15.
Cordle, J., Redfieldz, C., Stacey, M., van der Merwe, P.A., Willis, A.C., Champion, B.R., Hambleton, S., and Handford, P.A. (2008). Localization of the delta-like-1-binding site in human Notch-1 and its modulation by calcium affinity. J Biol Chem *283*, 11785-11793.
Costantini, D.L., Villani, D.F., Vallis, K.A., and Reilly, R.M. (2010). Methotrexate, paclitaxel, and doxorubicin radiosensitize HER2-amplified human breast cancer cells to the Auger electron-emitting radiotherapeutic agent (111)In-NLS-trastuzumab. J Nucl Med *51*, 477-483.
D'Souza, B., Miyamoto, A., and Weinmaster, G. (2008). The many facets of Notch ligands. Oncogene *27*, 5148-5167.

Davidson, T.J., Harel, S., Arboleda, V.A., Prunell, G.F., Shelanski, M.L., Greene, L.A., and Troy, C.M. (2004). Highly efficient small interfering RNA delivery to primary mammalian neurons induces MicroRNA-like effects before mRNA degradation. J Neurosci *24*, 10040-10046.
Davies, A.J. (2007). Radioimmunotherapy for B-cell lymphoma: Y90 ibritumomab tiuxetan and I(131) tositumomab. Oncogene *26*, 3614-3628.
de Haard, H.J., van Neer, N., Reurs, A., Hufton, S.E., Roovers, R.C., Henderikx, P., de Bruine, A.P., Arends, J.W., and Hoogenboom, H.R. (1999). A large non-immunized human Fab fragment phage library that permits rapid isolation and kinetic analysis of high affinity antibodies. J Biol Chem *274*, 18218-18230.
Deftos, M.L., He, Y.W., Ojala, E.W., and Bevan, M.J. (1998). Correlating notch signaling with thymocyte maturation. Immunity *9*, 777-786.
Deftos, M.L., Huang, E., Ojala, E.W., Forbush, K.A., and Bevan, M.J. (2000). Notch1 signaling promotes the maturation of CD4 and CD8 SP thymocytes. Immunity *13*, 73-84.
Derossi, D., Joliot, A.H., Chassaing, G., and Prochiantz, A. (1994). The third helix of the Antennapedia homeodomain translocates through biological membranes. J Biol Chem *269*, 10444-10450.
Dievart, A., Beaulieu, N., and Jolicoeur, P. (1999). Involvement of Notch1 in the development of mouse mammary tumors. Oncogene *18*, 5973-5981.
Donnenberg, V.S., and Donnenberg, A.D. (2005). Multiple drug resistance in cancer revisited: the cancer stem cell hypothesis. Journal of clinical pharmacology *45*, 872-877.
Dontu, G., El-Ashry, D., and Wicha, M.S. (2004). Breast cancer, stem/progenitor cells and the estrogen receptor. Trends Endocrinol Metab *15*, 193-197.
Duarte, A., Hirashima, M., Benedito, R., Trindade, A., Diniz, P., Bekman, E., Costa, L., Henrique, D., and Rossant, J. (2004). Dosage-sensitive requirement for mouse Dll4 in artery development. Genes Dev *18*, 2474-2478.
Duchardt, F., Fotin-Mleczek, M., Schwarz, H., Fischer, R., and Brock, R. (2007). A comprehensive model for the cellular uptake of cationic cell-penetrating peptides. Traffic *8*, 848-866.
Duncan, A.W., Rattis, F.M., DiMascio, L.N., Congdon, K.L., Pazianos, G., Zhao, C., Yoon, K., Cook, J.M., Willert, K., Gaiano, N., *et al.* (2005). Integration of Notch and Wnt signaling in hematopoietic stem cell maintenance. Nat Immunol *6*, 314-322.
Dvorak, H.F. (2002). Vascular permeability factor/vascular endothelial growth factor: a critical cytokine in tumor angiogenesis and a potential target for diagnosis and therapy. J Clin Oncol *20*, 4368-4380.
Efstratiadis, A., Szabolcs, M., and Klinakis, A. (2007). Notch, Myc and breast cancer. Cell Cycle *6*, 418-429.
Ekberg, H., Backman, L., Tufveson, G., and Tyden, G. (1999). Zenapax (daclizumab) reduces the incidence of acute rejection episodes and improves patient survival following renal transplantation. No 14874 and No 14393 Zenapax Study Groups. Transplant Proc *31*, 267-268.
Ellisen, L.W., Bird, J., West, D.C., Soreng, A.L., Reynolds, T.C., Smith, S.D., and Sklar, J. (1991). TAN-1, the human homolog of the Drosophila notch gene, is broken by chromosomal translocations in T lymphoblastic neoplasms. Cell *66*, 649-661.
Eramo, A., Lotti, F., Sette, G., Pilozzi, E., Biffoni, M., Di Virgilio, A., Conticello, C., Ruco, L., Peschle, C., and De Maria, R. (2008). Identification and expansion of the tumorigenic lung cancer stem cell population. Cell Death Differ *15*, 504-514.

Fan, X., Khaki, L., Zhu, T.S., Soules, M.E., Talsma, C.E., Gul, N., Koh, C., Zhang, J., Li, Y.M., Maciaczyk, J., *et al.* (2010). NOTCH pathway blockade depletes CD133-positive glioblastoma cells and inhibits growth of tumor neurospheres and xenografts. Stem Cells *28*, 5-16.
Fan, X., Matsui, W., Khaki, L., Stearns, D., Chun, J., Li, Y.M., and Eberhart, C.G. (2006). Notch pathway inhibition depletes stem-like cells and blocks engraftment in embryonal brain tumors. Cancer Res *66*, 7445-7452.
Fan, X., Mikolaenko, I., Elhassan, I., Ni, X., Wang, Y., Ball, D., Brat, D.J., Perry, A., and Eberhart, C.G. (2004). Notch1 and notch2 have opposite effects on embryonal brain tumor growth. Cancer Res *64*, 7787-7793.
Farnie, G., and Clarke, R.B. (2007). Mammary stem cells and breast cancer--role of Notch signalling. Stem Cell Rev *3*, 169-175.
Farnie, G., Clarke, R.B., Spence, K., Pinnock, N., Brennan, K., Anderson, N.G., and Bundred, N.J. (2007). Novel cell culture technique for primary ductal carcinoma in situ: role of Notch and epidermal growth factor receptor signaling pathways. J Natl Cancer Inst *99*, 616-627.
Felici, F., Castagnoli, L., Musacchio, A., Jappelli, R., and Cesareni, G. (1991). Selection of antibody ligands from a large library of oligopeptides expressed on a multivalent exposition vector. J Mol Biol *222*, 301-310.
Fischer, A., and Gessler, M. (2007). Delta-Notch--and then? Protein interactions and proposed modes of repression by Hes and Hey bHLH factors. Nucleic Acids Res *35*, 4583-4596.
Fischer, M., Yen, W.C., Kapoun, A.M., Wang, M., O'Young, G., Lewicki, J., Gurney, A., and Hoey, T. (2011). Anti-DLL4 inhibits growth and reduces tumor-initiating cell frequency in colorectal tumors with oncogenic KRAS mutations. Cancer Res *71*, 1520-1525.
Frankel, A.D., and Pabo, C.O. (1988). Cellular uptake of the tat protein from human immunodeficiency virus. Cell *55*, 1189-1193.
Fryer, C.J., Lamar, E., Turbachova, I., Kintner, C., and Jones, K.A. (2002). Mastermind mediates chromatin-specific transcription and turnover of the Notch enhancer complex. Genes Dev *16*, 1397-1411.
Fryer, C.J., White, J.B., and Jones, K.A. (2004). Mastermind recruits CycC : CDK8 to phosphorylate the notch ICD and coordinate activation with turnover. Molecular Cell *16*, 509-520.
Futaki, S., Suzuki, T., Ohashi, W., Yagami, T., Tanaka, S., Ueda, K., and Sugiura, Y. (2001). Arginine-rich peptides. An abundant source of membrane-permeable peptides having potential as carriers for intracellular protein delivery. J Biol Chem *276*, 5836-5840.
Gale, N.W., Dominguez, M.G., Noguera, I., Pan, L., Hughes, V., Valenzuela, D.M., Murphy, A.J., Adams, N.C., Lin, H.C., Holash, J., *et al.* (2004). Haploinsufficiency of delta-like 4 ligand results in embryonic lethality due to major defects in arterial and vascular development. Proc Natl Acad Sci U S A *101*, 15949-15954.
Gallahan, D., and Callahan, R. (1987). Mammary tumorigenesis in feral mice: identification of a new int locus in mouse mammary tumor virus (Czech II)-induced mammary tumors. J Virol *61*, 66-74.
Gallahan, D., and Callahan, R. (1997). The mouse mammary tumor associated gene INT3 is a unique member of the NOTCH gene family (NOTCH4). Oncogene *14*, 1883-1890.
Gallahan, D., Jhappan, C., Robinson, G., Hennighausen, L., Sharp, R., Kordon, E., Callahan, R., Merlino, G., and Smith, G.H. (1996). Expression of a truncated Int3

gene in developing secretory mammary epithelium specifically retards lobular differentiation resulting in tumorigenesis. Cancer Res *56*, 1775-1785.
Gao, C., Mao, S., Lo, C.H., Wirsching, P., Lerner, R.A., and Janda, K.D. (1999). Making artificial antibodies: a format for phage display of combinatorial heterodimeric arrays. Proc Natl Acad Sci U S A *96*, 6025-6030.
Garces, C., Ruiz-Hidalgo, M.J., Font de Mora, J., Park, C., Miele, L., Goldstein, J., Bonvini, E., Porras, A., and Laborda, J. (1997). Notch-1 controls the expression of fatty acid-activated transcription factors and is required for adipogenesis. J Biol Chem *272*, 29729-29734.
Gentle, M.E., Rose, A., Bugeon, L., and Dallman, M.J. (2012). Noncanonical Notch signaling modulates cytokine responses of dendritic cells to inflammatory stimuli. J Immunol *189*, 1274-1284.
Giovannini, C., Gramantieri, L., Chieco, P., Minguzzi, M., Lago, F., Pianetti, S., Ramazzotti, E., Marcu, K.B., and Bolondi, L. (2009). Selective ablation of Notch3 in HCC enhances doxorubicin's death promoting effect by a p53 dependent mechanism. J Hepatol *50*, 969-979.
Giovannini, C., Lacchini, M., Gramantieri, L., Chieco, P., and Bolondi, L. (2006). Notch3 intracellular domain accumulates in HepG2 cell line. Anticancer Res *26*, 2123-2127.
Goletz, S., Christensen, P.A., Kristensen, P., Blohm, D., Tomlinson, I., Winter, G., and Karsten, U. (2002). Selection of large diversities of antiidiotypic antibody fragments by phage display. J Mol Biol *315*, 1087-1097.
Gounder, M.M., and Schwartz, G.K. (2012). Moving forward one Notch at a time. J Clin Oncol *30*, 2291-2293.
Green, M., and Loewenstein, P.M. (1988). Autonomous functional domains of chemically synthesized human immunodeficiency virus tat trans-activator protein. Cell *55*, 1179-1188.
Griffiths, A.D., Malmqvist, M., Marks, J.D., Bye, J.M., Embleton, M.J., McCafferty, J., Baier, M., Holliger, K.P., Gorick, B.D., Hughes-Jones, N.C., *et al.* (1993). Human anti-self antibodies with high specificity from phage display libraries. EMBO J *12*, 725-734.
Gros, E., Deshayes, S., Morris, M.C., Aldrian-Herrada, G., Depollier, J., Heitz, F., and Divita, G. (2006). A non-covalent peptide-based strategy for protein and peptide nucleic acid transduction. Biochim Biophys Acta *1758*, 384-393.
Groth, C., and Fortini, M.E. (2012). Therapeutic approaches to modulating Notch signaling: current challenges and future prospects. Seminars in cell & developmental biology *23*, 465-472.
Grudzien, P., Lo, S., Albain, K.S., Robinson, P., Rajan, P., Strack, P.R., Golde, T.E., Miele, L., and Foreman, K.E. (2010). Inhibition of Notch signaling reduces the stem-like population of breast cancer cells and prevents mammosphere formation. Anticancer Res *30*, 3853-3867.
Gu, F., Ma, Y., Zhang, Z., Zhao, J., Kobayashi, H., Zhang, L., and Fu, L. (2010). Expression of Stat3 and Notch1 is associated with cisplatin resistance in head and neck squamous cell carcinoma. Oncol Rep *23*, 671-676.
Guilmeau, S., Flandez, M., Mariadason, J.M., and Augenlicht, L.H. (2010). Heterogeneity of Jagged1 expression in human and mouse intestinal tumors: implications for targeting Notch signaling. Oncogene *29*, 992-1002.
Haines, N., and Irvine, K.D. (2003). Glycosylation regulates Notch signalling. Nat Rev Mol Cell Biol *4*, 786-797.

Hallbrink, M., Floren, A., Elmquist, A., Pooga, M., Bartfai, T., and Langel, U. (2001). Cargo delivery kinetics of cell-penetrating peptides. Biochim Biophys Acta *1515*, 101-109.
Han, J., Ma, I., Hendzel, M.J., and Allalunis-Turner, J. (2009). The cytotoxicity of gamma-secretase inhibitor I to breast cancer cells is mediated by proteasome inhibition, not by gamma-secretase inhibition. Breast Cancer Res *11*, R57.
Hansen, J.E., Fischer, L.K., Chan, G., Chang, S.S., Baldwin, S.W., Aragon, R.J., Carter, J.J., Lilly, M., Nishimura, R.N., Weisbart, R.H., *et al*. (2007). Antibody-mediated p53 protein therapy prevents liver metastasis in vivo. Cancer Res *67*, 1769-1774.
Hawkins, R.E., Russell, S.J., and Winter, G. (1992). Selection of Phage Antibodies by Binding-Affinity - Mimicking Affinity Maturation. Journal of Molecular Biology *226*, 889-896.
Hayashi, I., Takatori, S., Urano, Y., Miyake, Y., Takagi, J., Sakata-Yanagimoto, M., Iwanari, H., Osawa, S., Morohashi, Y., Li, T., *et al.* (2012). Neutralization of the gamma-secretase activity by monoclonal antibody against extracellular domain of nicastrin. Oncogene *31*, 787-798.
Hellstrom, M., Phng, L.K., Hofmann, J.J., Wallgard, E., Coultas, L., Lindblom, P., Alva, J., Nilsson, A.K., Karlsson, L., Gaiano, N., *et al*. (2007). Dll4 signalling through Notch1 regulates formation of tip cells during angiogenesis. Nature *445*, 776-780.
Helms, W., Lee, H., Ammerman, M., Parks, A.L., Muskavitch, M.A., and Yedvobnick, B. (1999). Engineered truncations in the Drosophila mastermind protein disrupt Notch pathway function. Dev Biol *215*, 358-374.
Hemmati, H.D., Nakano, I., Lazareff, J.A., Masterman-Smith, M., Geschwind, D.H., Bronner-Fraser, M., and Kornblum, H.I. (2003). Cancerous stem cells can arise from pediatric brain tumors. Proc Natl Acad Sci U S A *100*, 15178-15183.
Henriques, S.T., and Castanho, M.A. (2008). Translocation or membrane disintegration? Implication of peptide-membrane interactions in pep-1 activity. J Pept Sci *14*, 482-487.
Hirata, H., Yoshiura, S., Ohtsuka, T., Bessho, Y., Harada, T., Yoshikawa, K., and Kageyama, R. (2002). Oscillatory expression of the bHLH factor Hes1 regulated by a negative feedback loop. Science *298*, 840-843.
Hoey, T., Yen, W.C., Axelrod, F., Basi, J., Donigian, L., Dylla, S., Fitch-Bruhns, M., Lazetic, S., Park, I.K., Sato, A., *et al*. (2009). DLL4 blockade inhibits tumor growth and reduces tumor-initiating cell frequency. Cell Stem Cell *5*, 168-177.
Holt, L.J., Basran, A., Jones, K., Chorlton, J., Jespers, L.S., Brewis, N.D., and Tomlinson, I.M. (2008). Anti-serum albumin domain antibodies for extending the half-lives of short lived drugs. Protein engineering, design & selection : PEDS *21*, 283-288.
Hoogenboom, H.R. (2005). Selecting and screening recombinant antibody libraries. Nat Biotechnol *23*, 1105-1116.
Hori, K., Fostier, M., Ito, M., Fuwa, T.J., Go, M.J., Okano, H., Baron, M., and Matsuno, K. (2004). Drosophila deltex mediates suppressor of Hairless-independent and late-endosomal activation of Notch signaling. Development *131*, 5527-5537.
Hosotani, R., Miyamoto, Y., Fujimoto, K., Doi, R., Otaka, A., Fujii, N., and Imamura, M. (2002). Trojan p16 peptide suppresses pancreatic cancer growth and prolongs survival in mice. Clin Cancer Res *8*, 1271-1276.
Hrabe de Angelis, M., McIntyre, J., 2nd, and Gossler, A. (1997). Maintenance of somite borders in mice requires the Delta homologue DII1. Nature *386*, 717-721.

Hsieh, J.J., Zhou, S., Chen, L., Young, D.B., and Hayward, S.D. (1999). CIR, a corepressor linking the DNA binding factor CBF1 to the histone deacetylase complex. Proc Natl Acad Sci U S A *96*, 23-28.
Hudecz, F., Banoczi, Z., and Csik, G. (2005). Medium-sized peptides as built in carriers for biologically active compounds. Med Res Rev *25*, 679-736.
Hufton, S.E., Moerkerk, P.T., Meulemans, E.V., de Bruine, A., Arends, J.W., and Hoogenboom, H.R. (1999). Phage display of cDNA repertoires: the pVI display system and its applications for the selection of immunogenic ligands. J Immunol Methods *231*, 39-51.
Hugo, H., Ackland, M.L., Blick, T., Lawrence, M.G., Clements, J.A., Williams, E.D., and Thompson, E.W. (2007). Epithelial--mesenchymal and mesenchymal--epithelial transitions in carcinoma progression. J Cell Physiol *213*, 374-383.
Hulleman, E., Quarto, M., Vernell, R., Masserdotti, G., Colli, E., Kros, J.M., Levi, D., Gaetani, P., Tunici, P., Finocchiaro, G., *et al.* (2009). A role for the transcription factor HEY1 in glioblastoma. Journal of cellular and molecular medicine *13*, 136-146.
Ignatovich, I.A., Dizhe, E.B., Pavlotskaya, A.V., Akifiev, B.N., Burov, S.V., Orlov, S.V., and Perevozchikov, A.P. (2003). Complexes of plasmid DNA with basic domain 47-57 of the HIV-1 Tat protein are transferred to mammalian cells by endocytosis-mediated pathways. J Biol Chem *278*, 42625-42636.
Isaacs, J.D. (2009). Antibody engineering to develop new antirheumatic therapies. Arthritis research & therapy *11*, 225.
Iso, T., Kedes, L., and Hamamori, Y. (2003). HES and HERP families: multiple effectors of the Notch signaling pathway. J Cell Physiol *194*, 237-255.
Iso, T., Sartorelli, V., Chung, G., Shichinohe, T., Kedes, L., and Hamamori, Y. (2001). HERP, a new primary target of Notch regulated by ligand binding. Mol Cell Biol *21*, 6071-6079.
Itoh, M., Kim, C.H., Palardy, G., Oda, T., Jiang, Y.J., Maust, D., Yeo, S.Y., Lorick, K., Wright, G.J., Ariza-McNaughton, L., *et al.* (2003). Mind bomb is a ubiquitin ligase that is essential for efficient activation of Notch signaling by Delta. Dev Cell *4*, 67-82.
Izon, D.J., Aster, J.C., He, Y., Weng, A., Karnell, F.G., Patriub, V., Xu, L., Bakkour, S., Rodriguez, C., Allman, D., *et al.* (2002). Deltex1 redirects lymphoid progenitors to the B cell lineage by antagonizing Notch1. Immunity *16*, 231-243.
Jafar-Nejad, H., Norga, K., and Bellen, H. (2002). Numb: "Adapting" notch for endocytosis. Dev Cell *3*, 155-156.
Jain, R.K. (1990). Physiological barriers to delivery of monoclonal antibodies and other macromolecules in tumors. Cancer Res *50*, 814s-819s.
Jarriault, S., Brou, C., Logeat, F., Schroeter, E.H., Kopan, R., and Israel, A. (1995). Signalling downstream of activated mammalian Notch. Nature *377*, 355-358.
Jarriault, S., Le Bail, O., Hirsinger, E., Pourquie, O., Logeat, F., Strong, C.F., Brou, C., Seidah, N.G., and Isra l, A. (1998). Delta-1 activation of notch-1 signaling results in HES-1 transactivation. Mol Cell Biol *18*, 7423-7431.
Jhappan, C., Gallahan, D., Stahle, C., Chu, E., Smith, G.H., Merlino, G., and Callahan, R. (1992). Expression of an activated Notch-related int-3 transgene interferes with cell differentiation and induces neoplastic transformation in mammary and salivary glands. Genes Dev *6*, 345-355.
Joliot, A., Pernelle, C., Deagostini-Bazin, H., and Prochiantz, A. (1991). Antennapedia homeobox peptide regulates neural morphogenesis. Proc Natl Acad Sci U S A *88*, 1864-1868.

Joliot, A., and Prochiantz, A. (2004). Transduction peptides: from technology to physiology. Nat Cell Biol *6*, 189-196.
Jones, P.T., Dear, P.H., Foote, J., Neuberger, M.S., and Winter, G. (1986). Replacing the complementarity-determining regions in a human antibody with those from a mouse. Nature *321*, 522-525.
Joo, Y.H., Jung, C.K., Kim, M.S., and Sun, D.I. (2009). Relationship between vascular endothelial growth factor and Notch1 expression and lymphatic metastasis in tongue cancer. Otolaryngology--head and neck surgery : official journal of American Academy of Otolaryngology-Head and Neck Surgery *140*, 512-518.
Kakarala, M., and Wicha, M.S. (2007). Cancer stem cells: implications for cancer treatment and prevention. Cancer journal *13*, 271-275.
Kale, A.A., and Torchilin, V.P. (2007). Enhanced transfection of tumor cells in vivo using "Smart" pH-sensitive TAT-modified pegylated liposomes. Journal of drug targeting *15*, 538-545.
Kao, H.Y., Ordentlich, P., Koyano-Nakagawa, N., Tang, Z., Downes, M., Kintner, C.R., Evans, R.M., and Kadesch, T. (1998). A histone deacetylase corepressor complex regulates the Notch signal transduction pathway. Genes Dev *12*, 2269-2277.
Katayose, D., Wersto, R., Cowan, K.H., and Seth, P. (1995). Effects of a recombinant adenovirus expressing WAF1/Cip1 on cell growth, cell cycle, and apoptosis. Cell growth & differentiation : the molecular biology journal of the American Association for Cancer Research *6*, 1207-1212.
Kipriyanov, S.M., Little, M., Kropshofer, H., Breitling, F., Gotter, S., and Dubel, S. (1996). Affinity enhancement of a recombinant antibody: formation of complexes with multiple valency by a single-chain Fv fragment-core streptavidin fusion. Protein Eng *9*, 203-211.
Kirkpatrick, R.B., Ganguly, S., Angelichio, M., Griego, S., Shatzman, A., Silverman, C., and Rosenberg, M. (1995). Heavy chain dimers as well as complete antibodies are efficiently formed and secreted from Drosophila via a BiP-mediated pathway. J Biol Chem *270*, 19800-19805.
Klinakis, A., Szabolcs, M., Politi, K., Kiaris, H., Artavanis-Tsakonas, S., and Efstratiadis, A. (2006). Myc is a Notch1 transcriptional target and a requisite for Notch1-induced mammary tumorigenesis in mice. Proc Natl Acad Sci U S A *103*, 9262-9267.
Koch, U., and Radtke, F. (2007). Notch and cancer: a double-edged sword. Cell Mol Life Sci *64*, 2746-2762.
Kohler, G., and Milstein, C. (1975). Continuous cultures of fused cells secreting antibody of predefined specificity. Nature *256*, 495-497.
Kontermann, R.E. (2004). Intrabodies as therapeutic agents. Methods *34*, 163-170.
Kopan, R. (2012). Notch signaling. Cold Spring Harbor perspectives in biology *4*.
Korkaya, H., and Wicha, M.S. (2007). Selective targeting of cancer stem cells: a new concept in cancer therapeutics. BioDrugs : clinical immunotherapeutics, biopharmaceuticals and gene therapy *21*, 299-310.
Kousparou, C.A., Yiacoumi, E., Deonarain, M.P., and Epenetos, A.A. (2012). Generation of a selectively cytotoxic fusion protein against p53 mutated cancers. BMC cancer *12*, 338.
Koutsokeras, A., and Kabouridis, P.S. (2009). Secretion and uptake of TAT-fusion proteins produced by engineered mammalian cells. Biochim Biophys Acta *1790*, 147-153.
Kovall, R.A., and Hendrickson, W.A. (2004). Crystal structure of the nuclear effector of Notch signaling, CSL, bound to DNA. EMBO J *23*, 3441-3451.

Kuroda, K., Han, H., Tani, S., Tanigaki, K., Tun, T., Furukawa, T., Taniguchi, Y., Kurooka, H., Hamada, Y., Toyokuni, S., *et al.* (2003). Regulation of marginal zone B cell development by MINT, a suppressor of Notch/RBP-J signaling pathway. Immunity *18*, 301-312.
Kurooka, H., and Honjo, T. (2000). Functional interaction between the mouse notch1 intracellular region and histone acetyltransferases PCAF and GCN5. J Biol Chem *275*, 17211-17220.
LaBarge, M.A. (2010). The difficulty of targeting cancer stem cell niches. Clin Cancer Res *16*, 3121-3129.
Lagerholm, B.C. (2007). Peptide-mediated intracellular delivery of quantum dots. Methods Mol Biol *374*, 105-112.
Lakin, N.D., and Jackson, S.P. (1999). Regulation of p53 in response to DNA damage. Oncogene *18*, 7644-7655.
Lamar, E., Deblandre, G., Wettstein, D., Gawantka, V., Pollet, N., Niehrs, C., and Kintner, C. (2001). Nrarp is a novel intracellular component of the Notch signaling pathway. Genes Dev *15*, 1885-1899.
Le Borgne, R., Bardin, A., and Schweisguth, F. (2005). The roles of receptor and ligand endocytosis in regulating Notch signaling. Development *132*, 1751-1762.
Le Friec, G., Sheppard, D., Whiteman, P., Karsten, C.M., Shamoun, S.A., Laing, A., Bugeon, L., Dallman, M.J., Melchionna, T., Chillakuri, C., *et al.* (2012). The CD46-Jagged1 interaction is critical for human TH1 immunity. Nat Immunol *13*, 1213-1221.
Lee, C.W., Raskett, C.M., Prudovsky, I., and Altieri, D.C. (2008). Molecular dependence of estrogen receptor-negative breast cancer on a notch-survivin signaling axis. Cancer Res *68*, 5273-5281.
Lewin, M., Carlesso, N., Tung, C.H., Tang, X.W., Cory, D., Scadden, D.T., and Weissleder, R. (2000). Tat peptide-derivatized magnetic nanoparticles allow in vivo tracking and recovery of progenitor cells. Nat Biotechnol *18*, 410-414.
Li, K., Li, Y., Wu, W., Gordon, W.R., Chang, D.W., Lu, M., Scoggin, S., Fu, T., Vien, L., Histen, G., *et al.* (2008). Modulation of Notch signaling by antibodies specific for the extracellular negative regulatory region of NOTCH3. J Biol Chem *283*, 8046-8054.
Lin, L., Mernaugh, R., Yi, F., Blum, D., Carbone, D.P., and Dang, T.P. (2010). Targeting specific regions of the Notch3 ligand-binding domain induces apoptosis and inhibits tumor growth in lung cancer. Cancer Res *70*, 632-638.
Lin, S.E., Oyama, T., Nagase, T., Harigaya, K., and Kitagawa, M. (2002). Identification of new human mastermind proteins defines a family that consists of positive regulators for notch signaling. J Biol Chem *277*, 50612-50620.
Linardou, H., Epenetos, A.A., and Deonarain, M.P. (2000). A recombinant cytotoxic chimera based on mammalian deoxyribonuclease-I. Int J Cancer *86*, 561-569.
Lindgren, M., and Langel, U. (2011). Classes and prediction of cell-penetrating peptides. Methods Mol Biol *683*, 3-19.
Liu, Z.J., Xiao, M., Balint, K., Smalley, K.S., Brafford, P., Qiu, R., Pinnix, C.C., Li, X., and Herlyn, M. (2006). Notch1 signaling promotes primary melanoma progression by activating mitogen-activated protein kinase/phosphatidylinositol 3-kinase-Akt pathways and up-regulating N-cadherin expression. Cancer Res *66*, 4182-4190.
Logeat, F., Bessia, C., Brou, C., LeBail, O., Jarriault, S., Seidah, N.G., and Israel, A. (1998). The Notch1 receptor is cleaved constitutively by a furin-like convertase. Proc Natl Acad Sci U S A *95*, 8108-8112.
Luo, D., and Saltzman, W.M. (2000). Synthetic DNA delivery systems. Nature Biotechnology *18*, 33-37.

Maier, M.M., and Gessler, M. (2000). Comparative analysis of the human and mouse Hey1 promoter: Hey genes are new Notch target genes. Biochem Biophys Res Commun *275*, 652-660.
Mailhos, C., Modlich, U., Lewis, J., Harris, A., Bicknell, R., and Ish-Horowicz, D. (2001). Delta4, an endothelial specific notch ligand expressed at sites of physiological and tumor angiogenesis. Differentiation; research in biological diversity *69*, 135-144.
Mani, S.A., Guo, W., Liao, M.J., Eaton, E.N., Ayyanan, A., Zhou, A.Y., Brooks, M., Reinhard, F., Zhang, C.C., Shipitsin, M., *et al.* (2008). The epithelial-mesenchymal transition generates cells with properties of stem cells. Cell *133*, 704-715.
Marks, J.D., and Bradbury, A. (2004). Selection of human antibodies from phage display libraries. Methods Mol Biol *248*, 161-176.
Marks, J.D., Hoogenboom, H.R., Bonnert, T.P., Mccafferty, J., Griffiths, A.D., and Winter, G. (1991). By-Passing Immunization - Human-Antibodies from V-Gene Libraries Displayed on Phage. Journal of Molecular Biology *222*, 581-597.
Marvin, D.A. (1998). Filamentous phage structure, infection and assembly. Curr Opin Struct Biol *8*, 150-158.
Matsuno, K., Diederich, R.J., Go, M.J., Blaumueller, C.M., and Artavanis-Tsakonas, S. (1995). Deltex acts as a positive regulator of Notch signaling through interactions with the Notch ankyrin repeats. Development *121*, 2633-2644.
Mayer, M., Kies, U., Kammermeier, R., and Buchner, J. (2000). BiP and PDI cooperate in the oxidative folding of antibodies in vitro. J Biol Chem *275*, 29421-29425.
McCafferty, J., Griffiths, A.D., Winter, G., and Chiswell, D.J. (1990). Phage antibodies: filamentous phage displaying antibody variable domains. Nature *348*, 552-554.
McGuinness, B.T., Walter, G., FitzGerald, K., Schuler, P., Mahoney, W., Duncan, A.R., and Hoogenboom, H.R. (1996). Phage diabody repertoires for selection of large numbers of bispecific antibody fragments. Nat Biotechnol *14*, 1149-1154.
McLaughlin, P., Grillo-Lopez, A.J., Link, B.K., Levy, R., Czuczman, M.S., Williams, M.E., Heyman, M.R., Bence-Bruckler, I., White, C.A., Cabanillas, F., *et al.* (1998). Rituximab chimeric anti-CD20 monoclonal antibody therapy for relapsed indolent lymphoma: half of patients respond to a four-dose treatment program. J Clin Oncol *16*, 2825-2833.
Meng, R.D., Shelton, C.C., Li, Y.M., Qin, L.X., Notterman, D., Paty, P.B., and Schwartz, G.K. (2009). gamma-Secretase inhibitors abrogate oxaliplatin-induced activation of the Notch-1 signaling pathway in colon cancer cells resulting in enhanced chemosensitivity. Cancer Res *69*, 573-582.
Mhashilkar, A.M., Bagley, J., Chen, S.Y., Szilvay, A.M., Helland, D.G., and Marasco, W.A. (1995). Inhibition of HIV-1 Tat-mediated LTR transactivation and HIV-1 infection by anti-Tat single chain intrabodies. EMBO J *14*, 1542-1551.
Mittal, S., Subramanyam, D., Dey, D., Kumar, R.V., and Rangarajan, A. (2009). Cooperation of Notch and Ras/MAPK signaling pathways in human breast carcinogenesis. Molecular cancer *8*, 128.
Moellering, R.E., Cornejo, M., Davis, T.N., Del Bianco, C., Aster, J.C., Blacklow, S.C., Kung, A.L., Gilliland, D.G., Verdine, G.L., and Bradner, J.E. (2009). Direct inhibition of the NOTCH transcription factor complex. Nature *462*, 182-188.
Mondon, P., Dubreuil, O., Bouayadi, K., and Kharrat, H. (2008). Human antibody libraries: a race to engineer and explore a larger diversity. Frontiers in bioscience : a journal and virtual library *13*, 1117-1129.

Morohashi, Y., Kan, T., Tominari, Y., Fuwa, H., Okamura, Y., Watanabe, N., Sato, C., Natsugari, H., Fukuyama, T., Iwatsubo, T., *et al.* (2006). C-terminal fragment of presenilin is the molecular target of a dipeptidic gamma-secretase-specific inhibitor DAPT (N-[N-(3,5-difluorophenacetyl)-L-alanyl]-S-phenylglycine t-butyl ester). J Biol Chem *281*, 14670-14676.
Morris, M.C., Depollier, J., Mery, J., Heitz, F., and Divita, G. (2001). A peptide carrier for the delivery of biologically active proteins into mammalian cells. Nat Biotechnol *19*, 1173-1176.
Morris, M.C., Deshayes, S., Heitz, F., and Divita, G. (2008). Cell-penetrating peptides: from molecular mechanisms to therapeutics. Biol Cell *100*, 201-217.
Morris, M.C., Vidal, P., Chaloin, L., Heitz, F., and Divita, G. (1997). A new peptide vector for efficient delivery of oligonucleotides into mammalian cells. Nucleic Acids Res *25*, 2730-2736.
Morrison, S.L., Johnson, M.J., Herzenberg, L.A., and Oi, V.T. (1984). Chimeric human antibody molecules: mouse antigen-binding domains with human constant region domains. Proc Natl Acad Sci U S A *81*, 6851-6855.
Mullendore, M.E., Koorstra, J.B., Li, Y.M., Offerhaus, G.J., Fan, X., Henderson, C.M., Matsui, W., Eberhart, C.G., Maitra, A., and Feldmann, G. (2009). Ligand-dependent Notch signaling is involved in tumor initiation and tumor maintenance in pancreatic cancer. Clin Cancer Res *15*, 2291-2301.
Muller, M., Affolter, M., Leupin, W., Otting, G., Wuthrich, K., and Gehring, W.J. (1988). Isolation and sequence-specific DNA binding of the Antennapedia homeodomain. EMBO J *7*, 4299-4304.
Mumm, J.S., Schroeter, E.H., Saxena, M.T., Griesemer, A., Tian, X., Pan, D.J., Ray, W.J., and Kopan, R. (2000). A ligand-induced extracellular cleavage regulates gamma-secretase-like proteolytic activation of Notch1. Mol Cell *5*, 197-206.
Nam, Y., Sliz, P., Song, L., Aster, J.C., and Blacklow, S.C. (2006). Structural basis for cooperativity in recruitment of MAML coactivators to Notch transcription complexes. Cell *124*, 973-983.
Nam, Y., Weng, A.P., Aster, J.C., and Blacklow, S.C. (2003). Structural requirements for assembly of the CSL.intracellular Notch1.Mastermind-like 1 transcriptional activation complex. J Biol Chem *278*, 21232-21239.
Nickoloff, B.J., Qin, J.Z., Chaturvedi, V., Denning, M.F., Bonish, B., and Miele, L. (2002). Jagged-1 mediated activation of notch signaling induces complete maturation of human keratinocytes through NF-kappaB and PPARgamma. Cell Death Differ *9*, 842-855.
Niesner, U., Halin, C., Lozzi, L., Gunthert, M., Neri, P., Wunderli-Allenspach, H., Zardi, L., and Neri, D. (2002). Quantitation of the tumor-targeting properties of antibody fragments conjugated to cell-permeating HIV-1 TAT peptides. Bioconjug Chem *13*, 729-736.
Nishimura, M., Isaka, F., Ishibashi, M., Tomita, K., Tsuda, H., Nakanishi, S., and Kageyama, R. (1998). Structure, chromosomal locus, and promoter of mouse Hes2 gene, a homologue of Drosophila hairy and Enhancer of split. Genomics *49*, 69-75.
Noguera-Troise, I., Daly, C., Papadopoulos, N.J., Coetzee, S., Boland, P., Gale, N.W., Lin, H.C., Yancopoulos, G.D., and Thurston, G. (2006). Blockade of Dll4 inhibits tumour growth by promoting non-productive angiogenesis. Nature *444*, 1032-1037.
O'Brien, C.A., Kreso, A., and Jamieson, C.H. (2010). Cancer stem cells and self-renewal. Clin Cancer Res *16*, 3113-3120.

O'Connell, D., Becerril, B., Roy-Burman, A., Daws, M., and Marks, J.D. (2002). Phage versus phagemid libraries for generation of human monoclonal antibodies. J Mol Biol *321*, 49-56.
Oehlke, J., Scheller, A., Wiesner, B., Krause, E., Beyermann, M., Klauschenz, E., Melzig, M., and Bienert, M. (1998). Cellular uptake of an alpha-helical amphipathic model peptide with the potential to deliver polar compounds into the cell interior non-endocytically. Biochim Biophys Acta *1414*, 127-139.
Ordentlich, P., Lin, A., Shen, C.P., Blaumueller, C., Matsuno, K., Artavanis-Tsakonas, S., and Kadesch, T. (1998). Notch inhibition of E47 supports the existence of a novel signaling pathway. Mol Cell Biol *18*, 2230-2239.
Osipo, C., Patel, P., Rizzo, P., Clementz, A.G., Hao, L., Golde, T.E., and Miele, L. (2008). ErbB-2 inhibition activates Notch-1 and sensitizes breast cancer cells to a gamma-secretase inhibitor. Oncogene *27*, 5019-5032.
Oswald, F., Kostezka, U., Astrahantseff, K., Bourteele, S., Dillinger, K., Zechner, U., Ludwig, L., Wilda, M., Hameister, H., Knochel, W., *et al.* (2002). SHARP is a novel component of the Notch/RBP-Jkappa signalling pathway. EMBO J *21*, 5417-5426.
Oswald, F., Liptay, S., Adler, G., and Schmid, R.M. (1998). NF-kappaB2 is a putative target gene of activated Notch-1 via RBP-Jkappa. Mol Cell Biol *18*, 2077-2088.
Oswald, F., Tauber, B., Dobner, T., Bourteele, S., Kostezka, U., Adler, G., Liptay, S., and Schmid, R.M. (2001). p300 acts as a transcriptional coactivator for mammalian Notch-1. Mol Cell Biol *21*, 7761-7774.
Oswald, F., Winkler, M., Cao, Y., Astrahantseff, K., Bourteele, S., Knochel, W., and Borggrefe, T. (2005). RBP-Jkappa/SHARP recruits CtIP/CtBP corepressors to silence Notch target genes. Mol Cell Biol *25*, 10379-10390.
Paganetti, P., Calanca, V., Galli, C., Stefani, M., and Molinari, M. (2005). beta-site specific intrabodies to decrease and prevent generation of Alzheimer's Abeta peptide. J Cell Biol *168*, 863-868.
Pajerowski, A.G., Nguyen, C., Aghajanian, H., Shapiro, M.J., and Shapiro, V.S. (2009). NKAP is a transcriptional repressor of notch signaling and is required for T cell development. Immunity *30*, 696-707.
Palm, C., Netzereab, S., and Hallbrink, M. (2006). Quantitatively determined uptake of cell-penetrating peptides in non-mammalian cells with an evaluation of degradation and antimicrobial effects. Peptides *27*, 1710-1716.
Palomero, T., Lim, W.K., Odom, D.T., Sulis, M.L., Real, P.J., Margolin, A., Barnes, K.C., O'Neil, J., Neuberg, D., Weng, A.P., *et al.* (2006). NOTCH1 directly regulates c-MYC and activates a feed-forward-loop transcriptional network promoting leukemic cell growth. Proc Natl Acad Sci U S A *103*, 18261-18266.
Panares, R.L., and Garcia, A.A. (2007). Bevacizumab in the management of solid tumors. Expert Rev Anticancer Ther *7*, 433-445.
Pandya, K., Meeke, K., Clementz, A.G., Rogowski, A., Roberts, J., Miele, L., Albain, K.S., and Osipo, C. (2011). Targeting both Notch and ErbB-2 signalling pathways is required for prevention of ErbB-2-positive breast tumour recurrence. Br J Cancer *105*, 796-806.
Paschke, M. (2006). Phage display systems and their applications. Applied microbiology and biotechnology *70*, 2-11.
Patel, N.S., Dobbie, M.S., Rochester, M., Steers, G., Poulsom, R., Le Monnier, K., Cranston, D.W., Li, J.L., and Harris, A.L. (2006). Up-regulation of endothelial delta-like 4 expression correlates with vessel maturation in bladder cancer. Clin Cancer Res *12*, 4836-4844.

Patel, N.S., Li, J.L., Generali, D., Poulsom, R., Cranston, D.W., and Harris, A.L. (2005). Up-regulation of delta-like 4 ligand in human tumor vasculature and the role of basal expression in endothelial cell function. Cancer Res *65*, 8690-8697.
Pece, S., Serresi, M., Santolini, E., Capra, M., Hulleman, E., Galimberti, V., Zurrida, S., Maisonneuve, P., Viale, G., and Di Fiore, P.P. (2004). Loss of negative regulation by Numb over Notch is relevant to human breast carcinogenesis. J Cell Biol *167*, 215-221.
Perez, F., Joliot, A., Bloch-Gallego, E., Zahraoui, A., Triller, A., and Prochiantz, A. (1992). Antennapedia homeobox as a signal for the cellular internalization and nuclear addressing of a small exogenous peptide. J Cell Sci *102 (Pt 4)*, 717-722.
Petcherski, A.G., and Kimble, J. (2000). Mastermind is a putative activator for Notch. Curr Biol *10*, R471-473.
Pini, A., Viti, F., Santucci, A., Carnemolla, B., Zardi, L., Neri, P., and Neri, D. (1998). Design and use of a phage display library. Human antibodies with subnanomolar affinity against a marker of angiogenesis eluted from a two-dimensional gel. J Biol Chem *273*, 21769-21776.
Pooga, M., Hallbrink, M., Zorko, M., and Langel, U. (1998). Cell penetration by transportan. FASEB J *12*, 67-77.
Porter, R.R. (1973). Structural studies of immunoglobulins. Science *180*, 713-716.
Poungpair, O., Pootong, A., Maneewatch, S., Srimanote, P., Tongtawe, P., Songserm, T., Tapchaisri, P., and Chaicumpa, W. (2010). A human single chain transbody specific to matrix protein (M1) interferes with the replication of influenza A virus. Bioconjug Chem *21*, 1134-1141.
Prabhu, N.S., Blagosklonny, M.V., Zeng, Y.X., Wu, G.S., Waldman, T., and El-Deiry, W.S. (1996). Suppression of cancer cell growth by adenovirus expressing p21(WAF1/CIP1) deficient in PCNA interaction. Clin Cancer Res *2*, 1221-1229.
Purow, B.W., Haque, R.M., Noel, M.W., Su, Q., Burdick, M.J., Lee, J., Sundaresan, T., Pastorino, S., Park, J.K., Mikolaenko, I., *et al.* (2005). Expression of Notch-1 and its ligands, Delta-like-1 and Jagged-1, is critical for glioma cell survival and proliferation. Cancer Res *65*, 2353-2363.
Qin, H., Du, D., Zhu, Y., Li, J., Feng, L., Liang, Y., and Han, H. (2005). The PcG protein HPC2 inhibits RBP-J-mediated transcription by interacting with LIM protein KyoT2. FEBS Lett *579*, 1220-1226.
Qin, H., Wang, J., Liang, Y., Taniguchi, Y., Tanigaki, K., and Han, H. (2004). RING1 inhibits transactivation of RBP-J by Notch through interaction with LIM protein KyoT2. Nucleic Acids Res *32*, 1492-1501.
Quintana, E., Shackleton, M., Sabel, M.S., Fullen, D.R., Johnson, T.M., and Morrison, S.J. (2008). Efficient tumour formation by single human melanoma cells. Nature *456*, 593-598.
Raafat, A., Bargo, S., Anver, M.R., and Callahan, R. (2004). Mammary development and tumorigenesis in mice expressing a truncated human Notch4/Int3 intracellular domain (h-Int3sh). Oncogene *23*, 9401-9407.
Reedijk, M., Odorcic, S., Chang, L., Zhang, H., Miller, N., McCready, D.R., Lockwood, G., and Egan, S.E. (2005). High-level coexpression of JAG1 and NOTCH1 is observed in human breast cancer and is associated with poor overall survival. Cancer Res *65*, 8530-8537.
Reedijk, M., Odorcic, S., Zhang, H., Chetty, R., Tennert, C., Dickson, B.C., Lockwood, G., Gallinger, S., and Egan, S.E. (2008). Activation of Notch signaling in human colon adenocarcinoma. Int J Oncol *33*, 1223-1229.

Reichert, J.M. (2001). Monoclonal antibodies in the clinic. Nat Biotechnol *19*, 819-822.
Reichert, J.M. (2012). Marketed therapeutic antibodies compendium. MAbs *4*, 413-415.
Ricci-Vitiani, L., Lombardi, D.G., Pilozzi, E., Biffoni, M., Todaro, M., Peschle, C., and De Maria, R. (2007). Identification and expansion of human colon-cancer-initiating cells. Nature *445*, 111-115.
Richardson, J.H., Sodroski, J.G., Waldmann, T.A., and Marasco, W.A. (1995). Phenotypic knockout of the high-affinity human interleukin 2 receptor by intracellular single-chain antibodies against the alpha subunit of the receptor. Proc Natl Acad Sci U S A *92*, 3137-3141.
Ridgway, J., Zhang, G., Wu, Y., Stawicki, S., Liang, W.C., Chanthery, Y., Kowalski, J., Watts, R.J., Callahan, C., Kasman, I., *et al.* (2006). Inhibition of Dll4 signalling inhibits tumour growth by deregulating angiogenesis. Nature *444*, 1083-1087.
Rizzo, P., Miao, H., D'Souza, G., Osipo, C., Song, L.L., Yun, J., Zhao, H., Mascarenhas, J., Wyatt, D., Antico, G., *et al.* (2008). Cross-talk between notch and the estrogen receptor in breast cancer suggests novel therapeutic approaches. Cancer Res *68*, 5226-5235.
Roegiers, F., and Jan, Y.N. (2004). Asymmetric cell division. Current opinion in cell biology *16*, 195-205.
Ronchini, C., and Capobianco, A.J. (2001). Induction of cyclin D1 transcription and CDK2 activity by Notch(ic): implication for cell cycle disruption in transformation by Notch(ic). Mol Cell Biol *21*, 5925-5934.
Roth, J.A., Swisher, S.G., and Meyn, R.E. (1999). p53 tumor suppressor gene therapy for cancer. Oncology (Williston Park) *13*, 148-154.
Rousselle, C., Smirnova, M., Clair, P., Lefauconnier, J.M., Chavanieu, A., Calas, B., Scherrmann, J.M., and Temsamani, J. (2001). Enhanced delivery of doxorubicin into the brain via a peptide-vector-mediated strategy: saturation kinetics and specificity. J Pharmacol Exp Ther *296*, 124-131.
Salat, D., Liefke, R., Wiedenmann, J., Borggrefe, T., and Oswald, F. (2008). ETO, but not leukemogenic fusion protein AML1/ETO, augments RBP-Jkappa/SHARP-mediated repression of notch target genes. Mol Cell Biol *28*, 3502-3512.
Sansone, P., Storci, G., Giovannini, C., Pandolfi, S., Pianetti, S., Taffurelli, M., Santini, D., Ceccarelli, C., Chieco, P., and Bonafe, M. (2007). p66Shc/Notch-3 interplay controls self-renewal and hypoxia survival in human stem/progenitor cells of the mammary gland expanded in vitro as mammospheres. Stem Cells *25*, 807-815.
Santagata, S., Demichelis, F., Riva, A., Varambally, S., Hofer, M.D., Kutok, J.L., Kim, R., Tang, J., Montie, J.E., Chinnaiyan, A.M., *et al.* (2004). JAGGED1 expression is associated with prostate cancer metastasis and recurrence. Cancer Res *64*, 6854-6857.
Satoh, Y., Matsumura, I., Tanaka, H., Ezoe, S., Sugahara, H., Mizuki, M., Shibayama, H., Ishiko, E., Ishiko, J., Nakajima, K., *et al.* (2004). Roles for c-Myc in self-renewal of hematopoietic stem cells. J Biol Chem *279*, 24986-24993.
Sawant, R.M., Hurley, J.P., Salmaso, S., Kale, A., Tolcheva, E., Levchenko, T.S., and Torchilin, V.P. (2006). "SMART" drug delivery systems: double-targeted pH-responsive pharmaceutical nanocarriers. Bioconjug Chem *17*, 943-949.
Sawyer, C., Embleton, J., and Dean, C. (1997). Methodology for selection of human antibodies to membrane proteins from a phage-display library. Journal of Immunological Methods *204*, 193-203.

Saxena, M.T., Schroeter, E.H., Mumm, J.S., and Kopan, R. (2001). Murine notch homologs (N1-4) undergo presenilin-dependent proteolysis. J Biol Chem *276*, 40268-40273.
Schatton, T., Murphy, G.F., Frank, N.Y., Yamaura, K., Waaga-Gasser, A.M., Gasser, M., Zhan, Q., Jordan, S., Duncan, L.M., Weishaupt, C., *et al.* (2008). Identification of cells initiating human melanomas. Nature *451*, 345-349.
Scheinfeld, N. (2003). Adalimumab (HUMIRA): a review. Journal of drugs in dermatology : JDD *2*, 375-377.
Schier, R., and Marks, J.D. (1996). Efficient in vitro affinity maturation of phage antibodies using BIAcore guided selections. Human antibodies and hybridomas *7*, 97-105.
Schier, R., McCall, A., Adams, G.P., Marshall, K.W., Merritt, H., Yim, M., Crawford, R.S., Weiner, L.M., Marks, C., and Marks, J.D. (1996). Isolation of picomolar affinity anti-c-erbB-2 single-chain Fv by molecular evolution of the complementarity determining regions in the center of the antibody binding site. J Mol Biol *263*, 551-567.
Schroeder, T.J., First, M.R., Mansour, M.E., Hurtubise, P.E., Hariharan, S., Ryckman, F.C., Munda, R., Melvin, D.B., Penn, I., Ballistreri, W.F., *et al.* (1990). Antimurine antibody formation following OKT3 therapy. Transplantation *49*, 48-51.
Schutze-Redelmeier, M.P., Gournier, H., Garcia-Pons, F., Moussa, M., Joliot, A.H., Volovitch, M., Prochiantz, A., and Lemonnier, F.A. (1996). Introduction of exogenous antigens into the MHC class I processing and presentation pathway by Drosophila antennapedia homeodomain primes cytotoxic T cells in vivo. J Immunol *157*, 650-655.
Schwarze, S.R., Ho, A., Vocero-Akbani, A., and Dowdy, S.F. (1999). In vivo protein transduction: delivery of a biologically active protein into the mouse. Science *285*, 1569-1572.
Sestan, N., Artavanis-Tsakonas, S., and Rakic, P. (1999). Contact-dependent inhibition of cortical neurite growth mediated by notch signaling. Science *286*, 741-746.
Shaw, P.A., Catchpole, I.R., Goddard, C.A., and Colledge, W.H. (2008). Comparison of protein transduction domains in mediating cell delivery of a secreted CRE protein. Biochemistry *47*, 1157-1166.
Shawber, C., Nofziger, D., Hsieh, J.J., Lindsell, C., Bogler, O., Hayward, D., and Weinmaster, G. (1996). Notch signaling inhibits muscle cell differentiation through a CBF1-independent pathway. Development *122*, 3765-3773.
Shi, Y., Downes, M., Xie, W., Kao, H.Y., Ordentlich, P., Tsai, C.C., Hon, M., and Evans, R.M. (2001). Sharp, an inducible cofactor that integrates nuclear receptor repression and activation. Genes Dev *15*, 1140-1151.
Shimizu, K., Chiba, S., Kumano, K., Hosoya, N., Takahashi, T., Kanda, Y., Hamada, Y., Yazaki, Y., and Hirai, H. (1999). Mouse jagged1 physically interacts with notch2 and other notch receptors. Assessment by quantitative methods. J Biol Chem *274*, 32961-32969.
Silhol, M., Tyagi, M., Giacca, M., Lebleu, B., and Vives, E. (2002). Different mechanisms for cellular internalization of the HIV-1 Tat-derived cell penetrating peptide and recombinant proteins fused to Tat. Eur J Biochem *269*, 494-501.
Singh, S.K., Clarke, I.D., Terasaki, M., Bonn, V.E., Hawkins, C., Squire, J., and Dirks, P.B. (2003). Identification of a cancer stem cell in human brain tumors. Cancer Res *63*, 5821-5828.

Singh, S.K., Hawkins, C., Clarke, I.D., Squire, J.A., Bayani, J., Hide, T., Henkelman, R.M., Cusimano, M.D., and Dirks, P.B. (2004). Identification of human brain tumour initiating cells. Nature *432*, 396-401.
Slamon, D.J. (1987). Proto-oncogenes and human cancers. N Engl J Med *317*, 955-957.
Snijders, A.M., Schmidt, B.L., Fridlyand, J., Dekker, N., Pinkel, D., Jordan, R.C., and Albertson, D.G. (2005). Rare amplicons implicate frequent deregulation of cell fate specification pathways in oral squamous cell carcinoma. Oncogene *24*, 4232-4242.
Snyder, E.L., and Dowdy, S.F. (2005). Recent advances in the use of protein transduction domains for the delivery of peptides, proteins and nucleic acids in vivo. Expert Opin Drug Deliv *2*, 43-51.
Somia, N., and Verma, I.M. (2000). Gene therapy: trials and tribulations. Nat Rev Genet *1*, 91-99.
Song, L.L., and Miele, L. (2007). Cancer stem cells--an old idea that's new again: implications for the diagnosis and treatment of breast cancer. Expert Opin Biol Ther *7*, 431-438.
Song, L.L., Peng, Y., Yun, J., Rizzo, P., Chaturvedi, V., Weijzen, S., Kast, W.M., Stone, P.J., Santos, L., Loredo, A., *et al.* (2008). Notch-1 associates with IKKalpha and regulates IKK activity in cervical cancer cells. Oncogene *27*, 5833-5844.
Stewart, K.M., Horton, K.L., and Kelley, S.O. (2008). Cell-penetrating peptides as delivery vehicles for biology and medicine. Org Biomol Chem *6*, 2242-2255.
Stocks, M. (2005). Intrabodies as drug discovery tools and therapeutics. Curr Opin Chem Biol *9*, 359-365.
Strebe, N., Guse, A., Schungel, M., Schirrmann, T., Hafner, M., Jostock, T., Hust, M., Muller, W., and Dubel, S. (2009). Functional knockdown of VCAM-1 at the posttranslational level with ER retained antibodies. J Immunol Methods *341*, 30-40.
Studier, F.W. (2005). Protein production by auto-induction in high density shaking cultures. Protein expression and purification *41*, 207-234.
Stylianou, S., Clarke, R.B., and Brennan, K. (2006). Aberrant activation of notch signaling in human breast cancer. Cancer Res *66*, 1517-1525.
Suchting, S., Freitas, C., le Noble, F., Benedito, R., Breant, C., Duarte, A., and Eichmann, A. (2007). The Notch ligand Delta-like 4 negatively regulates endothelial tip cell formation and vessel branching. Proc Natl Acad Sci U S A *104*, 3225-3230.
Swiatek, P.J., Lindsell, C.E., del Amo, F.F., Weinmaster, G., and Gridley, T. (1994). Notch1 is essential for postimplantation development in mice. Genes Dev *8*, 707-719.
Takahashi, K., Tanabe, K., Ohnuki, M., Narita, M., Ichisaka, T., Tomoda, K., and Yamanaka, S. (2007). Induction of pluripotent stem cells from adult human fibroblasts by defined factors. Cell *131*, 861-872.
Tammam, J., Ware, C., Efferson, C., O'Neil, J., Rao, S., Qu, X., Gorenstein, J., Angagaw, M., Kim, H., Kenific, C., *et al.* (2009). Down-regulation of the Notch pathway mediated by a gamma-secretase inhibitor induces anti-tumour effects in mouse models of T-cell leukaemia. Br J Pharmacol *158*, 1183-1195.
Tamura, K., Taniguchi, Y., Minoguchi, S., Sakai, T., Tun, T., Furukawa, T., and Honjo, T. (1995). Physical interaction between a novel domain of the receptor Notch and the transcription factor RBP-J kappa/Su(H). Curr Biol *5*, 1416-1423.
Tanaka, T., and Rabbitts, T.H. (2008). Functional intracellular antibody fragments do not require invariant intra-domain disulfide bonds. J Mol Biol *376*, 749-757.
Tang, X., Molina, M., and Amar, S. (2007). p53 short peptide (p53pep164) regulates lipopolysaccharide-induced tumor necrosis factor-alpha factor/cytokine expression. Cancer Res *67*, 1308-1316.

Taniguchi, Y., Furukawa, T., Tun, T., Han, H., and Honjo, T. (1998). LIM protein KyoT2 negatively regulates transcription by association with the RBP-J DNA-binding protein. Mol Cell Biol *18*, 644-654.
Theisen, D.M., Pongratz, C., Wiegmann, K., Rivero, F., Krut, O., and Kronke, M. (2006). Targeting of HIV-1 Tat traffic and function by transduction-competent single chain antibodies. Vaccine *24*, 3127-3136.
Thurston, G., Noguera-Troise, I., and Yancopoulos, G.D. (2007). The Delta paradox: DLL4 blockade leads to more tumour vessels but less tumour growth. Nat Rev Cancer *7*, 327-331.
Tonon, G., Modi, S., Wu, L., Kubo, A., Coxon, A.B., Komiya, T., O'Neil, K., Stover, K., El-Naggar, A., Griffin, J.D., *et al.* (2003). t(11;19)(q21;p13) translocation in mucoepidermoid carcinoma creates a novel fusion product that disrupts a Notch signaling pathway. Nat Genet *33*, 208-213.
Trachsel, E., Bootz, F., Silacci, M., Kaspar, M., Kosmehl, H., and Neri, D. (2007). Antibody-mediated delivery of IL-10 inhibits the progression of established collagen-induced arthritis. Arthritis research & therapy *9*, R9.
Tsuji, M., Shinkura, R., Kuroda, K., Yabe, D., and Honjo, T. (2007). Msx2-interacting nuclear target protein (Mint) deficiency reveals negative regulation of early thymocyte differentiation by Notch/RBP-J signaling. Proc Natl Acad Sci U S A *104*, 1610-1615.
Uyttendaele, H., Marazzi, G., Wu, G., Yan, Q., Sassoon, D., and Kitajewski, J. (1996). Notch4/int-3, a mammary proto-oncogene, is an endothelial cell-specific mammalian Notch gene. Development *122*, 2251-2259.
VanderWielen, B.D., Yuan, Z., Friedmann, D.R., and Kovall, R.A. (2011). Transcriptional repression in the Notch pathway: thermodynamic characterization of CSL-MINT (Msx2-interacting nuclear target protein) complexes. J Biol Chem *286*, 14892-14902.
Visintin, M., Quondam, M., and Cattaneo, A. (2004). The intracellular antibody capture technology: towards the high-throughput selection of functional intracellular antibodies for target validation. Methods *34*, 200-214.
Vives, E., Brodin, P., and Lebleu, B. (1997). A truncated HIV-1 Tat protein basic domain rapidly translocates through the plasma membrane and accumulates in the cell nucleus. Journal of Biological Chemistry *272*, 16010-16017.
Vo, K., Amarasinghe, B., Washington, K., Gonzalez, A., Berlin, J., and Dang, T.P. (2011). Targeting notch pathway enhances rapamycin antitumor activity in pancreas cancers through PTEN phosphorylation. Molecular cancer *10*, 138.
Vogel, C.L., Cobleigh, M.A., Tripathy, D., Gutheil, J.C., Harris, L.N., Fehrenbacher, L., Slamon, D.J., Murphy, M., Novotny, W.F., Burchmore, M., *et al.* (2002). Efficacy and safety of trastuzumab as a single agent in first-line treatment of HER2-overexpressing metastatic breast cancer. J Clin Oncol *20*, 719-726.
Wallberg, A.E., Pedersen, K., Lendahl, U., and Roeder, R.G. (2002). p300 and PCAF act cooperatively to mediate transcriptional activation from chromatin templates by notch intracellular domains in vitro. Mol Cell Biol *22*, 7812-7819.
Wang, J., Wakeman, T.P., Lathia, J.D., Hjelmeland, A.B., Wang, X.F., White, R.R., Rich, J.N., and Sullenger, B.A. (2010). Notch promotes radioresistance of glioma stem cells. Stem Cells *28*, 17-28.
Wang, Q., and Greene, M.I. (2008). Mechanisms of resistance to ErbB-targeted cancer therapeutics. J Clin Invest *118*, 2389-2392.
Weerkamp, F., Luis, T.C., Naber, B.A., Koster, E.E., Jeannotte, L., van Dongen, J.J., and Staal, F.J. (2006). Identification of Notch target genes in uncommitted T-cell

progenitors: No direct induction of a T-cell specific gene program. Leukemia *20*, 1967-1977.
Wei, P., Walls, M., Qiu, M., Ding, R., Denlinger, R.H., Wong, A., Tsaparikos, K., Jani, J.P., Hosea, N., Sands, M., *et al.* (2010). Evaluation of selective gamma-secretase inhibitor PF-03084014 for its antitumor efficacy and gastrointestinal safety to guide optimal clinical trial design. Mol Cancer Ther *9*, 1618-1628.
Weiner, L.M., Surana, R., and Wang, S. (2010). Monoclonal antibodies: versatile platforms for cancer immunotherapy. Nat Rev Immunol *10*, 317-327.
Weng, A.P., Millholland, J.M., Yashiro-Ohtani, Y., Arcangeli, M.L., Lau, A., Wai, C., Del Bianco, C., Rodriguez, C.G., Sai, H., Tobias, J., *et al.* (2006). c-Myc is an important direct target of Notch1 in T-cell acute lymphoblastic leukemia/lymphoma. Genes Dev *20*, 2096-2109.
Weng, A.P., Nam, Y., Wolfe, M.S., Pear, W.S., Griffin, J.D., Blacklow, S.C., and Aster, J.C. (2003). Growth suppression of pre-T acute lymphoblastic leukemia cells by inhibition of notch signaling. Mol Cell Biol *23*, 655-664.
Westhoff, B., Colaluca, I.N., D'Ario, G., Donzelli, M., Tosoni, D., Volorio, S., Pelosi, G., Spaggiari, L., Mazzarol, G., Viale, G., *et al.* (2009). Alterations of the Notch pathway in lung cancer. Proc Natl Acad Sci U S A *106*, 22293-22298.
Whitmore, L., and Wallace, B.A. (2008). Protein secondary structure analyses from circular dichroism spectroscopy: methods and reference databases. Biopolymers *89*, 392-400.
William, D.A., Saitta, B., Gibson, J.D., Traas, J., Markov, V., Gonzalez, D.M., Sewell, W., Anderson, D.M., Pratt, S.C., Rappaport, E.F., *et al.* (2007). Identification of oscillatory genes in somitogenesis from functional genomic analysis of a human mesenchymal stem cell model. Dev Biol *305*, 172-186.
Wilson, J.J., and Kovall, R.A. (2006). Crystal structure of the CSL-Notch-Mastermind ternary complex bound to DNA. Cell *124*, 985-996.
Wright, M.J., and Deonarain, M.P. (2007). Phage display of chelating recombinant antibody libraries. Mol Immunol *44*, 2860-2869.
Wu, L., Aster, J.C., Blacklow, S.C., Lake, R., Artavanis-Tsakonas, S., and Griffin, J.D. (2000). MAML1, a human homologue of Drosophila mastermind, is a transcriptional co-activator for NOTCH receptors. Nat Genet *26*, 484-489.
Wu, L., Sun, T., Kobayashi, K., Gao, P., and Griffin, J.D. (2002). Identification of a family of mastermind-like transcriptional coactivators for mammalian notch receptors. Mol Cell Biol *22*, 7688-7700.
Wu, Y., Cain-Hom, C., Choy, L., Hagenbeek, T.J., de Leon, G.P., Chen, Y., Finkle, D., Venook, R., Wu, X., Ridgway, J., *et al.* Therapeutic antibody targeting of individual Notch receptors. Nature *464*, 1052-1057.
Wu, Y., Cain-Hom, C., Choy, L., Hagenbeek, T.J., de Leon, G.P., Chen, Y., Finkle, D., Venook, R., Wu, X., Ridgway, J., *et al.* (2010). Therapeutic antibody targeting of individual Notch receptors. Nature *464*, 1052-1057.
Xue, Y., Gao, X., Lindsell, C.E., Norton, C.R., Chang, B., Hicks, C., Gendron-Maguire, M., Rand, E.B., Weinmaster, G., and Gridley, T. (1999). Embryonic lethality and vascular defects in mice lacking the Notch ligand Jagged1. Hum Mol Genet *8*, 723-730.
Yabe, D., Fukuda, H., Aoki, M., Yamada, S., Takebayashi, S., Shinkura, R., Yamamoto, N., and Honjo, T. (2007). Generation of a conditional knockout allele for mammalian Spen protein Mint/SHARP. Genesis *45*, 300-306.

Yan, M., Callahan, C.A., Beyer, J.C., Allamneni, K.P., Zhang, G., Ridgway, J.B., Niessen, K., and Plowman, G.D. (2010). Chronic DLL4 blockade induces vascular neoplasms. Nature *463*, E6-7.
Yang, Z.J., and Wechsler-Reya, R.J. (2007). Hit 'em where they live: targeting the cancer stem cell niche. Cancer Cell *11*, 3-5.
Yao, J., and Qian, C. (2010). Inhibition of Notch3 enhances sensitivity to gemcitabine in pancreatic cancer through an inactivation of PI3K/Akt-dependent pathway. Medical oncology *27*, 1017-1022.
Yu, J., Vodyanik, M.A., Smuga-Otto, K., Antosiewicz-Bourget, J., Frane, J.L., Tian, S., Nie, J., Jonsdottir, G.A., Ruotti, V., Stewart, R., *et al.* (2007). Induced pluripotent stem cell lines derived from human somatic cells. Science *318*, 1917-1920.
Zebedee, S.L., Barbas, C.F., 3rd, Hom, Y.L., Caothien, R.H., Graff, R., DeGraw, J., Pyati, J., LaPolla, R., Burton, D.R., Lerner, R.A., *et al.* (1992). Human combinatorial antibody libraries to hepatitis B surface antigen. Proc Natl Acad Sci U S A *89*, 3175-3179.
Zhao, Y., Katzman, R.B., Delmolino, L.M., Bhat, I., Zhang, Y., Gurumurthy, C.B., Germaniuk-Kurowska, A., Reddi, H.V., Solomon, A., Zeng, M.S., *et al.* (2007). The notch regulator MAML1 interacts with p53 and functions as a coactivator. J Biol Chem *282*, 11969-11981.
Zhao, Y., Lou, D., Burkett, J., and Kohler, H. (2001). Chemical engineering of cell penetrating antibodies. J Immunol Methods *254*, 137-145.
Zheng, L., Baumann, U., and Reymond, J.L. (2003). Production of a functional catalytic antibody ScFv-NusA fusion protein in bacterial cytoplasm. J Biochem *133*, 577-581.